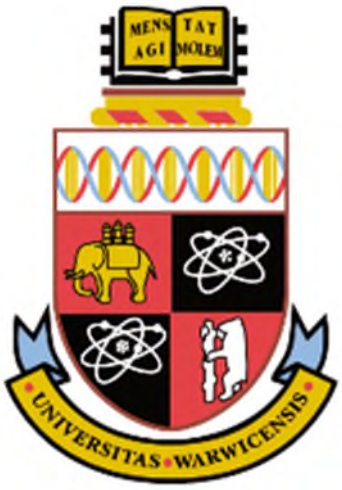

Glyoxalase 1 overexpression-associated multi-drug resistance in cancer chemotherapy

By Hafsa Abbas

A thesis submitted in partial fulfilment of the requirements

for the degree of

Doctor of Philosophy in Medical Sciences

Warwick Medical School

University of Warwick

July 2020

TABLE OF CONTENTS

LIST OF FIGURES

LIST OF TABLES

Acknowledgement

I would like to initiate my acknowledgement by thanking Allah, The Most High for giving me the strength, faith, patience, and ability in order to complete this interesting Ph.D. project. The pursuit of knowledge and reason is crucial for one to progress in life and help make a difference.

In the Glorious Quran, Allah the Most High states

‘"Recite: In the name of thy Lord who created man from a clot. Recite: And thy Lord is the Most Generous Who taught by the pen, taught man that which he knew not." (96:1-5)

I would like to thank my family especially my parents and siblings for their unlimited love, sacrifice, prayers and doing their best to support me morally, emotionally, financially, motivating me to improve for the better and accompanying me to national and international conferences because without them as well as several close friends, I would not have had any financial support.

I would like to thank my husband, Najib, for being patient, understanding and showering me with his love and care, for loving me for who I am and not what I am and always pushing me forward and supporting me with my career goals in life.

I would like to thank my supervisors, Professor Paul Thornalley and Dr Naila Rabbani for their selflessness, effort, sharing their knowledge and expertise, guiding me towards my PhD project and shaping me to be a good researcher.

I would like to thank my local supervisor, Dr Daniel Mitchell for his support and time after Professor Thornalley and Dr Rabbani left.

I would like to thank the post-doctoral researchers, Dr Mingzhan Xue, Dr Sabah Pasha and Dr Attia Anwar for sharing their expertise in experimental methods and giving advice based on their research experiences.

I would like to thank current and past members of the Protein Damage and Systems Biology group for your company and support during my time here.
I would like to thank Warwick Medical School especially the CSRL team for organising seminars, social events, great laboratories, organising orders, and symposiums to discuss current research, meet with other groups and creating a great medical and scientific atmosphere of learning and development for PhD students and staff members.

I would like to thank my Upgrade Panel: Dr Martin Weikert, Dr Mark Christian and Dr Jason Madden for their advice and support during the process.

I would like to thank University of Warwick for its great facilities, resources and organising beneficial courses such as SkillsForge, Postgraduate Certificate for Transferrable Skills and other courses and activities to improve our current skills, gain new skills and meet other research students from other departments creating an interdisciplinary atmosphere as part of Continuous Professional Development.

Ultimately, everyone mentioned above had a significant contribution to my current status. Thank you all.

Dedication

I would like to thank Allah, my family especially my parents, siblings and husband for being my golden source of strength.

Declaration

I am fully aware and understand the regulations by the University of Warwick concerning plagiarism. All the work presented in this thesis were performed by myself under the supervision of Professor Paul Thornalley and Dr Naila Rabbani. This work was not previously submitted to any other type of degree. The work presented below (including the data analysis) was carried out by the author, Hafsa Waseela Abbas.

ABSTRACT

Glyoxalase 1 (Glo1) overexpression is found in refractory tumours and this project aims to characterise the resistance to clinical anticancer drugs by Glo1 overexpression in the human HEK-293 tumour cell line *in vitro* and investigate drug-induced increased methylglyoxal and related cytotoxicity as a likely cause.

HEK-293 cells had high Glo1 expression and activity that was increased up to 5-fold when stably transfected with a pIRES2-EGFP-GLO1 plasmid with respect to empty vector control using G-418. Dose-response studies determined the median growth inhibitory concentration and showed that Doxorubicin, Mitomycin C, Taxol, Methotrexate and Mechlorethamine had the highest Glo1-linked multi-drug resistance. There was drug-induced increased glycolysis and flux of methylgloxal formation *in vitro.* Transient transfection of GLO1 siRNA, the cell-permeable Glo1 inhibitor S-p-bromobenzylglutathione cyclopentyl diester, exogenous methylglyoxal and hypoxia potentiated the cytotoxicity of anti-tumour drugs and increased dicarbonyl stress. Stable isotopic LC-MS/MS analysis revealed that Mitomycin C enhanced glutathione (GSH) depletion whereas Mechlorethamine increased GSH levels. There were increased methylglyoxal levels in drug-treated HEK-293 cells *in vitro.*

Overall, decreasing Glo1 expression and activity increased MG toxicity and sensitivity to anti-tumour drugs. Anti-tumours drugs are not direct Glo1 inhibitors and may be influenced by unrecognised downstream signalling mechanisms on glycolysis and MG metabolism.

LIST OF ABBREVIATIONS

2-DE	2-Dimensional gel electrophoresis
3-DG	3-Deoxyglucosone
3DG-H	hydroimidazolones
3-NT	3-Nitrotyrosine
3'UTR	3' untranslated region
4-HNE	4-hydroxynonenal
5-HMF	5-Hydroxymethylfurfural
5′-MTHF	5'-methyl-tetrahydrofolate
5'UTR	5' untranslated region
AA	Acetaldehyde
ACL	ATP citrate lyase
ACS	Ammonium persulphate
Acetyl CoA	acetyl coenzyme A
ACTB	β-actin gene
ADH	Alcohol dehydrogenase
AGEs	Advanced glycation endproducts
Ago2	argonaute
AICAR	Aminoimidazole carboxamide ribotide transformylase
AKR	Aldoketo reductase
Akt	Protein kinase B
ALDH	Aldehyde dehydrogenase
AP-2α	Activating enhancer-binding protein 2 alpha
APT	aminoglycoside 3'-phosphotransferase
AraC	cytarabine
ARE	Antioxidant response elements
ARI	Aldose reductase inhibitor
ATCC	American Type Culture Collection
ATF4	transcription factor 4

ATM	Ataxia telangiectasia
ATP	adenosine triphosphate
AUC	Space under the curve
Bax	Bcl-2-associated X
BCA	Bicinchoninic acid
Bcl-2	B-cell lymphoma 2
BCRP	breast cancer resistance protein
Bgl II	*Bacillus globigii*
BMT	Bone Marrow Transplant
BON-1	metastatic human carcinoid pancreatic tumour cell line
BSA	Bovine serum albumin
BSG	basigin
BSO	buthionine sulfoximine
CAIX	Carbonic anhydrase IX
CBP	CREB binding protein
CCLE	Cancer Cell Line Encyclopedia
CD147	cluster of differentiation 147
cDNA	Complementary deoxyribonucleic acid
CEdG	N2-(1-carboxytheyl) deoxyguanosine
CEL	Nε(1-carboxyethyl) lysine
CFS	Common fragile sites
Cis-diamminedichloroplatinum	cisplatin
CHIP	HSP70-interacting protein
CHO	chinese hamster ovary
CLL	Chronic lymphocytic leukaemia
CMA	Nε-carboxymethyl-lysine
CMC	S-carboxymethylcysteine
CMdG	N2-carboxymethyl-deoxyguanosine
CML	Nε-carboxymethyl-lysine

CML	chronic myelogenous leukaemia
CNV	Copy number variation
COX-2	cyclooxygenase
ctDNA	Circulating tumour DNA
CVD	Cardiovascular disease
CXCR4	C-X-C chemokine receptor type 4
CYCLO	cyclo,5,10, methenyl-FH4-cyclohydroxylase
CYP2E1	cytochrome p450 2E1
CYP3A4	cytochrome P450 3A4
DCP	Dicarbonyl proteome
DETAPAC	diethylenetriaminepentaacetic acid
dG	deoxyguanosine
DGV	The Database of Genomic Variants
DHAP	Dihydroxyacetone phosphate
DHF	dihydrofolate
DHFR	dihydrofolate reductase
DJ-1	protein deglycase
DM	diabetes mellitus
DMBA	Dimethylbenz(a)anthracene
DMEM	Dulbecco’s modified eagle's medium
DMF	Dimethylformamide
DMSO	dimethylsulphoxide
DNA	Deoxyribonucleic Acid
DNA-PK	DNA-dependent protein kinase
DSB	DNA strand breaks
DSC	desmocollin
DSG	desmoglein
dT	deoxythymine
DTT	Dithiothreitol

ECCC	European Collection of Cell Cultures
ECL	Enhanced chemiluminescence
ECM	extracellular matrix
ECMV	encephalomyocarditis cytomegalovirus virus
EDF4	E2F-binding to the transcription factor
EDTA	Ethylenediaminetetraacetic acid
EGF	Epidermal Growth Factor
eGFP	Enhanced Green Fluorescent Protein
EGFR	epidermal growth factor receptor
EMA	Europeans Medicines Agency
EMT	epithelial-mesenchymal transition
ER	endoplasmic reticulum
ERK	extracellular regulated
esRAGE	Endogenous secreted RAGE
F-1,6-BP	fructose 1,6-bisphosphate
F3K	fructosamine-3-kinase
FADH	flavin adenine dinucleotide
FBS	Foetal bovine serum
FDA	Food and Drug Administration
FDXR	ferredoxin reductase
FGF	fibroblast growth factor
FH	Fumarate Hydratase
FH2	dihydrofolate
FH4	tetrahydrofolate
FiH-1	Factor Inhibition Hypoxia Inducible Factor
FL	Nε-(1-deoxy-D-fructos-1yl) lysine
FPGS	folylpolyglutamate synthetase
G-6-P	glucose-6-phosphate
GA3P	glyceraldehyde 3-phosphate

GAPDH	glucose-6-phosphate (G-6-P) dehydrogenase
GAR	glycinamide ribotide
GC_{50}	Median growth inhibitory concentration
GCL	γ-glutamylcysteine ligase
GC-MS	gas chromatography with mass spectrometry
GCS	glutamylcysteine synthetase
gdC	5-glycolyldeoxycytidine
GdG	3-(2'-deoxyribosyl)-6,7-dihydro-6,7-dihydroxyimidazo[2,3-b] purin-9(8) one
GF	Growth factor
GGT	γ-glutamyl-transpeptidase
G-H1	Nδ-(5-hydro-4-imidazolon-2-yl)ornithine
Glc	glucose
Glo1	Glyoxalase 1
Glo2	Glyoxalase 2
GLS	Glutaminase
Glu	polyglutamate
GLUT	Glucose transporter
GP70	embigin
GPCR	G protein-coupled receptors
GPX	glutathione peroxidase
GRE	glucocorticoid responsive element
GSH	Reduced glutathione
GSSG	Oxidized glutathione
GSR	Glutathione reductase
GST	Glutathione S-transferase
GTPases	guanosine triphosphatase
HAGH	Hydroxyacylglutathione hydrolase
HB	hepatitis B virus

HBPC-GSH	hydroxy-N-bromophenylcarbamoyl)glutathione
HCC	hepatocellular carcinoma
HCV	Hepatitis C
HDL	high density lipoproteins
HDL	high density lipoproteins
HEK-293	Human embryonic kidney 293
HEPES 4-	4-(2-hydroxyethyl)-1-piperazineethanesulfonic acid
HER-2	human epidermal growth factor receptor 2
HIF	Hypoxia-inducible factor
HIF-1	Hypoxia-Inducible Factor 1
HIV	Human immunodeficiency virus
HK	hexokinase
HK-2	hexokinase-2
HLA-DR	Human Leukocyte Antigen - antigen D-Related
HO-1	haem oxygenase-1
HPLC	high phase liquid chromatography
HPV	human papillomavirus
HR	homologous recombination
HRE	hypoxia response elements
HSV TK	herpes simplex virus thymidin kinase
iASPP	inhibitor of apoptosis-stimulating protein of p53
IGF-2	insulin-like growth factor-2
IGFBP2	insulin-like growth factor binding protein 2
IL-8	interleukin 8
IKB-alpha	I-kappa-B-alpha
ING4	Inhibitor of growth protein 4
iNOS	inducible nitric oxide synthase

IQGAP1	IQ Motif Containing GTPase Activating Protein 1
IRE	Insulin response element
IRES	internal ribosome entry site
IS	Internal standard
JMJD2A	lysine-specific histone demethylase
JNK	c-Jun N-terminal kinase
K_{ATP}	ATP sensitive K^+
kb	kilobase
KDM4A	lysine-specific histone demethylase
Keap1	Kelch-like ECH-associated protein 1
KLHL	Kelch-like gene
Km	Michaelis-Menten constant
LC-MS/MS	Liquid chromatography with coupled tandem mass spectrometry
LDH	Lactate dehydrogenase
LDL	Low density lipoproteins
LOD	Limit of Detection
LOX	Lysyl oxidase
MAPK	Mitogen activated protein kinases
MARE	MAF recognition elements
mCAR	murine coxsackievirus and adenovirus receptor
MCM	Mini chromosome maintenance
MCS	Multiple cloning sites
MCT	monocarboxylate transporters
MDA	malondialdehyde
MDM2	mouse double minute 2
MDR	Multi-drug resistance
MDR1	multi-drug resistance protein 1
MDT	Multidisciplinary team

MeCN	acetonitrile
MeOH	methanol
MG	methylglyoxal
MGdG	3-(2′-deoxyribosyl)-6,7-dihydro-6,7-dihydroxy-6-methylimidazo-[2,3-b] purine-
MG-H1	Nδ-(5-hydro-5-methyl-4-imidazolon-2-yl) ornithine
MGMT	Methyl-guanine-DNA methyltransferase
MHC	Major histocompatibility complex
MHRA	Medicines and Healthcare products Regulatory Agency
MMLV	Moloney Murine Leukaemia Virus
MMP	Matrix metalloproteases
MPTP	Mitochondrial Permeable Transition Pore
MRE	Metal Response Element
MRP	multixenobiotic resistance protein
MMR	Mismatch repair proteins
MRM	Multiple reaction monitoring
mRNA	Messenger ribonucleic acid
MS	methionine synthase
mTOR	mammalian target of rapamycin
mTORC1	mammalian target of rapamycin complex 1
MTA	Microtubule-targeting agents
MXR	mitoxantrone resistance protein
NaCl	sodium chloride
NAD^+	Nicotinamide adenine dinucleotide (oxidized form)
NADH	Nicotinamide adenine dinucleotide (reduced form)
NADPH	nicotinamide adenine dinucleotide phosphate
Neor	neomycin resistant

NER	Nucleotide excision repair
NF-κB	nuclear factor kappa-light-chain-enhancer of activated B cells
NHEJ	non-homologous end joining
NO	Nitric oxide
Nrf2	Nuclear factor erythroid 2-related factor 2
NSCLC	non-small cell lung cancer
ODS	octadecylsilica
ORF	Open reading frame
p14ARF	alternate reading frame protein
p65	nuclear factor-kappa B
PARK7	Parkinsonism Associated Deglycase
PARP	poly (ADP-ribose) polymerases
PBS	Phosphate buffered saline
PCA	perchloric acid
PCR	Polymerase chain reaction
PD	population doubling
PDGF-B	platelet-derived growth factor-B
PDH	pyruvate dehydrogenase
PDK-1	phosphoglycerate kinase
PERK	PKR-like endoplasmic reticulum kinase
P-gp	Permeability-glycoprotein 1
PGAM5	serine/threonine protein phosphatase
PHD	Prolyl Hydroxylase Domain isoforms
pI	Isoelectric point
PI3K	phosphatidylinositol 3-kinase
pIRES2-EGFP	Empty vector
pIRES2-GLO1-EGFP	Glo1 vector
PKC	Protein kinase C
PKM2	pyruvate kinase isozymes M1/M2

POLH	DNA polymerase Eta
PPP	pentose phosphate pathway
pRb	retinoblastoma
Pst I	*Providencia stuartii*
PTEN	Phosphatase and tensin
PVDF	polyvinyl difluoride
pVHL	von Hippel-Lindau
Pyr	pyruvate
RAGE	Receptor of Advanced Glycation End-products.
real-time RT-PCR	real-time reverse transcription-polymerase chain reaction
RFC	reduced folate carrier
RISC	RNA induced silencing complex
RNAi	RNA interference
RNS	reactive nitrogen species
ROS	reactive oxygen species
RT-PCR	reverse transcription-polymerase chain reaction
SAX-SPE	strong anion-exchange solid-phase extraction
SCAN-1	spinocerebellar ataxia with axonal neuropathy
SCLC	Small cell lung cancer
SD	Standard deviation
SDS	Sodium dodecyl sulphate
SH	sulfhydryl
siRNA	Small interfering ribonucleic acid
S-p-BrBzGSHCp2	S-p-bromobenzylgluthathione () diester.
sRAGE	c-terminal truncated soluble RAGE
SREBP1	Sterol regulatory element-binding transcription factor 1

STAT1	signal transducer and activator of transcription 1
SUMO	small ubiquitin-related modifier
SVCT2	Sodium Vitamin C Transporter 2
TCA	tricarboxylic acid
TCA	trichloroacetic acid
TDP1	tyrosyl-DNA phosphodiesterase-1
TEMED	N, N, N', N'-tetramethylethylene-1,2-diamine
TFA	Trifluoroacetic acid
TFAP2A	activating enhanced binding protein 2 alpha
TGF-β	transforming growth factor beta
THF	tetrahydrofolate
TLR	Toll-like receptors
TME	tumour microenvironment
TNF	Tumour necrosis factor
TNM	Tumour Node Metastasis
Tris base	Tris(hydroxymethyl)-aminomethane
TS	thymidylate synthase
TU	Transcription units
UKCCCR	United Kingdom Coordinating Committee on Cancer Research
UTR	untranslated region
VEGF	vascular endothelial growth factor

1. Introduction

1.1 Cancer

1.1.1 The hallmarks of Cancer

Cancer is an assembly of diseases characterized by uncontrolled cell growth and the distribution of cells from the primary site of origin to other parts of the body (metastasis) through the blood or lymph (Knox, 2010). Many types of human cells may potentially become cancerous whereby they acquire abnormal proliferative and invasive characteristics of malignant transformation (Pecorino, 2016). Hanahan and Weinberg (2011) have defined the hallmarks of cancer that consists of six biological abilities required for the multi-step development of tumours – Figure 1. This comprises of self-sufficiency to growth signals, evading anti-growth signalling mechanisms to proliferate, inhibiting apoptosis, inducing angiogenesis, invasion, and metastasis (Hanahan and Weinberg, 2011). This framework guides researchers on how to understand the molecular mechanisms and develop treatments for tumours.

However, they have identified additional characteristics that increase cancer progression: evading the immune system, promoting inflammation, reprogramming of energy metabolism and genomic instability. Cancer genomes are highly unstable where some genetic alterations are intragenic whereas the majority of the genetic mutations of the clonal origin have a functional loss (aneuploidy) which creates genetic diversity causing multifactorial functions (Cahill *et al.*, 1999; Marx, 2002, Hanahan and Wienberg, 2011; Moses *et al.*, 2018). Moreover, there are non-immortalised stromal cells besides tumour cells that form part of the tumour microenvironment that contributes to tumour development and progression (Moses *et al.*, 2018).

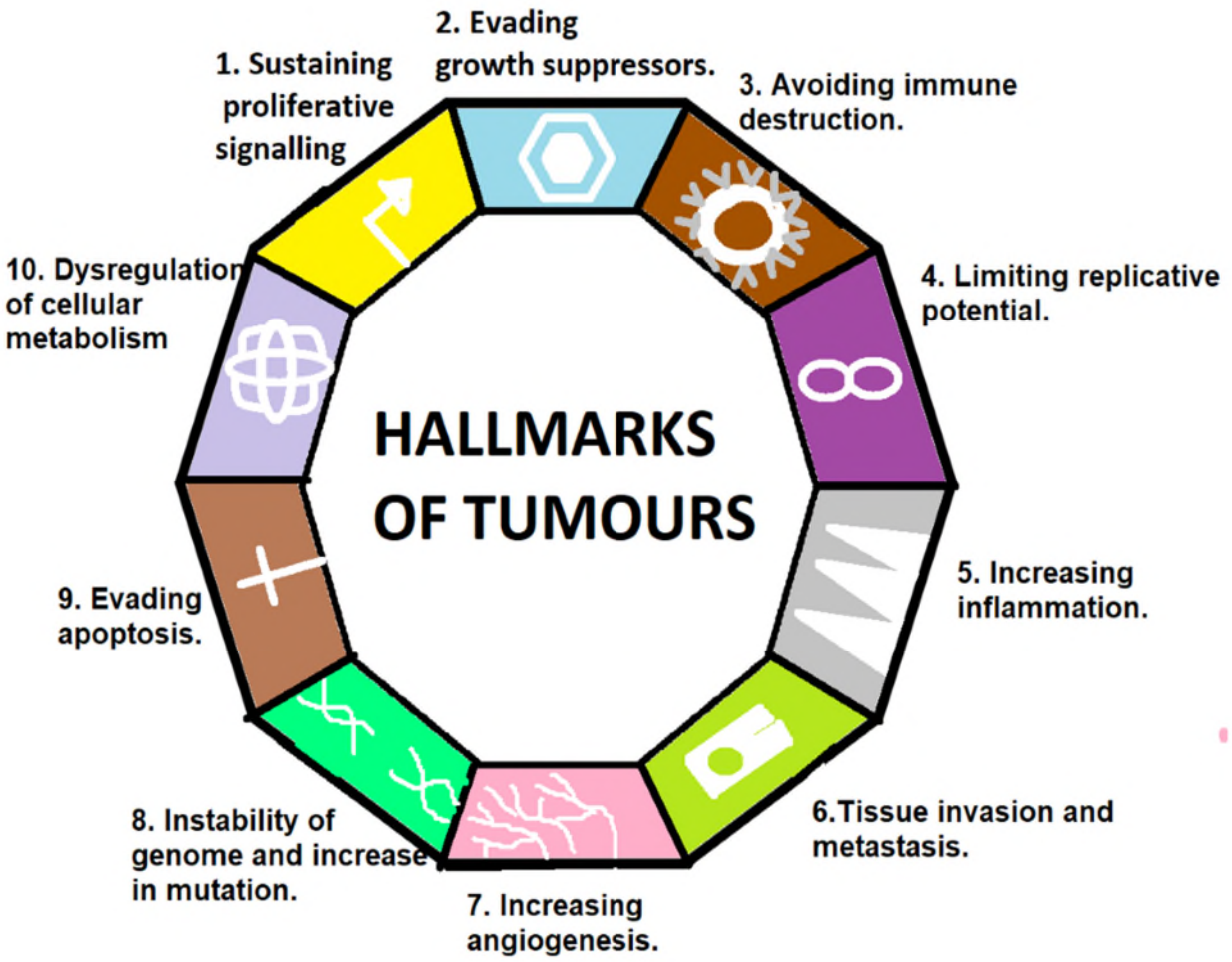

Figure 1: The hallmarks of cancer (Adapted from: Hanahan and Weinberg, 2011)

The ten hallmarks of cancer that characterise the tumour phenotype.

The morphological appearance of several forms of pre-malignant lesions, hyperplasia and dysplasia is caused by genetic, epigenetic and chromosomal alterations where some are inherited and can also be acquired in response to errors in cell division or environmental exposure to ultraviolet radiation and the tobacco smoke that damage deoxyribonucleic acid (DNA) (Esteller, 2000; Yokota, 2000). This disrupts the signalling mechanisms that control cellular functions and proliferation (Sadikovic *et al.*, 2008). An accumulation of these genetic mutations induces the formation of primary tumours – Figure 2. The cellular phenotype changes as mutations accumulate further progresses to expand and invade to form metastatic tumours maintaining the malignant phenotype of tumour cells (Yokota, 2000).

The two antithetical genetic types in oncogenesis are tumour suppressor proteins and proto-oncogenes (Shen *et al.*, 2018; Botezatu *et al.* 2016; Schwab and Amler, 1990; Varkondi *et al.*, 2005). Proto-oncogenes during genetic diversity can cause tumours cells to proliferate uncontrollably whereas tumour suppressor proteins prevent cells from degenerating into tumour cells (Shen *et al*, 2018; Croce, 2008; Klein and Klein, 1986). Other genes exhibit both functions (Shen *et al*., 2018).

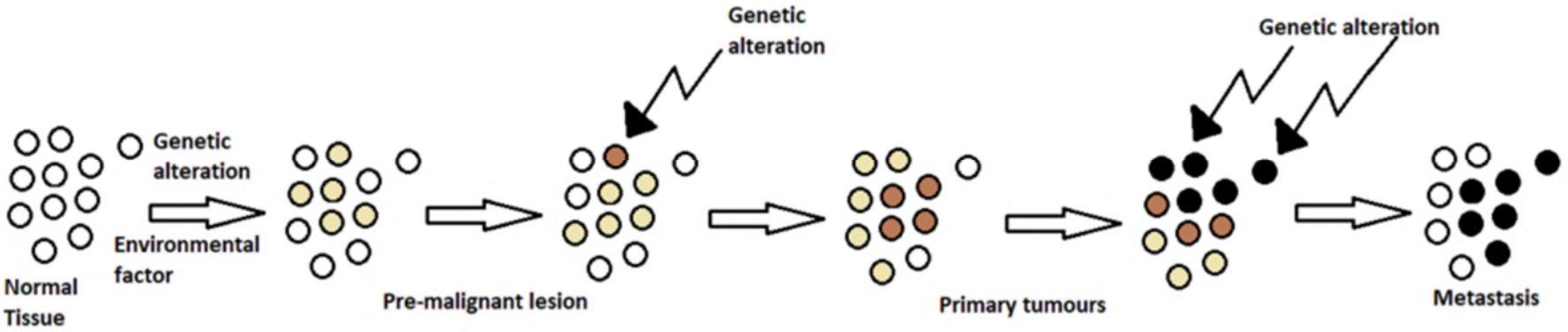

Figure 2 The key stages in cancer progression (Adapted from: Yokota, 2000)

Genetic alterations and environment stress can cause the normal cells to produce pre-malignant lesions. Additional genetic mutations form the primary tumours which undergoes expansion and invasion leading to metastasis.

Key: Normal cells ○, pre-malignant cells ○, tumour cells with no metastatic ability ● and tumour cells with metastatic ability ●.

1.1.1.1 Dysregulation of cellular metabolism

This project focuses on one of the major hallmarks of cancer, reprogramming of metabolic activity in cells which facilitates other hallmarks of cancer such as self-sufficiency in growth signals and evading apoptosis which is a major element in chemotherapeutic resistance and was discovered by Dr Otto Warburg (Phan *et al.*, 2014; Ward and Thompson, 2012, Warburg, 1923). Overexpression of the cytosolic enzyme, glyoxalase 1 (Glo1) is found in clinical refractory tumours and is a negative survival factor in cancer therapy (Rabbani *et al.*, 2018). Glo1 is the first line of defence that catalyses the detoxification and metabolism of reactive α-aldehydes or dicarbonyl metabolites such as methylglyoxal (MG) to the relatively non-toxic metabolic product, D-lactate to protect host systems from cell dysfunction and disease (Rabbani and Thornalley, 2014a, Thornalley, 2003a; Rabbani *et al*., 2014b, Xue *et al*., 2012).

Reprogramming of cellular metabolic activity is characterized by the following tumour cellular bioenergetic mechanisms: elevated glycolysis, pentose phosphate pathway (PPP), lipid metabolism, glutaminolysis and other metabolic mechanisms that provide tumour cells energy and metabolites for progression (Phan *et al*., 2014; Ward and Thompson, 2013; Kalyanaraman, 2017). Metabolites can also be oncogenic by influencing cell signalling and differentiation (Phan *et al.*, 2014; Cazzaniga and Bonanni, 2015). Thus, as illustrated in Figure 3, molecular pathways have an impact on metabolic programming. For instance, the phosphatidylinositol 3-kinase/ protein kinase B (PI3K/Akt) signalling pathway increases glucose consumption through the glucose transporter GLUT-1 (Buzzai *et al*., 2005; Vasseur *et al*., 2009). This, in turn, increases glycolytic flux. GLUT-1 expression is increased on the plasma membrane stimulating hexokinase and can associate with glucose via phosphorylation (Deprez *et al.* 1997; Suls *et al*., 2009; Kalyanaraman, 2017). Other mechanisms of increasing glycolytic metabolism are the activation of phosphofructokinase-1 and biosynthetic pathways such as the synthesis of fatty acids and cholesterol that need acetyl-coA (Kohn *et al*., 1996; Wakil *et al*., 1957).

In normal cells, glucose undergoes a catabolic reaction to pyruvate which is converted to acetyl coenzyme A (acetyl-CoA) to facilitate in the tricarboxylic

acid (TCA) cycle. This generates the electron carriers, nicotinamide adenine dinucleotide (NADH) and flavin adenine dinucleotide (FADH) for energy production. Each glucose molecule can produce a maximum of 36 adenosine triphosphate (ATP) in response to the mitochondrial respiratory chain. Glycolysis is utilized when the supply of oxygen is restricted (Dumas *et al*., 2017; Phan *et al.*, 2014). On the other hand, glycolysis is utilized in cancer cells even when there are high amounts of oxygen present (DeBerardinis *et al.* 2008). Cancer cells upregulate glucose transporters to increase glucose uptake predominantly GLUT-1, GLUT-2, GLUT-3 and GLUT-4 (Phan *et al.*, 2014). However, glucose consumption can be suppressed by p53 by halting the transcription and expression of Glut1, Glut3 and Glut4 (Schwartzenberg-Bar-Yoseph *et al*., 2004).

Another difference between normal and tumour cells is how the end-product of glycolysis, pyruvate, is processed. Majority of pyruvate is converted to acetyl-CoA for the TCA cycle whereas some are utilized to produce lactate or alanine (Phan *et al*., 2014). In tumour cells, lactate is produced predominantly because of the upregulation of the enzyme lactate dehydrogenase (LDH). This allows tumour cells to facilitate the oxidation of NADH to nicotinamide adenine dinucleotide - oxidised form, (NAD^+) and thereby maintain a high glycolytic rate (DeBerardinis *et al*., 2008; Dang, 1999; Kalyanaraman, 2017). Tumours may also access nutrients from the blood via monocarboxylate transporters (Phan *et al*., 2014).

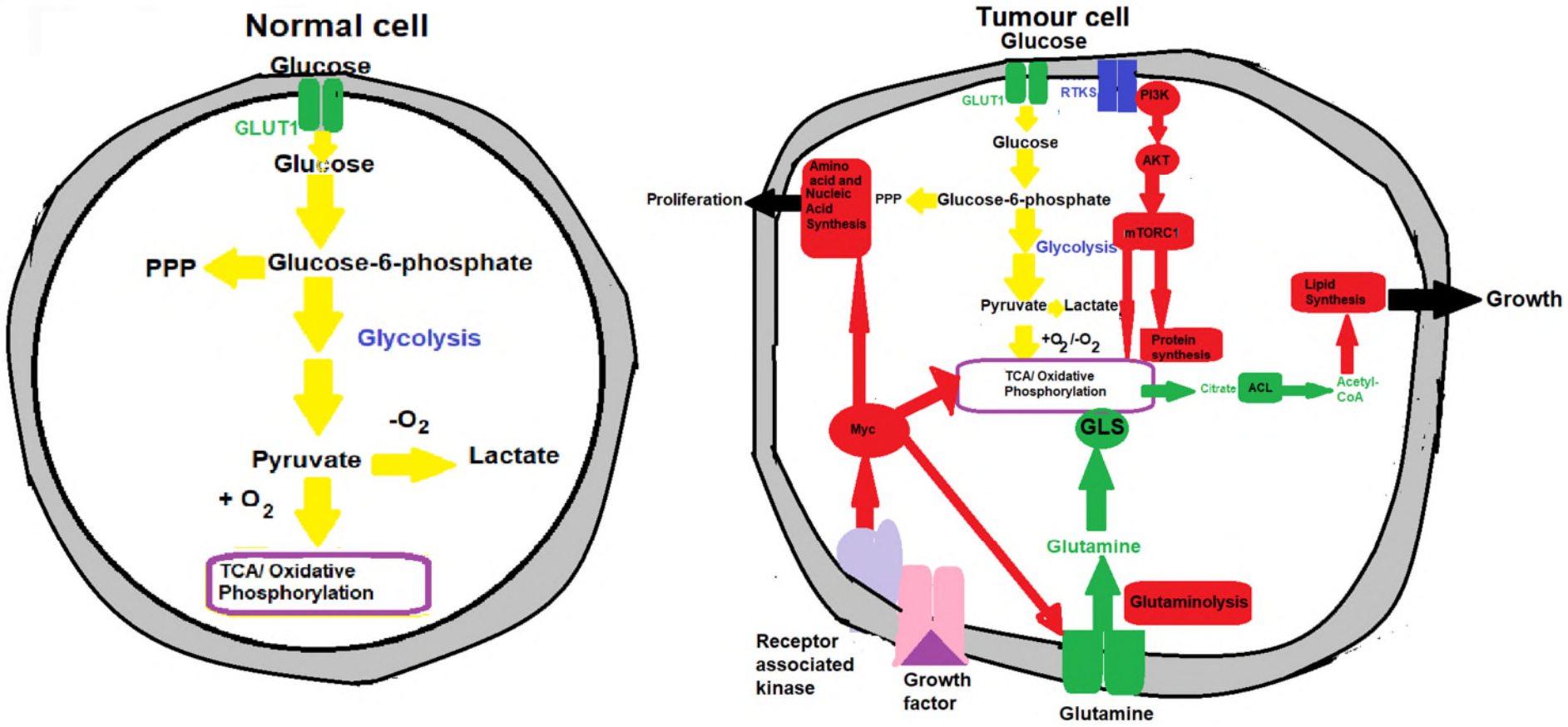

Figure 3: Metabolic reprogramming in cancer (Adapted from: Ward and Thompson, 2012)

Dysregulated metabolism caused by tumours are characterized by elevated glycolysis, increased oxidative phosphorylation, PPP, glutaminolysis, increased nucleic and amino acid production to provide energy and metabolites required for tumours to develop.

The pentose phosphate pathway (PPP) comprises of two mechanisms: oxidative and non-oxidative. In the oxidative pathway, the glycolytic intermediate glucose-6-phosphate is converted to ribulose-5-phosphate to generate the cofactor nicotinamide adenine dinucleotide phosphate (NADPH). NADPH is crucial for detoxification, protection from oxidative stress induced by the cytotoxicity of the anti-cancer drugs, biosynthetic reactions and the production of glutathione (Kalyanaraman, 2017; Phan *et al*., 2014). Ribose-5-phosphate is required for nucleotide synthesis. The non-oxidative PPP pathway produced glyceraldehyde-3-phosphate and fructose-6-phosphate (Jonas *et al*., 1992). PPP has a significant impact on tumour progression predominantly chemotherapeutic resistance, proliferation, invasion, apoptosis and metastasis which aligns it as a therapeutic target by effectively inhibiting the metabolic enzymes to eliminate tumour cells with minimal cellular damage to the normal cells (Cazzaniga and Bonanni, 2015; Phan *et al*., 2014).

Moreover, oxygen plays a significant role in regulating energy metabolism and the glyoxalase system where hypoxia is a phenomenon that occurs in most malignant tumours. Hypoxia is defined as the non-physiological level of oxygen caused by an imbalance between the supply and consumption of oxygen. There are three states of oxygen: normoxia (also known as physoxia), physiological hypoxia and pathological hypoxia (Aoife *et al*., 2003; Muz *et al*., 2015). Normoxia is defined as the normal oxygen concentration in healthy tissues, which varies widely between the organs due to diversified blood vessel network and metabolic activity. It ranges in human tissues between *ca.* 9.5 % O_2 in the renal cortex (partial pressure of oxygen pO_2 72 mmHg) to 4.6% O_2 in the brain (pO_2 35 mmHg). Pathological hypoxia is defined as 1% (8 mmHg) and the homeostatic mechanisms do not respond effectively to the oxygen levels that decline. For instance, ischaemia and related hypoxia can occur acutely (e.g. stroke) or chronically – for examples, as occurs in some tissues in (diabetes). In tumours, pathological hypoxia is a microenvironment factor that increases the propagation and survival of the tumour (Durand, 1991; Giaccia, 1996; Muz *et al*., 2015).

It has been hypothesised that hypoxia increases tumour growth by elevating the flux of MG formation via anaerobic glycolysis (Eales *et al,* 2016; Hu *et al*., 2003; Muz *et al.* 2015; Rabbani *et al*., 2017; Shafie *et al.,* 2016; Kumagai *et*

al., 2008). The glycolytic response is enhanced by the overexpression of GLUT-1 and hexokinase that increases glucose uptake (Semenza *et al.*, 1994; Semenza *et al.*, 1996a; Semenza *et al.*, 1996b). This enhances the ability of tumour cells to catabolize glucose, increase cell growth via the synthesis of their precursors and maintain the production of ATP and induce chemotherapy resistance under low oxygen tension conditions (Semenza *et al.*, 1994; Semenza *et al.*, 1996a; Semenza *et al.*, 1996b).

Other features of hypoxia include the ability to switch to glycolysis for energy supply by altering cell metabolism identified by Warburg, preventing apoptosis and upregulation of growth factors and proteins associated with invasion such as urokinase-type plasminogen activator (Aiofe *et al.*, 2003; Czekay *et al*., 2003; Krishnamachary *et al*., 2003; Warburg, 1956). The growth factors that are stimulated by hypoxia are epidermal grow factor (EGF), insulin-like growth factor-2 (IGF-2); platelet-derived growth factor-B (PDGF-B) and transforming growth factor-beta (TGF-β) (Koong *et al*., 2000). Moreover, hypoxia downregulates adhesion molecules to facilitate tumour cell attachment and can cause other hallmarks of cancer such as metastasis where there is attainment of epithelial-to-mesenchymal transition (EMT) phenotype causing cell mobility and metastasis (Azad *et al*., 2008; Mimeault *et al*., 2012; Muz *et al*., 2014; Muz *et al*., 2015).

Tumour hypoxia is a characteristic feature that occurs in solid tumours due to an insufficient supply of oxygen caused by exponential cellular proliferation and inadequate vascular supply (Aoife *et al*., 2003; Vaupel and Mayer 2007). Thus, it is an adverse prognostic indicator and deleterious factor associated with tumour malignant progression, aggressive phenotype and resistance to therapy by inducing cell quiescence (Aoife *et al*., 2003; McKeown, 2014; Vaupel and Mayer, 2007). Tumour hypoxia may impair disease-free survival for patients with cervical cancer, soft tissue sarcomas whereas in head and neck cancer it is a prognostic indicator for survival (Vaupel and Mayer, 2007). This has improved the use of endogenous markers such as hypoxia-related proteins HIF-1 alpha, GLUT-1 and exogenous bio-reductive drugs had significance for the patient outcome (Vaupel and Mayer, 2007). It also increases the risk of metastasis and mortality rate in breast cancer (Semenza, 2016)

1.1.2 Epidemiology of cancers

The prevalence of cancer increases every year and there was an incidence of 303,135 cases in 2016 where lung (12.7%), breast (15.2%), prostate (13.4%) and bowel cancers (15.3%) account for more than 50% of the cases of all ages in total (Office for National Statistics, 2018). This excludes the number of patients with non-melanoma skin cancers (Office for National Statistics, 2018). It is projected that the number of cancer cases is *ca.* 243,690 and 270,261 for females and males respectively in 2035 where breast and prostate cancer will be the most prevalent (Smittenaar *et al*., 2016). In addition, it is projected that *ca.* 95,961 females and 116,585 males will die in 2035 (Smittenaar *et al*., 2016). The increased burden of cancer cases and mortality rates stresses the importance of identifying risk factors.

1.1.3 Risk factors of cancers

Current epidemiological evidence suggests that lifestyle factors play a pivotal role in increasing the risk of cancer and can also significantly decrease its burden (Curry *et al*., 2003). Fifty percent of patients with the most prevalent tumours: lung, breast, colorectal and prostate cancers can be treated for modifiable risk factors (Ezzati *et al*, 2002). Table 1 presents a summary of modifiable risk factors tumours. People who are overweight are at risk of several tumours of the glands, gastrointestinal tract, brain, gynaecological, endocrine and the blood. For instance, breast (post-menopausal, liver, meningioma, ovary, thyroid and multiple myeloma (Calle *et al.*, 2003; Fedewa *et al.* 2017). It has been reported that obesity accounts for 14% and 20% of the mortality rates caused by tumours in men and women respectively (Calle *et al*. 2003).

Table 1: Preventative measures of modifiable risk factors for various cancers (Adapted from: Stein and Colditz, 2004).

Tumour	Avoid tobacco use	Physical activity	Healthy, balanced diet	Limit alcohol intake	Limit sexual activity	Avoid sun exposure	Taking screening tests	Maintain a healthy weight
Bladder	X		X					
Breast		X	X	X			X	X
Cervical	X				X		X	
Colorectal	X	X	X	X			X	X
Throat	X		X	X				X
Kidney	X							X
Lung	X		X					
Oral	X		X	X		X		
Pancreatic	X		X					
Prostate			X				X	
Skin						X		
Stomach	X		X					
Uterus								X

Another modifiable risk factor is physical activity, it reduces the risk of many types of tumours: liver, colorectal, breast, lung, prostate, oesophageal and kidneys by performing a moderate exercise for 30 minutes for most days of the week (Stein and Colditz, 2004; Pate *et al*., 1995; Fedewa *et al.*, 2017; Giovannucci *et al*., 1996; World Cancer Research Fund and American Institute for Cancer Research, 2007). It is estimated that physical activity decreases the risk of colon cancer by 50% due to the modification of the bile acid metabolism, decreasing the gastrointestinal transit time and less contact with potential carcinogens (Colditz *et al*, 1997; Martinez *et al*., 1999; McTiernan *et al.*, 1998). Increased physical activity also decreases the circulating concentrations of growth factors and hormones such as insulin and prostaglandins reducing the risk of diabetes and improving immunity respectively (McKeown-Eyssen, 1994; Martinez *et al*., 1999).

Other strategies of cancer prevention include reducing tobacco use which includes cigarettes, cigars, electric and avoiding smoking environment (second-hand smoke) that accounts for 5 million deaths annually (Ezzati *et al.*, 2002; Doll *et al.*, 1994). It contributes to 30% of all tumours and is the major cause of 90% of cases related to lung cancer (Ezzati *et al*., 2002). The pivotal role of tobacco in developing carcinogenesis and cancer progression demonstrates its significance in developing preventative measures. For instance, it delivers carcinogens to the site, causing inflammation and it affects the physical protective barriers to the human body (Ezzati *et al.*, 2002). Hecht (1999) reported that carcinogens, nitrosamines and polycyclic aromatic hydrocarbons that reside in the tobacco smoke were metabolized by secretion and/or linking with the DNA to form adducts. DNA adducts lead to apoptosis and the miscoding mutations of vital genes such as p53 caused genetic stability (Minna *et al.*, 2002). This consequently causes further damage and induces tumour development.

A number of studies focused on identifying the interconnection between diet and cancer (Feskanich *et al.*, 2000). Eating a balanced diet composed of fruits, vegetables, fish, poultry and whole grain reduces the risk of cancers of the mouth, oesophageal, stomach, larynx and the oestrogen receptor-negative breast tumours (Colditz *et al.*, 1996; Curry *et al*., 1993; World Cancer Research Fund and American Institute for Cancer Research, 2007; Fedewa *et al.* 2017).

They contain minerals, vitamins and fibre. Ezzati *et al.* (2002) reported 2.7 million deaths annually are associated with inadequate dietary intake causing a global burden. In addition, consuming less red meat such as veal, beef and lamb increases the intake of dietary fibres and this decreases the risk of pancreatic and colorectal cancer (Fedewa *et al*., 2017). This is due to the production of carcinogens whilst cooking of animal proteins at elevated temperatures. Other studies reported it is due to the elevated concentration of animal fat. Giovannucci (1999) conducted a study where he investigated the connection between prostate cancer and tomatoes. He discovered tomatoes reduced the risk of prostate cancers by 40-50% in men and it has been reported that carotenoid lycopene is the causative effect of this protection.

The association of alcohol with tumour development can be initially described by the mortality rates where there are more than 1.8 million deaths (Ezzati *et al*., 2002). Thun *et al*., reported that despite alcohol being a risk factor for the increase in mortality rates associated with cancer, moderate consumption of alcohol reduces the risk of diabetes and cardiovascular disease (Thun *et al*., 1997). It is the primary cause of oral, oesophageal, colorectal and breast cancer (Fedewa *et al*., 2017; Stein and Colditz, 2004). There is also evidence of its association with liver and pancreatic cancer (Fedewa *et al.*, 2017). Alcohol increases the risk of cancer due to three major respects: transports carcinogens to the basal layer of the mucosa, it acts as a solvent permitting carcinogen to penetrate the mucosa and increases cell turnover (Stein and Colditz, 2004).

Moreover, the enzyme alcohol dehydrogenase (ADH) metabolises alcohol to acetaldehyde (Sapkota and Wyatt, 2015). After when cytochrome p450 2E1 (CYP2E1) is stimulated, it produces reactive oxygen species (ROS), for instance, hydrogen peroxide, superoxide and hydrogen radicals (Sapkota and Wyatt, 2015). This predominantly occurs during chronic alcohol consumption. This facilitates the peroxidation of lipids and the production of 4-hydroxynonenal (4-HNE) and malondialdehyde (MDA) forms hybrid, DNA and protein adducts (Sapkota and Wyatt, 2015). Heavy consumption of alcohol has also been associated with liver and other conditions such as hypertension, complications during pregnancies and addiction (Stein and Colditz, 2004). A combination of tobacco smoking and alcohol increases the risk of cancer significantly (Fedewa *et al*., 2017).

Preventative measures include educating the public about the benefits and risks of alcohol use.

Another behavioural factor is ultraviolet radiation that increases the risk of tumours of the lip and different forms of skin cancers (Stein and Colditz, 2004). This includes malignant melanoma, basal cell carcinoma and squamous cell carcinoma. However, these are highly curable (Fedewa *et al*., 2017). Majority of skin cancer-related deaths are linked to invasive melanoma and a recent study estimated that *ca.* 230,000 cases will be prevented between the year periods 2020 - 2030 if an inclusive cancer prevention programme will be applied (Fedewa *et al.*, 2017). Current preventative measures include limited sun exposure, sunscreen, protective clothing such as hats and sunglasses decreases risk (Fedewa *et al.*, 2017). The use of fair skin colour and family history is insufficient data to identify those that are at risk of disease (English and Armstrong, 1988).

Several infectious agents have been associated with causing tumorigenesis. For instance, *Helicobacter pylori* cause gastric lymphoma and cancer. More than half of the global population is infected with this bacterium but are unaware (Fedewa *et al.*, 2017). Human immunodeficiency virus (HIV) increases the risk of cancers of the cervix, Kaposi sarcoma and non-Hodgkin lymphoma (Fedewa *et al.*, 2017). It is estimated 2.9 million deaths annually are caused by unsafe sexual acts due to the transmission of the virus and other oncogenic viruses (Ezzati *et al*, 2002). There is evidence that a combination of causes increases the rate of cancer. For instance, people who smoke and have HIV have a higher rate of immunosuppression and lung cancer (Fedewa *et al.*, 2017; Schiffman *et al.*, 2007).

Infection with human papillomavirus (HPV) accounts for cervix, anal, vulvar, vaginal and penile tumours (Fedewa *et al.*, 2017; Morrison *et al.* 1997). There is also a risk of other cancers: Chronic infections with Hepatitis B virus (HBV) and Hepatitis C (HCV) causes liver cancer and increases the risk for non-Hodgkin lymphoma (Fedewa *et al.* 2017). Preventative measures to lower the risk of infectious agents being transmitted include the use of vaccines, needle exchange programmes for drug users, educating the public on safer sexual

practices, the use of treatment for prophylactic infections and screening for blood donors (Koutsky *et al*., 2002).

Screening for breast, colorectal and cervical cancer and in some cases of prostate cancer reduce the burden of cancer due to early detection and effective treatment of pre-malignancy and malignancy cases reducing mortality rates (Fedewa *et al*., 2016); Hoffmann *et al*., 2009; Levin *et al*., 2008; Paci, 2012; Schiffman *et al*., 2007; Schröder *et al*., 2009; Stein and Colditz, 2004; Taplin *et al*., 2004). Some medications have protective effects of cancers, for instance, oral contraceptive pills and non-steroidal anti-inflammatory drugs such as aspirin decreases the risk of ovarian cancers and colorectal cancer. Conversely, the use of oestrogen and postmenopausal hormone therapy increases the incidence of endometrial and breast cancer respectively (Stein and Colditz, 2004).

1.1.4 Treatment of cancer using chemotherapy

Chemotherapy is one of the four types of cancer therapy, other treatments being surgery, radiotherapy, and immunotherapy (Luqmani, 2005; Kartal-Yandim *et al*., 2016). This project focuses on the resistance to chemotherapy but in order to understand the various mechanisms, an overview of the main types of chemotherapeutic treatments is required. The dual role of chemotherapy is to kill cancer cells and have systemic effects (Huang *et al*., 2017). Chemotherapeutic agents can be utilized in several ways: alone, with other agents, concurrent with radiotherapy and as targeted therapy (Lundqvist *et al.*, 2015).

The use of chemotherapy was initiated in the 20th century with attempts to develop chemicals that may affect the disease (De Vita and Chu, 2008). In 1955, the Cancer Chemotherapy National Service Centre was established in the USA to oversee an anticancer drug development programme. The benefits of having a combinatorial approach in chemotherapy were recognised after treating acute child leukaemia in the 1960s and 1970s to maximise potency and efficacy (De Vita and Chu, 2008). During this period, chemotherapy improved markedly to provide effective treatment for some solid tumours such as germ cell, childhood malignancy and haematological malignancies (Tsuruo, 2003). For instance, the capacity for chemotherapeutic drugs to treat advanced Hodgkin's disease was discovered (De Vita and Chu, 2008). Despite this success, the effectiveness of

chemotherapy is limited by MDR and adverse side effects (Tsuruo, 2003; Tsuruo *et al.*, 2003). Chemotherapy has a small therapeutic window in comparison to drugs of other forms. There is the possibility of serious clinical adverse effects and hence the optimum and safe dose of an anti-cancer drug for a patient is difficult to achieve (Lundqvist *et al.*, 2015).

There are several types of goals for chemotherapeutic treatment that need to be considered. For a curative intention, adverse effects are accepted if the probability rate for the patient to be cured is high. However, if the aim of the treatment is to increase the timespan for survival, the balance between the advantages of treatment and its adverse effects are carefully considered and optimised (Lundqvist *et al.*, 2015). If treatment has a dominant palliative aim to alleviate symptoms, there is a small likelihood of adverse effects. Tumour cells pass through various phases of the cell cycle and are chemosensitive apart from the G_0 phase; resting state (Lundqvist *et al.*, 2015). There is a prolonged survival in patients who progress slowly and live for a long period of time, their tumours become less chemosensitive because most cells are in the resting phase at each treatment cycle.

There are several classes of chemotherapy, based on modes of action. Anti-cancer drugs typically target proliferating cells that are more responsive to classes of drugs such as DNA alkylating and intercalating agents, topoisomerase inhibitors, mitotic inhibitors, and anti-metabolites (Luqmani, 2005).

1.1.4.1 DNA alkylating agents

DNA alkylating agents have been utilized for cancer treatment for over 60 years (Ralhan and Kaur, 2007). They directly act on DNA forming crosslinks with the N-7-guanine residues. This causes interstrand and intrastand DNA strand breaks (DSB) leading to irregular base pairing that prevents cell division and cell apoptosis (Ralhan and Kaur, 2007; Thirumaran *et al*., 2007). Figure 4 illustrates the mechanism of action of alkylating agents. Methyl-guanine-DNA methyltransferase (MGMT) repairs genetic changes and decreases the activity of the anti-cancer drug (Martinez-Cardus *et al*., 2015). Their clinical efficacy is limited due to drug resistance and systemic toxicity. There is evidence that the potency of alkylating agents increases in combination with other anti-cancer

agents. For instance, inhibitors of topoisomerase, phosphatases and other DNA repair enzymes (Ralhan and Kaur, 2007). Anti-vascular agents and multi-drug resistance proteins also improve efficacy. Novel developments are in progress to enhance the sensitivity of cancer cells to DNA alkylating agents. For instance, naphthalamides and selective androgen receptor are amongst the examples of novel modulators (Ralhan and Kaur, 2007).

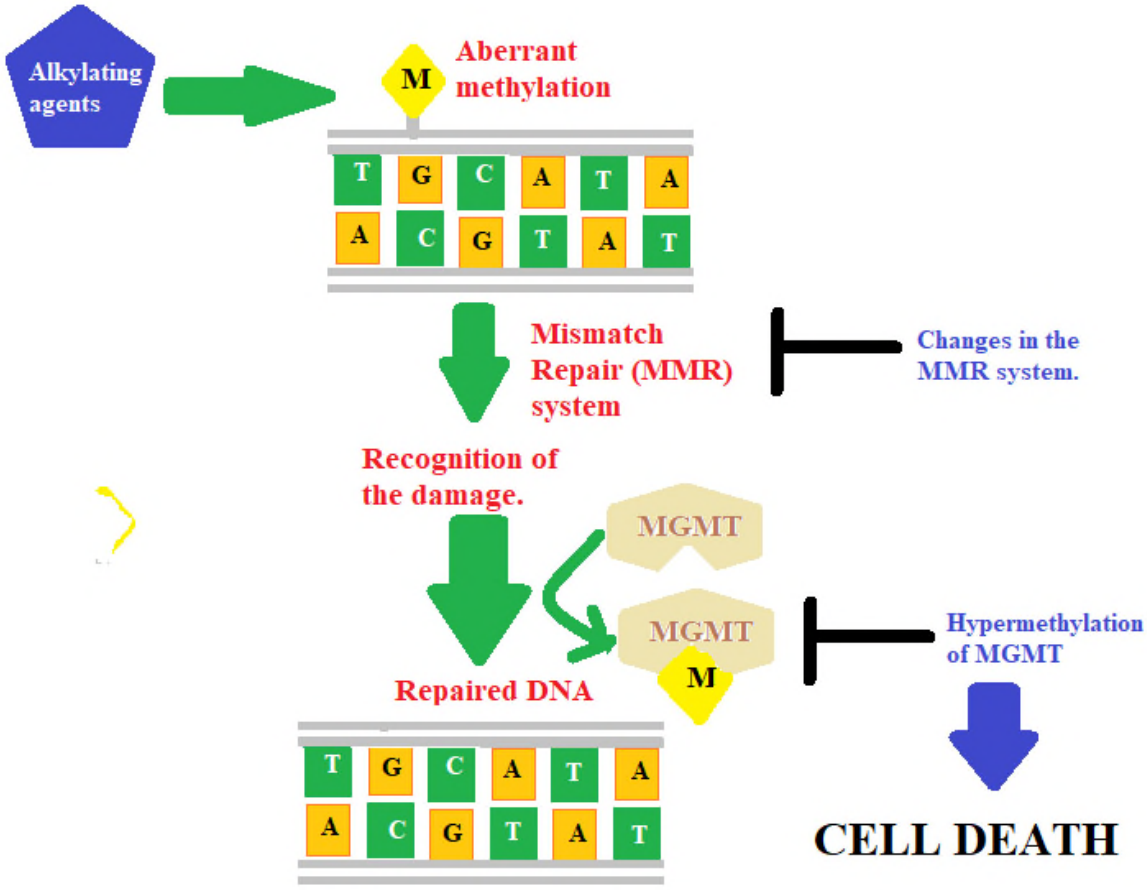

Figure 4: Mechanism of action of DNA alkylating agents (Adapted from: Martinez-Cardus *et al.*, 2015).

DNA alkylating agents cause DNA strand breaks leading to irregular base pairing that prevents proliferation and increase cell apoptosis.

The DNA alkylating agents employed in this study are Mechlorethamine Hydrochloride, Mitomycin C, and cisplatin. Mechlorethamine is a nitrogen mustard derivative that is utilized in palliative treatment for some tumours (Dobson *et al.*, 2008; Newton, 2012; Thirumaran *et al.*, 2007). It has a wide clinical anti-tumour spectrum with efficacy in various types of tumours. For

instance, Hodgkin lymphoma, chronic lymphocytic leukaemia, bronchogenic carcinoma and chronic myelogenous leukaemia and other lymphomas (Newton, 2006; Thirumaran *et al*., 2007). It has also been used for the treatment of neurological tumours: for instance, gliomas, however, it is associated with causing seizures and cerebral edema (Newton, 2006; Newton, 2012). At high doses, it is utilized for the preparation of bone marrow transplantation (Newton, 2012). Additionally, mechlorethamine is used in combination therapy with vincristine and prednisone for the treatment of Hodgkin's lymphoma (Kwok *et al*., 2017). It is administered intravenously and has limited stability and short half-life (Kwok *et al*., 2017).

Mitomycin C is a bio-reductive alkylating agent and anti-tumour antibiotic that is predominantly stimulated under anaerobic conditions (Verweij and Pinedo, 1990). It is utilized for gastric cancer and pancreatic adenocarcinoma. It has been utilized for the treatment of advanced breast cancer where there was a 20-30% response rate (Godfrey, 1988). However, an adverse effect of utilizing mitomycin C is an increase in haematological toxicity but this has been reduced when low doses are utilized (Godfrey, 1988).

The most effective chemotherapeutic agent for solid tumours is cis-diamminedichloroplatinum (cisplatin) (Cohen and Lippard, 2001). It is a crystalline powder whose colour varies between white, yellow, and orange. The metal compound is soluble in N, N-dimethylformamide (DMF) and is slightly water-soluble (Dasari and Tchounwou, 2014). It is utilized for a variety of neoplasms, for instance, sarcomas, carcinomas breast, lung, kidney, cancers of the ovaries and bladder (Dasari and Tchounwou, 2014).

Cisplatin is composed of a double-charged platinum ion bordered by four ligands (Goodsell, 2006). There are two types of ligands: amine ligands on the left create a stronger interaction with the platinum ion (Dasari and Tchounwou, 2014). The chloride ions form a bond with DNA bases (Goodsell, 2006). The platinum-based compound that induces cell cycle arrest and apoptosis by producing DNA adducts - Figure 21 (Cohen and Lippard, 2001). The two predominant adducts formed are 1,2-intrastrand d(GpG) adducts 1,2-intrastrand d(ApG) adducts in a 90% to 10% proportion. Other adducts such as 1,3-intrastrand d(GpXpG) adducts

are formed increasing the toxicity of cisplatin. It also influences the DNA repair mechanisms, crosslinks with purine bases on DNA and stimulates the intrinsic and extrinsic apoptotic mechanisms, down-regulating anti-apoptotic proteins and proto-oncogenes (Rosenberg and Van Camp, 1970; Roberts and Fraval, 1978; Dasari and Tchounwou, 2014; Kelland, 2007; Ozben, 2007).

Cisplatin produces ROS and lipid peroxidation which induces oxidative stress damaging cellular proteins, DNA, and lipids (Saad *et al*., 2004). The extrinsic apoptotic pathway produces ROS via the activated Fas ligand, a type 2 transmembrane protein that stimulates the downstream signalling events leading to apoptosis (Gupta *et al.* 2012). On the other hand, in the intrinsic apoptotic pathway, ROS aids in the release of cytochrome c by stimulating B-cell lymphoma 2 (Bcl-2) and Bcl-xL proteins and preventing the activation of Bcl-2-associated X protein (Martindale and Holbrook, 2002).

There are also several kinases involved in cell signalling pathways influenced by cisplatin. Protein kinase C (PKC) plays a pivotal role in inducing signal transduction and the regulation of cells (Basu and Sivaprasad, 2007; Dasari and Tchounwou, 2014). Cisplatin stimulates extracellular signal-regulated kinase (ERK) via the mitogen-activated protein kinases (MAPK) causing cell cycle arrest and DNA repair via p53 (Chang and Karin, 2001). The stereoisomers of cisplatin, cis and trans, activates c-Jun N-terminal kinase or stress-activated protein kinase (JNK) in response to DNA damage and apoptosis (Johns *et al*., 2007). The p38 MAPK pathway also regulates cisplatin-induced apoptosis (Cuadrado *et al*., 2007).

The cofactor reduced glutathione (GSH) plays a significant role in monitoring the inner mitochondrial permeability and enzymatic function in order to maintain the sulfhydryl (SH) groups in the reduced state. When the SH group cannot be maintained, they become deactivated. Amongst the toxicities stimulated by cisplatin is nephrotoxicity where there is a reduced intracellular concentration of GSH and SH-groups. NADH helps to maintain the reduced state of the SH groups. The depletion of NADH and GSH prevents the enzymatic activity of several dehydrogenases (Aggarwal, 1998). This induces oxidative phosphorylation, increases the synthesis of hydroxyl radicals and in turn oxidative

stress that degrades the integrity of the membranes (Dasari and Tchounwou, 2014).

Resistance to cisplatin develops intrinsically and after administration (Kartalou and Essigmann, 2001; Rabik and Dolan, 2007). This has been observed in lung, colorectal and ovarian cancers. Another form of resistance is the association of cisplatin to GSH which inactivates the platinum compound and prevents the formation of cisplatin-adducts (Huang *et al*., 2017). The increased expression of glutathione S-transferase (GST-π) isoenzyme has been linked with intrinsic resistance to cisplatin (Rowinsky *et al*. 1993).

In response to resistance and relapse from cisplatin treatment, other platinum compounds have been developed such as bile acid derivatives where it increases cytotoxicity and overcame cisplatin resistance (Rodriguez-Fernandez *et al*., 2009). Carboplatin is another platinum compound that is utilized for the treatment of the lung, head, and ovaries. In comparison to cisplatin, it has slow DNA-binding kinetics and low reactivity that reduces side effects such as nephrotoxicity (Go and Adjei, 1999; Natarajan *et al*., 1999). However, its limitation is suppressing the blood cells and platelets (Canetta *et al*., 1985). Adjuvant therapy is another mechanism in overcoming resistance. There is evidence that a combination of paclitaxel and cisplatin was effective against ovarian cancer (McGuire *et al*., 1989; Einzig *et al*., 1992). Doxorubicin and cisplatin have also been effective against carcinomas of the salivary gland (Dreyfuss *et al*., 1987).

1.1.4.2 Topoisomerase inhibitors

Topoisomerases are ubiquitous enzymes found in archaebacteria, eubacteria and eukaryotes. Mammalian cells encode six topoisomerases whereas prokaryotes comprise of 4 topoisomerases whose function is to regulate DNA supercoiling (torsional tension) which is vital for the processes of transcription and replication (Pommier, 2013). Positive supercoiling causes DNA tightening and inhibits strand separation evading the polymerases from performing its function. On the other hand, negative supercoiling extends the DNA strand separation facilitating the synthesis of irregular nucleic acid structures such as guanosine quartets, z-DNA and intramolecular hairpins and causing dysfunction of the RNA polymerases by stalling R-loops (Pommier, 2013; Ewesuedo and Retain 1997). This leads to the formation of DNA double-strand breaks (Gellert *et al*., 1976).

There are two types of topoisomerases. Topoisomerase I is a monomeric and highly conserved enzyme whose catalytic function is to cleave one strand of DNA. Topoisomerase II has two forms: heterotetrameric (bacteria) and homodimeric (humans) whose function is to cleave the duplex DNA strands and rest the supercoiled DNA preventing helical constraints (Denny and Baguley, 2003; Gellert *et al*., 1976; Lodish, 2000; Pommier, 2013; Thakur, 2011).

Topoisomerases eliminate supercoiling by various mechanisms, Type 1A enzyme transits one strand from the same DNA molecule through a transient break in the single or double strand formed by the topoisomerase in another duplex (Ewesuedo and Retain, 1997; Thakur 2011). Type 2A enzyme utilizes a duplex from the same DNA molecule using the same method that enters breakage of both strands. Both Type 1A and IIA undergo DNA cleavage by attaching their tyrosine residue to the 5’ end of the DNA whereas the 3’ end are bound tightly allowing the DNA to pass through. Type 1B generates 3’ phosphotyrosine bonds and allows the strand that is broken to rotate that is regulated around the 5’ end of the other strand (Ewesuedo and Retain, 1997; Husain *et al.,* 1994). Through the process of transesterification, topoisomerases share a common characteristic where the non-homologous families they cleave DNA utilizing the tyrosine as a nucleophile attacking the phosphodiester bond and re-ligate the backbone of the

double-stranded DNA molecule (Pommier, 2013; Wang 1971; Wang 1996). However, they differ in the form of DNA adduct produced.

Poly (ADP-ribose) polymerases (PARP) are activated by topoisomerase 1 in response to DNA damage but this is dependent on the processes of replication and transcription (Pommier, 2013). There is high synergism between the inhibitors of PARP and topoisomerase 1 and low synergism with topoisomerase 2. There is much interest directed to using small molecule inhibitors of DNA repair enzymes. It has been reported that PARP inhibitors increase sensitivity to camptothecin delaying DNA repair (Smith *et al*, 2005; Zhang *et al*., 2014). Several trials have been conducted for determining the combined therapeutic effect of radiotherapy and cytotoxic drugs (El-Khamisy *et al*., 2003).

Topoisomerase 1 play a significant role in human tumours especially in colorectal cancer where their increased expression of topoisomerase 1 mRNA and protein was observed (Husain *et al*., 1994). It significantly contributes to tumorigenesis, (Li and Liu, 2016). Paradoxically, the accumulation of topoisomerases induces cell death and is the mechanism of toxicity. However, Liu (1990) revealed that human cells naturally suppress the enzymatic activity of topoisomerases through small ubiquitin-related modifier (SUMO) modifications at the residues of lysine: K436 and K391. This decreases DNA damage induced by topoisomerase 1. These SUMOylations cause genetic instability, mutagenesis, and cancer development. In addition, mismatch repair proteins (MMR) account for 5% of colorectal cancers caused by a germline mutation of MMR. It has been hypothesised that MMR modulates response to topoisomerase 1 (Jacob *et al*, 2001). The topoisomerase I inhibitor utilized in this PhD project is camptothecin.

Camptothecin is a quinoline alkaloid that is utilized to treat various cancers (Venditto and Simanek, 2010). It was discovered by Wall and Wani (1996) who extracted it from the bark *'Camptotheca acuminata'* (Nyssaceae) However, the disadvantages of utilizing the anti-cancer drug is the deprived stability and solubility at physiological states (Venditto and Simanek, 2010). A year later, they discovered paclitaxel, a broad-spectrum chemotherapeutic agent that showed promise. Novel camptothecin derivatives have been developed to reduce the limitations and increase bioavailability (Venditto and Simanek, 2010).

Camptothecin has two forms: when active it is a lactone whereas when it is inactive it is a carboxylate. Lactone associates with the DNA-topoisomerase 1 complex preventing re-ligation of the DNA strands; this causes apoptosis. Preclinical studies have demonstrated its anti-tumour effect in several experimental murine tumour models in *in vivo* studies and human tumour xenografts of the breast, lung, malignant melanoma and colon (Ewesuedo and Ratain, 1997). It is toxic to cells in the S-phase causing growth arrest in G-2 phase and stimulates chromosomal DNA fragmentation by preventing DNA of chromosomal DNA by inhibiting DNA synthesis through strand scission (Venditto and Simanek, 2010).

Another functional role of camptothecin is the stimulation of the ribonucleic acid (RNA) synthesis of the dihydrofolate reductase (DHFR) gene. It caused a high accumulation of RNA polymerases in the 5' end of the DHFR gene preventing elongation (Ljungman *et al.,* 1996). Its pentacyclic ring structure facilitates in its anti-tumour activity predominantly the D and E rings and is most effective in high-proliferating cells (Ljungman *et al.,* 1996). The water-soluble derivatives of camptothecin, topotecan and irinotecan, were developed by the modification of the A and B rings (Venditto and Simanek, 2010; Dancey and Eisenhauer, 1996).

Topoisomerase II is the target for antineoplastic agents (Larsen *et al*, 2003). There are two broad types of inhibitors of topoisomerase II: topoisomerase II poisons and catalytic inhibitors (Bower *et al*., 2010; Larsen *et al*., 2003; Andoh and Ishida 1998; Nitiss, 2009). Topoisomerase II poisons specifically stabilize the cleavage complex. Examples include clinically active chemotherapeutic agents such as doxorubicin and etoposide (Nitiss, 2009; Nitiss and Nitiss 2014). This increases the number of covalent complexes between topoisomerase II and DNA. Catalytic inhibitors act on other areas of the catalytic cycle to kill cancer cells such as preventing the binding of ATP (novobiocin) and interference between the linkage of cleaving complex (merbarone) that can affect other targets (Larsen *et al*., 2003; Nittis, 2009).

Other modes of action of topoisomerase II inhibitors blocks the catalytic cycle causing DNA damage which subsequently affects replication and

transcription (Serre and Duguet, 2003; Andersen *et al*., 1989; Nittis, 2009). Several compounds prevent the enzymatic activity of topoisomerase II and DNA cleavage. An example is bisdioxopiperazine which induces non-competitive inhibition of the ATPase activity (Jain, 2017; Nittis, 2009). Several novel secondary metabolites are produced by plants to prevent adverse side effects. For instance, polyphenols, alkaloids and quinones have been used to improve the treatment of cancer by preventing the enzymatic activity of DNA topoisomerases (Malpathak and Baikar, 2010).

Cancer researchers have a major interest in topoisomerase II inhibitors particularly etoposide and doxorubicin that mediate DNA damage and their clinical activities in various human tumours in the initiation and curative stages (McClendon and Osheroff, 2007; Nittis, 2009). The aim is to improve further understanding of their mechanism to maximise the efficacy of anti-cancer drugs whilst minimizing risks of secondary malignancies (McClendon and Osheroff, 2007).

One of the topoisomerase II inhibitors utilised in this study is doxorubicin that has been utilized to treat solely and in combination with other drugs for various cancers. It is the first line of treatment for cancers of the breast, thyroid, bladder, and blood malignancies (Watt and Hickson, 1994). Besides their inhibitory effect on topoisomerase II activity, it intercalates DNA and produces ROS (Watt and Hickson, 1994). Another way in how doxorubicin exerts its anti-tumour effects is through the cleavage of the transcription factor CREB 3L1 (Patel and Kaufmann, 2012). Cardiotoxicity is one of the adverse effects of doxorubicin causing nuclear and mitochondrial damage (Watt and Hickson, 1994).

However, there have been recent developments on doxorubicin where a liposomal encapsulated version is available for treatment of patients with Kaposi sarcoma, multiple myeloma, and advanced stages of ovarian and breast tumours. It increases anti-tumour activity and plasma circulation time decreasing the risk of cardiomyopathy (Kwok *et al.* 2017). Novel findings discovered several *de novo* and acquired mechanisms of resistance that contribute to decreased sensitivity of doxorubicin (Lovitt *et al*., 2018).

Etoposide is another topoisomerase inhibitor utilised in this study. It is a semi-synthetic demethylepipodophyllotoxin derivative utilized for a broad spectrum of solid tumours such as tumours of the endocrine, germline, small cell lung cancer, neuroblastomas, and sarcomas (Baldwin and Osheroff, 2005; Watt and Hickson, 1994). It has been used for patients with testicular cancer who had previous surgery, radiation therapy or the former chemotherapeutic agents did not improve his or her condition. Moreover, etoposide has also been utilized as a part of a combination therapeutic strategy for breast cancer (Höffken, 1982; Nichols, 1992). In comparison to podophyllotoxins, it functions independently from tubulin. Another function of etoposide that differs from that of doxorubicin is the mechanism of trapping etoposides succeed in doing this to both topoisomerase 2 α and β to prevent the carcinogenesis of secondary leukaemia whereas doxorubicin targets solely topoisomerase II-β (Watt and Hickson, 1994).

1.1.4.3 Dihydrofolate reductase inhibitors

Methotrexate is another anti-tumour drug that is utilized in this project. It is a folate analogue that inhibits dihydrofolate reductase (DHFR), tetrahydrofolate (THF) and the production of pyrimidines and purines (Jolivet *et al*., 1983; Hagner and Joerger, 2010; Llado *et al*., 2009; Gracia-Cazana *et al.*, 2016, Keystone *et al*., 2017, Lima *et al*., 2014). Folates are essential in the *de novo* production of thymidylate, purines and pyrimidines that are critical for DNA in mammalian cells (Hagner and Joerger, 2010; Ndiaye *et al.*, 2010). They belong to a family of B9 vitamins and folic acid undergoes two consecutive steps of reduction mediated by DHFR: to dihydrofolate (DHF) followed by a further reduction to THF (Hagner and Joerger, 2010). The dietary form of folate is 5′-methyl-THF (5′-MTHF). MTHF is a cofactor for the conversion of homocysteine to methionine, catalysed by methionine synthase (Hagner and Joerger, 2010; Touroutoglou and Pazdur, 1995). The progressive addition of glutamates to the γ-carboxyl residues by the enzyme folylpolyglutamate synthetase (FPGS) to its main substrate THF produces folate polyglutamates (Hagner and Joerger, 2010).

Folate analogues were initially developed based upon the functional and molecular aspects of thymidylate synthase (TS) and folate (Touroutoglou and Pazdur, 1995; Schweitzer *et al*., 2010). It is also dependent on the activity of the

reduced folate carrier (RFC) proteins which normally function for cellular entry and polyglutamation by FPGS (Touroutoglou and Pazdur, 1995; Hagnet and Jorger, 2010). Methotrexate is utilized for the treatment of leukaemias, lymphomas and cancers of the lung, breast and head cancer (Hagner and Joerger, 2010; Lehman, 2002; Schweitzer *et al*., 2010; Touroutoglou and Pazdur, 1995).

1.1.4.4 Microtubule-targeting agent

Microtubule-targeting agents (MTA) affect microtubule dynamics by influencing the normal mechanism of the mitotic spindle formation and disassembly, causing cell cycle arrest and apoptosis (van Vuuren *et al*., 2015; Rohena and Mooberry, 2014; Mukhtar *et al*., 2014). Microtubules are highly dynamic, intracellular cytoskeleton framework and have vital cellular functions that are induced by the polymerization by α and β dimers at either side of the microtubules (Jordan *et al*. 2005; van Vuuren *et al*., 2015; Risinger *et al*., 2009; Risinger *et al*., 2011). They are involved in processes of growth, intracellular trafficking, motility, division and adapting to various conditions of the environment (Jordan *et al*. 2005; van Vuuren *et al*., 2015; Risinger *et al*., 2009; Risinger *et al*., 2011)

MTAs are used in the treatment of solid and haematopoietic tumours. They are anti-mitotic agents that reduce the rate of cell proliferation and act on the polymerization of the spindle (van Vuuren *et al*., 2015). Tubulin is the monomer of microtubules and MTAs associate with tubulin to induce its anti-cancer response (Yang and Horwitz 2017). MTAs are divided into two groups: microtubule-stabilizing agents activate polymerization of microtubules, stabilize, and increase the mass of the polymer (van Vuuren *et al*., 2016). An example of this is Paclitaxel which is utilized in this study. Microtubule destabilisers which prevents polymerization, reduces the rate of the transition between metaphase and anaphase by blocking mitosis and inducing apoptosis (Jordan *et al*. 2005; Dumontet and Jordan, 2010; Nolte *et al*., 2016; van Vuuren *et al*., 2016; Risinger *et al*., 2009; Risinger *et al*., 2011). An example is Vincristine utilized in this study.

Recent evidence emphasizes that stimulation of the mammalian target of rapamycin (mTOR) is dependent on the dynein-mediated transport. Thus, MTA

causes dysfunction of microtubules by preventing the activation of the AKT/mTOR signalling mechanism preventing cell proliferation (van Vuuren *et al*., 2015). This signifies the various mechanisms to induce mitotic arrest.

Toxicology reports emphasise that the paclitaxel concentration (> 10nM) prevents the proliferation of the endothelial cells (van Vuuren *et al*., 2015; Risinger *et al*., 2009; Risinger *et al*., 2011; Chang *et al*., 1993; Murphy *et al.*, 1993; Weaver, 2014). Paclitaxel stimulates the phosphorylation of various proteins that can stimulate survival mechanisms. For instance, Bcl-2, Cox-2 and Akt (van Vuuren *et al*., 2015). This consequently induces cell death. Several protein kinase enzymes are involved such as MAPK and p53. The stimulation of the apoptosome (caspase-9/Apaf-1/cytochrome c) in the mitochondrial apoptotic pathway leads to the activation of caspase-3 enzymes (Mekhail and Markman, 2002). However, Ofir *et al.* discovered that procaspase-9 is not activated following treatment with paclitaxel in *in vitro* studies: human leukaemia (e.g. HL-60), ovarian (e.g. SKOV3) and the breast cancer cell line (e.g. MCF-7) (Ofir *et al*., 2002). This emphasises that it is cell type specific. Alternatively, Lin *et al.* (2000) revealed that taxol-induced apoptosis is via ROS independent pathway. Combination therapy has proved effective especially in metastatic breast cancer. It is composed of cisplatin and platinum compound (Xu *et al.* 2010).

Vincristine is a plant alkaloid extracted from periwinkle that is utilized to treat acute lymphoblastic leukaemia and other lymphoid malignancies (Douer, 2016; Stengel *et al*., 2008). However, despite its capacity to be utilized in combined therapy and mechanism of action, it is prescribed to patients minimally due to the potential risk of experiencing neurotoxicity (Douer, 2016). Vincristine disrupts microtubule synthesis in the mitotic spindle causing cell arrest at metaphase. It also prevents replication and induces cell death (Douer, 2016). Other functions include interference with the synthesis of nucleic acids and proteins by prohibiting contact with glutamic acid (Douer, 2016). Microtubule disruptors such as vincristine cause growth arrest in G2/M phase by stimulating the G_2-M checkpoint (Bhat and Setaluri, 2007). This induces p53-independent apoptosis and cells can escape at this checkpoint. Vincristine can also stimulate the G1-S checkpoint leading to p53-dependent cell death (Bhat and Setaluri, 2007).

1.1.4.5 Resistance to Chemotherapy

Cancer chemotherapy is one of the treatment modalities for cancer which has effectively improved treatment for several solid tumours such as childhood malignancy, haematological malignancies, and germ cell tumours. Resistance to chemotherapy is, however, a major factor as to why patients who have refractory tumours become unresponsive to various cancer treatments and have high mortality rates (Holohan *et al*., 2013; Patel and Rothenberg, 1994; Baskar *et al*., 2012). Failure to respond to cancer chemotherapy is linked to multidrug resistance (MDR) and adverse side effects (Tsuruo, 2003; Tsuruo *et al*., 2003). This was found in the treatment of local, disseminated, and recurrent human tumours (Luqmani, 2005; Patel and Rothenberg, 1994). For instance, the resistance mechanisms to platinum-based chemotherapeutic agents are through several varied pathways (Liu, 2009). Several pharmacodynamic and pharmacokinetic causes of MDR have been discovered and addressed by countermeasures. This emphasises that the management of cancer remains to be a challenge.

MDR is a multifactorial phenomenon that is influenced by various mechanisms that limit response to drug-induced inhibition of tumour growth - Figure 5 (Luqmani, 2005; Harris and Hochhauser, 1992). Alterations in the expression and activity of enzymes (e.g. topoisomerase II) and drug-metabolising enzymes, membrane transport (p-glycoprotein, ABC transporters), deactivation of drugs in response to the conjugation with glutathione and increased DNA repair of cancer cells that fail to undergo apoptosis due to mutated proteins that have a functional role in cell cycle such as p53 (Housman *et al*., 2014; Luqman, 2005). This increases degradation and promotes the inhibition of anti-cancer drugs. Epigenetic effects and the heterogeneity of the cells at the tumour site also plays a pivotal role in resistance to chemotherapy (Byler and Sarkar, 2014; Housman *et al*., 2014; Sarkar *et al*., 2013). Extracellular matrix proteins and cell adhesion molecules on stromal cells associated with the cell adhesion molecule on cancer cells (Housman *et al*., 2014). Cancer and stromal cells also secrete factors that regulate epithelial-mesenchymal transition (EMT) (Housman *et al*. 2014).

Therapeutic attempts have been made to strategically overcome MDR. For instance, the inhibition of drug efflux by adenosine triphosphate-binding cassette

(ABC) transporter proteins led to the discovery of promising compounds (Fletcher *et al.*, 2010; Luqmani, 2005; Szakacs *et al.*, 2004). Other therapeutic targets include nuclear factor kappa-light-chain-enhancer of activated B cells (NFκB), proteasome, Ras monoclonal antibodies, immunotoxins, gene therapy Ras have been discovered (Wilkens, 2015; Wang *et al.*, 2004; Adams *et al.*, 1999; Luqmani, 2005). Angiogenesis and the altered expression of the Bcl-2 protein involved in apoptosis and other physiological factors have also been investigated (Fujita *et al.*, 2005; Kirkin *et al.*, 2004).

The current standard is the use of combination therapy of different cytotoxic drugs has been investigated to increase therapeutic efficacy and narrow the cycle interval to allow the recovery of the bone marrow (Luqman, 2005). P-glycoprotein inhibitors with adjuvant therapy and protein kinase inhibitors have also been experimented to delay the onset of resistance to chemotherapy (Luqman, 2005). Nevertheless, with the increasing prevalence and cancer mortality rates, it is likely there remain causes of MDR unaddressed and impairing current traditional therapies. This necessitates further research and this project aims to discover the intervention of the overlooked glyoxalase system in the development of MDR.

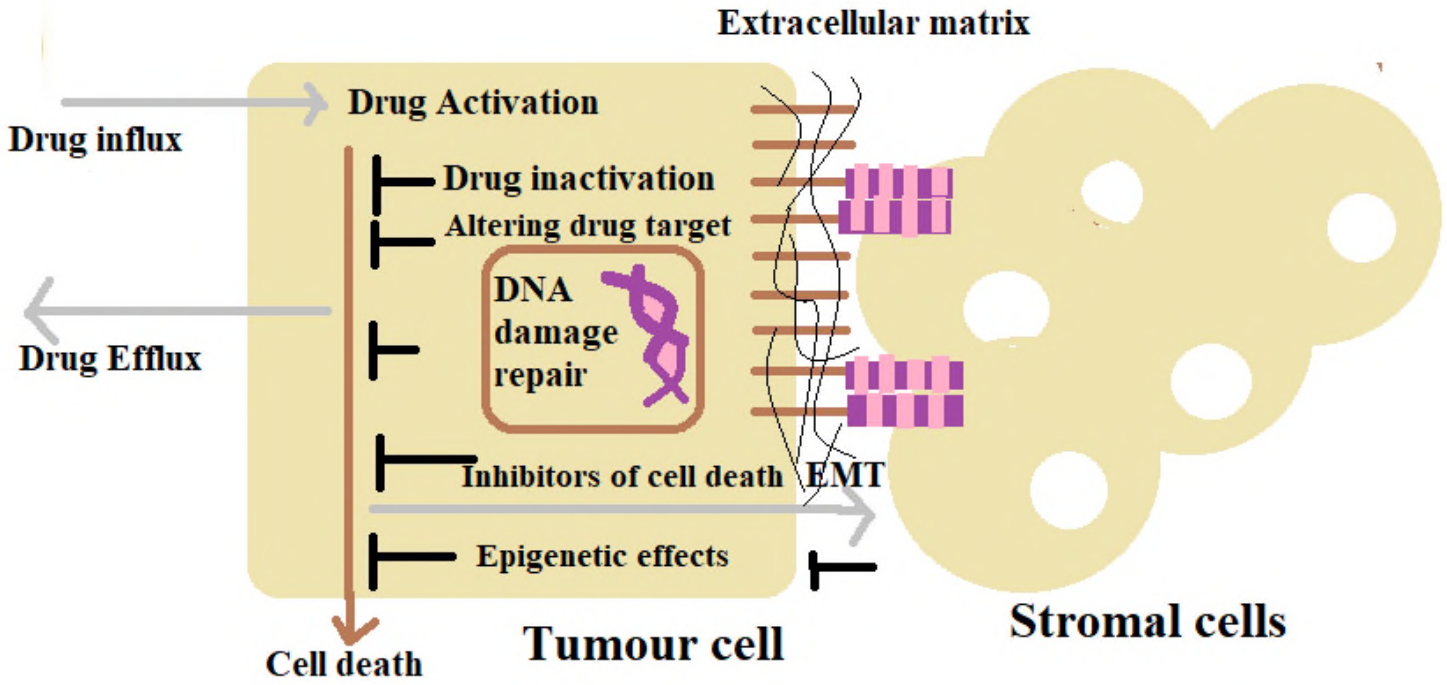

Figure 5: Mechanisms of resistance to chemotherapy (Adapted from: Housman *et al.* 2014).

There are many types of resistance mechanisms that can occur against each and every effect anti-tumour drug which includes: increased drug efflux, decreased drug uptake, increased DNA repair mechanisms, altering drug target, evading drug-induced cell death, inhibiting epigenetic effects and the activation of detoxification systems.

The primary mechanism of MDR is the enhancement of drug efflux (Ughachukwu and Unekwe 2012). There are two types of transporter protein superfamilies: ABC transporter and the solute carrier transporter (Liu, 2009). ABC transporters are energy-requiring efflux pump whose role is to emit chemotherapeutic agents from the cancer cells (Liu, 2009). The solute carrier transporter facilitates the uptake of chemotherapeutic agents to cells (Liu, 2009).

ABC transporters are transmembrane proteins and are important regulators at the plasma membrane that transport several substances (Housman *et al*., 2014; Xue and Liang, 2012). For instance, they are highly expressed in the liver and intestinal epithelium where they pump drugs into the intestinal lumen and bile duct to protect the body (Borst and Elferink, 2002; Housman *et al*., 2014). Other functions include preserving the blood-brain barrier (Housman *et al*., 2014; Schinkel *et al*., 1994). Their structures differ from protein to protein and are distinguished by the presence of two domains: the variable transmembrane domain and a conserved nucleotide binding domain (Chang and Roth, 2001). The efflux mechanism initiates when the substrate attaches to the transmembrane domain. This triggers ATP hydrolysis at the nucleotide binding site which causes an alteration in their conformation. This causes the substrate to undergo exocytosis (Sauna and Ambudkar, 2001; Shukla *et al.* 2007). Despite the efflux conducted by ABC transporters, it is a physiological mechanism that occurs normally, it can also occur in cancer cells where there are three types of transporters whose presence are found in drug resistant cancers (Housman *et al*., 2014).

The second type of transporter is the Permeability-glycoprotein 1 (P-gp) otherwise known as the multi-drug resistance protein 1 (MDR1). It is a 170 kDa glycoprotein comprises of 1280 amino acids and resides at the plasma membrane along the gastrointestinal tract where its primary location is the small intestine where anti-cancer drugs administered orally can be absorbed through the epithelium (Thorn *et al*., 2005; Xue and Liang, 2012; Wacher *et al*., 2001). It is also situated in several sites such as around the blood-brain barrier, placenta, colon, renal, testes and pancreas (Schinkel, 1999; Zhou *et al.* 2008). However, its location differs in cancer-resistant cell lines where it resides in the mitochondrial cristae, rough endoplasmic reticulum, and the Golgi apparatus (Solazzo *et al*.,

2009; Wong *et al*., 2006). It is widespread through several drug-resistant tumours such as cancers of the kidneys, pancreatic, breast, lung liver and leukaemias (Gottesman and Pastan, 2015). On the other hand, other cancers such as lung, ovarian and oesophageal cancer have low expression of P-gp (Gottesman and Pastan, 2015).

P-gp can also indirectly deactivate by stimulating the expression of cytochrome P450 3A4 (CYP3A4) (Bendayan *et al*., 2006). Dietrich *et al.* discovered that a high expression of P-gp influences the bioavailability of several anti-cancer drugs such as Imatinib, doxorubicin and paclitaxel (AlFarouk *et al*., 2015; Dietrich *et al*. 2001a; Dietrich *et al*., 2001b; Schellens *et al*., 2000**;** Sparreboom and Baker, 2016). The high expression of P-gp correlates with the overexpression of proteins that function as receptor tyrosine kinase in the MAPK pathway such as HRas and ERK-1 / 2. This is why inhibitors of tyrosine kinase and HSP90 chaperone protein can down-regulate the expression of P-gp (Zanini *et al*. 2017). The expression can be relieved by the presence of growth factors such as Fibroblast Growth Factor (FGF) and Epidermal Growth Factor (EGF) (Segerer *et al.* 2018).

The third type is called the breast cancer resistance protein (BCRP) otherwise known as the multixenobiotic resistance protein, ABCG2, mitoxantrone resistance protein (MXR) or ABCP (Litman *et al.*, 2002). It emits large, positively charged, hydrophobic molecules that can protect normal cells from xenobiotic effects and maintains the homeostasis of folate and haem (Alfarouk *et al*., 2015; Gottesman and Pastan, 2015). If cancer cells do not have MRP nor P-gp, MXR comes in position for causing resistance (Noguchi *et al*., 2009).

However, by using the tyrosine kinase inhibitor, Gefitinib, it inhibits BRCP causing transporter dysfunction, decreasing drug efflux and preventing drug resistance (Gottesman and Pastan, 2015; Yanase *et al*. 2004; Yanase *et al*. 2006). Doyle *et al.* discovered that oestrogen plays a pivotal role in regulating the expression of BCRP whereby 17b estradiol was able to downregulate its expression in breast cancer cells. This enhanced the sensitivity of anti-cancer drugs such as anthracyclines (Doyle *et al*.,1998). The three types of ABC transporters have a broad substrate specificity and can efflux several different

anti-cancer drugs such as taxanes, vinca alkaloids and anthracyclines from the cells (Gottesman *et al*., 2002).

Hydrophilic nanoparticles can improve the stability and solubility of chemotherapeutic agents by inhibiting the drug efflux, increasing the half-life, exposure time and to treat resistant cancer cells (Xue and Liang, 2012). Nanoparticles can be modified with image moieties, antibodies, anti-cancer drugs and specific to increase the accumulation of the anti-cancer drugs (Xue and Liang, 2012). Patil and Panyam (2009) discovered that siRNA-based nanoparticles can modulate drug resistance by decreasing the expression of MDR1 in combination with an anti-cancer drug (Patil and Panyam, 2009). This was successfully established with doxorubicin (Wang *et al*., 2018; von Roemeling *et al*., 2017).

Alterations to the drug targets such as modifications and mutations to their expression and signal transduction mechanism can cause chemotherapy resistance (Housman *et al*., 2014). For instance, some anti-cancer drugs target the topoisomerase II enzyme which causes damage to the coiling of DNA and prevents synthesis. However, when topoisomerase II is genetically mutated it leads to drug resistance (Stavrovskaya, 2000).

Another example of how genetic mutations cause drug resistance are beta-tubulins that affect the mechanism of action of paclitaxel in ovarian cancers (Mehta *et al.*, 2009). Chromosomal rearrangements in the structure of anaplastic lymphoma kinase have been found in lymphoma (Housman *et al*., 2014; Holohan *et al*., 2013). This emphasizes how drug target alterations cause drug resistance.

Anti-cancer drugs that target signalling kinases such as epidermal growth factor receptor (EGFR) family are associated with cellular proliferation. (Housman *et al.*, 2014). For example, there is a high level of expression of human epidermal growth factor receptor 2 (HER2) tyrosine kinase in *ca.* 30 % of breast cancers and resistance to anti-cancer drugs can result in targeting the kinase for a significantly long period of time (Housman *et al*., 2014; Holohan *et al*., 2013; Lal *et al*., 2003). Another example of an alteration that causes resistance in breast cancer treatment is the malfunction of the oestrogen receptor signalling that influences the antagonistic activity of tamoxifen causing cancer progression (Shou *et al*., 2004)

Inactivation of drugs is another prominent mechanism in how cancer resistance arises. For instance, the nucleoside drug, cytarabine (AraC) is utilized in the treatment of acute leukaemia and is stimulated to form AraC-triphosphate following phosphorylation (Zahreddine and Borden, 2013). Resistance to AraC can occur when there is a mutation or down-regulation in this mechanism. Another example of drug inactivation is resistance to platinum-based drugs caused by glutathione which activates the detoxification mechanism (Mehta and Fok, 2009).

Another example of drug inactivation is through the detoxifying enzymes Glutathione S-transferase (GSTs). GSTs can inhibit the MAPK pathway and when highly expressed it increases detoxification of the anti-cancer drugs reducing cellular damage and cytotoxicity (Manolitsas *et al*., 1997).

There have been several recent developments with the aim to decrease patient-specific resistance. For instance, a bio-printed chip of the pathological characteristics of patients with native tumours can be created to determine drug combinations that increase tumour killing. For instance, a chip has been reconstituted for glioblastoma containing decellularised extracellular matrix, tumour cells and vascular endothelial cells from the brain tissue. They underwent concurrent treatment with chemoradiation and the oral DNA-alkylating agent temozolomide and revealed they were ineffective (Yi *et al.* 2019). This suggests how this methodology can be used to determine the first line of treatment of patients with cancer.

Another technique that can assist patients with metastatic solid tumours is molecular profiling. Treatments can be approved based on the molecular testing of genomic drivers of tumourigenesis rather than the location of tumour (El-Deiry *et al.* 2019). This is known as precision oncology. However, initially, there have been low matching rates with monotherapies due to several limitations such as the drug availability, deterioration of patients with advanced tumours and limited gene panels (Sicklick *et al.* 2019). The current clinical trial paradigm for personalised medicine is to optimize heterogeneous tumours with multidrug regimens to yield a higher matching score and increase the progression-free and overall survival rates (Sicklick *et al.* 2019).

Moreover, the pentose phosphate pathway (PPP) induces chemotherapeutic resistance by various mechanisms: it facilitates DNA damage repair by assisting in nucleotide synthesis, PPP provides cancer cells with NADPH that protects cancer cells from oxidative stress-induced by chemotherapy. It increases tumour survival during treatment by reducing the intracellular levels of reactive oxygen species limiting access of cancer cells to mitochondrial respiration (Phan *et al.*, 2014; Wallace, 2012). Increasing the flux of PPP causes the levels of glutathione and glucose-6-phosphate dehydrogenase to increase, this decreases the accumulation of drugs in cancer cells (Phan *et al*., 2014; Riganti *et al*., 2012).

Ultimately, there are a number of mechanisms that induce chemotherapy resistance; however, the focus of this project is the role of Glo1-linked multidrug resistance in cancer chemotherapy. To understand the pathophysiological mechanisms, the structure and function of the glyoxalase system and its role in MG metabolism is addressed.

1.2 The glyoxalase system

1.2.1 Introduction

The glyoxalase system is a cytosolic enzymatic system that consists of two enzymes: glyoxalase 1 (Glo1) and glyoxalase 2 (Glo2) and a catalytic amount of the cofactor reduced glutathione (GSH) (Thornalley, 2003a, Thornalley, 2008). The enzymatic system is present in eukaryotes and most prokaryotic organisms (Rabbani and Thornalley, 2018a, Rabbani *et al*., 2016, Thornalley, 1990). It is found in animals, plants, fungi, bacteria, and protists (Xue *et al.*, 2011).

The primary role of the glyoxalase system is to catalyse the detoxification and metabolism of reactive α-aldehydes or dicarbonyl metabolites such as methylglyoxal (MG) to the relatively non-toxic metabolic product, D-lactate via the intermediate S-D-lactoylglutathione *in vivo* (Rabbani and Thornalley, 2014a, Thornalley, 2003a). MG is the major substrate of the glyoxalase pathway in physiological systems (Rabbani *et al*., 2016). This, in turn, protects host systems from cell dysfunction and disease (Rabbani *et al*., 2014b, Xue *et al*., 2012). Other functions of the glyoxalase system are to regulate the

microtubule assembly, control growth and glycolytic bypass in microbial systems (Thornalley, 2003a).

The process of detoxification consists of two sequential reactions to prevent an increase of reactive α-oxoaldehydes and its associated reactions – Figure 6. Glo1 catalyses the isomerisation of the hemithioacetal formed non-enzymatically from MG and GSH to form the intermediate S-D-lactoylglutathione (Shinohara *et al*., 1998). Glo2 catalyses the hydrolysis of S-D-lactoylglutathione to form D-lactate and GSH is regenerated. However, other substrates have a different intermediate, for instance, glyoxal is converted to glycolate via the intermediate glycolylglutathione whereas hydroxypyruvaldehyde is converted to L-glycerate via S-L-glyceroylglutathione (Clelland and Thornalley, 1991, Jerzykowski *et al.*, 1973).

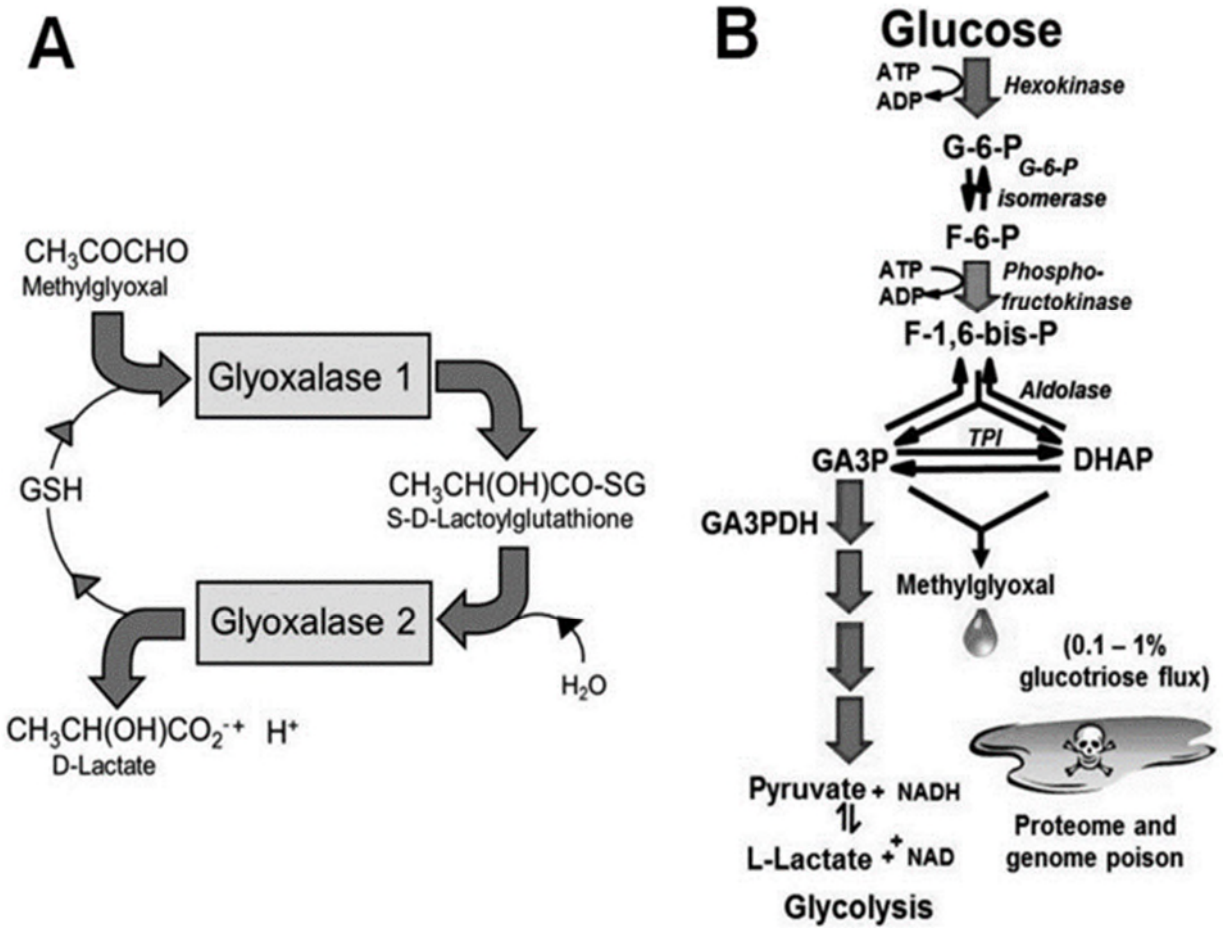

Figure 6: The glyoxalase system.

(A) The glyoxalase system. (B) “Leakage” of metabolic flux from the Embden-Meyerhof pathway by non-enzymatic degradation of triosephosphates to form MG (Rabbani and Thornalley, 2014c).

1.2.1.1 Historical development

The glyoxalase system was discovered in 1913 independently by: (i) Carl Neuberg, and concurrently (ii) Henry Drysdale Dakin and Harold Ward Dudley (Dakin and Dudley, 1913; Neuberg, 1913). In the late 1920s, Neuberg did further experiments where he revealed there was an association between MG and the glyoxalase system in glycolysis where the enzymatic system catalyses the conversion of MG to lactate (Neuberg and Kobel 1929). However, Neuberg's findings were opposed by Embden who found that glycolysis produced only the L-enantiomer of lactate whereas with the addition of methylglyoxal to tissues he found both L- and D-lactate (Neuberg and Kobel, 1929).

Furthermore, Embden revealed that fructose 1,6-bisphosphate (F-1,6-BP) was converted into 3-phosphoglycerate; an oxidation product of glyceraldehyde-3-phosphate (GA3P) (Warburg and Christian, 1939, Meyerhof., 1933). F-1,6-BP was fragmented into two triosephosphates, GA3P and dihydroxyacetone phosphate (DHAP). He also hypothesised that 3-phosphoglycerate was a precursor of pyruvate and L-lactate (Embden, 1932). His findings on the alternative glycolytic intermediates were consolidated by Otto Meyerhof. This led to the introduction of the Embden–Meyerhof pathway that involves the conversion of glucose into L-lactate (Embden 1932; Meyerhof, 1933).

Moreover, further developments were made between the years 1930s and 1950s which advanced and shaped our current understanding of the characteristics and physiological aspects of the glyoxalase system. The leading investigators of this period were: Karl Lohmann who discovered GSH, Juda Quastel and Maurice Jowett who revealed that GSH and MG interacted to form a hemithioacetal substrate, and Samuro Yamazoye who showed that the hemithioacetal is converted to S-D-lactoylglutathione (Jowett and Quastel, 1933; Lohmann, 1932; Yamazoye, 1936). The distribution of the glyoxalase system in living organisms was studied by Edward Morgan and Frederick Gowland-Hopkins who discovered it occurred widespread in living organisms (Hopkins and Morgan, 1945).

Efraim Racker found that there were two sequential metabolic steps of glyoxalase system catalysed by Glo1 and Glo2, respectively, and that the terminal product of metabolism of MG was D-lactate (Racker, 1951; Thornalley, 1990).

The terminal protein stereoselectivity for D-lactate was subsequently analysed by Ekwall and Mannervik who confirmed the unexpected finding of Racker (Ekwall and Mannervik, 1973). In 1960, a study was conducted on the human arterial tissue where the results put an emphasis on the functional role of Glo1 and how low activity of Glo1 influences the ageing process and increased the risk of cardiovascular disease (Kirk, 1960).

With the role of MG and the glyoxalase system being dissociated from glycolysis, further investigations were conducted on the function of the glyoxalase system. The glyoxalase system was hypothesised to be a regulator of growth control and high doses of exogenous MG provide novel cancer treatment: MG was hypothesised to be a 'retine' that restricts growth whereas Glo1 was seen as a 'promine' that counteracts this effect (Szent-Györgyi *et al*., 1967; Szent-Gyorgyi *et al*., 1963). However, the subsequent finding of other, more potent and effective growth factors and their receptors led to this hypothesis being rejected.

Bonsignore *et al*. revealed that GA3P underwent non-enzymatic hydrolysis to form MG (Bonsignore *et al.*, 1973). The arginine-directed protein glycation induced by MG was discovered by Takahashi and was later revealed to be the major protein adduct: hydroimidazolone (MG-H1) (Ahmed *et al*. 2002, Henle *et al*., 1994; Takahashi, 1977; Thornalley *et al*., 2003). MG-derived advanced glycation endproducts (AGEs) were quantified using a stable isotopic dilution analysis liquid chromatography-tandem mass spectrometry (LC-MS/MS) (Thornalley *et al*., 2003).

In 1988, it was discovered that the formation of MG was elevated in erythrocytes that were incubated in high glucose concentrations *in vitro* (Thornalley, 1988). This led to the detection of other metabolites of D-lactate and S-D-lactoylglutathione that were increased in patients with diabetes in comparison to healthy participants which emphasises that there is an increase in Glo1 activity (Atkins and Thornalley, 1989; Thornalley *et al*., 1989).

Vince and Wadd pursued the hypothesis that elevated concentrations of MG were toxic to tumour cells and proposed a novel strategy to achieve this: by targeting Glo1 with small molecule inhibitors. The Glo1 inhibitors derived from

glutathione thioethers may be effective anti-cancer agents via the accumulation of MG (Vince and Wadd, 1969).

The molecular and structural characteristics of the glyoxalase enzymes and their catalytic mechanisms were detected in the 1970s-1990s. Wilson and his colleagues discovered that Glo1 gene was an inherited factor associated with the body mass index (BMI) and part of the obesity genome (Wilson *et al.*, 1991). Glyoxalase enzymes were purified and characterized by several groups – as reviewed (Rabbani and Thornalley, 2014b). The non-enzymatic degradation of triosephosphates – GA3P and DHAP, to form MG was characterized using a specific and validated MG assay under physiological state conditions (Phillips and Thornalley, 1993). This represents a minor "leak" of *ca.* 0.05% - 0.1 % glucotriose flux from the Embden-Meyerhof pathway. Despite this low level, the high reactivity of MG with protein and DNA required effective and efficient metabolism of MG to suppress these reactions to low, tolerable levels (Phillips and Thornalley, 1993).

The physiological function of the glyoxalase pathway has been accepted to be a natural damage protective system by detoxifying potent reactive MG that otherwise induces dicarbonyl glycation and forms advanced glycation end-products (AGEs) (Lo *et al.,* 1994a; Lo *et al*., 1994b). It was also discovered during the same year that aminoguanidine prevented the formation of AGEs by preventing the development of diabetic complications (Lo *et al*., 1994a). This suggests a fundamental and conserved role required by all glycolytic life forms unless there is an alternative, compensatory route to MG detoxification (Thornalley, 2003a).

Up to the 1990s, glyoxalase research was still lacking an effective inhibitor of Glo1 *in situ.* Despite the development of potent Glo1 inhibitors by Vince and Wadd in 1969, it lacked cell permeability and hence could not reach the Glo1 receptor in the cytoplasm of cells. This was resolved in 1992 by Lo and Thornalley who produced a cell permeable Glo1 inhibitor, S-*p*-bromobenzylgluthathione (SpBrBzGSH) diester that exerted its anti-tumour effects *in vitro* and *in vivo* by the accumulation of MG leading to apoptosis, anoikis and necrosis. The diesterification provided a pro-drug modification that

facilitated cell permeability inside the cells forming the active Glo1 inhibitor. It also stabilised Glo1 inhibitors from extracellular degradation by ɣ-glutamyl transferase (Lo and Thornalley, 1992; Thornalley, 1996; Thornalley *et al*., 1996). This was further developed by Creighton and co-workers (Creighton *et al*., 2003).

Several *in vitro* and *in vivo* studies revealed there was an increase in the concentration of MG and MG-derived AGEs but there was a reduction in Glo1 and Glo2 activities; this is associated with oxidative stress and ageing (McLellan and Thornalley, 1989; Abordo *et al.*, 1999, Dunn *et al.*, 1991, Ahmed *et al.*, 1997; Sharma-Luthra and Kale, 1994; Baynes, 1991). This was also observed in patients with type 2 diabetes mellitus who underwent metformin therapy where there was a reduction in the concentration of MG in plasma (Beisswenger *et* al., 1999). Shinohara and colleagues discovered that overexpression of Glo1 in endothelial cells reduced the accumulation of MG and the production of associated AGEs *in vitro* (Shinohara *et al.*, 1998). This suggests how Glo1 is the major enzyme involved in MG metabolism.

Sakamoto *et al*. revealed there was an association between GLO1 overexpression and MDR in cancer chemotherapy (Sakamoto *et al*., 2000). MDR is defined as the innate and/or acquired aptitude of tumour cells to avoid the drug-induced tumour growth inhibition (Alfarouk *et al*., 2015). It is the central mechanism in how tumours develop chemotherapeutic resistance and remains a continuous, central challenge for medicine today in the treatment of disseminated and local disease (Luqmani, 2005; Persidis, 1999). It was also discovered that MDR is connected to the overexpression of Glo1 in tumour cells lines *in vitro* and tumour-bearing mice *in vivo*; this was lifted by the S-*p*-bromobenzylgluthathione diester (Sakamoto *et al*., 2001).

Further developments were also made in understanding the genetic basis of Glo1 in the late 2000s. Redon and his colleagues identified Glo1 after constructing a copy number variation (CNV) map. This led to the introduction of the non-transcribed region of the Glo1 gene that played a major role in increasing the amplification of the Glo1 gene (Redon *et al*., 2006; Cahan *et al*., 2009). In 2007, Zender and his colleagues conducted a genome-wide study consisting of tumour suppressor genes and discovered that Glo1 was linked to the functional

role of tumour suppression which in turn influences the production of MG-derived nucleotide AGEs: MG-derived imidazopurinine (MGdG) and N_2-(1-carboxytheyl)deoxyguanosine (CEdG); these are associated with mutagenesis and DNA instability *in vivo* (Zender *et al*; 2008, Santarius *et al*., 2010). The level of Glo1 gene expression was discovered to be influenced by the lifespan of *Caenorhabditis elegans*. When Glo1 was overexpressed in *Caenorhabditis elegans,* the median lifespan was increased *ca.* 30%; and when Glo1 was silenced by transfecting with Glo1 small interfering ribonucleic acid (siRNA), the median lifespan was decreased by *ca.* 50% (Morcos *et al.*, 2008).

In 2010, Santarius *et al*. revealed that a driver of increased Glo1 expression was, in some cases, increased GLO1 copy number in tumours that have innate MDR. Highest prevalence of increased GLO1 copy number was found in breast cancer (22%), non-small cell lung cancer (NSCLC) (11%) and small cell lung cancer (SCLC) (16%) of 520 human tumours were assessed (Santarius *et al.*, 2010).

Another cause of Glo1 overexpression was discovered in 2012. The transcription factor nuclear factor-erythroid 2 p45 subunit related factor 2 (Nrf2) binds to a regulatory antioxidant response element (ARE) in the 5'-untranslated regions of exon-1 of the mammalian GLO1 gene to increase the basal and inducible expression of Glo1 (Xue *et al.*, 2012). This increases the detoxification and metabolism of MG to protect cells from oxidative stress-induced damage (Xue *et al*., 2012).

Besides, Nrf2 can also increase intracellular levels of GSH (Frandsen *et al*., 2017). The activation of Nrf2 increases the transcription of proteins under the states of stress and cytotoxicity by ROS and anti-tumour drugs respectively to initiate antioxidant defence mechanisms (Surh *et al*., 2008). Amongst the products of Glo1 is GST, glutamylcysteine synthetase (GCS) and haem oxygenase-1 (HO-1) (Serafini *et al*., 2010). Under the resting phase, Nrf2 associates with its negative regulator, Kelch-like ECH-associated protein 1 (Keap1) to form a complex and is sequestered into the cytoplasm where it undergoes subsequent ubiquitination by Cullin-3 and is transferred to the proteasome for degradation (Frandsen *et al.* 2017; Kobayashi *et al.* 2004; Kobayashi *et al*., 2006).

Since Glo1 is a tumour suppressor protein, small molecule Nrf2 activators and Glo1 inducers developed from dietary bioactive compounds may be utilized to increase the mRNA expression, protein, and enzymatic activity of Glo1 to prevent tumour progression. Other therapeutic uses of Glo1 inducers is to treat vascular diabetic complications and act as dietary supplements to promote healthy ageing (Rabbani *et al*, 2018; Rabbani *et al*., 2014, Xue *et al*., 2011).

Currently, we are in the position of joining the bridge between the regulatory process of the glyoxalase system and its effects on physiological stress, chemotherapeutic resistance, ageing, and disease to develop novel pharmaceutical strategies.

1.3 Glyoxalase 1

1.3.1 Molecular characteristics and structure

Human Glo1 has a molecular mass of 42 kDa by sequence whereas its mass is determined experimentally by gel filtration is 46 kDa. The isoelectric point (pI) value is in the range of 4.8 - 5.1 (Thornalley, 2003a; Thornalley, 1990). Human Glo1 is a dimeric protein and each subunit consists of 184 amino acids with a molecular mass of 21 kDa by sequence (Thornalley, 2003a). The two monomers are associated by non-covalent bonds (Birkenmeier *et al.*, 2010). Each monomer contains two, structurally equivalent domains that have risen by a gene duplication and 3D domain swapping of the N-and C-terminal domains (Thornalley, 2003a; Thornalley, 2003c). One domain comprises residues 31-104 amino acids and the other domain residues 124-183. These domains are linked by two regions: 20 amino acid connecting region and a long N-terminal region. Each domain also contains a βαββββ-motif and a mixed β-sheet. When the subunits undergo dimerization, a β-barrel structure is formed that contains the active site. The dimers have enzymatic activity whereas the individual monomers do not (Thornalley, 2003a).

The expression and activity of Glo1 is found in different organisms, from prokaryotes to eukaryotes but the prosthetic metal ion varies. For example, the Glo1 found in the bacteria *Escherichia coli* is a dimeric Ni^{2+}-metalloenzyme

whereas the Glo1 found in humans is a dimeric Zn^{2+}- metalloenzyme with a stoichiometry of one zinc ion per monomer (Marmstål *et al*., 1979; Thornalley, 2003a). The crystal structures of human and bacterial Glo1 has been solved to 1.7 and 1.5 Å resolution (Cameron *et al*., 1997).

The prosthetic Zn^{2+} binding site in the human Glo1 consists of two structurally equivalent residues from each domain: Gln-33A, Glu-99A, His-126B, Glu-172B and two water molecules. It is organised in an octahedral coordination whereas the Ni^{2+} binding site of bacterial Glo1 comprises His-5A, Glu-56A, His-74B, Glu-122B and two water molecules (Thornalley, 2003a). In human Glo1, the active site is located in the dimer interface particularly in the β-barrel motifs. This can be compared to other enzymatic structures, several studies have highlighted that Glo1 belongs to the bleomycin resistance protein and Fe^{2+} dependent dihydroxybiphenyl dioxygenase (Cameron *et al*., 1997). The substrate and prosthetic Zn^{2+} ions interact with the side chains from both subunits (Thornalley, 2003a).

1.3.2 Genetics and polymorphism

The GLO1 gene encodes two subunits and is expressed at a diallelic genetic locus on chromosome six found between the centromere and Human Leukocyte Antigen - antigen D-Related (HLA-DR). The genetic locus is 6p21.2 (38,751,680 - 38,778,930) whereas the GLO1 gene consists of 27,250 bp, six exons and five introns (Thornalley, 2003a; Tripodis *et al*., 1998). The length of the GLO1 gene is ~12.0kb (Gale and Grant, 2004).

GLO1 has two alleles, GLO_1 and GLO_2 in heterozygotes, which are inherited autosomally in a co-dominant technique (Thornalley, 1991). GLO^1 arises via mutation whereas the GLO^2 allele is the ancestral allele. The difference between them is caused by the point mutation at position 332 in cDNA sequence (Thornalley, 2003a). Thus, the possible genotypes of the human GLO1 are GLO1(1-1), GLO1(1-2) and GLO1(2-2). These allozymes represent the homozygous and heterozygous expressions of the diallelic gene in all tissues. This common polymorphism is produced by the mutation C419A in the coding region giving rise to amino acid residue polymorphism Ala111Glu (A111E). The expression of GLO^1 produces a Glo1 subunit with Ala111, whereas the

expression of GLO^2 produces a subunit with Glu111 (Degaffe *et al.*, 2008, Kim *et al*., 1995).

Allozymes may be distinguished by their molecular shapes and charge densities which are resolved by ion-exchange chromatography and gel electrophoresis (Kim *et al*., 1995). Human population genetic studies revealed that the GLO_1 allele-frequency is at its highest in native tribes in Alaska, 0.67 – 0.85 and decreases geographically from the South and East to Europe and South America, through Africa, the Middle East and India, to the very low GLO1 allele frequencies of the Far East and Oceania, 0–0.16 (Thornalley, 1991). Deletion of GLO1 is embryonically lethal in mice and humans unless the compensatory increased expression of MG reductase occurs (Arai *et al*., 2010).

The GLO1 promoter region presented in Figure 7 consists of several binding sites for regulatory elements that vary in position and are hot spots for an increase in the functional copy number. The human GLO1 promoter region is 982 bp and the main elements present are: metal responsive element (MRE) positioned from -647 to -654bp, glucocorticoid responsive element (GRE) (-363 to -368bp), activating enhanced binding protein 2 alpha (TFAP2A) (-24 to -32bp), insulin response element (IRE) (-842 to -848 bp), antioxidant response element ARE-1 (-10 to -19), ARE-2 (-252 to -261), ARE-3 (1051 to -1060), The activating enhancer binding protein 2 alpha (AP-2α) and E2F-binding to the transcription factor EDF4 (Ranganathan *et al.,* 1999; Lewis *et al*., 2010; Donato *et al*. 2018; Xue *et al.,* 2012; Conboy *et al*., 2007).

Some of the functionalities, IRE and MRE were validated by reporter assays where there was an increase in the transcriptional response (2-fold) due to the exposure of zinc chloride and insulin (Ranganathan *et al*., 1999). No functional activity was established for the GRE but there was activity in hormone response element (HRE) which decreased the expression of GLO1 (Ranganathan and Tew, 1993; Ranganathan *et al*., 1999; Zhang *et al*., 2012).

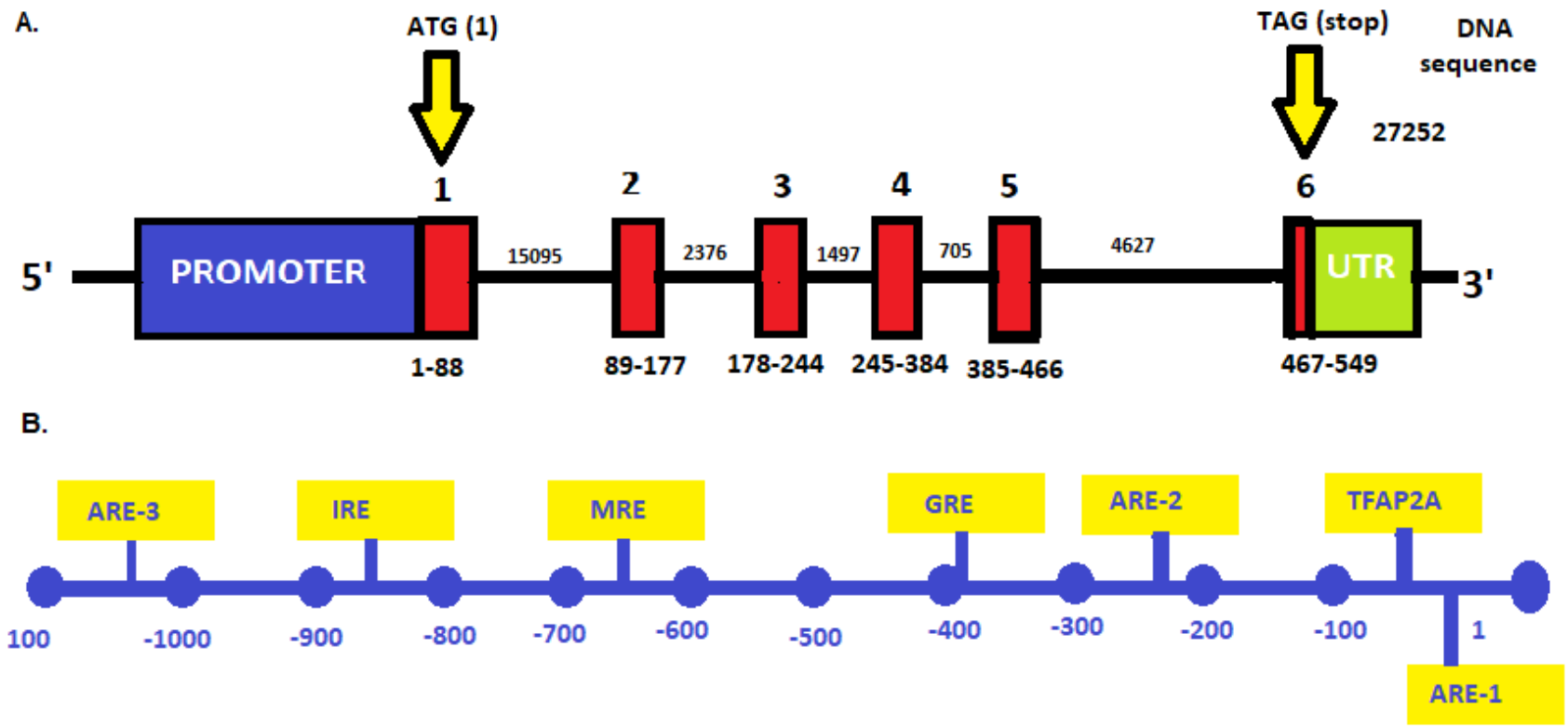

Figure 7: The structure of the human GLO1 gene (Adapted from Shafie *et al*., 2014)

(A) A schematic presentation of the different domains in the human GLO1 gene (Blue: promoter region, red: exon, green: untranslated region.

(B) Promoter sequence of human GLO1 with positions of regulatory elements (Yellow)

1.3.2.1 Copy number variation (CNV) of GLO1 gene

Advances in technology provided an insight into the genetic rearrangement of various sites in the genome of a species. These could be deletions, duplications, inversions, and insertions that cause alterations in the structural arrangement of chromosomes and genes. Copy number variation (CNV) is defined as a genomic segment of at least 50 bp that differs in copy number based on the comparison of two or more genomes (Zarrei *et al.*, 2015). This can cause genetic diversity that has been revealed in mammalian species and plays an influential role in evolution and susceptibility to disease (Choy *et al*.,2010, Freeman, 2006; Schrider and Han, 2010; Kehrer-Sawatzki, 2006; Shlien and Malkin, 2009).

There was an increase in GLO1 CNV and this can be found in adipose, hypothalamus and hematopoietic cells (Cahan *et al.*, 2009). Williams and his colleagues identified GLO1 locus as a hotspot for CNV in mice strains that are undergoing duplications. The duplication is associated with increasing the levels of GLO1 expression (Shafie *et al*., 2014 Williams *et al*., 2009; Cahan *et al.* 2009; Perry *et al*., 2008).

1.3.3 Enzyme kinetics and catalytic mechanism

Glo1 is the first line of defence in how MG and associated reactive metabolites such as glyoxal and 3-deoxyglucosone (3-DG) are removed in most human tissues (Rabbani *et al*. 2014, Thornalley, 1993; Shinohara *et al*., 1998; Thornalley, 2003a, Thornalley, 2003b). Glo1 catalyses the isomerisation of the hemithioacetal formed non-enzymatically from the reaction of MG and GSH to form the corresponding α-hydroxyacid, S-D-lactoylglutathione (Phillips and Thornalley, 1993; Thornalley, 2003a). In cells and tissues *in vivo*, this decreases the steady-state concentration of α-oxoaldehydes and associated glycation reactions (Thornalley, 1999). Glo1 has a broad specificity for α-oxoaldehydes such as glyoxal $(CHO)_2$), MG (CH_3COCHO), hydroxypyruvaldehyde ($HOCH_2COCHO$), 4,5-dioxovaleric acid $HO_2C(CH_2)_2COCHO$ and other acyclic glyoxal derivatives (Rabbani and Thornalley, 2012a). The K_M and kcat values decrease as the hydrophobicity of the side chain of the glyoxal derivative substrate increases (Van der Jagt *et al*., 1975). For human Glo1 interacting with the GSH-

MG hemiothioacetal, $CH_3COCHOH$-SG, the Michaelis-Menten constant (K_M) is 71-130 µM and the turnover number kcat is 7-11 x 10^4 min^{-1} (Thornalley, 2003a).

The catalytic reaction consists of a proton transfer in the hemithioacetal from C-1 to C-2 to produce an ene-diol intermediate (Thornalley, 2003a). This is followed by rapid ketonization to form the thioester product (Thornalley, 2003a). Two types of stereoisomers are formed in the pre-equilibrium forming the hemithioacetal: R - and S-substrate diastereoisomers. Glo1 accepts them both and once bound to the active site, it displaces the water molecules in the metal ion primary co-ordination shell. There is a difference in the catalytic base found in both types of diastereoisomers: Glu-172 is the base for the S-substrate diastereoisomer whereas Glu-99 is the base for the R-substrate diastereoisomer. Glu-172 can re-protonate the ene-diol to produce the R-2- hydroxyacylglutathione product (Rabbani and Thornalley, 2014b; Rabbani and Thornalley, 2008a; Thornalley, 2003a).

1.3.4 Glo1 expression, transcriptional regulation, and post-translational modification

In the adult human tissues and blood cells the basal expression 0.2 µg Glo1 protein per mg total protein. This was increased up to 2-fold in foetal tissues (Larsen *et al*., 1985). The expression of Glo1 can decrease causing accumulation of MG in three major respects: when levels of Glo1 are suppressed *in situ* by GSH depletion, the expression of Glo1 is decreased by siRNA silencing and in the presence of cell permeable Glo1 inhibitors (Abordo *et al*. 1999; Thornalley, 1993; Thornalley *et al*. 1996; Thornalley, 2003b, Xue *et al*. 2017).

The expression of Glo1 may also be decreased by the activation of the cell-surface receptor for advanced glycation end-products (RAGE), although the mechanism remains unclear (Bopp *et al*. 2008; Reiniger *et al*., 2010; Zeng *et al*., 2012). The function of RAGEs is to act as decoy receptors for the ligands and influence RAGE-ligand interactions and signal transduction pathways (Park *et al*., 1998; Vazzana *et al.* 2009). For instance, Mitogen activated protein kinases (MAPK), phosphoinositol-3-kinase (PI3K), Rho GTPase, Jak/STAT, extracellular regulated (ERK) and c-Jun N-terminal kinase (JNK) (Hejab *et al*., 2012; Vazzana *et al*., 2009).

Endothelial RAGE binds with circulating AGEs causing endothelial dysfunction which activates nicotinamide adenine dinucleotide phosphate oxidase (Hejab *et al*., 2012; Vazzana *et al*., 2009). This increases the synthesis of ROS and nuclear transcription factors such as NF-kB. NF-kB is translocated to the nucleus and initiates target gene transcription such as E-selectin, ICAM-1 and endothelin-1 (Vazzana *et al.* 2009; Sparvero *et al.*, 2009). This highlights the importance of RAGE as a central player for several pathological states: chronic inflammaion, diabetes and atherosclerosis (Bopp *et al.*, 2008; Hejab *et al.*, 2012). Moreover, the expression of Glo1 can be decreased by the activation of hypoxia-inducible factor 1α; see Section 1.10 (Zhang *et al.*, 2012; Zhang *et al*., 2015).

During post-translational processing of human Glo1, the N-terminal Met is removed, and the remaining N-terminal Ala is blocked by acetylation (Xue *et al.* 2011). There is a vicinal disulphide bridge between the cysteine residues 19 and 20 and a mixed disulphide with glutathione on cysteine-139. Cysteine-139 may also form an intra-molecular disulphide with cysteine-61. *N*-Acetylation and the oxidation state of C19/C20 did not affect Glo1 activity whereas glutathionylation strongly inhibited Glo1 activity *in vitro* (Birkenmeier *et al.*, 2010).

Glo1 is modified by S-nitrosylation by the reaction with nitric oxide (NO) on cysteine-139. The presence of both C19 and C20 were influential on S-nitrosylation which occurred preferentially on the acidic, α-form of Glo1. The NO-responsive form of Glo1 is the basic, reduced form of Glo1 without intramolecular disulphide bonding (De Hemptinne *et al*., 2007). Glo1 is a substrate for calcium, calmodulin-dependent protein kinase II and is phosphorylated at Thr-107 preferentially but not exclusively on the basic, reduced and NO-responsive form (Santarius *et al*., 2010; de Hemptinne *et al*., 2009; De Hemptinne *et al*., 2007, Birkenmeirer *et al*., 2010).

The expression of Glo1 was quantified in NIH3T3 mouse fibroblasts in a genome-wide study by Selbach and colleagues (Schwanhäusser *et al*., 2011). For Glo1, the number of copies per cell of mRNA and protein was: mRNA – 22 (median of transcriptome 17); and protein – *ca.* 584,000 (median of proteome *ca.* 50,000). The half-lives of mRNA and protein were mRNA – 7.8 h (median of transcriptome 9 h); and for protein, 179 h (median of proteome *ca.* 46 h). The

transcription rate (molecules per cell per h) was: 2.4 (median for transcription, 1.8). The translation rate (molecules protein per molecule mRNA per h) was: 750 (median for genome-wide translation, 117). The view emerging from this is that Glo1 has protein abundance *ca.* 10-fold higher and half-life 4-fold higher than the median value. The quantitative level of Glo1 protein is in reasonable agreement with that estimated for the human tissues by immunoassay of *ca.* 0.2 µg per mg protein or Glo1 is *ca.* 1/5000th of total protein (Larsen *et al.*, 1985). Glo1 is a highly efficient enzyme and so these relatively high levels of protein probably reflect a requirement for high *in situ* activity. There were 677 Glo1 proteins detected from the overall 5028 proteins and was present in the top 13% of proteins detected by abundance. This is similar abundance to that of other glycolytic enzymes – such as transketolase.

There have been a few comprehensive studies of the relationships between the levels of transcripts and proteins they encode in mammals. In a genetic approach in which natural variations were used to perturb both transcript levels and protein levels amongst the inbred strains of mice, in quantifying levels of the 7,185 most heritable transcripts and 486 related proteins, the mRNA levels of Glo1 had one of the strongest correlations with Glo1 protein; r = 0.87). Only 50% of the genes tested had a significant correlation of mRNA and protein and the average correlation was r = 0.27 (Ghazalpour *et al.*, 2011). The post-transcriptional mechanisms that converted Glo1 mRNA into Glo1 protein are relatively constant – at least in the liver, and the half-life of Glo1 may be little changed in good health. This suggests that Glo1 shows a moderate increase in proteolysis on the activation of autophagy (Kristensen *et al.*, 2008).

1.3.5 The association between glyoxalase 1 and cancer

1.3.5.1 Glyoxalase 1 as a tumour suppressor protein

Increased MG concentration may cause increased DNA strand breaks, cytotoxicity and mutation frequencies mediated by the increased production of MG-derived imidazopurinone adducts and glyoxal-derived nucleotides of DNA (Rabbani *et al*., 2018; Thornalley *et al*., 2010; Xue *et al*., 2016). This is countered by the nucleotide excision repair (Thornalley, 2003a; Thornalley, 2003b). In studies of liver carcinogenesis, a p53 knockout Ras overexpression rodent model was utilized to scan for tumour suppressor genes (Zender *et al*., 2008). Hits were identified by the augmented tumour growth with selective gene silencing achieved by introducing pools of short hairpin RNAs into pre-malignant progenitor cells and selection for those that promote tumour formation after transplantation. Thirteen tumour suppressor genes (in addition to p53) were identified, including *Glo1* (Zender *et al*., 2008). If this rodent model translates to clinical carcinogenesis, an elevated expression of Glo1 is linked with reduced risk of cancer and this can be observed through the example of hepatocellular carcinoma (Rabbani *et al*., 2018; Xue *et al*., 2016). Therefore, Glo1 inducers can be utilized as a cancer therapeutic strategy for patients who are at high risk (Rabbani *et al*., 2017).

1.3.5.2 Glyoxalase 1 gene amplification in tumours

High Glo1 expression has been discovered in various clinical tumours as illustrated in Figure 8. For instance, lung, stomach, liver, skin, prostate, breast and colon cancer (Bair *et al*., 2010; Ranganathan *et al*, 1995; Rulli *et al.,* 2001; Geng *et al*., 2014; Cheng *et al.,* 2012; Amatschek *et al*., 2004; Davidson *et al*., 1999; Sakellariou *et al.* 2016; Fonseca-Sanchez *et al*., 2012; Zhang *et al.*, 2014; Zhou *et al*. 2015). Glo1 expression presented robust nuclear and cytoplasmic positivity where it is *ca.* 2-fold relative to normal tissues. Tumours that have an elevated expression and activity of Glo1 may have increased tumour growth with a high glycolytic rate.

There is a positive correlation between the GLO1 high copy number with the expression of Glo1 mRNA and protein and is a common feature in how multiple human malignancies progress. It is also positively correlated with tumour grade where the grade is based on how the morphological appearance of the tumour cells and growth patterns differ with normal cells, which is essential for the prognosis of patients (Fonseca-Sánchez *et al.*, 2010). Patients with grade 3 tumours have an undifferentiated, aggressive phenotype due to a loss of tubules and the elevated activity of mitosis where the 5-year overall survival rate is 50|% (Fonseca-Sánchez *et al.*, 2010).

On the other hand, patients with tumours with grade 1 and 2 have an overall survival rate of 90% and 75% respectively. This highlights the potential use of GLO1 as a novel biomarker for tumours and to diagnose patients with and without aggressive tumours (Fonseca-Sánchez *et al*., 2010). However, the presence of GLO1 in the nuclear fraction can be found in approximately 10% of tumours which illustrates the role of GLO1 in MG metabolism to prevent the formation of nuclear-advanced glycation end-products (Fonseca-Sánchez *et al.*, 2010).

Santarius *et al.* revealed that the cancer that had the highest expression of Glo1 gene amplification was breast cancer by (22%), followed by sarcomas at (17%) and NSCLC by (11%) (Santarius *et al*., 2010). In addition, triple negative breast cancers that do not comprise of HER-2, oestrogen and progesterone receptors have high GLO1 gene amplification (Shafie *et al*., 2014). This suggests

that the increase in the expression and activity of GLO1 implemented by tumour cells with an aggressive phenotype has been induced by the high intracellular levels of MG with high glycolytic rates. Therefore, GLO1 plays a significant role in when the tumour initiates, during malignant progression and treatment failure.

siRNA knockdown of Glo1 in tumours with high glycolytic rates increases the formation and cytotoxicity of methylglyoxal (Santarius *et al*., 2010). Xue *et al*. discovered that siRNA knockdown of Glo1 increases sensitivity to doxorubicin and in absence of the drug treatment in the metastatic human carcinoid pancreatic tumour cell line (BON-1) *in vitro (*Xue et al., 2016). This emphasises that Glo1 expression is associated with the resistance of doxorubicin in BON-1 cell lines and can be inhibited through the cell permeable Glo1 substrate inhibitor (Sakamoto *et al*., 2001; Santarius *et al.*, 2010).

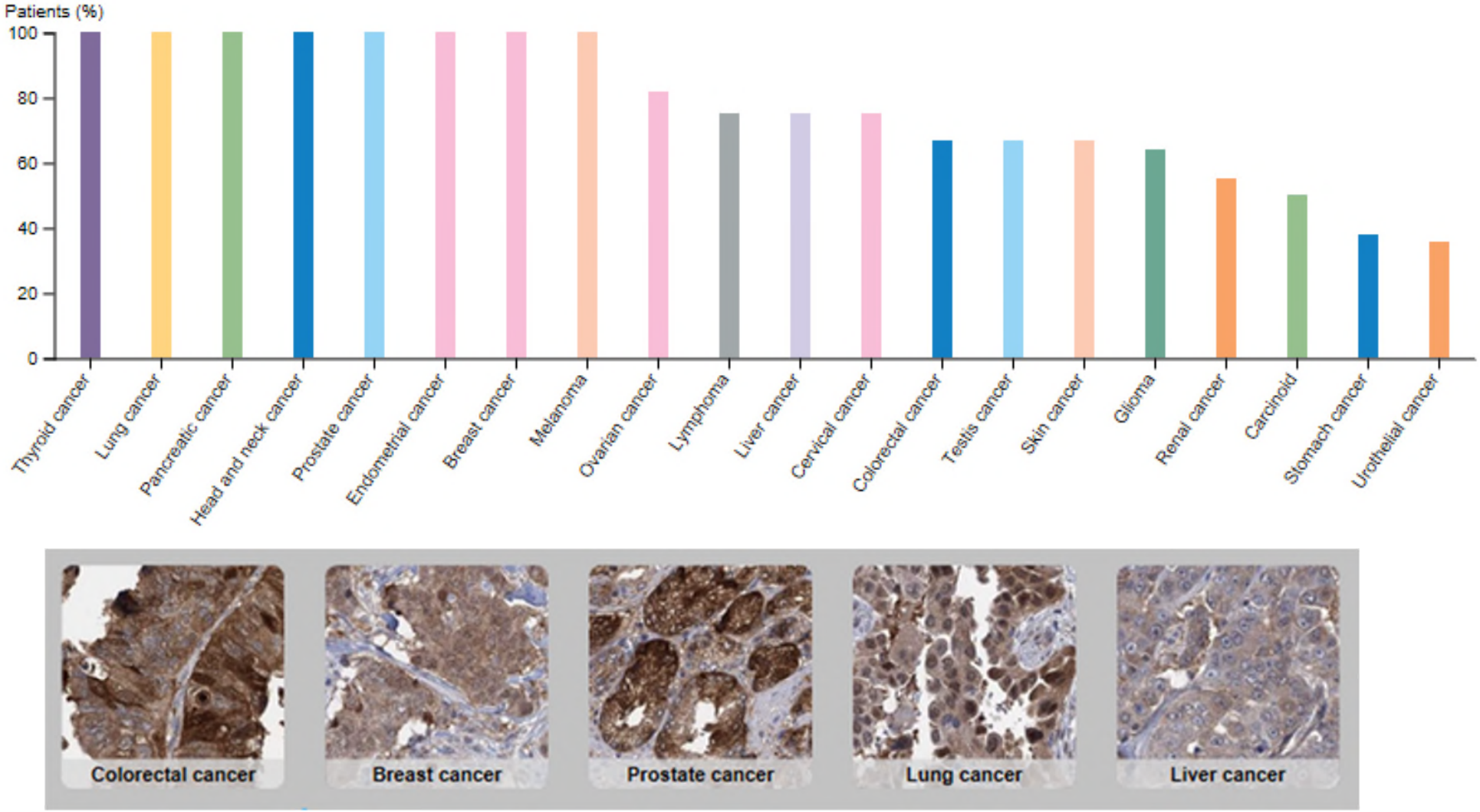

Figure 8: The Protein expression files of GLO1 in varied tumours. A. Quantitative analysis of the expression of Glo1 in different tumours B. The immunohistochemistry profile of protein expression of Glo1 (The Protein Atlas, 2018)

1.3.5.3 Overexpression of Glo1 causing multi-drug resistance

An elevated expression of Glo1 was found in clinical refractory tumours where Glo1 was discovered to be a negative survival factor for cancer treatment by preventing the accumulation of the cytotoxic MG which suppresses the ME-defrived glycation leading to the formation of AGEs (Rabbani *et al*., 2018, Beroukhim *et al*., 2010; Cheng *et al*., 2012; Xue *et al.*, 2016; Thornalley *et al*., 1996; Hudis and Gianni, 2011; Santarius *et al*., 2010). There are two main causes of Glo1-linked MDR: high glyoxalase 1 gene amplification and elevated transcriptional activity of Nrf2 via ARE-linked up-regulation of GLO1 transcription (Rabbani and Thornalley and Rabbani, 2011; Rabbani and Thornalley, 2015; Rabbani *et al*., 2017; Rabbani *et al*., 2018). Xue *et al*. discovered that Nrf2 undergoes translocational oscillations between the cytoplasm and the nucleus and this is associated with a stress-stimulated cytoprotective response which suggests that the stimulation of Nrf2 improves treatment of disease with current therapy (Xue *et al.*, 2015). Glo1 may contribute to both acquired and innate MDR but the degree of resistance is dependent on the types of chemotherapeutic agents (Rabbani and Thornalley, 2011a).

High Glo1 expression was discovered in hepatocellular carcinoma (HCC) where there was a low prevalence of GLO1 gene amplification (6%) which emphasises that increased expression of Nrf2 may cause high Glo1 expression reducing survival (Zhang *et al*., 2015; Thornalley *et al*., 2009). Nevertheless, despite there were recent advances in the modalities of treatment, HCC still has chemotherapeutic resistance (Hollebecque *et al.,* 2015).

Glo1-linked MDR was at first studied by Ranganathan *et al.* using fibroblasts as a model and they discovered that resistance increased to the anti-cancer drugs doxorubicin and mitomycin C (Ranganathan *et al.,* 1995). Tsuruo *et al*. also observed that Glo1 overexpression caused MDR in leukaemia cells. The DNA segment amplified in tumour GLO1 amplification was larger than in low level duplication in the healthy population (Shafie *et al*., 2014). However, Glo1 inhibitor improved the effectiveness of treatment for Glo1-mediated MDR tumour cell lines and tumour-bearing mice (Sakamoto *et al*., 2000; Hosoda *et al*., 2015; Santarius *et al*., 2010; Sakamoto *et al*., 2001). This indicates that current anti-

cancer drugs increase the cellular concentration of MG and cytotoxicity as part of their mechanism. This can be through directly inhibiting the expression and the modification by MG of the Mitochondrial Permeable Transition Pore (mtPTP) - Figure 9. mtPTP is a non-specific channel that resides in the inner mitochondrial membrane and translocates <1.5 kDa such as cyclophilin D and VDAC contributing to the formation of mtPTP (Rabbani *et al*., 2018; Vianello *et al*.,2012). MG modification of mtPTP stimulates the release of cytochrome c from mitochondria (Speer *et al*., 2003; Thornalley and Rabbani, 2011c). The third cell death mechanism induced by MG is the modification of DNA which causes DNA strand breaks resulting in replicative stress and caspase 2 induced apoptosis – "replication catastrophe" (Rabbani *et al.*, 2018).

Another study revealed that MG-induced apoptosis prevented proliferation, migration and invasion of colon cancer cells by down-regulating c-Myc protein. Consequently, this lowered glucose consumption, lactate, and ATP production and lowered c-Myc protein levels. This emphasises the anti-tumour role of MG in colon cancers (Du *et al*., 2000; Taniguchi *et al*. 2012).

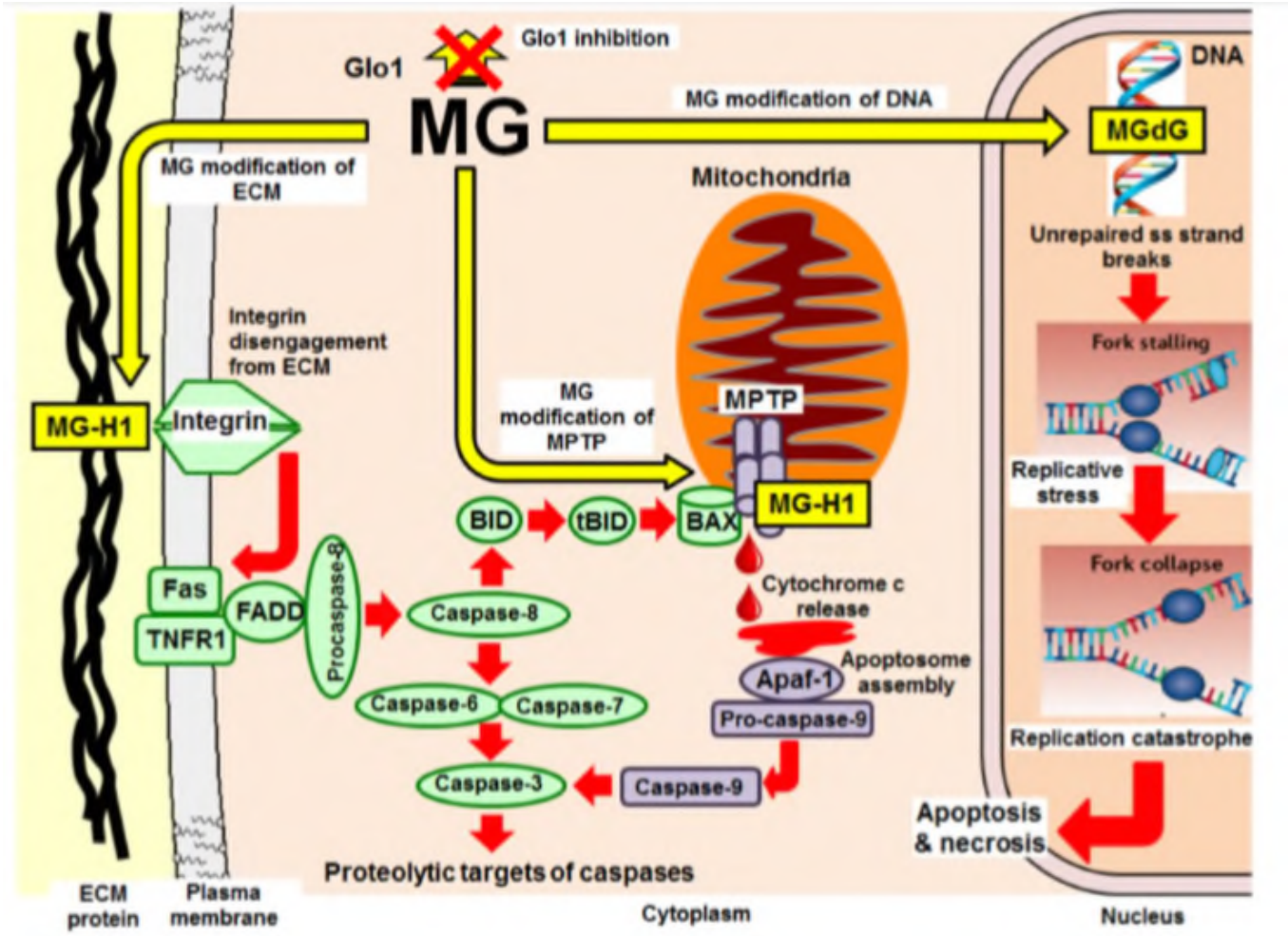

Figure 9: Cell death mechanisms stimulated by methylglyoxal (Rabbani *et al.*, 2017)

High levels of methyglyoxal can induce apoptosis, necrosis, and anoikis. There are three main mechanisms: the modification of the extracellular matrix (ECM), the modification of the mitochondrial permeable transition pore (MPTP) and the modification of DNA.

1.3.6 Therapeutic approaches to Glo1-linked MDR

1.3.6.1 Anti-tumour activity of glyoxalase 1 inhibitors

Vince and Wadd first proposed that inhibition of Glo1 might also lead to increased endogenous MG to cytotoxic levels and Glo1 inhibitors as a potential new class of anticancer therapeutic agents (Vince and Wadd, 1969). Their initial design of Glo1 inhibitors was based on GSH conjugates which were Glo1 substrate analogues. A prototype Glo1 inhibitor was S-p-bromobenzylglutathione; K_i for human Glo1 = 160 nM (Allen *et al.*, 1993b; Vince *et al.*, 1971). GSH conjugates have poor cell permeability and are unstable to cleavage by γ-glutamyl transferase on the cell surface and extracellular fluid.

These barriers to Glo1 inhibitor development were solved by Lo and Thornalley (1992) where cell permeability was facilitated and stability to γ-glutamyl transferase acquired by diesterification of GSH conjugate inhibitors. GSH conjugate diesters are prodrugs of Glo1 inhibitor and when delivered to the tumour, the ester groups were removed by non-specific esterases and the Glo1 inhibitor revealed. This led to the first evidence of potent antitumour activity of a Glo1 inhibitor prodrug *in vitro* and *in vivo* illustrated in Figure 10 (Lo and Thornalley, 1992; Thornalley *et al.*, 1996). The optimum ester derivative was *S-p*-bromobenzylglutathione cyclopentyl diester SpBrBzGSHCp2 (Thornalley *et al.*, 1996). SpBrBzGSHCp2 had antitumour activity *in vitro* and *in vivo* and lifted multidrug resistance against tumours with high Glo1 expression. SpBrBzGSHCp2 remains today the most effective treatment for some experimental MDR tumors in mice (Sakamoto *et al.*, 2001; Thornalley *et al.*, 1996).

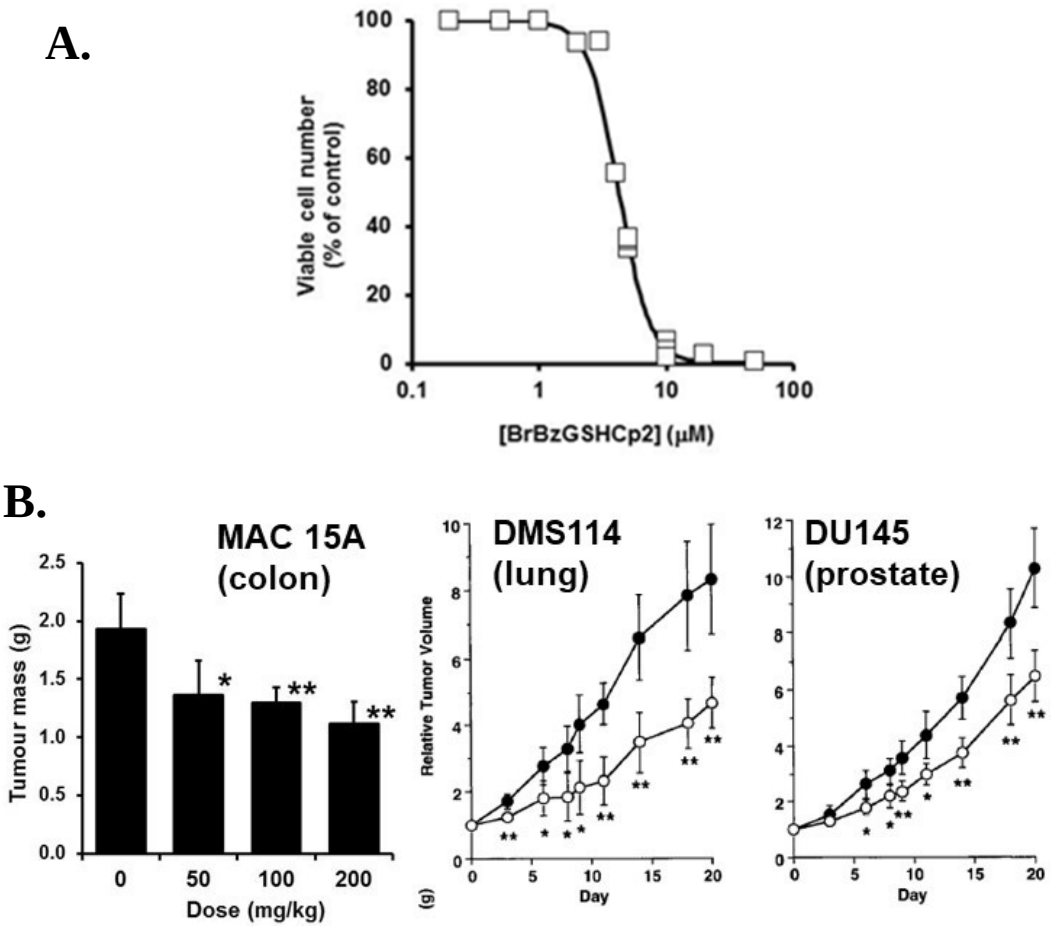

Figure 10: Experimental studies determining the effect of Glo1 inhibitor in *in vitro* and *in vivo* studies. (A) Inhibition of human leukaemia 60 cell growth by the cell-permeable Glo1 inhibitor prodrug, SpBrBzGSHCp2. The viable cell number (percentage of control %) decreases as the concentration of the Glo1 inhibitor increases. The most significant effect was with 200 mg/kg of the Glo1 inhibitor in comparison to the control. (B) Murine mouse models: MAC15A (colon), DMS114 (lung) and DU145 (prostate). MAC15A illustrates that as the dose of the Glo1 inhibitor (mg/kg) increases, the tumour mass decreases whereas for DMS114 and DU145 illustrate that the relative tumour volume increases as the duration of the incubation with the Glo1 inhibitor increases. The relative tumour volume can be determined by multiplying the absolute tumour volume of the respective tumour on the day by the absolute tumour volume of the same tumour on the baseline when the treatment was initiated. (Thornalley *et al.* 1996; Sakamoto *et al.* 2001).

Further developments of substrate analogue Glo1 inhibitors produced S-(N-aryl-N-hydroxycarbamoyl) glutathione and hydroxamate derivatives,

including bivalent inhibitors – two substrate analogue inhibitors with a linker structure where the inhibitor binds to both of the two active sites of Glo1. The most potent inhibitor of Glo1 has an inhibitor constant K_i values of 0.96 nM for human Glo1 (More and Vince, 2009; Murthy *et al.*, 1994; Zheng and Creighton, 2003). These inhibitors are based on the glutathione peptide backbone and hence require pro-drug ester modification for delivery into tumour cells and tissue. Delivery of the prodrug inhibitors is potentially impaired by plasma non-specific esterase where the essential prodrug modification maybe removed prior to tissue delivery.

Creighton and co-workers made the critical observation that plasma esterase activity of in-bred strains of laboratory mice have markedly higher plasma esterase activity than in human serum such that the half-life of S-(N-p-chlorobenzyl-N-hydroxycarbamoyl) glutathione ethyl diesters was *ca.* 9 h in human plasma but < 30 s in serum samples obtained from inbred strains of laboratory mice used to evaluate chemotherapeutic agents against murine tumours. Fortunately, esterase deficient DBA/2 C57BL/6 mice were identified that could be used for appropriate evaluation of these prodrugs. Potent anti-tumour activity *in vivo* of Glo1 inhibitor prodrugs was thereby achieved (Cameron *et al.*, 1999; Sharkey *et al.*, 2000).

Some other compounds have been claimed to be Glo1 inhibitors – such as methotrexate (K_i = 20 μM) and curcumin (K_i = 5.1 μM) (Bartyik *et al.*, 2004; Santel *et al.*, 2008). However, this is *ca.* 120 and 30-fold less potent than BrBzGSH. Peak plasma concentrations of methotrexate are *ca.* 16 μM in cancer chemotherapeutic use, so some anti-tumour activity of methotrexate may be linked to inhibition of Glo1. Extremely high doses of curcumin, 8 g per day, achieved peak plasma concentrations of *ca.* 1.8 μM and it is unlikely to provide potent inhibition of Glo1 *in vivo* (Cheng *et al.*, 2001; Widemann and Adamson, 2006). Delphinidin is a dietary anthocyanidin that is found in berry fruits and was found to inhibit human Glo1 (Ki = *ca.* 280 nM) but was *ca.* 10-fold less potent than SpBrBzGSHCp2 against HL60 cells *in vitro* (Takasawa *et al.*, 2010). Troglitazone inhibited Glo1 (Ki = *ca.* 8 μM) but peak plasma concentrations *in vivo* were only *ca.* 4 μM; suggesting this too is unlikely to be an effective Glo1 inhibitor (Loi *et al.*, 1999; Wu *et al.*, 2001). Anti-cancer drugs showing little

Glo1-mediated MDR are likely an optimum choice for tumours with high Glo1 expression (Thornalley and Rabbani, 2011b; Thornalley and Rabbani, 2011c).

Despite cell permeability of SpBrBzGSHCp2, relatively high doses (50-200 mg/kg) were required for antitumour activity in mice. This may have been due to the high esterase activity of mice – not present in human subjects. MG is metabolised by AKR enzymes that have been upregulated by Nrf2 and this causes overactivation in tumours (Rabbani *et al*., 2017). They are highly expressed in adenocarcinomas and there is evidence that AKR activity influences its potency (Rabbani *et al*., 2018). Moreover, there are some tumour cell lines that are resistant to Glo1 inhibitor and some are sensitive. A recent study discovered that there are Nrf2 activators that induce the expression of Glo1, AKR and dehydrogenase enhances to increase MG metabolism (Chen *et al.,* 2012).

1.3.6.2 Anti-tumour activity by silencing Glo1 by siRNA.

Small interfering ribonucleic acid (siRNA) is non-coding double-stranded RNA molecule that consists of 21-23 nucleotides with the 3′ two-nucleotide extended (Lam *et al.*, 2015). It is formed by the processing and cleavage of the long double-stranded RNA mediated by the enzyme RNase III-like enzyme Dicer (McNamara *et al.*, 2006; Dana *et al.* 2017). It is a potential therapeutic target due to its ability to evade specific genes in the treatment of cancer and other diseases (Dana *et al.* 2017). It has also been utilized as a tool to investigate the function of single genes *in vivo* and *in vitro*.

The siRNA can enter the cytoplasm where it directly associates with the multiprotein component complex called RNA induced silencing complex (RISC) (Hammond *et al.,* 2000). The RISC protein is part of the argonaute family (Ago2) (Meister *et al.,* 2004). The siRNA strands are separated where the strand with a stable 5'-end is incorporated into the RISC complex whereas the passenger strand leaves. The RNA interference is initiated by the anti-sense single-stranded siRNA that aligns and cleaves the target mRNA via the catalytic mechanism of the RISC protein causing degradation (Zamore *et al.,* 2000). The siRNA-RISC complex has also been linked with the nucleolus region where it can enter or leave the nucleus (Dana *et al.* 2017).

Previous studies have shown that GLO1 silencing can increase the concentration of MG and increase cell sensitivity to chemotherapeutic agents (Chen *et al*. 2017; Sakamoto *et al.* 2000; Hutschenreuther *et al*., 2016). This, in turn, increases anti-proliferative, apoptotic, and oxidative stress-induced effects (Bair *et al.* 2010, Xue *et al*., 2017). Chen *et al.* revealed that a combination of MG with GLO1 silencing further increases the synergistic inhibitory effect on cell viability and proliferation (Chen *et al*. 2017). This can be achieved through increased expression of the tumour suppressor signal transducer and activator of transcription 1 (STAT1) and the proapoptotic protein Bcl-2-associated X (Bax) and the reduction in the level of the enzyme metalloproteinase 9 (MMP9) and the B-cell lymphoma protein-2 (Bcl-2) where the latter consists of anti-apoptotic and pro-apoptotic proteins that modulate the cell cycle (Chen *et al.* 2017; Guo *et al.*, 2016). Bcl-2 plays a major role in regulating the intrinsic apoptotic pathway particularly in the mitochondrial release of cytochrome C and its ability to associate with Apaf-1 via the interaction with Bax (Guo *et al.* 2016). Moreover, Braun *et al.* revealed that the increased level of methylglyoxal that downregulate migration and invasion depend on the 53 kDa phosphoprotein, p53 (Braun *et al.* 2019; Berkers *et al*. 2013).

Moreover, recent studies have suggested that miRNAs also have a role in how Glo1 silencing can inhibit tumour progression. For instance, high levels of miR-137 can decrease the endogenous expression of GLO1 causing anti-proliferative effects in melanoma (Lv *et al.*, 2018).

1.3.6.3 Glo1 inducers

Dietary bioactive compounds were screened for their ability to induce expression of Glo1 or “Glo1 inducer” activity. The optimum Glo1 inducer was composed of two compounds: *trans*-resveratrol and hesperetin. Trans-Resveratol is a natural polyphenol found naturally in red grapes (Shakibaei *et al*., 2009). Its structure has 2 aromatic rings associated with methylene bridge and has trans isomers (Baur and Sinclair, 2006). Hesperetin is a flavanone that is naturally found in lemons, oranges and citrus fruits and could be used for natural traditional remedies (Khan *et al.,* 2014; Bai *et al.* 2016). The suggested mechanism of action involves anti-inflammatory activity – Figure 11. Clinical treatment with the Glo1 inducer decreased expression of RAGE in healthy human subjects (Xue *et al*., 2016). Decreased expression of RAGE may decrease tumour development, growth and metastasis which may also contribute to a cancer chemopreventive response (Taguchi et al., 2000).

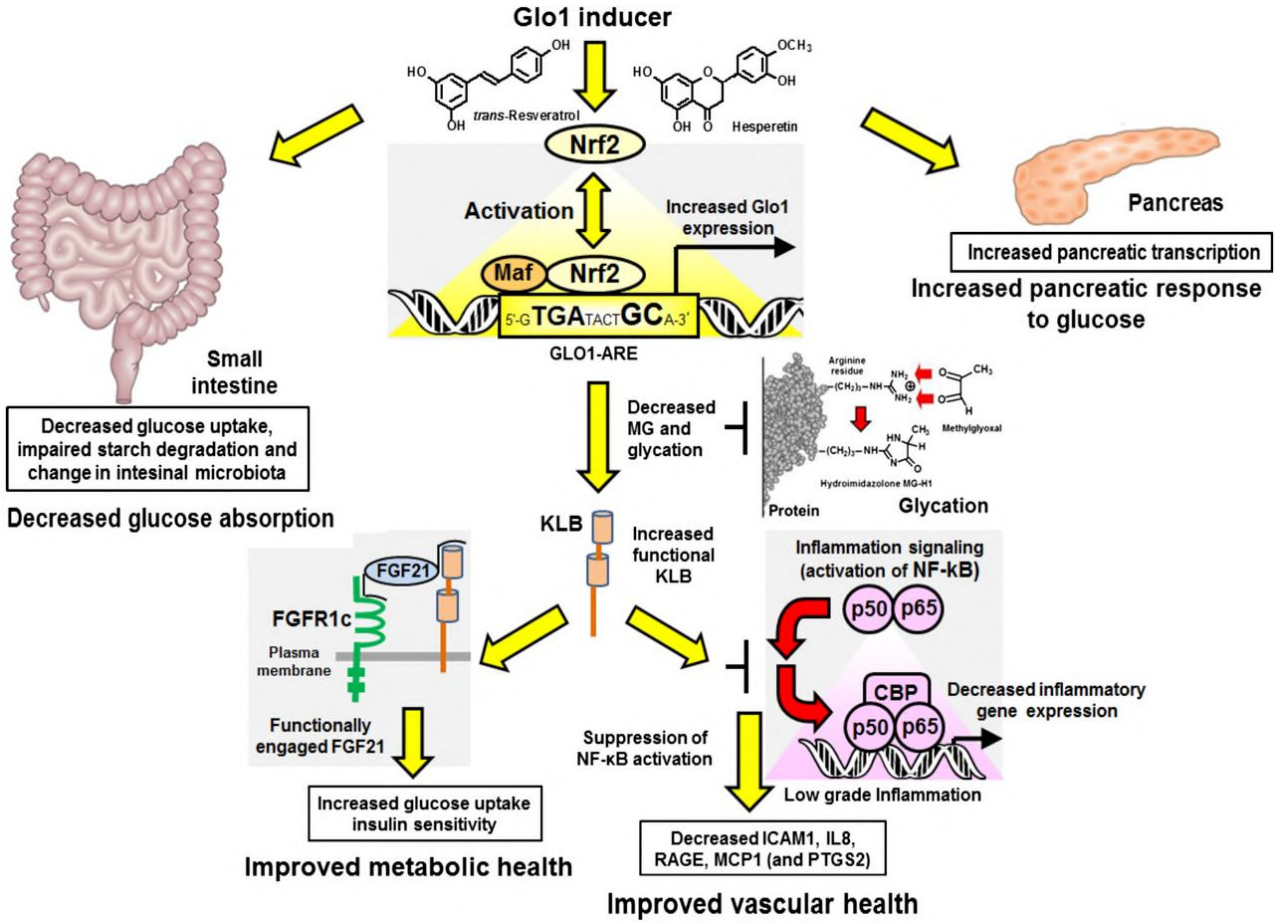

Figure 11: The role of Glo1 inducer in cancer and diabetes (Xue *et al.* 2016).

Glo1 inducer has a chemopreventative effect in non-malignant states where it can decrease the expression of RAGE which influences AGEs. Yellow and red arrows reflect improvements of health and suppression of damaging mechanisms respectively.

Moreover, resveratrol increases the cytotoxicity of anti-cancer drugs and this has been demonstrated through doxorubicin (Mitani *et al*., 2014). Under hypoxic conditions, MCF-7 breast cancer cells acquire doxorubicin-resistance and at a concentration of 10 µM, Mitani *et al.* discovered that resveratrol and one of its derivative 3,5-dihydroxy-4'-methoxy-trans-stilbene can alleviate this resistance (Mitani *et al*., 2014).

1.4 Glyoxalase 2

1.4.1 Structure

Human Glo2 is a monomeric zinc thiolesterase that consists of two major isoforms: mitochondrial Glo2 with a molecular mass of 33,806 Da and the cytosolic Glo2 with a molecular mass of 29, 200 Da (Xue *et al.*, 2011). The pI in both isoforms was 8.3 (Xue *et al*., 2011). Cytosolic Glo2 is composed of two domains: N-terminal that contains 1-173 amino acids and the C-terminal consist of 174-260 residues that are folded into five alpha helices (Cameron *et al*., 1999). It is a four-layered beta sandwich with two mixed β-sheets that is flanked with an α-helical domain and resembles that of metallo-β-lactamases (Cameron *et al.*, 1999; Xue *et al.*, 2011). The topology of the first half of the sandwich has a βββαβαββ whereas the second half is aligned at 20° to the first and consists of a βββββαβ unit. The βββββαβ motif from the two halves: β1β2β3α1β4 and β8β9β10α3β11 can be overlaid by a two-fold rotation. The residues 136-141 reside directly after β10 to create a β hairpin at 80° to the direction of β10. This is a fragment of an extended loop structure that is not present in the N-terminal half of the sandwich (Xue *et al*., 2011).

The active site of Glo2 contains the substrate binding site that spreads over the domain interface and binuclear metal ion-binding location (Cameron *et al*., 1999; Limphong *et al*., 2009; Xue *et al*., 2011). There are two metal ion binding sites that contain iron and zinc (Xue *et al*., 2011). The zinc site is a vital factor for the structure of the protein and the catalytic activity-substrate hydrolysis. The first metal-binding site consists of three conserved histidine residues linking water/hydroxide with aspartic acid. The second metal binding site contains two histidines that associate water/hydroxide ions that are fused with the water; these bounds terminally to aspartic acid and an associated aspartic acid

(Limphong *et al*., 2009). Besides, there is a hydroxide ion arranged to both metal ions and reside 2.9˚A from the carbonyl carbon of the substrate and acts as a nucleophile during catalysis (Xue *et al*., 2011). Moreover, there are several amino acids in the active site: lysine, arginine and histidine based on the chemical modification of Glo2 (Dragani *et al*., 1999).

The activity of Glo2 mainly takes place in the cytosol where it accounts 85-90%. The mitochondrial Glo2 does not play a major role in MG detoxification even when overexpressed (Cordell *et al.*, 2004). Therefore, MG and S-D-lactoylglutathione are produced in the cytosol where glycolysis takes place. However, there is a possibility that the mitochondrial Glo2 is involved in the regulation of the redox state because mitochondria are where ROS are mainly produced (Cordell *et al.*, 2004). Moreover, Rabbani *et al.* suggested it may play a role in hydrolysing S-acyl glutathione esters in mitochondria formed during the acyl exchange from acyl-CoA to GSH (Rabbani *et al*., 2014; Rabbani and Thornalley, 2015).

1.4.2 Genetics and Polymorphisms

HAGH (hydroxyacylglutathione hydrolase) is the gene for human Glo2 (Thornalley, 1990). It is localized on chromosome 16p13.3 (Xue *et al*., 2011). Genetic polymorphisms are rare and two genotypes are known: HAGH1 and HAGH2 (Allen *et al.*, 1993a; Thornalley, 1990). HAGH consists of 10 exons which are transcribed to dual distinct mRNA species from 9 and 10 exons that vary in function (Thornalley, 1993; Xue *et al*., 2011; Shafie *et al*., 2014). The 10-exon-derived transcript compromises of a termination codon between two initiating AUG codons and encodes the cytosolic form of Glo2 whereas the 9-exon-derived transcript encodes both the cytosolic and mitochondrial types whereby the AUG codon in the mRNA sequence initiates Glo2 to target mitochondria. On the other hand, the cytosolic Glo2 starts by the entry of the internal ribosome entry at a downstream AUG codon (Xue *et al*., 2011, Cordell *et al*., 2004, Choudhary *et al*. 2009).

1.4.3 Substrate specificity

Glo2 has broad substrate specificity for glutathione thiol esters, particularly S-2-hydroxyacylglutathione derivatives (Xue *et al.*, 2011). The glutathione moiety is tightly linked to the protein via glycine and cysteine residues. The γ-glutamyl does not interact with the protein. This varies with what has been observed in Glo1, whereby in the same ligand, the γ-glutamyl and glycine residues are involved in hydrogen-bonding interactions with the protein. The three basic residues that are in proximity to the carboxylate group of glycine: Lys-143, Lys-252 and Arg-249 (Rabbani and Thornalley, 2012b; Xue *et al.*, 2011). Lys-252 and Arg-249 form part of the α-helix of the second domain and within the range of the hydrogen-bonding distance of the carboxylate (Xue *et al.*, 2011). In addition, other hydrogen-bonding interactions solidify Arg-249 into a position whereby the carboxylate of Asp-253 and the carbonyl oxygen of Cys-141 is situated on the hairpin (Cameron *et al.*, 1999).

1.4.4 Enzyme Kinetics

Glo2 catalyses the hydrolysis of S-D-lactoylglutathione to GSH and D-lactate. The K_m is 146 M and the k_{cat} value is 727s^{-1} (Xue *et al.*, 2011). Glo2 is an efficient enzyme; the k_{cat}/K_m value is close to the diffusion limit using S-D-lactoylglutathione as the substrate (Cameron *et al.*, 1999). It has a broad optimum pH as Glo2 is isolated from human liver and have shown no difference in activity between the ranges 6.8 and 7.5 (Xue *et al.*, 2011). The catalytic mechanism involves a nucleophilic attack on C1 atom of the substrate by the active site bound water molecule (which has a low pKa value) (Xue *et al.*, 2011). The product is then formed by hydrolysing the C-S bond (Wendler *et al.*, 2009; Xue *et al.*, 2011; Cameron *et al.* 1999).

1.4.5 Glyoxalase 2 and its association with cancer

Despite the focus of the project is related to the role of Glo1 overexpression in multidrug resistance in cancer chemotherapy, it is important to highlight the role of Glo2 in tumours because it hydrolyses S-D-lactoylglutathione to the less toxic D-lactate (Martins *et al.*, 2001). Moreover, the regeneration of GSH from the oxidized glutathione produced from Glo1-catalysed reaction maintains the redox state within the cell. This represents a critical step in cellular defence against MG toxicity (Thornalley, 2008).

Xu and Chen (2006) revealed that Glo2 is a novel target of the transcription factors p63 and p73. Both p63 and p73 share a similar structural homology with the tumour suppressor p53 and can bind to p53 responsive element to activate some of its target genes such as mouse double minute 2 (MDM2), p21, DNA polymerase Eta (POLH) and ferredoxin reductase (FDXR) that aid in the development of cells (Harms *et al.*, 2004; El-Deiry *et al.*, 1993; Wu *et al.*, 1993; Liu and Chen, 2002). Mutations of p63 and p73 rarely occur in tumours. It can also upregulate the GLO2 gene by bounding to intron 1 on its gene.

Overexpression of cytosolic Glo2 protects cells from MG-induced cell death by inducing DNA damaged-induced apoptosis in a p53-dependent manner. Godbout *et al.* have shown that knockdown of GLO2 synergistically acts with cisplatin to induce apoptosis (Godbout *et al.*, 2002). This emphasises the association between p53 and the glyoxalase system in the normal development and pathogenesis of various human diseases especially in tumours (Moll and Slade, 2004).

There is evidence that there are high genetic expression and activity of Glo1 and Glo2 in breast and bladder cancer and this is due to the limited supply of oxygen during tumour progression where they increase aerobic glycolysis to produce sufficient energy and maintain balance (Rulli *et al*., 2001; Moll and Slade, 2004).

However, in other tumours, there are high levels of Glo1 but low Glo2 emphasising the role of these enzymes in chemotherapy resistance by decreasing MG. For instance, Antognelli *et al. d*iscovered that there are low levels in kidney

adenocarcinoma which emphasises the role of S-D-glutathione in supplying energy in high proliferating cells. It also highlights the importance of Glo1 inhibitors as anti-tumour drugs (Antognelli *et al.* 2006).

Ngyuen *et al.* revealed that Glo2 correlates with redox signalling and increases expression of oxidative genes, for instance, catalase, nicotinamide nucleotide transhydrogenase, hydroxyacid oxidase 1, hydroxyacid oxidase 2, paraoxonase 1, paraoxonase, epoxide hydrolase 2, arylamine N-acetyltransferase 1 and glutaredoxin. This suggests the significant role of Glo2 in hepatocellular carcinoma progression where elevated levels increase better clinical survival outcomes and is a potential prognostic marker of precision medicine and potential therapeutic target in its treatments (Ngyuyen *et al.* 2018).

Antognelli and Talesa (2018) revealed that Glo1 and Glo2 maintain the metastatic phenotype non-enzymatically in some malignant tumours via PTEN/PI3K/Akt/mTOR pathway involving pyruvate kinase isozymes M1/M2 (PKM2) and oestrogen receptor-alpha (ERα). Therefore, Glo1 silencing and the Glo2 ectopic expression (pCMV-GLO2) are needed to maintain migration, invasion and EMT (Antognelli and Talesa, 2018). Recent studies have suggested that Oleuropein, a bioactive plant-derived compound exhibits anti-tumour activity via the mitochondrial apoptotic pathway by upregulating mitochondrial Glo2 that is stimulated by the superoxide anion and the Akt signalling pathway by interacting with the proapoptotic protein Bax (Antognelli *et al.* 2019).

1.5 Other putative enzymatic pathways of MG detoxification

Aldehyde dehydrogenases (ADHs) and aldo-keto reductases (AKRs) also metabolise MG to contribute to the enzymatic defence against MG glycation. This prevents the formation of glycation adducts and repair damaged sites caused by early glycation (Allaman *et al*., 2015; Rabbani and Thornalley, 2014b; Thornalley, 2003). Nevertheless, both enzymes have a minor role in their metabolism compared to the glyoxalase system (Rabbani *et al*., 2016a; Rabbani and Thornalley, 2016).

MG is metabolised to hydroxyacetone (95%) and D-lactaldehyde by NADH-dependent aldo-ketoreductase isozyme 1B1 (aldose reductase) (Thornalley, 1994). Both products can then be reduced further by AKR to propanediol. This mechanism was observed using the yeast *Hunsenulu mrakii* as a model. Besides, studies have revealed that Glo1 activity exceeds AKR activity by >30-fold in all human tissues with exception of the renal medulla whereby the AKR expression is advanced (Rabbani *et al*., 2016).

There are two types of dehydrogenases: NAD^+-dependent betaine aldehyde dehydrogenase and $NADP_+$-dependent dehydrogenase which catalyses the oxidation of MG to form pyruvate (Rabbani *et al.* 2014; Rabbani *et al.*, 2016). This mechanism can be observed in the gram-negative bacterium; *Pseudomonas putida* as a model (Allaman *et al*., 2015). The expressions of AKRs, ADH and Glo1 under basal and inducible conditions are regulated by Nrf2 via regulatory AREs (Rabbani *et al*., 2016; Xue *et al*., 2012; Rabbani and Thornalley 2011a). Metabolism of MG and glyoxal by reductase occurs in the renal medulla where the expression of AKR outweighs that of Glo1 (Nishimura *et al.*, 1993).

There is a third type of glyoxalase called glyoxalase III. It is an MG oxidoreductase purified from *Escherichia coli* (Misra *et al*., 1995). Its distinctive functional role is to convert MG to D-lactate without utilizing the GSH cofactor and does not form the intermediate S-D-lactoylglutathione. The specificity constant of glyoxalase III in *E. coli* was discovered to be 7.4×10^8 $M^{-1}min^{-1}$ and this was *ca.*7,000 fold higher than the specificity constant found by Lee *et al.* 1.1×10^5 $M^{-1}min^{-1}$ (Lee *et al*., 2012, Clugston *et al*., 2004). Moreover, another oxidoreductase is DJ-I isoenzymes but has a significantly low specificity *ca.*

10,000-fold less in comparison to human Glo1. The low specific activity emphasises there is a limited role in MG metabolism *in vivo* (Rabbani and Thornalley, 2014b).

1.6 Glyoxalase-related metabolites

1.6.1 Reduced glutathione

The cofactor GSH is a linear tripeptide with a mass of 307 Da and is composed of three amino acids: L-cysteine, glycine and L-glutamate. It is highly abundant in cells and consists of more than 90% total cellular non-protein sulphur (Meister, 1988). The intracellular concentration of GSH is between 0.5 to 10 mM whereas the extracellular level is much lower (Lushchak, 2012).

The concentration of glutathione is high in the liver which is crucial for detoxification and is a natural part of the immune system. The levels of GSH is decreased by oxidative stress and low *in situ* glutathione reductase activity in diabetic patients (Thornalley *et al*., 1996). In the latter, this increases the risk of oxidative damage and glycation mediated by α-oxoaldehydes by lowering the activity of Glo1 (Thornalley *et al*., 1996).

GSH is a pivotal redox agent that is under homeostatic control between its synthesis, recycling and utilization. The formation of GSH consists of two enzymatically-controlled reactions that employ ATP: cysteine and glutamate condense by γ-glutamyl cysteinyl synthetase to form γ-glutamylcysteine**.** This is followed by conversion of γ-glutamylcysteine to GSH, catalysed by GSH synthetase (Franco *et al.,* 2007). The recycling of GSH is catalysed by glutathione reductase where nicotinamide adenine dinucleotide phosphate, reduced form (NADPH) is used to re-convert oxidised disulphide (GSSG) to GSH.

GSH is consumed in many processes, for instance, conjugation, oxidation and hydrolysis (Halliwell and Gutteridge, 1988). It is directly oxidized by ROS and reactive nitrogen species (RNS). It is also indirectly oxidized during the GSH-dependent peroxidase-catalysed reactions (Zhang and Forman, 2009). Conjugation with exogenous and endogenous electrophiles consumes a significant amount of cellular levels of GSH (Zhang and Forman, 2009). Extracellularly, GSH is hydrolysed by γ-glutamyl transpeptidase and the transfer process can

result in the glutamyl moiety of GSH to the peptides and amino acids or the glutamyl functional group to water to produce free glutamate (Zhang and Forman, 2009). As GSH is being consumed, the glutathione redox cycle keeps GSH repleted. γ-glutamyl transpeptidase and cysteinyl-glycine dipeptidase catalyse the degradation of GSH into its amino acid subunits (Griffith, 1999; Meister, 1988; Meister and Anderson, 1983).

The principle biological mechanism of GSH is to protect against ROS, RNS and electrophiles (Lushchak, 2012). GSH is the primary protectant of the skin, retina, lens and cornea against radiation. It has additional functions in the cells such as storing and transporting nitric oxide, facilitates the metabolism for oestrogens, prostaglandins and leukotrienes (Birben *et al*., 2012). It can also be used as a cofactor to detoxify several endogenous compounds and to reduce ribonucleotides to form deoxyribonucleotides (Deponte, 2013; Lushchak, 2012).

1.6.1.1 Reduced glutathione and its association with cancer

The homeostasis of the antioxidant GSH plays a significant role in various cell parameters, for instance, differentiation, proliferation and apoptosis (Balendiran *et al*. 2004). Increased production of GSH and NADPH combats the effects of the relatively elevated levels of oxidative and nitrosative stress which is often linked with chemotherapy-induced apoptosis (Hussain *et al.*, 2003; Cairns *et al.*, 2011; Couto *et al*. 2016). This has been found in various tumours, for instance, liver cancer, melanoma, NSCLC and medulloblastoma, making neoplastic tissues more resistant to chemotherapy (Carretero *et al.* 1999; Marengo *et al.* 2010; Joseph *et al.* 2002; Costantini *et al.* 2000; Yoo *et al*., 2019; Colvin *et al*., 1993). It is caused by high activities of the GSH-associated enzymes, for instance, γ-glutamylcysteine ligase (GCL) and γ-glutamyl-transpeptidase (GGT) and high expression of GSH-transporting export pumps (Estrela *et al.* 2006; O'Brien and Tew, 1996). GSH is effluxed by cells via GGT metabolism and is implied in tumour development (Pompella *et al.* 2007).

One of the chemotherapeutic agents in which GSH mediated resistance against are DNA alkylating agents and nitrogen mustards induce resistance by conjugating with glutathione and this reaction is catalysed by GST (Fujitani *et al.*, 2019). This suggests that the intracellular levels of GSH correlate with tumour

progression and drug resistance (Ballatori *et al*., 2009; Lv *et al*., 2019; Ortega *et al*. 2011). Low intracellular levels of GSH or the fluctuations of the GSH: GSSG ratio can increase susceptibility to oxidative stress and cytotoxicity of several chemotherapeutic agents without increasing toxicity to normal tissues (Lau *et al*., 2008; Russo *et al*., 1986; Hussain *et al*., 2003; Meister 1991).

Several mechanisms have been studied to deplete GSH and increase sensitivity to chemotherapy, for instance inhibiting GCL, buthionine sulfoximine (BSO) and glutathione analogues (Griffith, 1982; Wu and Batist, 2012). Recent studies have discovered that GCL induces depletion of GSH at a transcriptional level where Nrf2 binds to the ARE in the promoter region of genes encoded by GCL and GST (Yoo *et al*., 2019; Nguyen *et al*. 2009; Maher *et al*. 2007).

1.6.2 S-D-Lactoylglutathione

In the biological systems, S-D-lactoylglutathione is the physiological intermediate of the glyoxalase system (McLellan *et al*., 1993). It is synthesised endogenously from MG and GSH by Glo1 and is then metabolised to D-Lactate and GSH by Glo2 (Xue *et al*., 2011). The location of S-D-lactoylglutathione is restricted to the cytosol. This is due to S-D-lactoylglutathione incapable of crossing the biological membranes (McLellan *et al*., 1993).

S-D-lactoylglutathione is metabolised by three enzymes: thiolesterases, γ-glutamyl transferases and dipeptidases. Glo1 hydrolyses S-D-lactoylglutathione to GSH and D-lactate. However, when S-D-lactoylglutathione is in the extracellular compartment, γ-glutamyltransferase cleaves S-D-lactoylglutathione to S-D-lacoylcysteineylglycine. S-D-lactoylcysteinylglycine is then spontaneously rearranged to N-D-lactoylcysteinylglycine (Tate, 1975; Thornalley and Tisdale, 1988).

N-D-lactoylcysteine inhibits the synthesis of pyrimidines by preventing dihydro-oratase (Edwards *et al*., 1993, Edwards *et al*., 1996). The addition of exogeneous S-D-lactoylglutathione to human leukaemia cells, HL-60 cells results in cytotoxicity, growth arrest and preventing the synthesis of DNA where the growth inhibitory concentration (GC_{50}) was 82 and 72 µM respectively (Thornalley and Tisdale, 1988). It was discovered that the quantity of cells in G_0-G_1 phase was relatively higher than that of G_2-M phase (Hooper *et al*., 1987;

Hooper *et al.*, 1988). This cytotoxic effect was not observed with GSH, D-lactate and a combination of both. The inhibitory effect of S-D-lactoylglutathione on proliferation is stimulated by the prevention of uridylate synthesis (Edwards and Thornalley, 1994).

1.6.3 D-Lactate

There are two major stereoisomers of lactate formed in the human intermediary metabolism: D-Lactate and L-Lactate – Figure 12. The concentration of L-lactate is efficiently metabolised in humans and has higher fractional renal clearance than L-lactate (Connor *et al*.,1983). It is permeable to cell membranes through the inorganic anion transporter, specific lactate transporter and passive diffusion of unionised conjugate acid (Oh *et al*., 1985). D-Lactate is produced from the detoxification of methylglyoxal via the glyoxalase system in erythrocytes and is a measure of the flux of formation of MG in red blood cells and lens fibre cells (Phillips and Thornalley, 1993; Ranganathan *et al*. 1995). The concentration of D-lactate in the blood of normal healthy patients is 11.0 +/- 1.2 (mean +/- SE nmol/ml) whereas in diabetic patients there is a significant increase 20.0 +/- 1.3 (mean +/- SE nmol/ml) (McLellan *et al*., 1992a). The D-lactate concentration in plasma of healthy controls is 2 – 20 µM (De Vrese and Barth, 1991; McLellan *et al*., 1992a).

D-lactate can also be ingested in yoghurt and absorbed from the gut flora (Ohmori and Iwamoto, 1988; Mortensen *et al.*, 1991). The metabolism of D-lactate to pyruvate is via the 2-hydroxyacid dehydrogenase; a mitochondrial FAD-linked enzyme (Ohmori and Iwamoto, 1988; Phillips and Thornalley, 1993).

D-Lactate can be quantitatively measured by fluorescent end-point enzymatic assay and reverse phase high phase liquid chromatography (HPLC). The assay method comprises measuring the concentration by the production of NADH linked to the oxidation of D-lactate to pyruvate using the enzyme D-lactic dehydrogenase (McLellan *et al*., 1992a). In the HPLC method, D-Lactate is measured by the derivatization of pyruvate with 1,2-diaminobenzene (Ohmori *et al*., 1991).

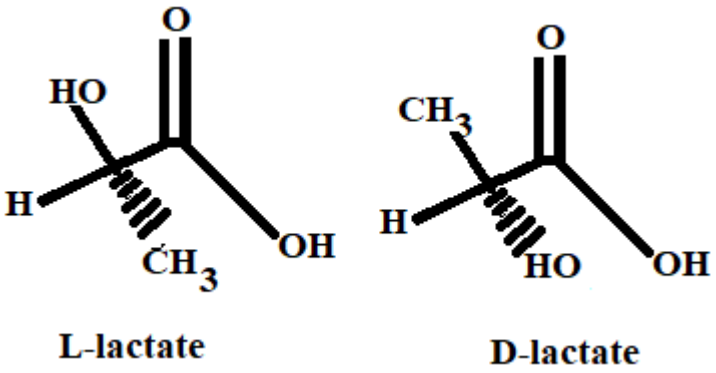

Figure 12 - Optical forms of lactate: L (+) and D (−) lactate. (Adapted from Lipsa *et al.* 2010). Lactic acid is chiral and has two optically active isomers. The two enantiomers are D-lactate and L-lactate and can be produced by fermentation from pyruvate via the enzyme lactate dehydrogenase. The other product from the reaction is NAD which is utilized in glycolysis to produce ATP.

1.6.3.1 The association of D-Lactate with cancer

Tumours have been associated with the dysregulation of glucose metabolism which increases the uptake of glucose and cause alterations in the metabolic fluxes where there is an increase in the conversion rate from pyruvate into lactate; this is known as the Warburg effect (Romero-Garcia *et al.,* 2016; Wu *et al.*, 2016). Both lactate and pyruvate are utilised by tumour cells to undergo Kreb's cycle and oxidative phosphorylation to increase the production of ATP, proliferation and the survival rate of the malignantly transformed cells (Pavlides *et al.*, 2012). This aids in the prognosis of patients with various tumours (Yao *et al.*, 2014). For instance, overexpression of LDH5 increases the risk of mortality by 60% emphasising poor clinical survival outcomes, more proliferation and advanced Tumour Node Metastasis (TNM) staging in patients with breast cancer (Huang *et al.* 2016a). Similar reports have been discovered in patients with cancers of the stomach, bladder, pancreas, colon and kidney (Sun *et al.,* 2015; Koukourakis *et al.*, 2016; Mohammad *et al.*, 2016; Koukourakis *et al.*, 2011; Girgis *et al.*, 2014).

Lactate is a monocarboxylate and it undergoes proton-associated transport alongside lactate and ketone bodies across the plasma membrane and into cells (Simchowitz and Textor, 1992). This is catalysed by monocarboxylate transporters (MCTs) that reside on the plasma membrane, for instance, neutrophils, tumour cells and erythrocytes (Halestrap, 2012; Simchowitz and Textor, 1992). MCTs have

distinctive affinities for substrates which influences the efflux and influx rate of lactate (Halestrap, 2012). MCT1 has low expression and is primarily involved in the importation of lactate. MCT2 is expressed in the neurons, kidney, and liver whereas MCT3 is found at the choroid plexus and the basolateral retinal pigment epithelium (Halestrap, 2012). MCT4 is primarily involved in the exportation of lactate and is expressed in the white skeletal muscle. Low levels of MCT4 can be found in the lungs, testis, placenta, leukocytes and glial cells such as astrocytes (Halestrap, 2012). Several tumours have been associated with the increased expression of MCT1 whereas MCT4 is linked with tumours associated with poor prognosis (Pinheiro *et al*. 2008).

Another factor that influences lactate secretion besides the substrate is the pH (Dimmer *et al*., 2000). The Warburg effect decreases the extracellular pH to 6.0 - 6.5 (Xie *et al*., 2014). Lactate can increase vascular endothelial growth factor (VEGF) signalling pathway via MCT1 and autocrine angiogenesis under normoxic conditions which can trigger the phosphorylation and degradation of I-kappa-B-alpha (IKB-alpha) stimulating the nuclear factor kappaB (NF-KBa)/interleukin 8 (IL-8) causing T-cell dysfunction and immunosuppression (van der Mijn *et al*., 2017; Goodwin *et al*., 2019; Fischer *et al*., 2007; Hunt *et al*., 2007; Vegran *et al*., 2011; Fukumura *et al*., 2001; Shi *et al.,* 2000). Lactic acidosis can also increase metastasis by increasing the production of MM9 (Kato *et al*., 2007; Wu *et al*., 2012).

1.6.4 Dicarbonyls

Dicarbonyl compounds such as α-oxoaldehydes are reactive intermediates and saccharide derivatives of the Maillard reaction to form AGES on functional arginine residues (Ahmed *et al*. 2008; Thornalley, 2005). The interrelationship between the degradation of glucose to form α-oxoaldehydes was discovered by Pinkus in 1898. This led to further developments in understanding their quantitative and functional role in the physiological systems. It is important to note that the α-oxoaldehydes are 20,000-fold more reactive than glucose to produce AGEs (Rabbani and Thornalley, 2008b; Thornalley, 2005). However, the concentration of dicarbonyl compounds in the physiological systems is 10,000 - 50,000 times lower than glucose (Thornalley, 2005).

The three main dicarbonyls are glyoxal, MG and 3-DG presented in Figure 13. The most reactive dicarbonyl that has a relatively high flux of formation *in vivo* and *in vitro* is MG which causes arginine-directed glycation to form AGEs (Ahmed, 2005; Thornalley 2005). For instance, the glycation of mitochondrial proteins induces damage by nitration and oxidation (Pun and Murphy, 2012; Thornalley, 2008; Thornalley and Rabbani, 2011a; Thornalley and Rabbani, 2011b).

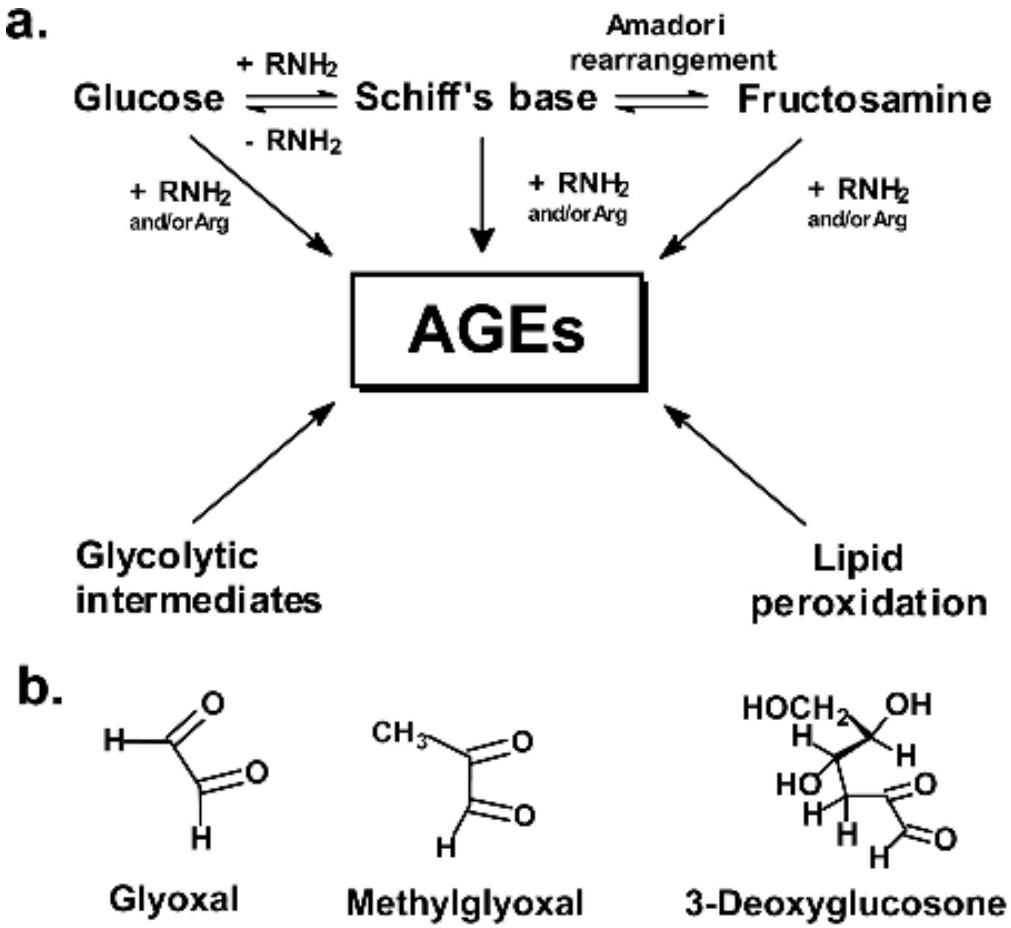

Figure 13: The Maillard Reaction and Physiological dicarbonyl metabolites (Rabbani and Thornalley, 2008a).

A. the Maillaird chemical reaction. B. Dicarbonyls. The Maillard reaction is a non-enzymatic reaction that increases the production of AGEs that contribute to ageing and the pathogenesis of diseases.

1.6.4.1 Advanced Glycation End-products (AGEs)

AGEs are a heterogenous group of compounds. AGEs are formed by the degradation of fructosamine-modified proteins and also by the glycation of proteins by dicarbonyls. Proteins susceptible to glycation by dicarbonyls are called the 'dicarbonyl proteome' (DCP) (Thornalley *et al*., 2003; Rabbani and Thornalley, 2008b). Protein damage *in vivo* are caused by early glycation – forming fructosamines, advanced glycation - forming AGEs, oxidation and nitration in the physiological systems – Figure 14. They are increased in many pathological conditions: diabetes, renal failure, arthritis, and other diseases and ageing (Beechtold *et al*., 2009; Geoffrion *et al*., 2014; Rabbani and Thornalley, 2008c; Rabbani and Thornalley, 2009; Thornalley and Rabbani, 2014b; Rabbani *et al*., 2016; Sparvero *et al*. 2009; Waris *et al*., 2015)**.**

An example of an early-stage glycation adduct is Nε-(1-deoxy-D-fructos-1yl) lysine (FL). It is formed from glucose and increases the concentration of glucose. Fructosamine 3-phosphokinase repairs this intracellularly (Rabbani and Thornalley, 2008b; Thornalley and Rabbani, 2014b). Methionine sulphoxide is an example of an oxidation adduct. It is formed by exposing to hydrogen peroxide, peroxynitrite and hypochlorite (Thornalley and Rabbani, 2014b).

Other AGEs are also formed in physiologically systems from lysine but limitedly: Nε(1-carboxyethyl)lysine (CEL) and Nε-carboxymethyl-lysine (CML) from MG and glyoxal, respectively. CML is mainly formed by the oxidative degradation of FL (Masania *et al*., 2016; Rabbani *et al*., 2016b). There are also bis(lysyl) crosslinks: MOLD and GOLD, and trace level formation of fluorescent AGEs – pentosidine and argpyrimidine (Rabbani and Thornalley, 2014b; Thornalley, 2008).

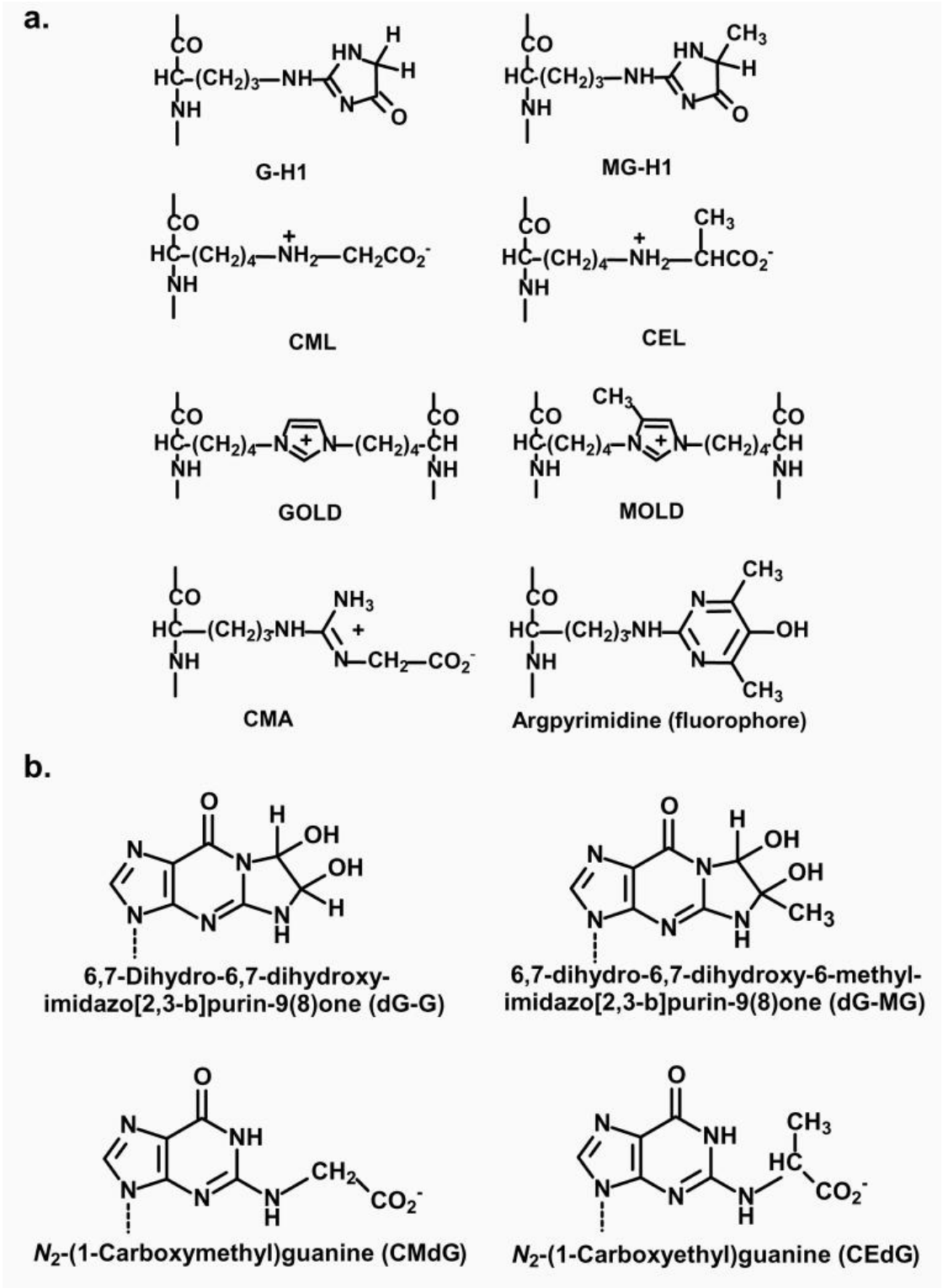

Figure 14 The advanced glycation end-products formed from protein and DNA glycation by glyoxal and methylglyoxal (Thornalley, 2008). A. protein-derived AGEs with a peptide backbone. B. DNA-derived AGEs with modifications in a nucleic acid base with the 3-(2′-deoxyribosyl) moiety.

1.6.4.2 Quantification of dicarbonyls

An ongoing problem is the reliable estimation of the α-oxoaldehyde metabolites, MG and glyoxal in the physiological systems due to three major respects: they may be synthesized by the degradation of glycolytic intermediates, monosaccharides and glycated proteins (Thornalley and Rabbani, 2014a; Thornalley and Rabbani; 2011a). They do not have strong chromophores necessary for spectrophotometric analysis. Interferences during sample processing can cause the estimates to be 10-1000-fold higher. One of the potential interferences is peroxidase as it catalyses the conversion of 1,2-diaminobenzene into trace amounts of these dicarbonyl compounds causing poor specificity (Thornalley and Rabbani, 2014a). This causes artefactual overestimation of glyoxal and MG measurement. In order to prevent this interference, sodium azide is added in the derivatizing buffer (Rabbani and Thornalley, 2014d; Thornalley and Rabbani, 2014a). Chemical derivatisation is vital to obtain sensitivity in the assay (Rabbani and Thornalley, 2014d; Thornalley, 2008; (McLellan *et al.*, 1992a).

The current method employed is the derivatisation with 1,2-diaminobenzene and two detection methods: LC-MS/MS with stable isotopic dilution analysis or via gas chromatography with mass spectrometry (GC-MS) (Ohmori *et al*., 1987; Rabbani and Thornalley, 2012a; Rabbani and Thornalley, 2014d; Selicharová *et al*., 2007; Thornalley and Rabbani, 2014a; Lopez-Clavijo *et al*., 2014). There are several advantages of utilizing 1,2-diaminobenzene, for instance, there is high reactivity at low, neutral and high pH, good adduct stability, high sensitivity and is commercially available in high purity (Cordeiro and Freire, 1996; Beisswenger *et al.,* 2005). However, it has poor sensitivity and the 1,2-Diaminobenzene degrades oxidatively to form glyoxal and methylglyoxal. The estimated concentrations of MG and glyoxal in human blood plasma are between 100 – 120 nM (Beisswenger *et al.*, 1999; Strzinek *et al*., 1972). The cellular concentrations of methylglyoxal and glyoxal are in the range 1-5 µM and 0.1 – 1 µM respectively (Dobler *et al*., 2006).

There are several reasons why the levels of methylglyoxal are measured: the characterization of medicinal products, for instance, dialysis fluids. Another reason is to develop therapeutics such as Glo1 inducer and Glo1 inhibitor

(Rabbani and Thornalley, 2014d). Thirdly, thermally processed beverages and foods can be characterized because dicarbonyls are produced from carbohydrates during Maillard reactions and Degen *et al.* discovered that the main dicarbonyl found in cookies, fruit juices and balsamic vinegars was 3-DG with a concentration of *ca*. 385 mg/kg, 410 mg/L and 2622 mg/L respectively (Degen *et al*., 2012). There were minimal concentrations of MG in these foods, but a higher concentration was established for manuka honey (Degen *et al*., 2012).

Similar reports have been discovered where the concentration of MG ranged between 48 and 742 mg/kg^{-1} and other studies discovered it to be within 189 to 835 mg/kg^{-1} (Mavric *et al*., 2008; Atrott and Henle 2009; Majtan, 2011). The level of MG in manuka honey may correlate with the anti-bacterial properties that manuka honey holds (Majtan, 2011). These concentrations are higher than 5-Hydroxymethylfurfural (5-HMF) which is a flavouring compound produced from the thermal dehydration of fructose in heat-processed food products (Morales, 2009).

Degen *et al*. discovered that the concentration in cookies, fruit juices and balsamic vinegar was *ca.* 448 mg/kg, 714 mg/L and 3760 mg/L, respectively. However, Ruiz-Matute *et al.* discovered that levels of 5-HMF in dried fruits are above 1 g/kg (Ruiz-Matute *et al*., 2010). Therefore, due to the presence of MG and glyoxal in food, the estimated dietary intake is between the ranges 5 to 20 mg/day and 20 to 160 mg/day for 3-DG and MG respectively (Degen *et al.*, 2012).

Thus, to investigate the effects of MG, there are two methods: Glo1 knockdown by siRNA and inhibiting Glo1 via the cell permeable inhibitors such as *S*-p-bromobenzylglutathione cyclopentyl diester ($SpBrGSHCp_2$) (Riboulet-Chavey *et al*., 2006; Thornalley *et al*., 1996). Validation of the estimates gained from the physiological samples such as plasma, animal tissue, plant tissue, and cultured cells can be performed by kinetic modeling of *in situ* rates of protein.

1.7 Dicarbonyl stress

Dicarbonyl stress is the abnormal accumulation of α-oxoaldehyde metabolites that are developed as a result of an imbalance between the formation of dicarbonyl metabolites and their metabolism as well as an enhanced exposure to exogenous dicarbonyls (Rabbani and Thornalley, 2015). This increases the glycation and modification of proteins and DNA leading to cell and tissue dysfunction which contributes to ageing and disease (Rabbani and Thornalley, 2014a; Rabbani and Thornalley, 2015). There is evidence that there is an increase of dicarbonyls particularly MG in diabetes, ageing human lens, renal failure and ageing (Rabbani and Thornalley, 2015). The reference ranges of the dicarbonyls in human plasma are 50 – 150 nM, 1- 4 μM in mammalian and plant cells (Rabbani and Thornalley, 2015).

There are a number of clinical implications of reactive dicarbonyls and their glycation adducts in pathological processes, ageing and diseases such as tumorigenesis, multi-drug resistance, neurodegenerative diseases and diabetes (Kuhla *et al.*, 2005; Morcos *et al.*, 2008; Rabbani and Thornalley, 2011; Thornalley, 2008; Thornalley and Rabbani, 2011a; Thornalley and Rabbani, 2011b). An increase in the expression of Glo1 in transgenic rats and mice prevented the development of diabetic complications: neuropathy, nephropathy and retinopathy (Brouwers *et al.*, 2011; Giacco *et al.*, 2014; Berner *et al.*, 2012; Maessen *et al.*, 2014). There was also evidence of an increase in GLO1 mRNA, protein and enzymatic activities in the early stage of Alzheimer's disease with levels decreasing during the advanced disease stage (Chen *et al.*, 2004; Kuhla *et al.*, 2007).

Similarly, there was *ca.* 50% reduction of the activity of Glo1 and a frameshift mutation of GLO1 forming a non-functional peptide in heterozygotes that have severe schizophrenia (Arai *et al.*, 2010). However, there was an increase of Glo1 mRNA, protein and activity and MG concentration in the mid-brain and cortex of alpha-synuclein knockout mice, in comparison to wild type controls (Kurz *et al.*, 2011). This emphasises that α-synuclein plays a role in regulating the mechanisms that suppress the formation and deletion of MG, thus the expression

of Glo1 is increased in response to stress (Kurz *et al*., 2011). These studies are of interest in relation to Parkinson's disease and other α-synuclein-related diseases.

Furthermore, there is evidence that low expression of Glo1 enhances the progression in cardiovascular disease (CVD) by increasing atherosclerosis in ApoE deficient mice (Makinen *et al*., 2014; Schalkwijk, 2015; Tikellis *et al*., 2014). Overexpression of Glo1 inhibited the apoptosis of cardiomyocytes, vascularity and angiogenesis (Blackburn *et al*., 2013, Ahmed *et al*., 2008, Vulesevic *et al.*, 2014). It was suggested that downregulation in hypoxia is associated with tissue ischaemia (Zhang *et al*., 2012).

There is also an emerging role of Glo1 in chronic kidney disease where there was a profound increase in the concentration of MG, 8-fold in comparison to control (Rabbani and Thornalley, 2012c; Rabbani and Thornalley, 2018a). An experimental study in rats revealed decreased development of renal senescence (Ikeda *et al.* 2011). A reduction in Glo1 expression by frameshift mutation was linked to a reduced glomerular filtration rate which may increase the risk of CVD (Ikeda *et al*., 2011; Miyata *et al*., 2001).

Several tumour cell lines have a high activity of Glo1 and are sensitive to Glo1 inhibitor, S-p-bromobenzylglutathione cyclopentyl diester (Sakamoto *et al*., 2001). There was high Glo1 expression found in refractory clinical tumours. The level of Glo1 expression is a negative survival factor in cancer treatment e.g. breasts cancer, lung cancer, neuroendocrine tumours and others (Rabbani *et al*, 2018; Xue *et al*., 2017). It was suggested that GLO1 gene amplification is one of the main causes of increased GLO1 expression in some human tumours (Santarius *et al.*, 2010). Overexpression of GLO1 is acquired by oncogene-linked malignant transformation (Rabbani *et al*, 2018). It also blocks the activity of several clinical anti-cancer drugs *in vitro.* Glo1 inhibitor, BBGD, improved effectiveness of treatment of MDR tumour-bearing mice *in vivo* (Sakamoto *et al.* 2000).

There have been reports of an anti-stress gene response induced by the increased expression of GLO1 via Toll-4 receptor to endotoxaemia (Rabbani *et al*., 2016).

1.7.1 Biochemical and physiological effects of glycation by methylglyoxal

1.7.1.1 Formation and metabolism of Methylglyoxal

MG formation is a fundamental aspect of the Embden-Meyerhof pathway. It is produced predominantly inside cells at a relatively high flux (0.05-0.1%). This is achieved by the non-enzymatic and enzymatic degradation and fragmentation of triosephosphate glycolytic intermediates in all organisms with anaerobic glycolysis as shown in Figure 15 (Rabbani and Thornalley, 2014a; Rabbani *et al*., 2016; Szent-Györgyi *et al*., 1967; Thornalley, 1994; Thornalley, 1996). It has a molecular mass of 72 Da and is highly toxic when in contact with proteins and DNA. The most abundant adduct is Nδ-(5-hydro-5-methyl-4-imidazolon-2-yl)-ornithine (MG-H1) (Rabbani and Thornalley, 2012c). A spontaneous small fraction, as a result, is leaked from the metabolic flux and is elevated with increased glucose metabolism. It can also occur from other metabolic ways: for instance, glyceroneogenesis, photosynthesis and gluconeogenesis where triosephosphate is also an intermediate (Thornalley 2005, Rabbani and Thornalley, 2015).

GA3P is 8-fold more reactive than DHAP in degrading to MG whereas the concentration ratio of DHAP: GA3P in cells *in situ* is *ca.* 9. Consequently, both GA3P and DHAP are approximately equally important sources in forming MG (Phillips and Thornalley, 1993). Nevertheless, MG formation represents a minor fate of triosephosphates based on studies conducted on erythrocytes, endothelial cells and fibroblasts whereby only 0.089% glucotriose were converted to MG (Rabbani *et al*., 2016). The overall rate of the cellular formation of MG was predicted to be *ca.* 125 μmol/kg cell mass per day whereby the adult human body mass and body cell mass is 70 kg and 25 kg respectively. This equates to an estimated whole-body rate of formation of *ca.* 3 mmol MG per day (Aronsson *et al*., 1978; Rabbani *et al*., 2016).

Other ways in how MG is formed are via the metabolism of acetone (the oxidation of acetone from ketone bodies is catalysed by cytochrome E4502 E1), monosaccharides via glucose glycation, threonine (degradation of this amino acid

via the aminoacetone) and proteins via glucose glycations (Rabbani *et al*., 2016; Thornalley, 1996, Thornalley, 2005). However, these are minor contributions especially the oxidation of acetone whose levels are elevated in diabetic ketoacidosis (Rabbani and Thornalley, 2014b). It has been reported that MG synthases can form MG enzymatically in bacteria but there is no evidence for the enzymatic formation of MG from triosephosphates found in the mammalian cells (Phillips and Thornalley, 1993). The formation of MG from enzymatic and non-enzymatic pathways is dependent on the type of organism (Thornalley, 2008).

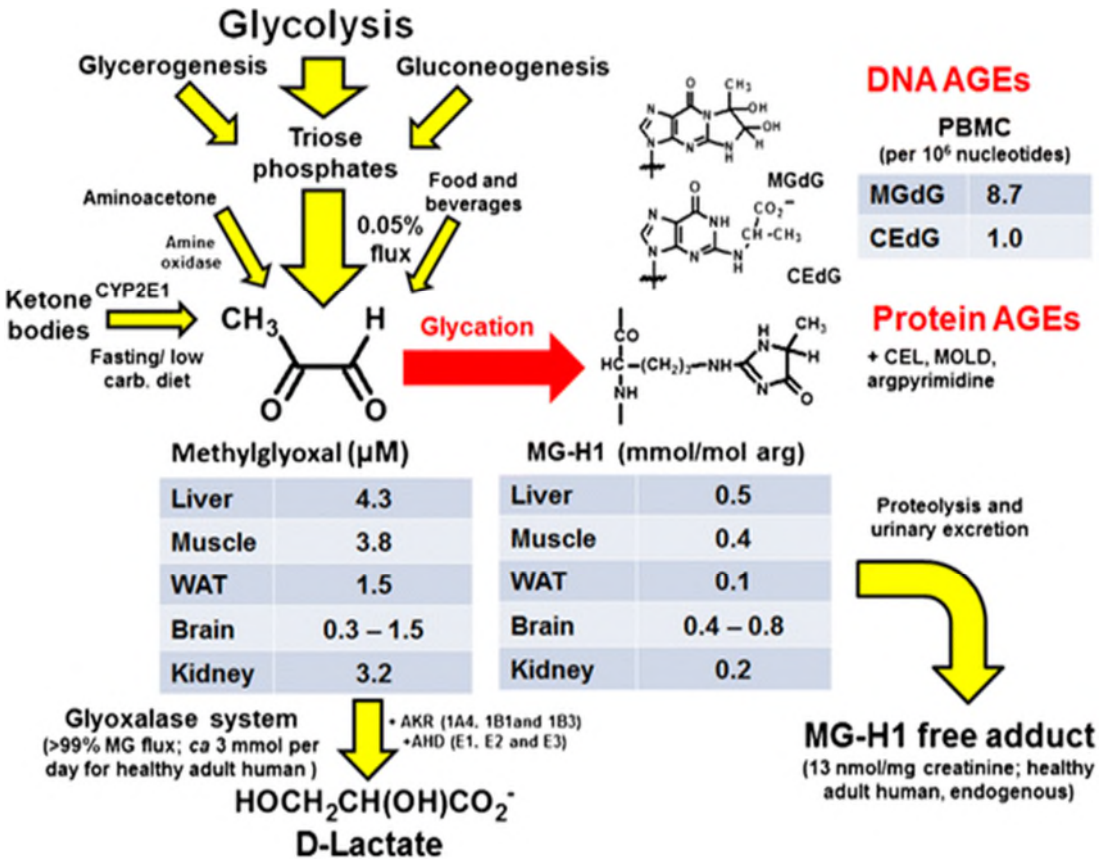

Figure 15: The sources of formation of methylglyoxal, metabolism and glycation of proteins and DNA *in vivo* (Rabbani *et al*., 2016). The levels of MG and MG-H1 adducts in tissues are for mice. The levels of the PBMC DNA AGEs, the MG metabolism by the glyoxalase system and the urinary excretion of MG-H1 are for human subjects. The concentration of methyglyoxal and MG-H1 is higher in the liver cells (4.3 μM) and 0.5 mmol/mol arg respectively in comparison to other cells however the levels of MG-H1 adduct varied in cells of the brain where in the range of 0.4 - 0.8 mmol/mol arg.

The level of efficiency of MG detoxification is dependent on the hemithioacetal formation. At pH 7 in aqueous solution, MG is present in solution in three forms under physiological conditions: unhydrated α-oxoaldehyde (1%), monohydrated (71%) and dehydrated forms (28%) (Thornalley, 1996; Rabbani and Thornalley, 2012a). The unhydrated form can produce the hemithioacetal that enters the active site of Glo1. The equilibrium is shifted towards the formation of the hemithioacetal when GSH is present resulting in the removal of MG from the glyoxalase system (Rabbani *et al*., 2016; Thornalley *et al*., 1999; Thornalley, 2003a).

The activity of glyceraldehyde-3-phosphate dehydrogenase (GADPH) may also influence the cellular concentration of triosephosphates and thereby the formation of MG (Karachalias *et al*., 2005; Rabbani *et al*., 2016). The low activity of GADPH results in the accumulation of triosephosphate which in turn increases the production of MG (Rabbani *et al*., 2016; Phillips and Thornalley, 1993).

1.7.1.2 Protein glycation by methylglyoxal

Glycation of proteins by MG is usually low, occurring on 1 - 5% protein but can increase in response to disease and ageing (Rabbani *et al.,* 2016). The major MG-derived protein glycation adduct, hydroimidazolone MG-H1, has a urinary excretion rate of healthy humans of *ca*. 10 μmol per day. This indicates that less than 1% of MG formed endogenously modifies proteins; the remainder, >99% is metabolised by the glyoxalase system as little MG is excreted (Rabbani *et al*., 2016).

MG reacts with arginine residues forming two adducts: dihydroxyimidazolidine and then hydroimidazolone MG-H1. The former is a minor unstable adduct whereas MG-H1 has a chemical half-life of *ca.* 12 days through slow reversibility of the formation reaction. This suggests that the protein content of hydroimidazolones can be decreased if the concentrations of MG and other precursor α-oxoaldehydes are lowered (Ahmed *et al*., 2003; Thornalley, 2008).

Protein glycation by MG is damaging because the arginine residues modified have a high probability of being located in the functional domains of proteins and

this modification results in loss of charge of the side chain guanidino group (Rabbani *et al*., 2016; Perkins *et al*., 2008; Duran-Jimenez *et al*., 2009). For instance, arginine residues in the GFOGER and RGD motifs of the integrin-binding domains of collagen IV that lines the blood vessel walls can undergo MG glycation. Modification of MG induces endothelial cell detachment, increasing the risk of thrombus formation, anoikis, contact with subendothelium and prevents angiogenesis (Rabbani and Thornalley, 2014a; Thornalley, 2008; Dobler *et al*., 2006; Yamagishi *et al*., 2005). The sites where arginine and lysine glycation are prone to take place have been hypothesised to be near positively and negatively charged amino acid residues that differ by 3-4 residues in the primary sequence. Nevertheless, this needs to be experimentally confirmed (Rabbani and Thornalley, 2012c).

After proteins are modified, they are mis-folded and undergo proteolysis in the proteasome. Cellular proteins have a median half-life of 32 hours (Gerner *et al*., 2002). Other MG-modified proteins undergo lysosomal degradation in macrophages and monocytes (Rabbani *et al*., 2016; Thornalley, 1996; Thornalley, 2008). Amongst the consequences of dicarbonyl glycation are: increased formation of ROS in response to the dysfunction of mitochondrial protein which in turn causes oxidative stress, mitochondrial-activated apoptosis and cell detachment from the extracellular matrix and anoikis (Morcos *et al*., 2008; Rabbani and Thornalley, 2015; Rabbani *et al.*, 2016b).

Protein glycation also causes covalent cross-linking of proteins producing resistance to proteolysis (Rabbani and Thornalley, 2012c; Thornalley, 2008). Non-sulfhydryl cross-links are also formed between proteins reducing the solubility of proteins triggering enzymatic digestion (Schnider and Kohn, 1981). This is crucial as they affect the extracellular matrix and connective tissues that consequently influence their structural properties and physiological function that increase with age (Cárdenas-Leon *et al*., 2009). For instance, the capillary basement membrane's thickness and rigidity is increased (Lee, 1993; Lee *et al*., 2016). Thus, AGEs influence the function of proteins and the interactions between proteins (Rabbani and Thornalley, 2012c).

Glycation of proteins affects the proteome in the living systems causing many pathological conditions. Protein modification is increased in diabetes and its vascular complications causing further damage (Thornalley *et al.,* 2003). Methylglyoxal modifies high density lipoproteins (HDL) and low-density lipoproteins (LDL). This reduces the concentration of HDL. MG modification of LDL leads to the formation of small atherogenic LDL (Godfrey *et al*., 2014; Rabbani *et al*., 2011a; Rabbani *et al*., 2011b). Modification of neural voltage gate sodium channels by MG increases hyperalgesia in patients with diabetic neuropathy (Bierhaus *et al.*, 2012). Glycation of plasminogen decreases the generation and function of plasmin in diabetes (Ajjan *et al*., 2013).

1.7.1.3 DNA glycation by methylglyoxal

DNA is susceptible to glycation by glyoxal and MG. Deoxyguanosine (dG) is the most reactive nucleotide towards dicarbonyl glycation under physiological conditions (Thornalley *et al.,* 2010). The main nucleotide AGEs derived from dicarbonyls are imidazopurinones. The glycation of DNA by glyoxal forms GdG, CMdG and gdC. Glycation of DNA by MG forms MGdG and CEdG. MGdG is the predominant nucleotide AGE. The MGdG content of DNA of the peripheral blood mononuclear cells of healthy human subjects was higher than the DNA oxidative damage adduct, 8-hydroxydeoxyguanosine. The formation of CEdG is linked with DNA depurination (Thornalley, 2003b; Thornalley, 2008). An increase in GdG and MGdG is associated with elevated mutation frequency, cytotoxicity and the production of DNA strand breaks (DSB) (Thornalley *et al*., 2010).

Nucleotide excision repair (NER) suppresses glycation of nucleotide and its detrimental effects (Murata-Kamiya *et al*., 1986, Murata-Kamiya *et al*., 1999, Pischetsrieder *et al*., 1999). A mutation by MG-derived nucleotide AGEs leads to carcinogenesis that may underly why Glo1 is considered a tumour suppressor protein (Zender *et al.,* 2008).

1.7.2 Biochemical and physiological effects of glycation by glyoxal

1.7.2.1 Formation and metabolism of Glyoxal

Glyoxal is an endogenous α-oxoaldehyde substrate and metabolite of the glyoxalase system (Thornalley and Rabbani, 2014a). It is produced in early and advanced glycation mechanisms from the slow, non-enzymatic oxidative degradation of glucose (Abordo *et al*., 1999). This is predominantly monosaccharides and saccharide derivatives. Glyoxal is also formed by the degradation of glycated proteins, Schiff's base adducts, lipid peroxidation and auto-oxidation of linoleic and linolenic acids (Loidl-Stahlhofen and Spitelier, 1994; Thornalley *et al*., 1999; Thornalley, 2005). The concentration of glyoxal in human blood is *ca*. 150 nM (Thornalley, 1999). It is present in aqueous solution in three hydration forms: unhydrated, monohydrate and dihydrate and can produce dimers.

1.7.2.2 Protein glycation by Glyoxal

Similarly, to methylglyoxal, the modification of proteins and nucleotides by glyoxal induces cell dysfunction and death. Glyoxal interacts with lysine, arginine and cysteine residues of protein to form the AGE adducts: Nε-carboxymethyl-lysine (CML), N_{ω}-carboxymethylarginine (CMA) and *S*-carboxymethylcysteine (CMC) respectively (Thornalley, 2008). Another arginine-derived adduct formed is N_{δ}-(5-hydro-4-imidazolon-2-yl)ornithine (G-H1) and its related isomers G-H2 and G-H3 (Ahmed *et al*., 2002; Thornalley, 2008).

1.7.2.3 DNA glycation by Glyoxal

In DNA glycation, the most reactive nucleotide under physiological conditions is deoxyguanosine (dG). The major nucleotide AGE is the imidazopurinone derivative 3-(2'-deoxyribosyl)-6,7-dihydro-6,7-dihydroxyimidazo [2,3-b]purin-9(8)one (GdG). However, other nucleotide AGEs have been reported which are CMdG and GdC (Anwar *et al*., 2018; Murata-Kamiya *et al*., 1998).

The host research group have created an LC-MS/MS based assay technique to quantify nucleotide adducts using acid nuclease digestion and isotopic dilution analysis (Fleming *et al*., 2008). Using this method, a major finding has been established: the level of GdG estimated in the human mononuclear leukocytes were

1.59 ± 0.08 adducts per 10^6 nucleotides (n=3). This emphasises how DNA glycation via glyoxal is a vital type of DNA damage quantitatively *in vivo*. Under physiological conditions, GdG is moderately stable and can be stabilised by forming single- and double-stranded DNA. Its presence has been associated with increased DNA mutations, strand breaks and cytotoxicity. Thus, glyoxal and methylglyoxal are efficiently metabolised by the glyoxalase system to glycolate and D-lactate respectively (Rabbani and Thornalley 2014b; Rabbani and Thornalley, 2016; Thornalley, 2008). The intermediate formed by the reaction with glyoxal by Glo1 is *S*-glycolylglutathione.

1.7.3 Biochemical and physiological effects of glycation by 3-deoxyglucosone

3-Deoxyglucosone (3-DG) is produced as a major carbonyl intermediate via the polyol pathway and the Maillard reaction (Kato *et al.*, 1988). In the early stage of the Maillard reaction, glucose reacts with protein amino groups non-enzymatically. This involves the conversion of reversible Schiff base adducts to stable, covalently bound N-terminal amines or lysine side chains called Amadori products (Ashraf *et al.*,2015; Kato *et al*., 1987; Kato *et al*., 1988; Tsukushi *et al*., 1999). The quantity of Amadori products is in proportion to the hyperglycaemic levels in diabetes mellitus (DM) (Tsukushi *et al*., 1999). During the intermediate phase of the Maillard reaction, the Amadori products under various dehydration and rearrangements form reactive dicarbonyl compounds such as 3-DG (Niwa *et al*., 1996; Niwa, 1999).

3-DG is a potent and reactive glycating agent that undergoes further reactions with proteins predominantly cysteine, arginine, and lysine to form AGEs (Niwa *et al*., 1996, Niwa, 1999). It also has several biological functions such as cellular toxicity (Lo *et al*., 1994a). However, the reaction of 3-DG with amino groups varies. For instance, irreversible reactions are formed when interacting with arginine and lysine residues resulting in protein polymerisation whereas with cysteine residues reversible hemithioacetal adducts are produced but has not been well characterised (Biemel *et al*., 2002; Edwards and Wedzicha, 1992). The predominant AGE is a mixture of isomeric hydroimidazolones (3DG-H). A further

AGE formed is pyrraline (Beisswenger *et al*., 2003a; Niwa, 1999; Tsukushi *et al*., 1999, Thornalley *et al*., 1999; Thornalley *et al*., 2003b).

The polyol pathway is also involved in 3-DG synthesis. The oxidized product of sorbitol is fructose and is converted into 3-DG *in vitro* involving sorbitol dehydrogenase (Igaki *et al*., 1990; Hayase *et al*., 1991; Hayase *et al.*, 1995; Kato *et al.*, 1987). Szwergold *et al.* discovered using the lens of diabetic rats that 3-DG is the hydrolytic product of fructose-3-phosphate which is enzymatically synthesised from fructose (Szwergold *et al.,* 1990).

A further source of the formation of 3-DG is the phosphorylation of fructoselysine by the enzyme fructosamine-3-kinase (F3K); this leads to the hydrolysis of fructoselysein-3-phosphate (Beisswenger *et al*. 2003a).

Ashraf *et al.* discovered that upon histone H3 glycation by 3-DG, it affects the structure and function of chromatin. This may be involved in uraemic and diabetic complications (Ashraf *et al*., 2015; Niwa, 1999). 3-DG is detoxified to 2-keto-3-deoxygluconic acid and 3-deoxyfructose via the enzymes 3-DG dehydrogenase and 3-DG reductase respectively (Brings *et al*., 2017; Niwa, 1999).

2.0 Project-specific background

Many refractory clinical tumours with high glycolytic rate have overexpression of Glo1 and it is hypothesised that an accumulation of methylglyoxal potentiates the cytotoxic effects of current chemotherapy treatment (Rabbani *et al*., 2017; Rabbani *et al*., 2018). The main physiological substrate of Glo1 is methylglyoxal. MG is efficiently metabolised by Glo1 to suppress the formation of damaging protein and DNA AGEs to low, tolerable levels (Thornalley, 2003b; Thornalley, 2008).

The activity of Glo1 can be suppressed *in situ* which can significantly accumulate methylglyoxal to toxic levels by three mechanisms investigated in this study: cell-permeable Glo1 inhibitors, Glo1 silencing and GSH depletion (Abordo *et al.* 1999; Thornalley, 1993; Thornalley *et al.* 1996; Thornalley, 1998a, Thornalley, 2003). High levels of methylglyoxal enhance protein and DNA glycation that may be involved in stimulating G1-induced growth arrest and apoptosis (Kang *et al.* 1996). Biswas *et al*. have shown that methylglyoxal can inhibit glycolysis and the flow of electrons via the mitochondrial complex I of the respiratory chain which are common characteristics of malignant cells (Biswas *et al*. 1997). This suggests how GLO1 is involved in the proliferation and survival of tumours and is a potential biomarker for diagnosis (Geng *et al*., 2014; Rabbani *et al*., 2018).

2.1 Cell culture models in cancer studies

2.1.1 HEK-293 cell line

The cell line utilized in this project is the human embryonic kidney 293 (HEK-293) cells. Graham *et al.* developed the semi-adherent embryonic renal tubular epithelial cell line with cell transformation produced by human adenovirus type 5 DNA (Graham *et al.*, 1977). HEK-293 cells have been used for many applications, for instance, cell biology, electrophysiology and biotechnology (Lin *et al*., 2014; Lemtiri-Chlieh and Ali, 2013; Stepanenko and Dmitrenko, 2015). Recent studies revealed that HEK-293 cells were used to produce glycoproteins to form adenoviral vaccines and protein therapies that have been approved by the Medicines and Healthcare products Regulatory Agency (MHRA), Europeans Medicines Agency (EMA) and the United States Food and Drug Administration (FDA) (Rijal *et al*., 2019; Chin *et al*., 2019; Dumont *et al.*, 2016). This implies the therapeutic use of HEK-293 cells where it has good biosafety risks from viral contamination (Dumont *et al*., 2016).

Until today, it is still debated on the origin of HEK-293 cells and whether they have a tumour-like phenotype. HEK-293 cells share morphological characteristics that are analogous to tumour cells. The mammalian cell line does not have an actin cap and has premature peripheral F-actin structures (Haghparast *et al.*, 2015). It has a round shape with a mean cell diameter of 15.5 ± 0.3 μm (Dietmair *et al.*, 2012). HEK-293 cells can detach from the substrate and its round shape did not cause significant changes to the structure of F-actin at the apical cell surface (Haghparast *et al.*, 2015).

HEK-293 cells are a low tumorigenic immortalized cell line that can undergo malignant transformation following the transfer of oncogenes via a non-classical mechanism that phenotypically present a neoplastic state (Ha *et al.*, 2010; Lin *et al.*, 2011; Canis *et al*., 2013). This increases the instability of the chromosomes that promote tumour progression and metastasis (Abdouh *et al*., 2014; Stepanenko and Dmitrenko, 2015; Gisselsson and Hoglund, 2005). This suggests that HEK-293 cells are not a model for mammalian cell line.

HEK-293 cells have a high proliferation rate where it has a population doubling (PD) time of 24 hours (Stepanenko and Dmitrenko 2015). Their

tumorigenicity increases with passage where it reaches 100% when the passage exceeds 65 whereas below passage 53, no tumours can be induced (Shen *et al*., 2008). This suggests that HEK-293 cells can become highly malignant.

2.1.1.1 Biochemical characteristics of HEK-293 cells.

HEK-293 cells can concomitantly co-metabolize glucose and lactate even through their exponential growth. The metabolic shift from the production of lactate to glucose and lactate metabolism is dependent on the pH where it is efficiently triggered at pH 6.8 (Liste-Calleja *et al.*, 2015). The two glucose transporters that are mainly expressed by HEK-293 cells are GLUT1 and GLUT3 where they increase the uptake of glucose and the flux of methylglyoxal formation – Figure 16 (Castro *et al*., 2008). They also express Sodium Vitamin C Transporter 2 (SVCT2) that facilitates in the uptake of ascorbic acid (Castro *et al*., 2008). Ascorbic acid is a hydrophillic anti-oxidant and cofactor in many enzymatic systems. It prevents the consumption of glucose during glutamatergic synaptic activity intracellularly. This increases the uptake of glutamate and sodium ions to induce glucose transport and metabolism and lactate efflux (Castro *et al*., 2008). It also prevents the transport of 2-deoxyglucose in HEK-293 cells. However, when the uptake of ascorbic acid is halted, glucose becomes the substrate that facilitates the glutamatergic transmission (Castro *et al*., 2008).

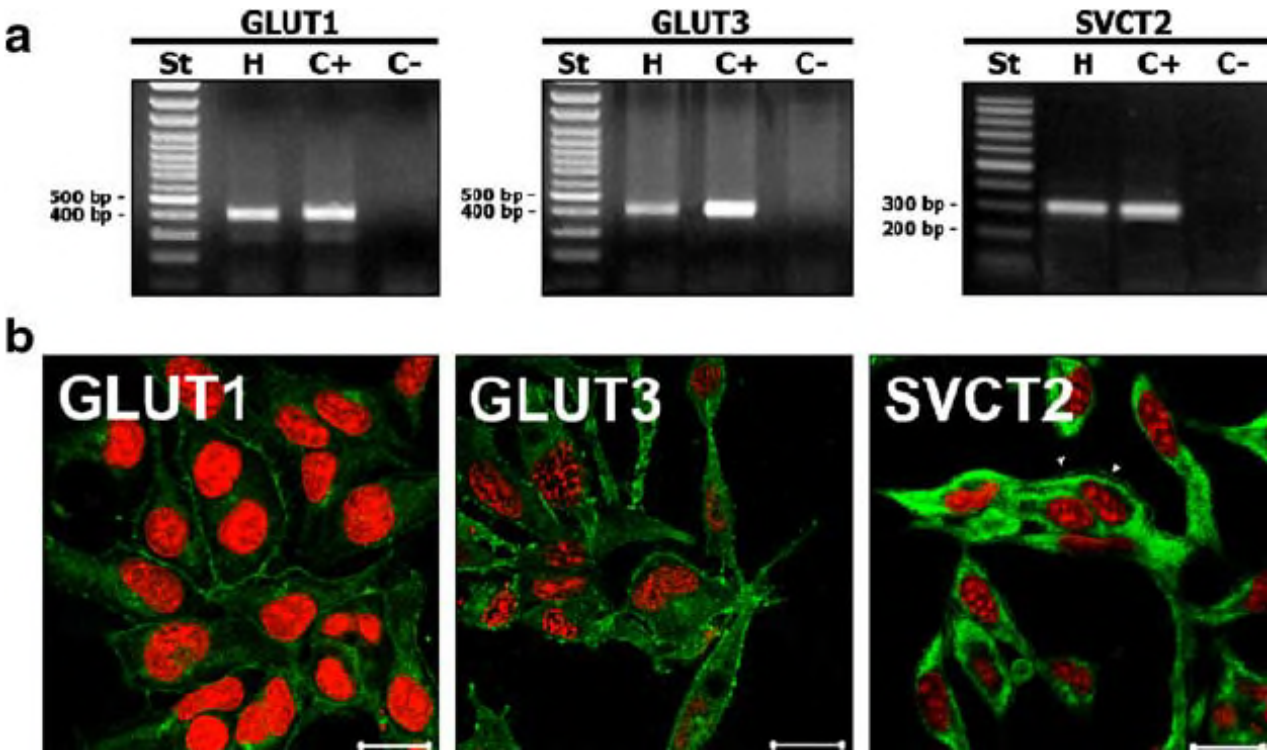

Figure 16: The expression of GLUT1, GLUT3 and SVCT2 in HEK-293 cells.

A reverse transcription – polymerase chain reaction qualitative analysis of the transporters: GLUT1, GLUT3 and SVCT2. (H) HEK-293 cells mRNA, 100 base pair (bp) DNA standard (st.). The rat brain mRNA as positive control (C+) and a negative control (C-). The expression of GLUT1 and GLUT2 was between 400 to 500 bp. The expression of SVCT2 was between 200 to 300 bp. B. Immunofluorescence analyses of the three transporters (green) where the nuclei were stained with propidium iodide (red). Scale bar, 20 µm. (Castro *et al.* 2008)

Another way in how a metabolic switch can occur from respiration to an increase in aerobic glycolysis and glutaminolysis is through the stabilization of hypoxia-inducible factor 1 (HIF-1) by the cytoplasmic enzyme called fumarase otherwise known as Fumarate Hydratase (FH) (Frezza *et al.* 2011; Lin *et al*., 2014). Focal deletions of fumarase can be found in kidney tumours (Linehan and Rouault, 2013).

HEK-293 cells are also efficient in the γ-carboxylation of glutamic acid and the sulfation of tyrosine which is required to produce therapies such as recombinant factors IX-Fc2 and Drotrecogin alfa (Kannicht *et al*., 2013; Peters *et al*., 2013). Other fermentative features of HEK-293 cells are the increase of ammonia and alanine (Lee *et al*. 2008, Nadeau *et al.* 2000; Lin *et al*., 2014).

2.1.1.2 Molecular characteristics of HEK-293 cells.

One of the advantages of utilizing HEK-293 cells is its ability to produce recombinant proteins and has high transfection efficiency to overexpress target genes of interest whereas vectors can be engineered synthetically to add introns and codons that are optimized (Kavsan *et al.*, 2011; Thomas and Smart, 2005; Gustafsson *et al*., 2004; Chin *et al*., 2019).

HEK293 cells are also involved in the post-translational modification and processing to increase the yield of target proteins in comparison to other mammalian cells such as chinese hamster ovary (CHO) cells (Bollin *et al.*, 2011; Ooi *et al*. 2016; Wurm, 2004; Mariati *et al.*, 2010). This suggests that the expression of the recombinant proteins in HEK-293 cells is dependent on two factors: delivery of the recombinant vector via transfection and the detection of expressed proteins.

HEK-293 cells can transform on chromosome 19 where there is a 332.5 kbp genomic region containing the adenoviral sequence insertion site, human adenovirus type 5 DNA E1A and E1B that express SV40 large T antigen (Graham *et al.* 1977; Lin *et al*., 2014; Stepanenko and Dmitrenko, 2015). It can be amplified to maintain the high copy number of the adenoviral sequence (Lin *et al*. 2014). The telomere of chromosome 1q can be rearranged via deletions and mutations causing ectopic expressions of genes, dysregulation of cell cycle control, primarily retinoblastoma gene (pRB) retinoblastoma and tumour suppressor p53 (Graham *et al*., 1977; Lin *et al*. 2014; Eisenberg, 2011; Londono-Vallejo, 2004). Most polymorphisms are heterozygous which decreased the rate of senescence in HEK-293 cells and increased the rate of proliferation (Louis *et al*., 1997; Ha *et al*., 2010; Graham *et al*., 1977; Wang *et al.*, 2008; Lin *et al*., 2011 Hamilton, M., *et al*. 2006). This highlights the potential of HEK-293 cells to form cancer influencing apoptotic mechanisms and can be applied in transfection experiments (Stepanenko and Dmitrenko, 2015).

Transfection is an analytical procedure to study the function and regulation of genes in cells. There are three types of transfection: biological, chemical and physical and have been further advanced to deliver nucleic acids (DNA and RNA) to specific subcellular structures by laser-microscope systems and have also combined with mRNA transfection (Kim and Eberwine, 2010). This can subsequently produce

recombinant proteins that can inhibit and increase expressions of specific genes in mammalian cells (Kim and Eberwine, 2010; Wurm, 2004).

However, it is dependent on the objective and experimental design wherein this project, stable and transient transfection are utilized to overexpress and knockdown GLO1 respectively (Lemtiri-Chlieh and Ali, 2013; Ooi *et al*., 2016; Spidel *et al*. 2016). Transient transfection was not performed to overexpress GLO1 as a member of the host team has conducted this previously. Wildtype and empty vector-transfected cells where the latter are used as control can form colonies and tumours of different size (Stepanenko and Dimitriko, 2015). The mechanism in how genetic material can be stably or transiently transfected is illustrated in Figure 17. In stable transfection, a selective marker such as green fluorescent protein (GFP) acts as a marker for transgenes integrated into the genome of HEK-293 cells and the expression of the transgene is sustained even after replication – Figure 17A (Kim and Eberwine, 2010; Bestvater *et al*., 2002; Lin *et al*., 2015). On the other hand, HEK-293 cells that are transiently transfected are expressed for a limited period and are not integrated into the genome and are more prone to losing the genetic expression via cell division and environmental factors – Figure 17B (Wurm, 2004; Pfeifer and Verma, 2001; Hamilton and Baulcombe, 1999; Kim and Eberwine, 2010).

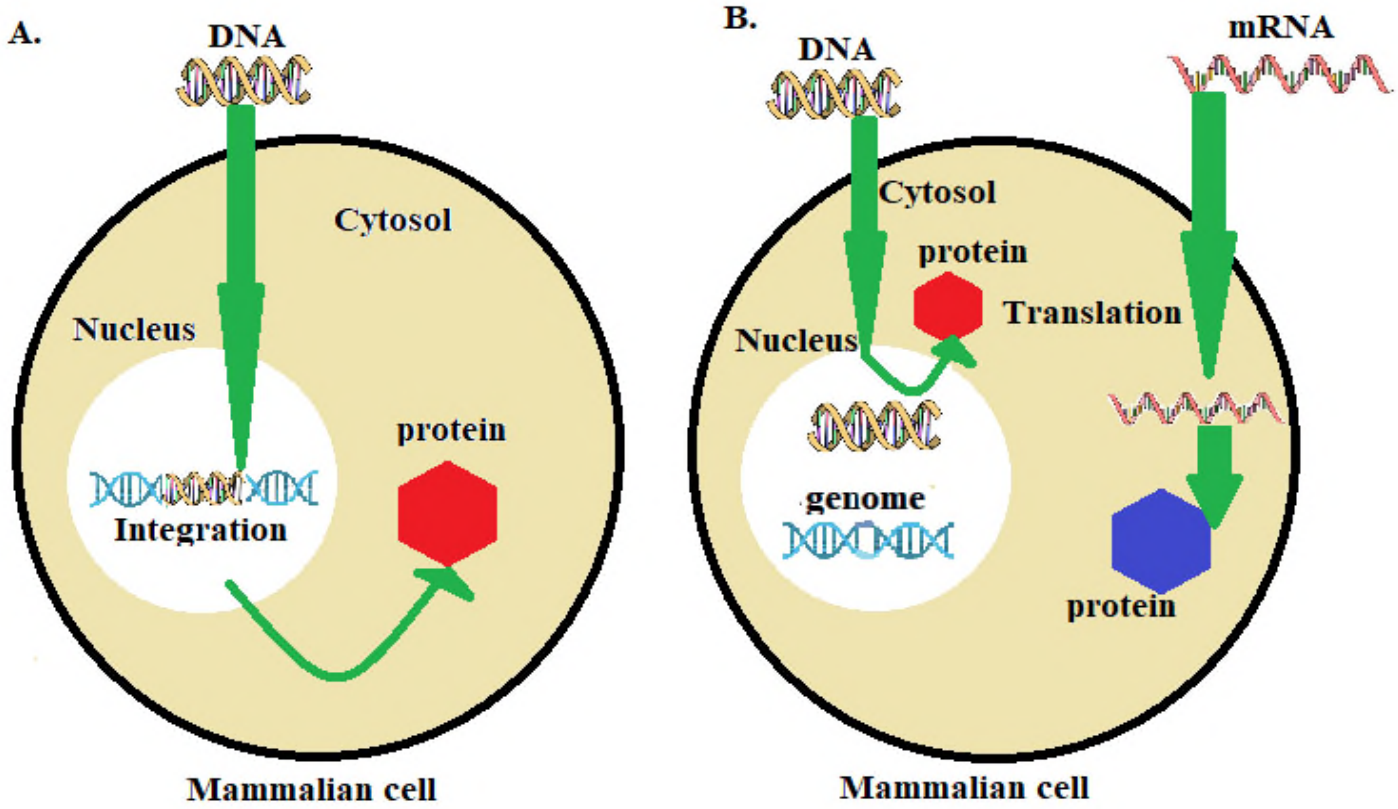

Figure 17 The mechanisms of stable and transient transfections (Adapted from Kim and Eberwine, 2010). (A) Stable transfection: foreign DNA is translocated to the nucleus and is integrated into the host genome to increase expression. (B) Transient transfection: foreign DNA is translocated into the nucleus but is not integrated into the genome. Foreign mRNA can undergo translation in the cytosol. The proteins expressed are presented as hexagons whereas the green arrows present the process of delivering nucleic acids.

For stable transfection, previous studies have discovered that HEK-293 cells can produce stable recombinant proteins using xenogenic genes as selection markers and antibiotic selection (Spidel *et al*. 2016). Lipofectamine 2000 is the transfection reagent used in this investigation. Lipofectamine 2000 is a liposome complex that transmits nucleic acids that resides in a phospholipid bilayer into cells by fusing with the cellular outer-membrane. This mode of action is known as lipofection. Advantages of using this transfection reagent are due to its high efficiency and minimal cell toxicity (Shi *et al.*, 2018).

In this project, the pIRES2-EGFP-GLO1 vector illustrated in Figure 18 is stably transfected into HEK-293 cells to overexpress GLO1 protein and enzymatic activity to analyse its effect on chemotherapeutic agents, cell metabolism, tumour proliferation and survival (Hutschenscheur *et al*. 2016). The pIRES2-EGFP consists of an internal ribosome entry site (IRES) of the encephalomyocarditis cytomegalovirus virus (ECMV). The IRES is situated between the multiple cloning site (MCS) and the enhanced green fluorescent protein (EGFP) region (Jackson *et al.*, 1990). This allows the gene of interest, GLO1, that contains the starting codon, ATG *a*nd the selection marker GFP to be translated from the 3' end of the singular bicistronic mRNA to enter the MCS (Jackson *et al*., 1990; Jang *et al.*; 1990; Cormack *et al*., 1996). EGFP is a red-shifted variant of wild-type form that has been optimised to increase fluorescence and gene expression in mammalian cells. The excitation and emission maximum wavelengths are 448 and 507 nm respectively (Cormack *et al*. 1996; Haas *et al*. 1996).

HEK-293 cells transfected with pIRES-EGFP-GLO1 plasmid are resistant to the aminoglycoside antibiotic G-418 and contains the neomycin and kanamycin-resistant genes (Gorman, 1985; Küng *et al*., 1997). G-418 eradicates mammalian cells by binding to 80S subunit of the ribosome, this prevents the elongation step in ribosomes preventing protein synthesis (Küng *et al*., 1997). They also express aminoglycoside 3'-phosphotransferase (APT) that covalently modifies G418 to 3'-phospho-G418. 3'-Phospho-G418 contains negligible potency and low affinity for prokaryotic and eukaryotic ribosomes (Davis *et al*., 1986).

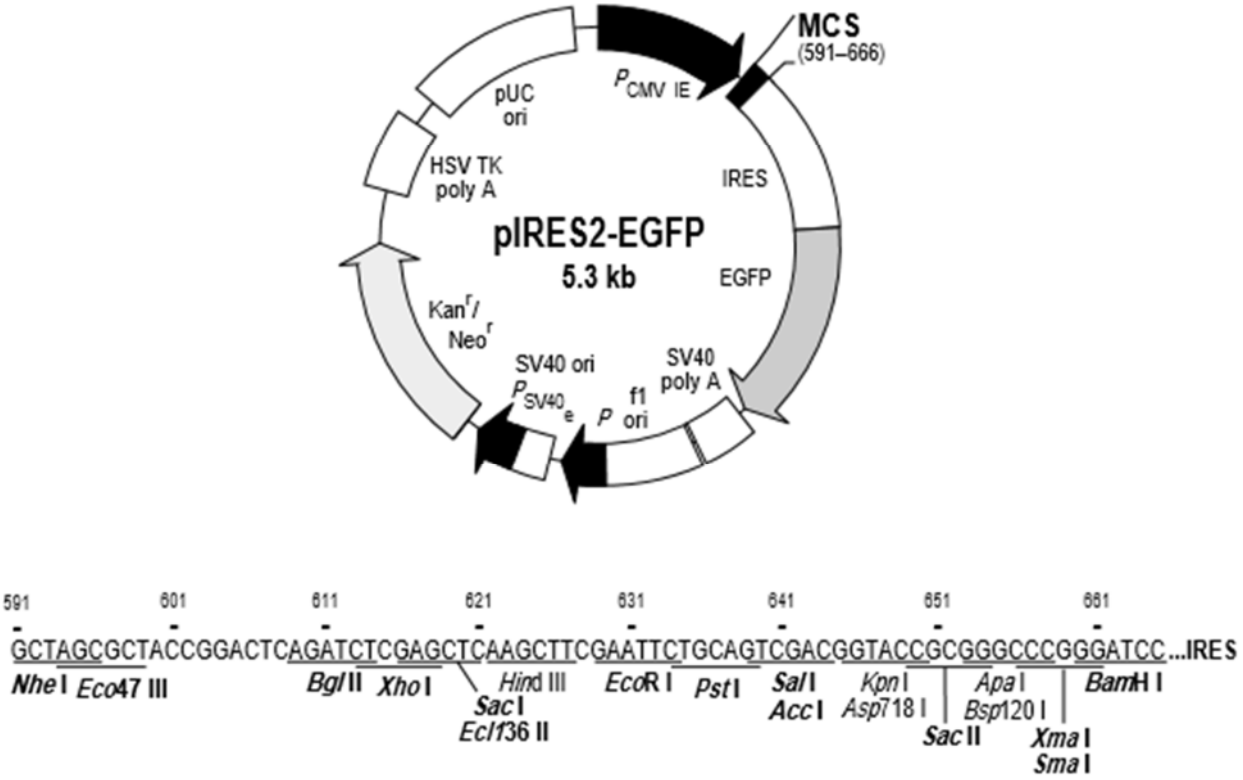

Figure 18: The restriction map and multiple cloning site for the pIRES2-EGFP vector (Clontech, 2019).

The EGFP encodes a mutant variant that consists of two amino acid substitution: Phenylalanine-64 (Phe-64) to Leucine. Serine-65 (Ser-65) to Threonine. There are more than 190 changes to the silent bases. The MCS is between the early promoter of CMV and the IRES sequence. The SV40 polyadenylation aids the GFP expression. The SV40 origin (ori) is for the replication of mammalian cells expressing the SV40 T antigen. The vector contains Tn5 gene that is resistant to the antibiotic's neomycin and kanomycin. The neomycin resistant (Neor) cassette comprises the SV40 early promoter. There are also polyadenylation sites in the herpes simplex virus thymidin kinase (HSV TK) gene that allows the selection of stable transfectant cells using G-418. The pUC origin (ori) of replication allows the bacterial transformation and propagation in *E-coli* to take place. The f1 origin allows the production of single-stranded DNA. The restriction sites are in bold and the two restriction enzymes are: *Bgl II* (Bacillus globigii) and *Pst I* (Providencia stuartii).

Previous studies have successfully overexpressed GLO1 in HEK-293 cells where there was a 20-fold increase in GLO1 mRNA, protein and activity in comparison to mock-transfected cells – Figure 19 (Hutschenreuther *et al*. 2016).

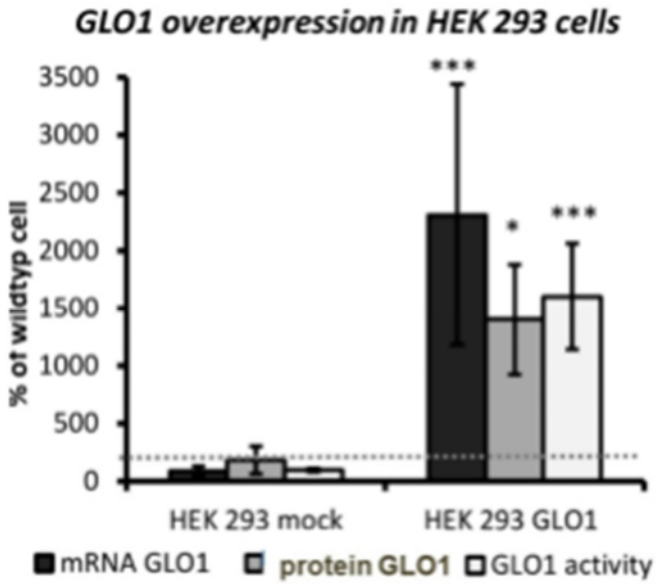

Figure 19: The effect of GLO1 overexpression in HEK-293 cells *in vitro* (Hutschenreuther *et al*. 2016).

Cytosolic cell extracts were used to measure the GLO1 mRNA, protein and enzymatic activity whereby the GLO1 protein and mRNA were normalized B-actin. The grey dashed line presents the wild-type cells (n=3). The GLO1 protein, mRNA and enzymatic activity increased significantly in comparison to the HEK-293 mock cells. Statistical Significance: * $p < 0.05$; ** $p < 0.01$; *** $p < 0.001$ (t-test) with respect to control.

Transient transfection of HEK-293 cells does not require inducible vectors nor does the mRNA need to be in the nucleus to be expressed and can be used for therapeutic purposes (Job and Eberwine, 2001; Sul *et al.* 2009; Sullenger and Gilboa 2002; Subedi *et al*. 2015). There are four sites that can undergo nucleoside modifications and are vital in the translation of mRNA: cap, open reading frame (ORF), poly-A tail, 5′ untranslated region (5′UTR) and 3′ untranslated region (3′UTR) (Subedi *et al*., 2015). Transient transfection can be used to overexpress GLO1 and produce soluble recombinant proteins via transient gene expression and target the

secretory pathway (Kaufman, 2003; Berlec and Strukelj, 2013; Thomas and Smart, 2008).

RNA interference (RNAi) is used to knockdown down specific genes and observes the phenotypic changes and potential to treat disease (Kim and Eberwine, 2010). In this project, small inhibitory RNA (siRNA) form the RNA-induced silencing complex (RISC) in the cell preventing the expression of target genes (Brazas and Hagstrom, 2005; Castanotto and Rossi, 2009). Lipid-mediated and virus-mediated delivery of siRNA is the two most common methods (Davis *et al*. 2000). Previous studies have successfully knocked down GLO1 by siRNA > 95% where they potentiated the toxicity of chemotherapeutic regimens in tumour cell lines – Figure 20 (Xue *et al*., 2017). The GC_{50} and logistic regression coefficient were calculated to determine the maximal concentration at which 50% of cell growth has been inhibited. The GC_{50} value and logistic regression coefficient with wild-type BON-1 was 3.06 ± 0.13 μM and $n = 2.23 \pm 0.20$. However, upon treatment of BON-1 with GLO1 siRNA with doxorubicin, the proliferation rate decreased by $27 \pm 2\%$ (Xue *et al*., 2017).

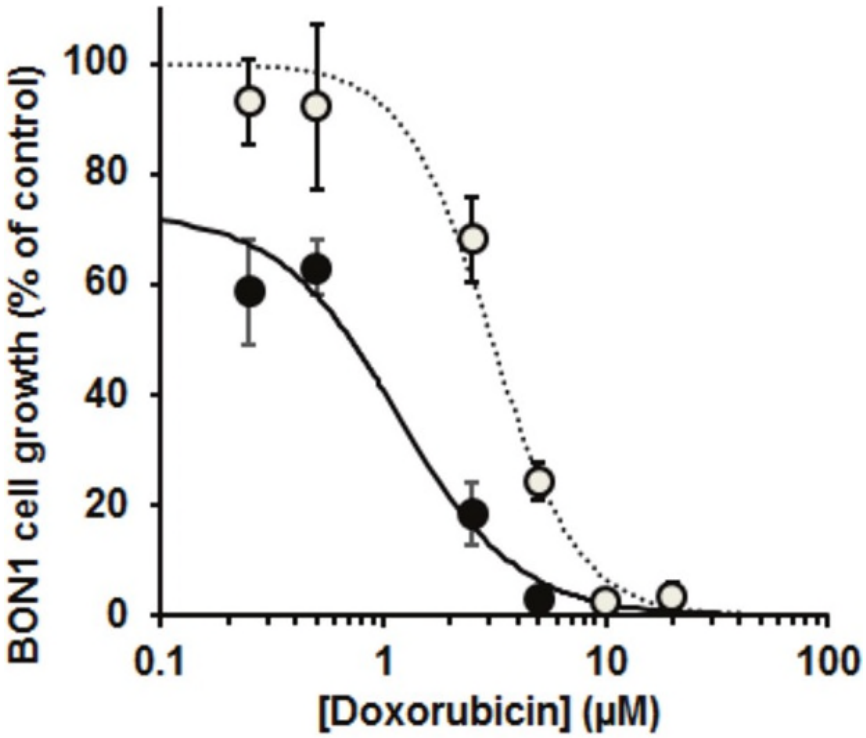

Figure 20: The dose-response curve presenting the effect of doxorubicin with and without silencing of GLO1 on the growth of BON-1 pancreatic neuroendocrine tumour cell line *in vitro* (Xue *et al.* 2017).

BON-1 was treated with doxorubicin at 6 different concentrations (μM): 0.25, 0.50, 2.5, 5, 10 and 20 μM. A concentration of 25 nM of Accell Human GLO1 SMART siRNA was used to silence GLO1. The higher the concentration of Doxorubicin, the more anti-proliferative effects it exerts. The GC50 value and logistic regression coefficient with wild-type BON-1 was 3.06 ± 0.13 μM and n = 2.23 ± 0.20. However, in combination with BON-1, cell growth decreased by 27 ± 2% (n = 3, P<0.001). Key: ○ and ---- represent the wild-type of BON1 cell line. ● and ▬ BON-1 with GLO1 silencing; Data mean ± SEM (n=3).

2.1.2 Human cancer cell lines

Human cancer cell lines are *in vitro* model systems that are widely used for experimentation under the right condition and control to develop anti-tumour drugs, study their mechanism of action and how MDR can develop (Gillet *et al*., 2013; Mirabelli *et al*. 2019; Masters, 2000). However, they do not have equal value where some have succeeded whereas others have failed and there is a continuous increase in the development of novel pre-clinical models *in vitro* (Gillet *et al*., 2013; Borrell, 2010; Weinstein, 2012).

The first tumour cell line was HeLa and was derived from cervical cancer cell lines by Henrietta Lacks in 1951 (Scherer *et al*., 1953). This subsequently led to the establishment of various cancer cell lines that were propagated as monolayer primary cultures *in vitro* or xenografts in tumour-bearing rodents *in vivo* (Mattern *et al*. 1988; Rockwell, 1980). Tumour cell lines can be obtained from the American Type Culture Collection (ATCC) and the European Collection of Cell Cultures (ECCC). Some of the most common cancer cell lines are summarised in Table 2. They differ in their anti-tumour drug response due to the complexity and biological mechanisms of the disease, percentage of oxygen, growth factors and their interaction with stromal and immune cells (Ferreira *et al.* 2013; Klijn *et al*., 2015; Ferriera, 2005). It is important to publish the tissue or cell type and immortality for each established cell line to be used in Biomedical research according to the United Kingdom Coordinating Committee on Cancer Research (UKCCCR) (Geraghty *et al.* 2014; Monks *et al.* 1991).

We are in a position where the molecular and cellular status of each cell line has been defined with accuracy in databases such as The Cancer Genome Atlas (TCGS) which mutations, copy number variations and the expression of genes and proteins and when contaminated with mycoplasma via omics technology (genomics, transcriptomics and proteomics) (Goodspeed *et al*. 2016; Barretina *et al*. 2012).

Table 2: Examples of tumour cell lines used in cancer research. Their morphological and mortality status have been described.

Name of cell line	Abbreviation	Morphology	Cell Origin	Immortalized status and age of sampling
Cervix adenocarcinoma	HeLa	Epithelial	*Homo sapiens*, Human	It was developed by Henrietta Lacks in 1951. The cells were obtained from a Black female patient aged 31.
Acute promyelocytic Leukaemia	HL-60	Promyelocyte	*Homo sapiens*, Human	It was developed by Collins 1987. The cells were obtained from Caucasian female patient aged 36.
Breast adenocarcinoma	MCF-7	Epithelial	*Homo sapiens*, Human	Caucasian female patient aged 69.
Pancreatic neuroendocrine tumor	BON -1	Lymph node from the carcinoid	*Homo sapiens*, Human	28 years old male patient.
pancreatic carcinoma	QGP-1	Epithelial-like from the islet cell origin of the cellosaurus tumour.	*Homo sapiens*, Human	61 year old male patient
Glioblastoma	U87MG	Epithelial	*Homo sapiens*, Human	Unknown male patient
Colon adenocarcinoma	HT-29	Epithelial	*Homo sapiens*	Caucasian female patient aged 44.
Lung carcinoma	A549	Human alveolar basal Epithelial	*Homo sapiens*, Human	They were developed by Giard *et al*.,1973. Caucasian male patient aged 58.
Hepatocellular carcinoma	HEP-G2	Epithelial	*Homo sapiens*	Caucasian male patient aged 15.
Chronic myeloid leukaemia	K-562	Lymphoblast	*Homo sapiens*	53 years old female patient.
SV40 transformed kidney	Cos7	Fibroblast	*Cercopithecus aethiops*	The grivet/African green monkey.
Grade IV Prostate adenocarcinoma	PC3	Epithelial	*Homo sapiens*,	62 years old male Caucasian patient.
Malignant melanoma	A375	Epithelial.	*Homo sapiens*,	Female patient aged 54
Burkitt's lymphoma	Raji	Lymphoblast	*Homo sapiens* humans	Black male patient aged 11
humn acute promyelocytic leukemia	NB4	premyomyoblast	*Homo sapiens* humans	Female patient aged 23 in second relapse in 1989.

2.1.3 Tumour Biopsies

Amongst the characteristics of tumour cells are uncontrollable growth, loss of attachment, invasion and metastasis. The ability for tumour cells in a neoplastic state to lose their cohesiveness can allow tumour biopsies or lesions to take place that requires a needle aspiration for microscopic examination and diagnosis (Shyamala *et al.* 2014). However, there is a risk of seeding these tumour cells into the interstitial tissue fluid to transfer through lymphatic veins or via vasculature to other organs or tissues (Shyamala *et al.* 2014).

Several tumour biopsies have been utilised in cancer research where there is a positive correlation between the quantity of GLO1 protein and tumour grade (Fonseca-Sánchez *et al.* 2012). This emphasises that GLO1 gene amplification correlates with upregulation of the Glo1 overexpression and are essential in the proliferation and progression of tumours. There is also evidence that upregulation of the serum level of AFP is linked with Glo1 overexpression in hepatocellular carcinoma that affects TNM staging (Zhang *et al*. 2014).

Abdul-Maksoud *et al*. discovered that GLO1 overexpression was higher in breast cancer tissue and even more so at advanced stages; highlighting its potential as a diagnostic and prognostic biomarker (Abdul-Maksoud *et al.* 2017; Nokin *et al*. 2019; Fonseca-Sanchez *et al.* 2012). Recent studies have discovered that in tumours that are highly malignant but has poor clinical outcome such as patients with paediatric diffuse midline glioma, liquid biopsy can be used to characterise and identify circulating tumour DNA (ctDNA) (Panditharatna *et al*., 2018).

2.2 Anti-cancer drugs used in this investigation.

A broad spectrum of anti-cancer drugs will be utilized in this study: mechlorethamine, camptothecin, methotrexate, doxorubicin, cisplatin, etoposide, mitomycin c and vincristine. The molecular structure, molecular mass, mechanism of action and therapeutic use are summarised in Table 3.

Table 3: The molecular mass, mode of action and examples of its the therapeutic use for the anti-cancer drugs utilized in this investigation.

Class	Anticancer drug	Molecular mass (Da)	Mechanism of action	Therapeutic applications	Reference
Nitrogen mustard	Mechlorethamine	156.05	DNA alkylation	Lung cancer; chronic leukaemia, Hodgkin's disease.	(Siddik, 2002; Siddik 2003)
Bioreductive alkylator	Mitomycin C	334.32	DNA alkylation	Bladder, gastric and skin cancers	(Iyer and Szybalski, 1963; Verweij and Pinedo, 1990)
Metal complex	Cisplatin	300.05	DNA-metal complexation	DNA-metal complexation.	
Anti-metabolite	Methotrexate	454.45	Dihydrofolate reductase inhibitor	Bone, lung, bladder, gynaecological cancers.	(Tian and Cronstein, 2007)
Topoisomerase inhibitors	Camptothecin	348.36	Topoisomerase I inhibitor	Ovarian and colorectal cancers	(Brangi *et al*., 1999)
	Doxorubicin	543.53	Topoisomerase II inhibitor	Breast, stomach, bladder and thyroid cancers.	(Tacar *et al*., 2013)
	Etoposide	588.56	Topoisomerase II inhibitor	Stomach cancer non-Hodgkin lymphoma.	(Van Maanen *et al.*, 1988)
Anti-tubulin	Taxol	853.91	Microtubule stabilisation	Brain, gynaecological, lung and pancreatic cancer.	(Koziara *et al*, 2005; Weaver, 2014)
	Vincristine	824.9	Microtubule disruption	Hodgkin's lymphoma, small cell cancer, leukaemia, neuroblastoma.	(Yoneda, 2010)

3.0 Aims and Objectives

The aim of this study is to characterise the level of MDR to clinical anti-cancer drugs by Glo1 overexpression in a model human tumour cell line *in vitro* and to investigate the MDR mechanism for drugs where it is most marked.

Objective 1: To characterise the glyoxalase system and dicarbonyl metabolism in HEK-293 cells under high glucose conditions *in vitro*.

The growth characteristics of HEK-293 cells was initially assessed by performing a growth curve *in vitro* to determine the time-point of evaluating the anti-tumour drug effect on cell growth. The viable cell number was deduced using trypan blue exclusion assay method. This was performed at low (5 mM) and high glucose (25 mM) concentration *in vitro*. There is evidence that glucose deprivation reduces the cell proliferation rate significantly causing a low yield of lactate production and low glycolytic rate (Siegwart *et al.* 1999).

The activities of the enzymes involved in the metabolism of the main dicarbonyl, methylglyoxal in HEK-293 cells was determined by validated methods using cytosolic cell extracts spectrophotometrically (Arai *et al*., 2014). Glo1 gene and protein in HEK-293 cells were measured by real-time reverse transcription-polymerase chain reaction (RT-PCR) and Western blotting, respectively (Xue *et al*. 2014).

The concentration of the endogenous metabolites, dicarbonyls and glutathione were measured in HEK-293 cell extracts by stable isotopic dilution analysis LC-MS/MS (Rabbani and Thornalley, 2014d). The normal concentration of dicarbonyls in mammalian cells is 1 – 4 μM and a level beyond this range causes dicarbonyl stress (Rabbani and Thornalley, 2015).

The fluxes of glucose consumption, and net L-lactate, D-Lactate formation were determined to give an insight into the effect of drug treatment on aerobic glycolysis and the formation of methylglyoxal respectively in HEK-293 cells i*n vitro*. D-glucose was measured in the cultured medium by enzymatic end-point absorbance assay whereas D-Lactate and L-lactate was measured in the cultured medium by enzymatic end-point fluorescence assay.

The effect of exogenous methylglyoxal on HEK-293 cells *in vitro* will be determined by conducting a concentration-response study. HEK-293 cells will be incubated for 48 h with varying concentrations of exogenous MG. There is evidence that exogenous MG affects the growth and sensitivity of HEK-293 cells *in vitro* (Kang *et al*., 1996; Santel *et al*, 2008).

Objective 2: To evaluate the growth inhibition and toxicity of anti-tumour drugs in stable transfectant HEK-293 cell lines with overexpression of Glo1 and empty vector control to assess the level of resistance associated with increased Glo1 expression *in vitro*.

Glo1 overexpression causes innate and acquired MDR in cancer treatment by Glo1 gene amplification and Nrf2 overactivation (MacLeod *et al*., 2016; Santarius *et al*. 2010; Thornalley and Rabbani, 2011c; Xue *et al*.; 2012b; Xue *et al*., 2015; Zhang *et al*. 2015). The level of MDR caused by Glo1 overexpression is unknown for current anti-anticancer drugs (Rabbani *et al.* 2018). According to the hypothesis, methylglyoxal accumulation may form part of the anti-tumour drug response to induce growth arrest and cytotoxicity in tumours with a high glycolytic rate. However, knowing that there is high GLO1 gene amplification and activity in tumours, screening for GLO1 gene in tumour biopsies can aid with optimising chemotherapeutic agents (Thornalley and Rabbani, 2011). The anti-tumour drug that has the least resistance can be the optimum choice for therapy (Rabbani *et al*. 2018).

To achieve the objective, HEK-293 cells are overexpressed with pIRES2-GLO1-EGFP plasmid by stable transfection and the empty vector is transfected with pIRES2-EGFP plasmid as a control to study the effect of a wide range of different anti-tumour drugs. HEK-293 wildtype and stable-transfectant cell lines were incubated with 6 different concentrations of the anti-tumour drug for 48 h. Viable cell number was assessed by the trypan exclusion assay. The median inhibitory concentration and logistic regression coefficient were deduced from the dose-response equation. This can then inform which anti-cancer drugs have the most resistance. Thereafter, the effect of the anti-cancer drugs that caused most resistance on the metabolic fluxes and glucose consumption will be explored.

Objective 3 To study the effect of Glo1 inhibitor and Glo1 silencing on MG metabolism and the potency of the chemotherapeutic drugs in HEK-293 cells under high glucose conditions in vitro

The level of Glo1 overexpression in tumour influences the level of sensitivity to the Glo1 inhibitor or Glo1 silencing that accumulates methylglyoxal to induce apoptosis, anoikus and necrosis (Rabbani *et al*. 2018; Thornalley, 1998b). To achieve this objective, the effect of anti-tumour drugs on HEK293 cell growth in combination with Glo1 inhibitor at GC_{50} concentration will be studied. The effect of Glo1 inhibitor and Glo1 silencing on the glyoxalase system and dicarbonyl metabolism in HEK-293 cells will also characterised.

To confirm Glo1 knockdown, HEK-293 cells were treated with siRNA for 72 h and the mRNA, enzymatic and protein levels of Glo1 were measured and were compared to scrambled siRNA that acted as a control. The anti-tumour drug that had the most resistance will be treated with Glo1 inhibitor and Glo1 silencing to determine their effect.

Objective 4: To determine the effect of hypoxia (3% oxygen) on the potency of anti-cancer drugs and Glo1 inhibitor BBGD in high glucose conditions *in vitro*

There is evidence that there is an increase in chemotherapy resistance under hypoxic conditions and it also decreases the expression of Glo1 and increase the flux of MG formation (Forristal *et al*., 2013; Shafie *et al*, 2016). The glyoxalase system and dicarbonyl metabolism will be explored under normoxic conditions (20% oxygen) and hypoxic condition (3% oxygen with 92% nitrogen) at 37°C. The effect on the anti-tumour drug that had the most resistance will also be explored to determine its effect under hypoxic conditions *in vitro*.

Objective 5: To explore why anti-tumour drugs suffer Glo1-linked MDR.

To achieve this objective, the direct and indirect effect of Glo1 on the anti-cancer drugs was established by determining the effect of Glo1 activity spectrophotometrically and the level of GSH depletion by stable isotopic LC-MS/MS respectively (Thornalley, 1998a). The level of methylglyoxal will also be measured in drug-treated HEK-293 cells by LC-MS/MS to explore the effect of the broad

spectrum of anti-cancer drugs that vary structurally and mechanistically on MG production.

4. Materials and Methods

4.1 Materials

4.1.1 Cell lines

The HEK-293 cell line was acquired from the American Type Culture Collection (ATCC) (Virginia, USA).

4.1.2 Cell culture

4.1.2.1 Reagents

HEK-293 cells were maintained in Dulbecco's Modified Eagles Medium (DMEM) containing phenol red, L-glutamine and glucose concentration 4500 mg/L (cat. no. 11965092, ThermoFisher, UK). The DMEM media was supplemented with a final concentration of 10% Foetal Bovine Serum (FBS) and 100 U penicillin/0.1 mg/mL Streptomycin. The FBS (cat.no. F7524), penicillin/streptomycin solution (10,000 U/mL penicillin with 10 mg/mL streptomycin in 0.9% sodium chloride, cat.no. P4333), Trypan blue powder (cat. no.76146), tissue culture-grade dimethylsulphoxide (DMSO, cat. no. D4540) were all purchased from Sigma-Aldrich (Poole, Dorset, UK).

4.1.2.2 Equipment

Corning cell-culture grade plastic polystyrene T25 cm^2 flasks (cat. No. CLS430639), T75cm^2 flasks (cat. no. CLS430641), 6-well plates (cat. no. CLS3516), 12-well plates (cat. no. 156367), 100 mm x 20 mm tissue-culture treated culture dishes (cat. no. P7612) and Stripette serological pipettes (cat. no. CLS4488) were all purchased from Sigma-Aldrich. The Neubauer Haemacytometer for cell counting (Model no. 0630410, Marienfeld-Superior) was from Paul Marienfeld GmbH & Co. KG (Lauda-Königshofen, Germany). The 150 µL cloning glass cylinders (cat.no. C1059) and the cloning discs (cat. no. Z374431) were from Sigma-Aldrich and the inverted microscope Nikon Eclipse TE2000-S (Nikon UK Limited, Kingston Upon Thames, Surrey, UK) was used to select uniform fluorescence transfected colonies.

4.1.3 Molecular, biological and transfection reagents

4.1.3.1 Stable Transfection of GLO1 overexpression

pIRES2-GLO1-EGFP plasmid and pIRES-EGFP plasmid were prepared by the host research team. The transfection reagent: Lipofectamine 2000 (cat. no. 11668027) and OptiMEM serum-supplemented media (cat.no 31985062) were purchased from ThermoFisher (Paisley, UK). DH5α™ Competent Cells *Escherichia coli* (11 x 10^6/mL) were purchased from Thermo Fisher (Paisley, UK) and stored at -80^{o}C. Luria Bertani (LB) broth, LB media and G-418 disulphate were obtained from Sigma-Aldrich. Geneticin G-418 (potency rating – a supplier estimates of bacterial growth inhibition, 700 µg/mg) was purchased from Fisher Scientific (Loughborough, UK). Reagents for fast, large-scale, anion-exchange-based plasmid DNA preparation (Hi-Speed Plasmid Mini and Midi prep kits) were purchased from QIAGEN (Manchester, UK).

4.1.3.2 Transient Transfection of GLO1 knockdown

Accell Human GLO1 SMART siRNA pool (cat.no E-012277-00-0020) and Accell non-targeting Control siRNA pool (cat.no D-001910-0X) were obtained from GE Healthcare Dharmacon (Buckinghamshire, U.K.). Lipofectamine *RNAiMAX* (cat. no. 13778030) and the OptiMEM reduced serum-supplemented media (cat. no. 31985062) were obtained from ThermoFisher (Paisley, UK). The OptiMEM media consisted of sodium pyruvate, L-glutamine, thymidine, 4-(2-hydroxyethyl)-1-piperazineethanesulfonic acid (HEPES), sodium bicarbonate, growth factors, hypoxanthine and trace elements.

4.1.4 Enzymes, substrates and cofactors

4.1.4.1 Molecular biology enzymes

Restriction enzymes Bgl II (*Bacillus globigii*) and Pst I(*Providencia stuartii* 164) were obtained from New England Biolabs (Hitchen, UK). A unit is defined as the quantity of enzyme needed to digest 1 µg of λ DNA in 1 hour at 37°C in a total reaction volume of 50 µL. Bioscript Moloney Murine Leukaemia Virus (MMLV). Reverse Transcriptase (10,000 units; BIO-27036) and is highly stable and sensitive for first-strand cDNA synthesis (Bioline, London).

4.1.4.2 Other enzymes

Trypsin/ethylenediaminetetra-acetic acid (EDTA) (cat. no. 4049), L-lactic dehydrogenase (cat. no. EC 1.1.1.27) and D-lactic dehydrogenase (EC 1.1.1.28) were purchased from Sigma-Aldrich. Trypsin-EDTA sterile-filtered solution was utilized in cell culture and comprised of 2.5 g porcine trypsin, 0.2 g EDTA-tetra sodium salt per litre of Hank's Balanced Salt Solution with phenol red. L-Lactic dehydrogenase was from bovine heart, type III, and had an activity of ≥ 1000 units/mg protein. D-Lactic dehydrogenase is lyophilised powder, purified from *Staphylococcus epidermidis* and had activity of ≥ 80 units/mg protein.

4.1.4.3 Substrates and cofactors

Methylglyoxal solution (40% w/w; cat. no. M0252-500ML), reduced L-glutathione (G4251-10G), S-D-lactoylglutathione (cat. no. L7140-25MG), glyoxal (40% w/w; cat. no. L0625), aminoguanidine hydrochloride (cat. no. 396494), L-lactic acid (cat. no. N7505-1G), D-lactic acid (cat. no. L0625), NAD^+ (cat. no. N0632-1G) and NADPH (cat. no. N7505-1G) were obtained from Sigma-Aldrich.

4.1.5 Antibodies

Monoclonal anti-Glo1 antibody produced in rat (cat. no. SAB4200193) and the anti-rat IgG antibody (cat. no. B7139) were purchased from Sigma-Aldrich (Dorset, UK). Anti-β-actin antibody (cat. no. ab8229) was purchased from Abcam (U.K).

4.1.6 Primers

The primers and probe for β-actin and Glo1 were pre-designed from Life Technology Ltd (Paisley, Scotland). The primers that were utilized for the amplification of cDNA for GLO1 mRNA are summarised below in Figure 21.

Primers	Forward	Reverse
GLO1	5'-ATGCGACCCAGAGTTACCAC-3'	5'-CCAGGCCTTTCATTTTACCA-3'
ACTB	5'-GGACTTCGAGCAAGAGATGG-3'	5'-AGCACTGTGTTGGCGTACAG-3'

Figure 21: The primers used for cDNA amplification for GLO1 and β-actin. The mRNA expression of GLO1 was normalized to β-actin.

4.1.7 Anticancer agents

Doxorubicin (cat. no. D1515-10MG), vincristine (cat. no. V8879-1MG), cisplatin (cat. no. 479306-1G), paclitaxel (cat. no. T7191-1MG), etoposide (cat. no. E1383-25MG), methotrexate (cat. no. 06563-5MG), *S*-(+)-Camptothecin (cat. no. C9911-100MG) and mitomycin C (from *Streptomyces caespitosus;* cat. no. M4287-2MG) were purchased from Sigma-Aldrich. Mechlorethamine (cat. no. C2942) were purchased from Cambridge Bioscience Ltd (Cambridge, UK). SpBrBzGSHCp2 was available in-house by the host research team. It was prepared by acid-catalysed esterification of S-p-bromobenzylglutathione and purified by column chromatography as described (Thornalley *et al.*, 1996).

4.1.8 Other reagents

Ammonium persulphate (ACS reagent grade, cat. no. 248614), β-mercaptoethanol (cat.no. M6250-10ML), 3',3",5',5"-tetrabromophenol sulfonphthalein sodium salt (bromophenol blue, electrophoresis grade; cat. no. 114405), diethylenetriaminepentaacetic acid (DETAPAC) (cat. no. D6518), Tween-20 (cat. no. P2287), DMF (cat. no. D4551)), Bovine serum albumin (cat. no. A9418-5G), Complete Lysis-M buffer (cat. No. 4719956001) , N,N,N',N'-tetramethylethylene-1,2-diamine (TEMED, ≥ 99% electrophoresis grade; cat. no. T9281-25ML), sodium phosphate monobasic (cat. no. 71505), hydrochloric acid (analytical grade, 1 N; HCl) (cat. no. H1758), trichloroacetic acid (TCA) (cat. no. T6399-5G) were purchased from Sigma-Aldrich. Filter paper, polyvinyl difluoride (PVDF) membrane were purchased from Bio-Rad (Hertfordshire, UK).

Perchloric acid (cat. no. A2296-1LB), sodium chloride (cat. no. 7647-14-5) and potassium bicarbonate (cat. no. 298-14-6), Tris(hydroxymethyl)-aminomethane (Tris base) (cat. no. 77-86-1), Perchloric acid (cat. no. A2296-1LB), sodium dodecyl sulphate (SDS) (cat. no. 28312B), SpectroTM multicolor broad range protein ladder 10-260 kDa, for 4 – 20% Tris-glycine SDS-PAGE (cat no. 26623), Glycine (cat. no. BP381-500) was purchased from Fisher Scientific (Loughborough, UK). Hydrazine hydrate (cat. no. 18412) was purchased from Fluka (Poole, Dorset, UK).

HyperLadder™ 1kb (cat. no. BIO-33053), agarose (cat. no. BIO-41026), Oligo $(dT)_{18}$ primer (cat. no. BIO-38029) is a single-stranded sequence of deoxythymine (dT) that was utilized to prime reactions catalysed by reverse transcriptase. dNTP mix set (cat. no. BIO-39044) contained dCTP, dTTP, dGTP and dATP. RiboSafe RNase Inhibitor (cat. no. BIO-65027) is a recombinant protein that inhibits a eukaryotic RNases, SensiMix™ SYBR® Low-ROX Kit (cat. no. QT625-05) were purchased from Bioline (London, UK).

4.1.9 Analytical and preparative kits

The glucose assay kit - hexokinase method (cat. no. GAHK20) - was purchased from Sigma-Aldrich. The RNAse mini kit (cat. no. 74106) was purchased from Qiagen (Manchester, UK). The Pierce BCA Protein Assay Kit (cat. no. 23227) was used to measure total protein concentration compared to protein standard at a wavelength of A562 nm was purchased from ThermoFisher. Enhanced chemiluminescence (ECL) reagent kit (cat. no. 34079) was purchased from Fisher Scientific, UK.

4.1.10 Mass spectrometry

4.1.10.1 Chromatographic materials

All solvents were HPLC graded: acetonitrile (cat. no. 75058), tetrahydrofuran (THF) (cat. no. 109999) and methanol (cat. no. 67561), were purchased from Fischer Scientific (Loughborough, UK). Formic acid (≥ 98%; cat. no. F0507-500ML) and Trifluoroacetic acid (TFA, ≥ 99.0% HPLC grade; cat. no. 302031). The column-BEH C18, 1.7 µm particle size column (100 x 2.1 mm) fitted with a (5 x 2.1 mm) pre-column was utilized for the dicarbonyl and glutathione assay and were purchased from Waters (Elstree, UK).

4.1.10.2 Calibration of stock solutions of dicarbonyls

High purity MG and 3-DG were prepared in-house by the host research team. MG was prepared by the method described by McLellan and Thornalley (McLellan and Thornalley, 1992a). 3-DG was prepared from glucose and toluidine by a combination of two methods described by Madson and Feather and Henle and Bachmann (Madson and Feather, 1981; Henle and Bachmann, 1996). Glyoxal (40% aqueous solution) was utilized without purification and was obtained from Sigma-Aldrich (Dorset, UK) was used without purification. The concentration of stock solutions of dicarbonyls was determined by the derivatization with aminoguanidine hydrochloride and measuring the absorbance at 320 nm spectrophotometrically of the 1,2,4-triazine derivatives. The concentration can then be deduced from the known molar extinction coefficient (Thornalley *et al.*, 2000).

4.1.11 Equipment

Corning clear 96 polystrene well plates (cat.no CLS9102), black polystyrene 96 well plates (cat. no. CLS3925), 100 mm x 20 mm dishes (cat.no P7612-360 EA), 6 well plate (cat. no. M9052-100EA), 12 well plate (cat. no. M9187-100EA) was obtained from Sigma Aldrich (Dorset, UK). Cryotube vials (1.8 ml; NUNC, cat. no. 363401) were purchased from Sigma-Aldrich (Dorset, UK). For real-time PCR, MicroAmp® optical adhesive film (cat. no. 4311971) and MicroAmp® optical 96-well reaction plate (cat. no. N8010560) were obtained from ThermoFisher Scientific. Special compressed gas mixture of 3% oxygen with nitrogen was purchased from CK Gas Products Ltd (Leicester, UK). HPLC

vials, caps, 200 µl glass inserts and plastic supports were purchased from Fisher Scientific (Loughborough, UK).

4.1.12 Instrumentation

For the quantification of protein assays, end-point absorbance assays and end-point fluorescence assay were performed using a FLUOstar OPTIMA microplate reader version 2.10 R2 was utilized from BMG Labtech (Ayelsbury, UK). The NanoDrop™ UV/visible spectrophotometer ND-1000 was from LabTech International (Uckfield, UK) and was used for the estimation of sample DNA and RNA content. AccuSpin 3R centrifuge and Heraeus Pico 17 centrifuge were purchased from Fisher Scientific (Loughborough, UK). A UVICON UV/VIS spectrophotometer (Northstar Scientific Limited, Sandy, UK) was used to determine activities of Glo1, Glo2, MG reductase and MG dehydrogenase. The centrifugal evaporator was a Savant Instruments SpeedVac and Applied Biosystems™ 7500 real-time PCR machine were from Thermo Fisher Scientific (Paisley, UK). Hypoxia chamber (cat. no. 27310) and single flow meter (cat. no. 27311) were from Stemcell Technologies (Manchester, UK).

A Criterion™ Cell electrophoresis chamber (cat. no. 1656020), Mini Trans-Blot Electrophoretic Transfer Cell (cat. no. 170-3930) and PowerPac™ Basic Power Supply (cat. no. 164-5050) were purchased from Bio-Rad (Hertfordshire, UK). Applied BiosystemsTM 7500 Real-time PCR machine was from Thermo Fisher (Paisley, UK). A gel imaging system for chemiluminescence, GeneGnome XRQ System was purchased from Syngene (Cambridge,UK).

Liquid chromatography-tandem mass spectrometry (LC-MS/MS) analysis was conducted using two instruments from Waters (Manchester, U.K.): AcquityTM UPLC system with a Quattro Premier XE tandem mass spectrometer and an AcquityTM UPLC system with a Xevo-TQS tandem mass spectrometer.

4.1.13 Software

Masslynx 4.1 software (Waters, Manchester, UK) was used to integrate the data for the dicarbonyl and glutathione assays. The GC_{50} value was calculated from the non-linear regression analysis using the Enzfitter program from Biosoft (Cambridge, UK). Densitometry of bands on Western blots was performed using Image J software from the National Institute of Health and Image Quant software

from GE Healthcare Life Sciences. The statistical package SPSS (v10) was made by SPSS Inc. (Chicago, USA).

4.2 Methodology

4.2.1 Culture of HEK-293 cells

HEK-293 cells were delivered frozen on dry ice and were stored in liquid nitrogen until use. Each vial contained 2 x 10^6 cells in 1 ml cryopreservative medium. When required, the solution was rapidly thawed on a water bath (37^{o}C) for 1 - 2 min. The cell suspension was transferred to a T-flask under aseptic conditions gently and mixed with 14 mL of pre-warmed culture DMEM medium containing high glucose (25 mM), L-glutamine (4 mM) and supplemented with 10 % (v/v) FBS, 100 U/mL penicillin/0.1 mg/ml streptomycin. The cell suspension was incubated at 37 ^{o}C, 5 % CO_2 and 100 % humidity and passed until cell fragments were removed and cell viability was >99%.

4.2.2 Normal growth conditions

HEK-293 cells were seeded at a density of 2 x 10^4 cells ml^{-1}. Cells were cultured in T75 cm^2 flasks to 80-90% confluence and routinely sub-cultured every three to four days. Cells were rinsed with 10 mL phosphate-buffered saline (PBS), 2 ml pre-warmed trypsin-EDTA solution added for 3-4 min, trypsin inhibited by addition of 10 ml pre-warmed growth medium and cells collected by centrifugation (150g, 5 min, 18 ^{o}C). The supernatant was removed and the cell pellet re-suspended with 5 ml pre-warmed growth medium. Trypan blue solution was prepared (0.25 % trypan blue in PBS) and the cell viability assessed by the Trypan blue exclusion method (Strober, 2001). The viable cells were > 98% consistently throughout. Aliquots of HEK-293 cells were prepared for cryostorage: 2 million cells in 1 mL of cryopreservative medium containing 60 % (v/v) FBS, 30 % complete growth medium and 10% DMSO.

4.2.3 Growth curve preparation

HEK-293 cells (20,000 cells per cm^2; 76000 cells per well in 12-well plates with 1 ml culture medium) were incubated for up to 4 days. Total cell number and viable cell number was counted every day for 4 days and a cell growth curve was constructed.

4.2.4 Characterisation of glyoxalase system and dicarbonyl metabolism in HEK-293 cells cultured *in vitro*.

HEK-293 cells were cultured in 25 mM glucose *in vitro* for three days in triplicate. Cell extracts were analysed for the activity of enzymes involved in MG metabolism: Glo1, Glo2, MG reductase and MG dehydrogenase. Glo1 mRNA and Glo1 protein levels were also quantified. The levels of dicarbonyls and glutathione in HEK-293 cells were also determined. The media samples were analysed to determine D-lactate, L-lactate and D-glucose levels.

A growth curve and the measurement of Glo1 activity, mRNA, protein and the metabolic fluxes were also performed for the following experiments:

- The effect of varying glucose concentration on HEK-293 cell growth *in vitro.*
- The effect of Glo1 overexpression on HEK-293 cell growth under 25 mM glucose conditions *in vitro*
- The effect of incubation with 7 µM Glo1 inhibitor, BBGD (2 x GC_{50}), on HEK-293 cell growth under 25 mM glucose conditions *in vitro*.
- The effect of Glo1 silencing on HEK-293 cell growth under 25 mM glucose conditions *in vitro.*
- The effect of hypoxia on HEK-293 cell growth under 25 mM glucose conditions *in-vitro*.

4.2.5 The effect of exogenous methylglyoxal on HEK-293 cell growth – dose-response study

Methylglyoxal was synthesised, purified and the concentration of aqueous stock solutions calibrated by McLellan and Thornalley (1992a). Sodium phosphate buffer (pH 7.4), 1 mM aminoguanidine hydrochloride with and without *ca.* 30 µM of the high purity methylglyoxal at 37 ^{o}C for 3 h in triplicate to derivatise MG by aminoguanidine to completion – Figure 22. The absorbance was recorded at 320 nm (Thornalley *et al*, 2000). The blank was corrected and the MG concentration was deduced in the stock solution. The molar extinction coefficient is 2.41 $mM^{-1}cm^{-1}$.

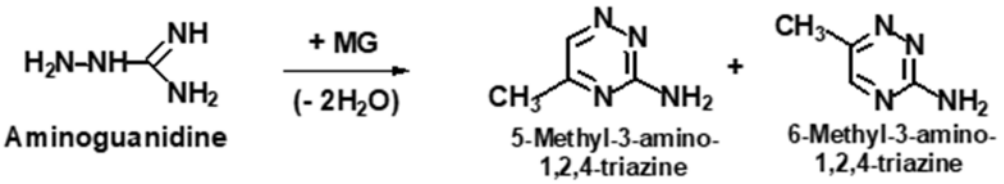

Figure 22: The derivatisation of high purity methylglyoxal solution. Aminoguanidine is a carbonyl scavenger and a prototype agent that prevents diabetic complications. It is pre-incubated with the physiological α-oxoaldehydes such as methylglyoxal to form isomeric 3-amino-1,2,4-triazine derivatives and prevent glycation by these agents *in vivo* and *in vitro*. The physiological conditions for this reaction are pH7.4 and 37^{o}C. The rate kinetics of the reaction of aminoguanidine with methylglyoxal were the same with unhydrated and monohydrated forms but the concentration of the initial reactant influences the ratio of the triazine derivatives (Thornalley *et al*, 2000).

Methylglyoxal was sterile filtered by centrifugation (10,000g, 5 min, 4 ^{0}C) at a concentration of 51.2 mM. HEK 293 cells (20,000 cells per cm^{2}; 76000 cells per well in 12-well plates with 1 ml culture medium) under high glucose (25 mM) concentrations *in vitro* and were incubated overnight to adhere to the plate. The following day, 100, 200, 400 µM of methylglyoxal was added with a 1:1 ratio with PBS. Each concentration and untreated controls were studied in triplicate. The plates were incubated for 48 hours. Cells were gently washed with 1 mL PBS then detached by incubation with 250 µL trypsin-EDTA. The cells and the

medium containing methylglyoxal were removed from the plate. Cells were collected by centrifugation (250 x g, 5 min) and the supernatant medium removed. The cells were re-suspended in fresh culture medium and a diluted sample was counted using a Neubauer haemocytometer. Each cell suspension was counted thrice, the number of viable and non-viable cells per mL deduced.

Viable and non-viable cell numbers were recorded to produce an MG concentration-response curve. Data were fitted to the dose-response equation $V=100 \times (GC_{50})^n / ((GC_{50})^n + ([MG])^n)$ where V is the viable cell number as a percentage of control cultures without the addition of MG, GC_{50} is the median growth inhibitory concentration value, [MG] is the concentration of MG and n is the logistic regression coefficient (also known as the Hill coefficient). Experimental data of V and [MG] were fitted by non-linear regression of V on [MG] using the programme EnzFitter programme (Biosoft, Cambridge, U.K.).

A time-course study on the effect of methylglyoxal on HEK-293 cell growth was also conducted. HEK-293 cells–were cultured at a cell density of 20,000 cells/cm^2 in 12-well plates containing 25 mM glucose media *in vitro*; there were independent triplicates. One plate was for the addition of the GC_{50} value of methylglyoxal, whereas the other plate contained control incubations in triplicate. The number of viable and non-viable cells was counted every day for three day.

4.2.6 Propagation of the glyoxalase 1 transfection vector

Escherichia coli DH5α cell suspension from cryostorage was thawed rapidly and kept on ice. pIRES2-GLO1-EGFP plasmid solution (0.5 – 1 µL; 286ng DNA per µL) was added and mixed gently with 0.1 mL competent *E. coli* in a sterile Eppendorf tube on ice (Jackson *et al*., 1990; Jang *et al*., 1990; Cormack *et al*., 1996). A tube containing no DNA was also prepared as a control. The solution was incubated on ice 20 min followed by incubation at 42 °C for two min. This was subsequently incubated on ice again for 1-2 min. LB medium (1 mL) was added. This solution was incubated for 30 - 0 min at 37 °C. Aliquots (10 – 300 µL) were pipetted onto an agar plate and gently smeared with sterile glass rod. Plates were then incubated overnight at 37 °C.

4.2.7 Bacterial transformation

pIRES2-EGFP plasmid (100 ng), GLO1 cDNA (500 ng) and T4 DNA ligase (200 U) were incubated at 4 ^{0}C in ligation buffer (50 mM Tris-HCl, 10 mM $MgCl_2$, 1 mM ATP, 10 mM DTT, pH 7.5) for four days. The products were transformed into DH5-α cells competent cells (heat shock method). An aliquot of the product (10-300 µL) were added to selective agar plates containing kanamycin 30 µg mL^{-1}. A few, well-formed, smooth-edged, isolated colonies from each plate were used to inoculate growth medium that also contained 30 µg mL^{-1} kanamycin. The restriction enzymes *Bgl II* and *Pst I* were used to obtain mini-preps and analytical digests by PCR method. These type II restriction endonuclease enzymes were chosen as studies have shown that the coding sequence of GLO1 can be easily obtained by digesting the vector with both enzymes. Plasmid DNA (1µg) and of *Bgl II* and *Pst I* (2.5 U) were incubated in 10X NEbuffer (100 mM NaCl, 50mM Tris-HCl, 10mM $MgCl_2$, 100µg/ml BSA pH 7.9 at 25°C to give a total volume of 20 µL. This was followed by incubation at 37^{o}C overnight to yield the following fragment sizes: 1662 bp and 3646 bp that were viewed on 1% agarose gel to check the identity of the GLO1 gene. The fragment size for GLO1 is between 500-600 bp – Figure 23.

Mini-preps were used to re-transform competent XL1 B cells and midipreps were conducted to purify pIRES2-GLO1-EGFP plasmid containing GLO1. The DNA concentration was measured by the NanoDrop spectrophotometry for GLO1 plasmid 286.0 ng/µL and empty plasmid 215 ng/µL. The correct insertion of the GLO1 cDNA into the Pgem-T Easy was established and thus the plasmids were digested with the restriction enzymes.

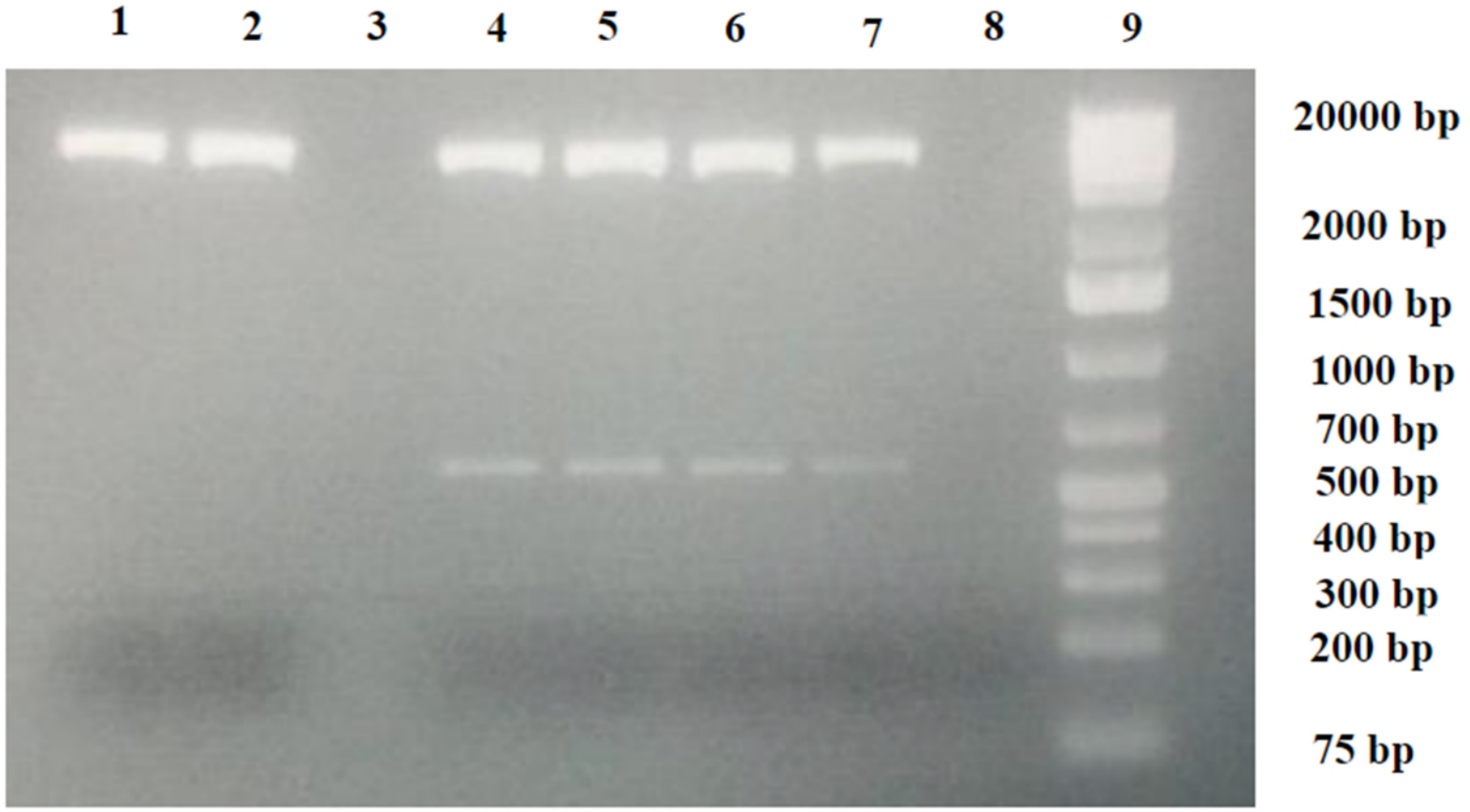

Figure 23: Analytical digests of the GLO1 plasmid and empty plasmid by conventional 1% agarose gel electrophoresis.

Lane 1: Empty plasmid; lane 2: empty plasmid; lane 4: GLO1 plasmid; GLO1 plasmid; lane 5: GLO1 plasmid; lane 6: GLO1 plasmid; lane 7: GLO1 plasmid; Lane 9: marker. The fragment sizes: 1662 bp and 3646 bp to check the identity of GLO1 gene. DNA Ladder utilized was GeneRuler 1 kb Plus DNA Ladder 75 – 20,000 bp.

4.2.8 Stable transfection of pIRES2-EGFP plasmid into HEK-293 cells

4.2.8.1 Preparation of transfected cells.

Transfection was conducted using Lipofectamine 2000 according to the manufacturer's instructions. Cells were seeded in 6-well plate at a density of 300,000 cells in 2 mL Transfection medium (DMEM, 10% FBS, no antibiotic). Lipofectamine 2000 (1 µg μL^{-1}; 2 µL) in a total volume of 100 µL OptiMEM serum-free medium was prepared. A separate solution of 1 µg plasmid DNA (GLO-1 plasmid 6.99 µl, Empty plasmid 9.30 µL) in 100 µl OptiMEM was also prepared. This was followed by incubation at room temperature for 5 min. The plasmid DNA solution and the Lipofectamine 2000 solution underwent fusion together to give a ratio for DNA: Lipofectamine 2000 as 1:4. This was followed by incubation for 20 min to allow transfection complexes to form between the two parties. An aliquot (200 µL) of OptiMEM-DNA-Lipofectamine 2000 solution was pipetted into each well of the 6 well plate drop-wise. Subsequently, the plate was mixed gently to provide a uniformed distribution of the mixture. The transfected cells were incubated at the following conditions: 37 ^{o}C, 5 % CO_2 in air, 100% humidity for 24 hours for adherence to occur and increase confluency. Visual quantification of EGFP-containing transfected cells was conducted using a fluorescence microscope (excitation maximum, 488 nm; emission wavelength, 507 nm).

4.2.8.2 Attempts to generate stably transfected cell lines.

After 48 h, cells were detached by trypsin and split to ~ 20% confluence and transfected cells were selected with sterile-filtered aminoglycoside antibiotic G-418 disulphate with fluorescence monitoring to detect transfected cells. Attempts were made to select transfected cells using the recommended dose 200-500 µg/ml (405 µg/mg potency) changing the media every two days. However, there was interference with non-transfected cells growth despite plasmid contains the neomycin gene. This was found even when increasing the concentration of G-418 to 2000 µg/mL (Sigma-Aldrich 405 µg/mg potency). Other methods to select the cell were via serial dilution using a 48 and 96 well plate, selecting colonies via the cycle and increasing the potency.

G-418 disulphate from Fischer Scientific (705 µg/mg) was utilized and an antibiotic kill curve was constructed varying the concentration from (200 – 2000 µg/ml) and were monitored daily for a period of 7 days – Figure 24. The purpose of the dose-response experiment is to define the minimum concentration of the selective antibiotic G-418 that can kill untransfected mammalian cells at a specific time to generate stable transfectant cell lines. Each cell line varies in their sensitivity to the antibiotic. The recommended doses provided by the supplier, 500 (µg/mL) failed to work and the optimal dose was gained at 2000 (µg/mL) and were used for further experiments.

Further studies involved transfected cell colonies selected using a cloning disc (3.2 mm) and glass cylinder selector. Transfected cell colonies with uniform fluorescence were selected using a cloning glass cylinder (8 mm, 150 µL) and cultured further with G-418 disulphate (705 µg/mg; 2 mg/mL) containing medium. In subsequent sub-culturing, G-418 concentration was decreased to 1 mg/mL. Glo1 activity and protein was assessed to determine the fold difference between Glo1 and empty stable transfectant cells. Colonies will be selected using a cloning disc (3.2 mm) and glass cylinder selector.

Figure 24: Microscopic images for the kill curve of G-418 antibiotic tested in HEK-293 cell lines. Qualitative analysis suggests that the viability of HEK-293 cells is in dependence of the concentration of the antibiotic monitored daily over the period of 8 days. The images reflect the adherent fraction of HEK-293 cells relative to confluency for Day 4, 6 and 8 after adding the G-418 antibiotic. The potency of the G-418 was 705 µg/mg where it was diluted to the concentration range (200 – 2000 µg/mL) and was compared to control (0 µg/mL). Each group consisted of technical replicates for 3 biological replicates. The images were taken using the Nikon microscope (Magnification, 40X).

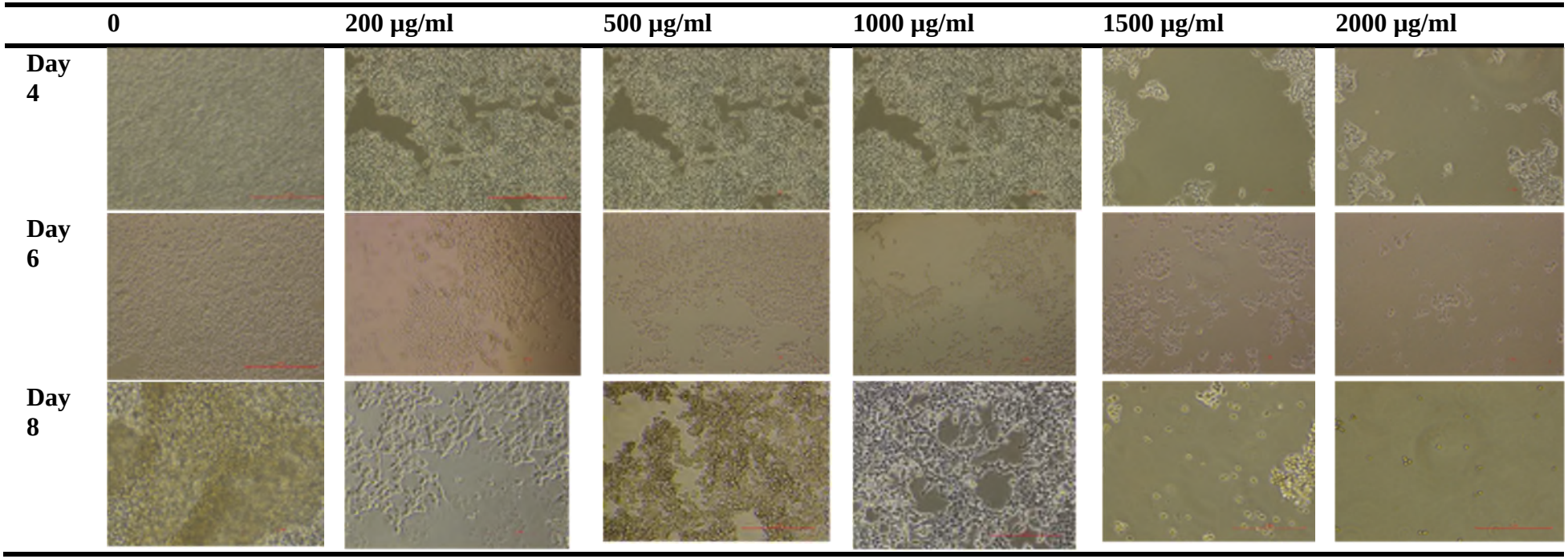

4.2.9 Transient transfection of Glo1 siRNA into HEK-293 cells

Cells were transfected with 48 nM Accell Human GLO1 SMART siRNA pool and 48 nM Accell non-targeting Control siRNA pool (GE Healthcare Dharmacon Inc, Little Chalfont, Buckinghamshire, U.K) with Lipofectamine *RNAiMAX* Transfection Reagent (Thermo Fisher Scientific, Paisley, U.K.) based on the manufacture's protocol for reverse transfection reaction. The complexes were prepared inside the well after which HEK-293 cells (1×10^5) in 12-well plate and 1 mL of DMEM containing high glucose (25 mM), L-glutamine (4 mM) and supplemented with 10 % (v/v) FBS, 100 U/ml penicillin/0.1 mg/ml streptomycin. Attempts were made to ensure Glo1 siRNA was knocked down by varying the concentrations from the recommended concentration (12 nM) given to extremely high concentrations (96 nM) to establish the dose that knocked down Glo1. This was confirmed by spectrophotometric measurement of Glo1 enzymatic activity, mRNA and protein levels to ensure >95% was decreased.

4.2.10 Anti-cancer drug concentration-response curves

4.2.10.1 Glo1 overexpression studies *in vitro*

Stock solutions of anti-cancer drugs were prepared in DMSO (100 mM), unless otherwise stated, and were sterile-filtered. Cisplatin stock solution was prepared in DMF. HEK 293 cells (20,000 cells per cm^2; 76000 cells per well in 12-well plates with 1 ml culture medium) were incubated overnight to adhere to the base of the plate. The following day, the culture medium was removed and replaced with medium containing the anti-cancer drug at the required concentration. Each concentration and untreated controls were studied in triplicate. The plates were incubated for 48 hours. Cells were gently washed with 1 mL PBS then detached by incubation with 250 µL trypsin-EDTA. The cells and the medium containing anti-cancer drug were removed from the plate. Cells were collected by centrifugation (250 x g, 5 min) and the supernatant medium removed. The cells were re-suspended in fresh culture medium and a diluted sample was counted using a haemocytometer. Each cell suspension was counted twice, the number of viable and non-viable cells per mL deduced. The viable cell number was expressed as a percentage of untreated control.

4.2.10.2 Glo1 inhibitor studies *in vitro*

The same procedure was conducted as described in Section 4.2.10.1. However, the constant GC_{50} value of Glo1 inhibitor 3.65 µM was added to each well containing varying concentrations of the anti-cancer drug. After 48 hours, the cell count was conducted via Trypan Blue exclusion assay.

4.2.10.3 Glo1 silencing studies *in vitro*

After 24 hours of transfection, the cells were incubated with and without the chemotherapeutic agent and were studied in triplicate. The stock solution of the chemotherapeutic agents was 50 mM in DMSO such that the maximum exposure to DMSO was 0.2 %. The plates were incubated for further 48 hours with the anti-cancer drug. Cells were gently washed with 1 mL PBS then detached by incubation with 250 µL trypsin-EDTA. The cells and the medium containing anti-cancer drug were removed from the plate. Cells were collected by centrifugation (250 x g, 5 min) and the supernatant medium removed. The cells were re-suspended in fresh culture medium and a diluted sample was counted using a Neubauer haemocytometer. Each cell suspension was counted thrice, the number of viable and non-viable cells per mL deduced. The viable cell number was expressed as a percentage of untreated control.

4.2.11 Hypoxia studies *in vitro*

Untransfected HEK-293 cells were seeded in a humidified atmospheric condition of 5% CO2 at 37^{o}C to adhere overnight before being exposed to hypoxic conditions for 72h. The cells were then placed in a hypoxia chamber filled with 3% oxygen with nitrogen. The procedure corresponded with the manufacturer's instructions (STEMCELL technologies, 2020). Excessive evaporation was prevented by placing two Petri dishes (100 mm x 20 mm) containing sterile water (10 – 20 mL) to the base of the chamber. A hermetical closure was performed by positioning the ring clamp. The gas tank was attached and the chamber was purged. The tank valve control was set at 8 – 10 psi clockwise whilst the flow meter was set at 20 L/min to remove oxygen for 4 minutes. The gas flow was subsequently turned off and the chamber was completely closed via the white clamps. A set of cell culture was placed in the conventional incubator as a control

The method carried out to construct a growth curve to determine the effect of a hypoxic environment on the proliferation rate of HEK-293 cells and the routine procedures to characterise the glyoxalase system and the dicarbonyl metabolism that correspond to Section 4.3. The anti-tumour drug that produced the most resistance was also experimented to determine their effect under normoxic and hypoxic conditions *in vitro.*

4.3 Analytical methods

4.3.1 Cell lysate preparation

Cell suspensions were centrifuged (250 x g, 5 min). The pellets (*ca.* 5×10^6 cells) were re-suspended in 300 µl PBS, pH 7.4, and centrifuged again. This was repeated 3 times to remove all extracellular protein. After the third wash, the pellets were stored at -80°C until further processing. Cell pellets were subsequently diluted in Lysis-M EDTA-free mammalian cell protein extraction reagent and the membranes were sedimented by centrifugation (14,000g, 20 min, 4°C). The supernatant was removed and used as lysate in protein quantification and subsequent enzymatic activity assays.

Previous attempts have been made to establish the above optimized method to extract proteins and ensure a good protein recovery to conduct further experiments. For instance, varying the number of cells, sonication method and protein assay reagent where the concentration of protein in cells lysates was initially measured by Bradford protein assay but it was incompatible with the Lysis M buffer as the detergent consists of NP40 and % sodium deoxycholate and the Bradford method is compatible up to 0.25% (Bradford, 1976, Compton and Jones, 1985). This is the reason why the BCA protein assay was utilized.

4.3.2 Total protein measurement

Protein concentration in the cell lysate was determined by the bicinchoninic acid assay (BCA) method. 1% (10 mg/ml) of Bovine serum albumin (BSA) solution was calibrated by UV absorption spectrophotometry. The molar extinction coefficient of BSA is 6.9 cm^{-1} at 279 nm (Peters, 1962). The assay was calibrated (0 - 2000 µg/µl protein) using the bovine serum albumin to be used as the standard at an absorbance of 595 nm. The standards, blanks and the samples were in triplicate (25 µl per well) with 200 µl of the Working reagent in a 96 well

clear microplate. The plate was thoroughly mixed on a plate shaker for the duration of 30 seconds. This was followed covering the plate and an incubation of 37°C for 30 minutes. The absorbance was then measured at 595 nm on plate reader. The protein concentration of the samples was obtained by the interpolation of the calibration curve. An example of a calibration curve is presented in Figure 25.

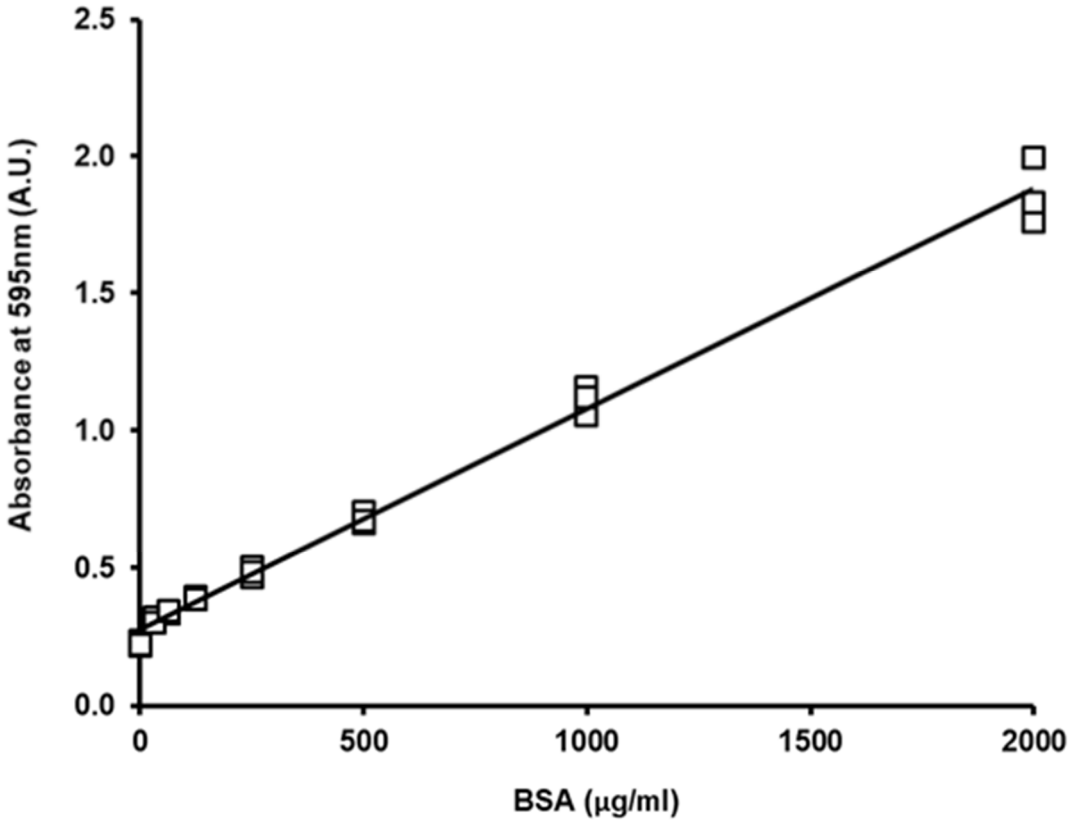

Figure 25: A calibration curve for determining the concentration of total protein using BSA as the protein reference standard. The albumin standard was formulated at 2 mg/mL in sterile water solution. 6 standards were utilized with varying concentrations within the range (0 – 2000 µg/ml). The X-axis is the protein concentration and the Y-axis is the absorbance measured at the wavelength 595 nm. Linear regression equation: Absorbance (arbitrary units) = (0.000800x + 0.275) x BSA standard (µg/ml); R2 = 0.993 (Data are mean ± SD; n = 3).

4.3.3 Characterisation of MG metabolism in HEK-293 cells.

4.3.3.1 Glo1 Activity

The activity of Glo1 was determined by measuring the initial rate of formation of S-D-lactoylglutathione from the hemithioacetal formed non-enzymatically from MG and GSH, followed spectrophotometrically at 240nm; $\Delta\varepsilon_{240}$ = 2.86 $mM^{-1}cm^{-1}$ – Figure 26 (Allen, *et. al*, 1993a).

Hemithioacetal was prepared by pre-incubation of MG (2 mM) with GSH (2 mM) at 37°C for 10 min in sodium phosphate buffer (500 µl, 100 mM, 37°C and pH 6.6). The cell extract (20 µl, prepared by lysing 5 x 10^6 cells in 100 µl lysis buffer and sedimenting cell membranes) was added and absorbance at 240 nm was monitored for 5 min. The activity of Glo1 is deduced from the initial increase in absorbance, corrected for homogenization buffer blank (Lysate M buffer). Glo1 activity is given in units per mg protein (the latter determined by BCA assay) where one unit of Glo1 activity is the amount of enzyme which catalyses the formation of 1 µmol of S-D-lactoylglutathione per minute under assay conditions.

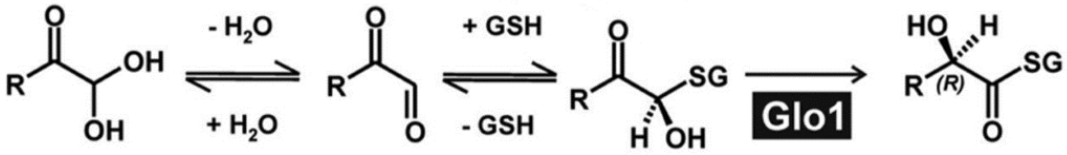

Figure 26: The metabolism of methylglyoxal by Glyoxalase 1

Glo1 catalyses the isomerization of the spontaneous reaction between the glutahionyl group of the tripeptide GSH and the aldehyde of MG to form hemithioacetal adduct: MG-GSH.

4.3.3.2 Glo2 Activity

Glo2 activity is determined by measuring the initial rate of hydrolysis of S-D-lactoylglutathione to GSH and D-lactate - Figure 27. The reaction is followed spectrophotometrically by following the decrease in A_{240} for which the change in molar absorption coefficient is $\Delta\varepsilon_{240}$ = 3.10 mM^{-1} cm^{-1} (Clelland and Thornalley, 1991). S-D-lactoylglutathione (0.3 mM, 100 µl, 4°C) was incubated in Tris-HCl buffer (100 mM, 500 µl, pH 7.4, 37°C) and water (37 °C, 380 µl). The cell lysate (20 µl, 5 x 10^6) was added and the absorbance was monitored for the duration of 5 min at 37°C. Glo2 activity is given in units per mg of protein or per million cells where one unit is the amount of enzyme that catalyses the hydrolysis of 1 µmol of *S*-D-lactoylglutathione per min under assay conditions (Allen *et al*., 1993b). Other S-2-hydroxyacyl-glutathione derivatives are hydrolysed to GSH and the aldonic acid (Reeves and Thornalley, 1993).

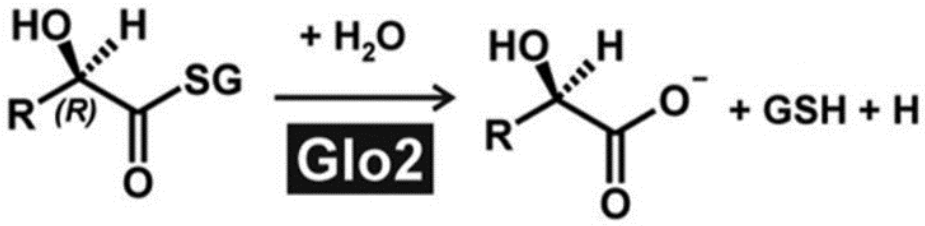

Figure 27: The hydrolysis of S-D-lactoylglutathione by Glyoxalase 2.

Glyoxalase II catalyses the terminal step of the glyoxalase system whereby S-D-lactoylglutathione is hydrolysed to reduced glutathione and the corresponding aldonic acid; D-Lactate.

4.3.3.3 MG reductase activity

NADPH-dependent aldoketo reductase is determined by measuring the initial rate of NADPH oxidation to $NADP^+$ by cell lysates (5×10^6) in the presence of MG and NADPH – Figure 28. This was followed spectrophotometrically at 340 nm for which the change in extinction coefficient is $\Delta\varepsilon_{340} = -6.20\ mM^{-1}cm^{-1}$. MG (20 mM in water, 50 µl) was incubated with NADPH (1 mM in water, 4°C, 100 µl) in sodium phosphate buffer (100 mM, 500 µl, pH 7.4, 37°C) and water (330 µl, 37°C) for 10 min. Cell lysate or lysate buffer (20 µl) for blank, added to a final volume of 1 ml the solution was mixed by inversion and the absorbance at 340 nm was measured for 5 min where the formation of hydroxyacetone (95%) and D-lactaldehyde is formed (Thornalley, 1994). It is measured in units where one unit catalyses the reduction of 1 µmol of MG per min under assay conditions.

$$NADPH + H^+ + CH_3COCHO \rightarrow NADP^+ + CH_3COCH_2OH + C_3H_6O_2$$

Methylglyoxal Hydroxyacetone lactoyladehyde

Figure 28: The metabolism of methylglyoxal by MG reductase

The 43 kDa enzyme has high specificity for methylglyoxal and is dependent upon NADPH that acts as an electron donor where it binds to its catalytic triad active site: Tyr-Lys-Ser to form hydroxyacetone (95%) and lactoyladehyde.

4.3.3.4 MG dehydrogenase activity

NAD^+-dependent MG dehydrogenase activity is determined by measuring the initial rate of NAD^+ reduction to NADH by cell lysates (5 x 10^6) in the presence of MG and NAD^+ - Figure 29 (Murata *et al.* 1975). This was followed spectrophotometrically at 340 nm for which the change in extinction coefficient is $\Delta\varepsilon_{340}$ = 6.20 $mM^{-1}cm^{-1}$. MG (20 mM in water, 50 µl) was incubated with NAD+ (1 mM in water, 4°C, 100 µl) in sodium phosphate buffer (100 mM, 500 µl, pH 7.4, 37°C) and water (330 µl, 37°C) for 10 min. Cell lysate or lysate buffer (20 µl) for blank, added to a final volume of 1 ml the solution was mixed by inversion and the absorbance at 340 nm was measured for 5 min. The activity of MG reductase is measured in units where one unit catalyses the reduction of 1 µmol of MG per minute under assay conditions.

$$NAD^+ + CH_3COCHO \rightarrow NADH + CH_3COCO^{2-}$$

Methylglyoxal Pyruvate

Figure 29: The metabolism of methylglyoxal by MG dehydrogenase.

Methylglyoxal dehydrogenase can detoxify MG into pyruvate which is then transferred into the tricarboxylic acid (TCA) via acetyl coA (Mostafa *et al*. 2018).

4.3.4 Assay of D-lactate

D-Lactate can cross plasma membranes by three mechanisms: non-ionic passive diffusion, the specific lactate transporter and the inorganic anion exchange system. Formation of D-lactate in cultured cells may therefore be measured by assaying D-lactate in the culture medium. An end-point enzymatic fluorometric assay was used to measure the flux of formation of D-lactate by HEK-293 cells (McLellan *et al*., 1992). This can be determined by measuring the concentration of D-lactate in the culture medium at baseline and end of the culture period. An aliquot of ice-cold 0.6 M perchloric acid (PCA) (1 m L) was added to the media (500 µL) to deproteinise samples. The sample mixture was vortexed and left on ice for 10 minutes to enable the protein precipitation. To sediment the precipitate, samples were centrifuged (7000 x g, 4 ^{0}C, 5 min). An aliquot of the supernatant (700 µl) was neutralised to pH 7 by adding potassium bicarbonate (2 M, 200 µl).

Samples were vortexed before centrifugation (7000 x g, 4 ^{0}C, 10 min) again to sediment potassium perchlorate. The samples were saturated in carbon dioxide and this was removed by centrifugal evaporator at room temperature under reduced pressure (20 mmHg) for the duration of 5 min. An aliquot of supernatant or D-Lactate standard solution (100 µl) was added in duplicates to each well of a 96-well black microplate containing of glycine hydrazine buffer (100 µl, 1.2 M glycine, 0.5 M hydrazine hydrate, 2.5 m M DETAPAC, pH 9.2) and NAD^{+} (4 mM, 25 µl). The reaction was initiated on the addition of D-lactic dehydrogenase enzyme (25 µl, 250 units per ml). The microplate was wrapped by foil sheet and incubated at 37 ^{0}C in the dark for 2 hours. A control was performed without the enzyme for each sample and used as a blank. The fluorescence of NADH was monitored at excitation 340 and emission 460 nm. The calibration standard curve was in the range of 0 - 6 nmol D-lactate/well – Figure 30.

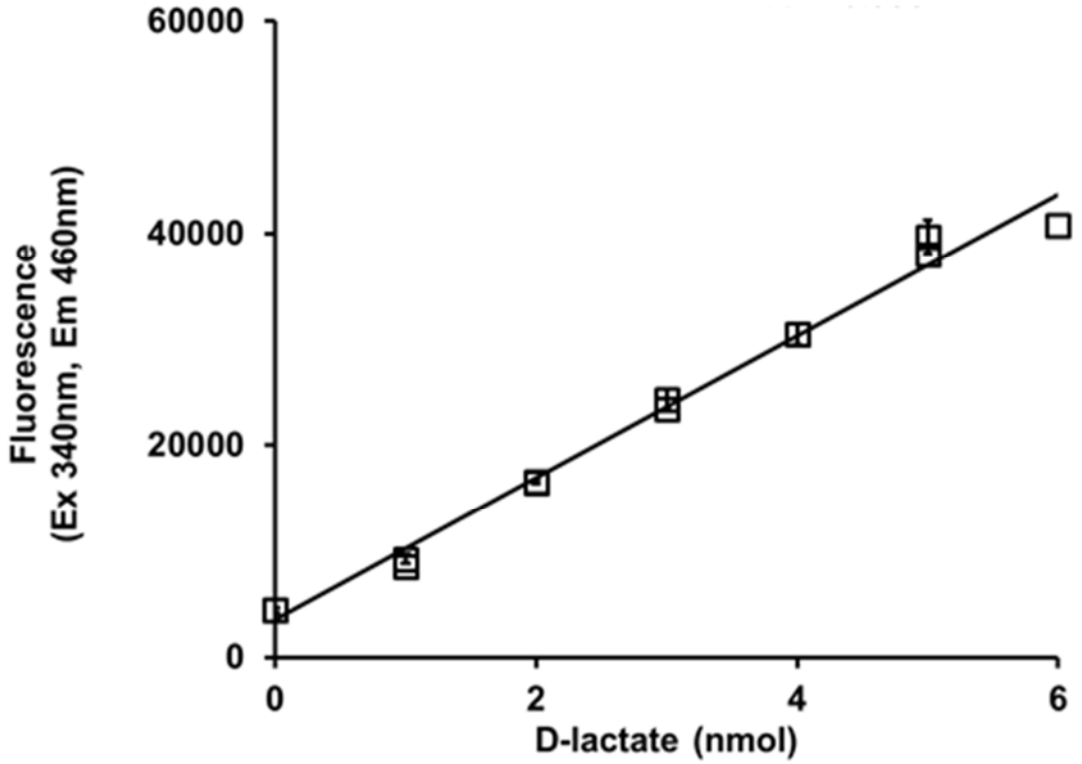

Figure 30: Calibration curve for D-lactate assay.

D-lactate has an anhydrous enzymatic purity of > 90%. It is oxidized enzymatically by D-Lactate dehydrogenase to pyruvate generating a fluorescent signal at the excitation wavelength 340nm and emission 460 nm in the presence of NAD^+. The amount of D-Lactate is proportional to the colorimetric product being formed. Linear regression equation: Fluorescence (arbitrary units) = (6685 ± 100) x D-lactate (nmol) + (3533 ± 217); $R^2 = 0.994$ (n = 21).

4.3.5 Assay of L-lactate

An aliquot of ice-cold 0.6 M PCA (1 mL) was added to the media (500 µL) to deproteinise samples. The mixture was vortexed and left on ice for 10 minutes to enable the protein precipitation. To sediment the precipitate, samples were centrifuged (7000 x g, 4 0C, 5 min). An aliquot of the supernatant (700 µl) was neutralised to pH 7 by adding potassium bicarbonate (2 M, 200 µl). Samples were vortexed before centrifugation (7000 x g, 4 ^{0}C, 10 min) again to sediment potassium perchlorate. An aliquot of L-Lactate standard solution (100 µl) was added to each well of a 96-well black microplate containing of glycine hydrazine buffer (100 µl, 1.2 M glycine, 0.5 M hydrazine hydrate, 2.5 mM DETAPAC, pH 9.2) and NAD^{+} (4 mM, 25 µl). For the supernatants, an aliquot of sample (10 µl) was added to each well, followed by an aliquot of deionized water (90 µl), glycine hydrazine buffer (100 µl) and NAD^{+} (25 µL). The media samples were diluted 10-fold with water to ensure the values will be within the range of the standards. The reaction was started on the addition of L-lactic dehydrogenase enzyme (25 µl, 250 units per ml). The microplate was wrapped by foil sheet and incubated at 37 ^{0}C in the dark for 2 hours. A control was performed without the enzyme and used as a blank. The fluorescence of NADH was monitored at excitation 340 and emission 460 nm. Calibration standard curve was in the range of 0 -10 nmol L-lactate/well and is presented in Figure 31.

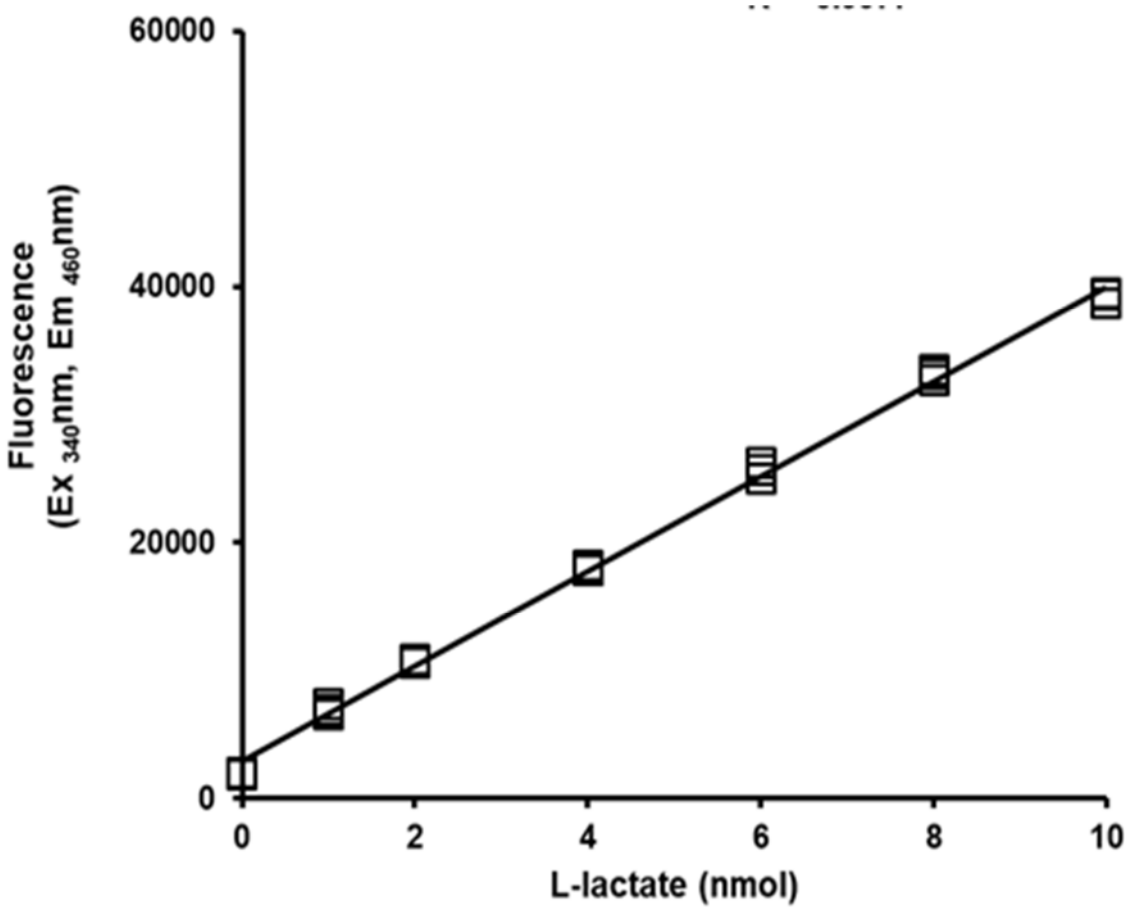

Figure 31: Calibration curve for the detection of L-lactate.

L-lactate is oxidized to form the pyruvate intermediate that is detected by a fluorescent signal at an excitation wavelength of 340 nm and emission of 460 nm; this is directly proportional to amount of lactate. The standard curve was linear from 0 to 10 nmol for L-lactate with a coefficient of determination of 0.988. Linear regression equation: Fluorescence = (3711 ± 88) x L-lactate (nmol) + (2905 ± 500); R2 = 0.998 (n = 21).

4.3.6 Assay of Glucose

The glucose concentration in cultured media samples was detected using an end-point enzymatic absorbance assay. Glucose in the samples is converted to 6-phosphogluconate via glucose-6-phosphate using the catalytic enzymes: hexokinase and glucose-6-phosphate dehydrogenase – Figure 32. Equimolar amounts of the phosphorylation of glucose are directly proportional to the yield and concentration of NADH formed from the reduction of NAD^+.

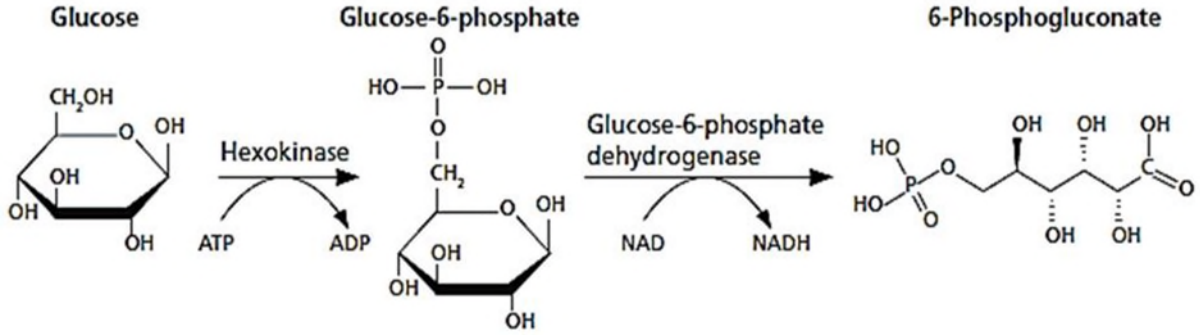

Figure 32: The detection of glucose via an enzymatic absorbance assay.

This coupled enzymatic reaction is catalysed by hexokinase and Glucose-6-phosphate dehydrogenase. At first, hexokinase catalyses the formation of D-glucose and ATP to produce Glucose-6-phosphate which is the initial substrate in a number of metabolic reactions: aerobic glycolysis, hexose monophosphate shunt pathway and the biosynthetic pathways: starch and glycogen. The concentration of Glucose-6-phosphate may reflection pathophysiological mechanisms in diabetes, cancer, oscillations and the depressive status of catabolites. Following the phosphorylation reaction, Glucose-6-phosphate is then catalysed by Glucose-6-phosphate dehydrogenase in the presence of NAD^+ to form 6-phosphogluconate and this is quantified at 340 nm. During the oxidation reaction, NAD^+ is reduced to NADH.

The samples were diluted to ensure the measured concentrations were within the standard curve range. Samples from low glucose were diluted 5-fold whereas samples in high glucose were diluted 20-fold with water. 2% of PCA (100 µl) to an aliquot of diluted culture medium (100 µl). The mixture was vortexed and left on ice for 10 minutes to enable the protein precipitation. Keep on ice for 10 min for the protein precipitate to develop fully. To sediment the precipitate, samples were centrifuged (6000 x g, 4 ^{0}C, 10 min). An aliquot of the supernatant (180 µl) was neutralised to pH 7 by adding potassium bicarbonate (1

M, 33 µl) *ca*. 7 with pH paper. Samples were vortexed before centrifugation (6000 x g, 4 ^{0}C, 10 min) again to sediment potassium perchlorate and remove the supernatant. The supernatant is then utilized in the glucose assay.

An aliquot of standard or diluted sample (25 µl) was added to each well of a microplate then the assay reagent (225 µl) was added. The assay mixture found in the commercial kit comprised of 1 mM ATP, 1.5 mM NAD+, 1 unit.ml hexokinase (HK) and 1 unit/ml glucose-6-phosphate (G-6-P) dehydrogenase (Sigma Aldrich). The plate was incubated at room temperature for 15 minutes for the NADH to form in the reaction mixture before the absorbance at 340 nm was read using the microplate reader. The standard curve was constructed between 0 – 1.5 mM D-glucose – Figure 33. The concentration of D-glucose in the sample was deduced from the equation of the line whereas the consumption of D-glucose was calculated by deducting the experimental measurements at the end of the culture period from the baseline media. The results were expressed in µmol/day/10^{6} cells.

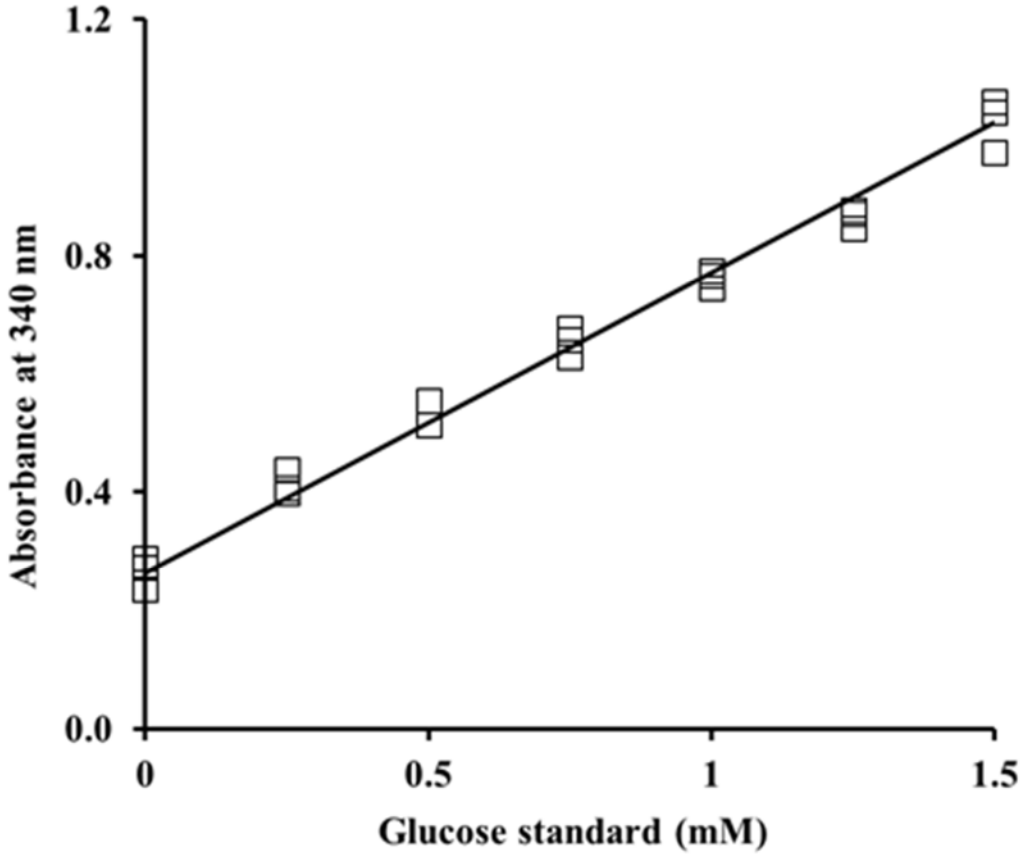

Figure 33: Calibration curve for the detection of D-glucose via enzymatic absorbance assay. The measured absorbance at the wavelength 340 nm after 15 minutes incubation was plotted against the concentration of glucose (mM). An increase in absorbance is positively correlated with the concentration of glucose. Linear regression equation: A340 (A.U.) = (0.509 ± 0.007) x D-glucose (mM) + (0.2622 ± 0.01); R^2 = 0.995 (n = 21).

4.3.7 Western blotting

Western blotting is used to detect specific proteins in a sample extract. A 10% polyacrylamide gel was prepared and removed from the gel cassette from the casting stand and placed into the electrode assembly into the clamping frame with the shorter plate facing forward. 1-fold dilution of prepared 10 x Electrophoretic buffer (25 mM Tris, 192 mM glycine, 0.1% SDS, pH 8.3) was poured into the Criterion electrophoresis cell (Bio-Rad Laboratories, 2018). Cytosolic extracts of HEK-293 cells (20 µg) were mixed in a one to one ratio with 4 X Laemmli buffer and were heated at 100 ^{o}C for 5 minutes to hydrolyse proteins and disulphide bonds (Laemmli, 1970). Once cooled, the sample mixture was loaded into the well and an aliquot of the pre-stained protein Spectra Multicolor Broad Range Protein Ladder (10 to 260kDa, 8 µl) was also added to a well to separate the samples by SDS-PAGE. The samples were electrophoresed at 120 V for 1 hour – Figure 34.

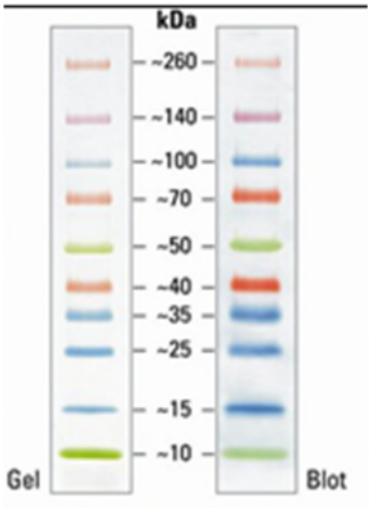

Figure 34: SDS-PAGE band profile of Spectra Multi-colour Broad Range Protein Ladder (ThermoFisher Scientific, 2020).

The protein ladder consists of 4 coloured chromophores: pink, blue, orange and green that can be bounded to the 10 pre-stained proteins with a molecular mass in the range of 10 to 260 kDa. This can be added directly for loading samples in gel electrophoresis and western blotting. The lot-to-lot variation is approximately 5% and is stored in (62.5 mM Tris phosphate at pH 7.5, 25 ^{o}C, 2 % (w/v) SDS, 33 % (v/v) glycerol 1 mM EDTA, 1 mM NaN3 and 10 mM DTT.

The separated proteins were transferred from the gel to PVDF membrane by the wet transfer method (Towbin, *et al.*, 1979). A wet transfer was performed at high intensity settings, 100 V for 1 hour to allow a limited time for transfer. It

involves using a cassette that consists of foam pads, polyacrylamide gel, PVDF membrane in the anode site and filter paper as shown in Figure 35 to ensure the proteins are transferring in the right manner. The sandwich is then submerged in transfer buffer (25 mM Tris, 192 mM Glycine, 10% Methanol (v/v), pH 8.3) (Towbin *et al*., 1979). The formulated buffer increases the buffering capacity, protein binding to the PVDF membrane particularly methanol to improve transfer efficiency.

The transfer membrane was then blocked with 5% (w/v) dried milk protein in Tris-buffered saline with Tween-20 (TBS-T buffer; 150 mM NaCl, 10 mM Tris/HCl pH 7.6 and 0.05% Tween-20). The membrane was then probed using anti Glo1 primary antibody produced from rat at an optimized concentration of 1 in 5,000 overnight at cold temperature 4^{o}C on a plate shaker at a steady speed if one intends to divide the procedure in two days.

However, if one has planned to do it in one day, the incubation period of the primary antibody is 1 hour on a plate shaker at a steady speed. Following the blotting with the primary Glo1 antibody, the membrane was washed three times with TBSTA buffer for 10 – 15 minutes. The membrane was then probed with the secondary antibody After blotting with the primary antibody, the membrane was washed three times with TBS-T buffer for 10 min. The blot was then divided into two where the HRP antibody of β-actin (1/8000) was added to the side that contains the molecular weight of β-actin. The other half containing the target Glo1 at a molecular weight of 21 kDa was probed with secondary antibody (anti-rat, 1/10000) on the plate shaker at a steady speed at room temperature for 1 hour. This followed by rinsing the blot several times with TBST. The blot was then developed with the ECL reagent. An image of the blot was taken from the imaging system for chemiluminescence; GeneGenome XRQ System (Syngene). The intensity of the Glo1 protein band was normalised to β-actin which is a protein loading control). Membranes were then quantified with ImageJ software where Glo1 blotting results were normalised to β-actin (protein loading control).

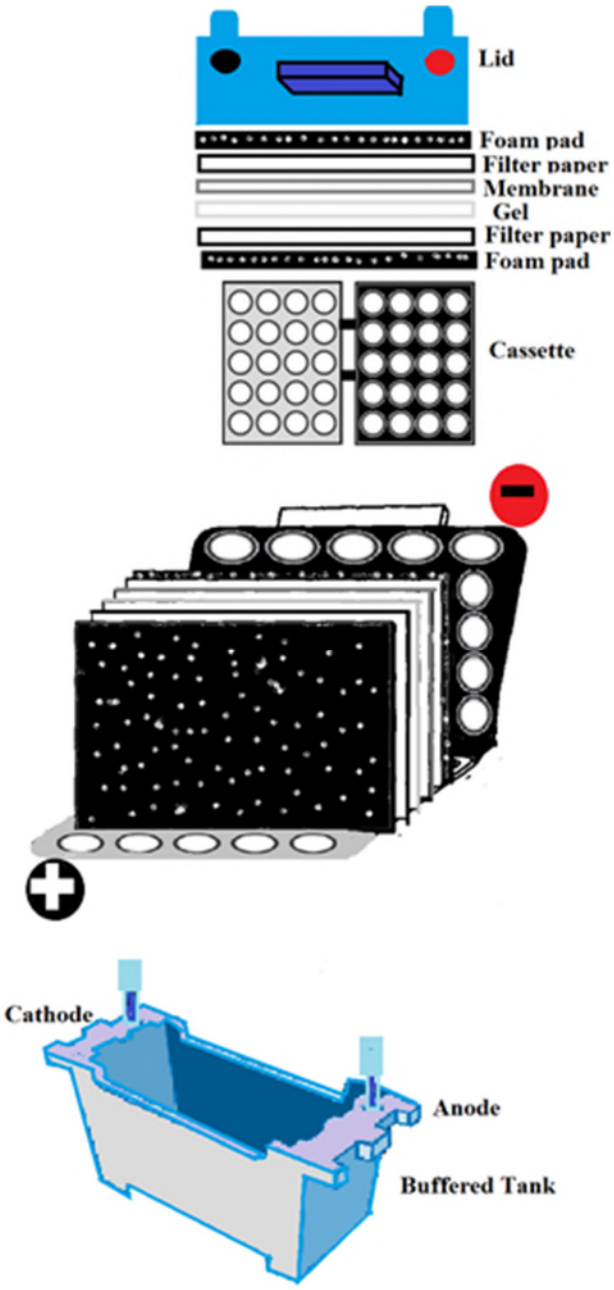

Figure 35: Layout of the western blot transfer setup (Adapted from Leinco Technologies, 2018). This step is key in transferring separated proteins from the gel to a solide support matrix to enable detection of specified proteins using antibodies. The gel is equilibrated in transfer buffer before placing into the sandwich that is pressed together in cassette that support the structure. The cassette is place into the tank vertically filled with transfer buffer.

4.3.8 Real-Time PCR quantitation

The relative copy number of GLO1 gene mRNA in HEK-293 cells was measured by real-time quantitative PCR. The procedure includes the extraction of mRNA, purification and reverse transcription to cDNA. The cDNA was quantified by measuring SYBR green dye as fluorescence in a PCR reaction. The SYBR green dye has high fluorescence when bound to double-stranded DNA and can cause intercalation between DNA bases.

4.3.8.1 Primer design

The primers and probe for Glo1 and ACTB were pre-designed primers probe mixture from Life Technology Ltd (Paisley, Scotland). The gene expression level was evaluated using 2(-ddCt) with ACTB as a reference gene for normalization for relative expression level. Dissociation plots otherwise known as melt curves were constructed for each assay plate to ensure the primers were working constantly – Figure 36.

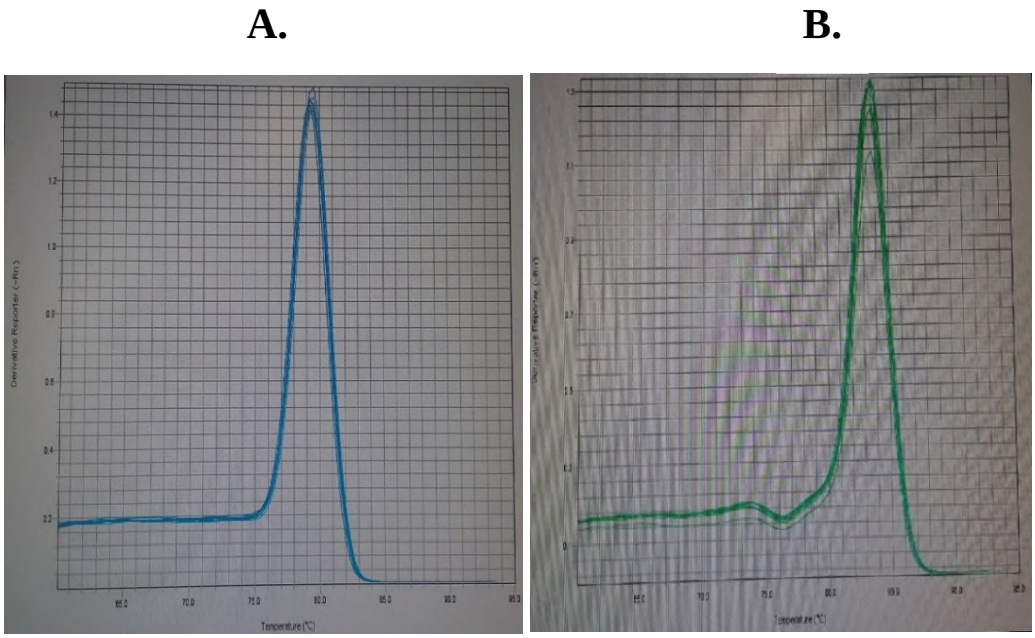

Figure 36: The melt curves for Beta-actin and Glo1.

(A) Beta-actin and (B) Glo1. The X-axis represents the temperature change whereas the Y axis presents the derivative of relative fluorescence divided by the derivative of temperature (dRFU/dT).

4.3.8.2 Sample preparation

HEK-293 cells were cultured in 25 mM glucose *in vitro* (1 x 10^5) in 12-well plate. Cells were transfected with 48 nM Accell Human GLO1 SMART siRNA pool or an Accell non-targeting Control siRNA pool (GE Healthcare Dharmacon Inc, Little Chalfont, Buckinghamshire, U.K) with Lipofectamine *RNAiMAX* Transfection Reagent (Thermo Fisher Scientific, Paisley, U.K.) based on the manufacture's protocol. After 72-hour incubation, the cells were collected and RNA extracts of the cells were prepared.

4.3.8.3 RNA extraction and purification

The Total RNA of HEK-293 cells (wildtype, GLO1 siRNA and scrambled siRNA) were extracted using the Qiagen RNeasy mini kit according to the manufacturer's instructions. HEK-293 cells under normoxic and hypoxic conditions were also conducted utilizing the same method as follows using the QIAGEN RNeasy mini kit according to the manufacturer's instructions. The samples were lysed by the addition of RLT lysis buffer (350 µL) containing β-mercaptoethanol and pipetting the suspension around 10 times. There is a high concentration of guanidine-thiocyanate present in the lysis buffer that acts as a chaotropic agent promoting cell lysis.

The lysed samples were then mixed with 70 % (v/v) ethanol to promote the binding conditions with RNA to the silica-based spin-column. To efficiently remove the impurities and contaminants present in the samples, they were washed thrice with multiple buffers: RW1, RPE with centrifugation. The procedure was then finalized by the addition of RNAse-free water. The quality and the concentration of RNA were measured using the NanoDrop 1000 spectrophotometer. 2 µL of the RNA sample was utilized and pure RNA were expected to give a ratio of 1.9 - 2.1 at A_{260} and A_{280}. The samples were diluted to 100 ng nucleic acid and the concentration was confirmed using the NanoDrop spectrophotometer.

4.3.8.4 Reverse transcription

Reverse transcriptase reaction was performed in 20 µL total volume with 100 ng total RNA extracts of HEK-293 (wildtype, Glo1 siRNA and scrambled siRNA) using the High-Capacity cDNA Reverse Transcription Kit (Applied Biosystems™) and run using an Eppendorf Mastercycler gradient. The priming pre-mix was prepared in RNase-free reaction tube: a total of 0.1 µg of RNA from cells were annealed with 10 µM oligo $(dT)_{18}$ (1 µL), 10 mM dNTP mix (1 µL) and RNase free water (10 µL) at 70°C for 5 min before incubation on ice for 1 min. The reaction pre-mix was prepared by the addition of 10U/µL RNase inhibitor (1 µL), 5 X Bioscript reaction buffer (4 µL) and 200 U/µL Bioscript reverse transcriptase (1 µL) in RNAse-free water. 10 µL of the reaction premix was added to the priming premix and mixed gently by pipetting. Samples were heated at 42 ^{0}C for 30 min. The reaction was terminated by incubating at 85^{0}C for 5 min and samples were chilled on ice. The synthesized cDNA was diluted 4-fold and were stored at -20 ^{0}C and repeated-thawing was avoided before analysis.

4.3.8.5 Analysis of gene mRNA expression by SYBR green

The method was utilized to measure the expression of mRNA of GLO1 gene and normalized to the housekeeping gene; Beta-actin. The synthesized cDNA was used to produce the standards and for samples.

4.3.8.6 Preparation of the standards for PCR

From each independent replicate (n=3) of HEK-293 cells (wildtype, empty vector and GLO1 overexpressed cells), 1 µg was combined together to one RNase-free reaction tube as standard curve stock. A 10-fold serial dilution was then constructed to custom standards over the range 0 – 1000,000 pg.

4.3.8.7 Preparation of the samples

The reverse transcription product cDNA was diluted 4-fold and were used for qRT-PCR to detect the expression level of the target gene; GLO1. In a 20 µL reaction volume, (2 µL) was added in a clear MicroAmp Optical 96 well reaction plate (Applied Biosystems™) in triplicate. The standards of the serially diluted cDNA values were run alongside the samples and were used for quantification using the β-actin as a reference gene. SensiMix™ SYBR Low-ROX Mastermix (10 µL), primer (0.5 µL) and nuclease free water (7.5 µL) was added to the well. The plate was sealed using a MicroAmp Optical adhesive film (Applied Biosystems™) and were centrifuged for several seconds. The mRNA expression of GLO1 was measured using the SYBR green technique on ABI 7500 real time PCR system. The initial reaction was at 95 °C for 10 min to stimulate the hot-start DNA polymerase, followed by 40 cycles at 95°C for 15 s and 60°C for 1 min. The standard curve is shown in Figure 37.

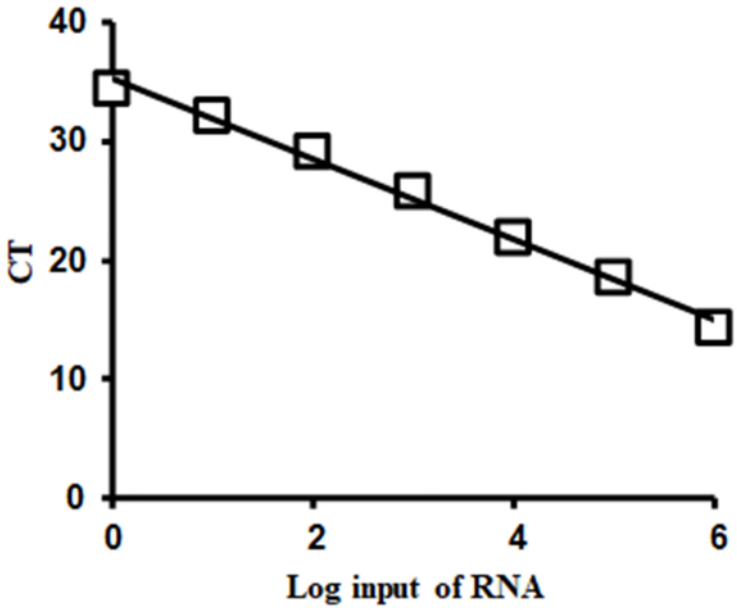

Figure 37: The calibration curve of real-time PCR.

The semi-log regression line point of the x axis that presents the log copies of mRNA per ml and the the y axis is the Ct value for each calibration standard. The slope (-3.05) is the estimation of the efficiency of the PCR amplification. The Linear regression equation: Threshold cycle = (-3.05 ± 34.9) x log input amount of mRNA + (34.4 ± 2.4); R^2 = 0.994 (n=21).

4.3.8.8 Data analysis

Following the completion of the PCR reaction, the cycle threshold (Ct) data was obtained for the control and the samples. Ct is defined as the number in which fluorescence crosses the threshold value. Delta Ct (dCt) is the difference between the target gene's Ct (Ct(t)) i.e GLO1 and the Beta-actin control (Ct(t)). The fold change was compared between samples and the linear equation in gene expression

$$dCt = Ct(t) - Ct(end)$$

$$ddCt = dCt(exp) - dCt(cal)$$

$$\text{Fold change} = 2(-ddCt)$$

4.3.9 Assay of dicarbonyls by stable isotopic dilution analysis LC-MS/MS

The amount of 3-DG, glyoxal and MG in the culture medium and HEK-293 cells incubated with and without the anti-cancer drugs were determined by utilizing 1,2-diaminobenzene for the derivatisation and quantification of the subsequent quinoxaline compounds by stable isotopic dilution analysis LC-MS/MS – Figure 38 (Rabbani and Thornalley, 2014d; McLellan *et al*., 1993).

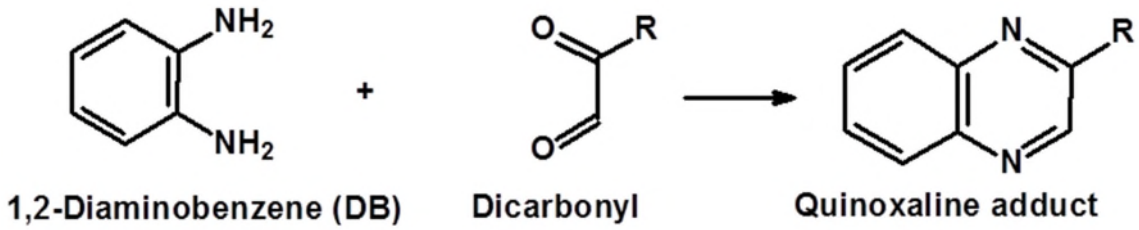

Figure 38: Derivatisation utilized in the dicarbonyl assay.

1,2-Diaminobenzene reacts with the dicarbonyl, this eliminates water and forms the Quinoxaline adduct, 6, 7-dimethoxy-2-methylquinoxaline. The derivatisation involves solid-phase extraction with HPLC under acidic conditions to prevent the synthesis of MG via triose phosphates (Rabbani and Thornalley, 2014d).

4.3.9.1 Sample preparation

Non-transfected HEK-293 cells (*ca*. 1 x 10^6 cells) were seeded overnight and the following day they were treated for three hours with two-fold the GC_{50} value of the following anti-tumour drugs that had high Glo1-linked MDR from the dose response studies: paclitaxel, mechlorethamine, doxorubicin, mitomycin c and methotrexate. These were compared with non-transfected cells and two amongst the anti-cancer drugs that had low Glo1-linked MDR. The cellular samples were washed with PBS at a minimal residue to eradicate any remaining media. They were centrifuged (250 x g, 5 min) to sediment detached cells. The supernatant was collected to be used for immediate analysis.

The cell pellets were de-proteinised by the addition of trichloroacetic acid (TCA)- saline solution (20% TCA, 0.9% sodium chloride (NaCl), 10 µl). The samples were vortexed well. An aliquot of water (40 µl) was added followed by 3% sodium azide in water (5 µl) to inhibit peroxidase activity (Rabbani and Thornalley, 2014d). Isotopic standard cocktail (5 µl; 2 pmol stable isotopic dicarbonyl) [$^{13}C_3$]MG, [$^{13}C_2$]glyoxal and [$^{13}C_6$]3DG were added to each sample. The samples were vortex mixed and centrifuged (6,000 g, 10 min, 4 °C) to sediment membranes. The supernatant (45 µl) was removed and added to 10 µl derivatisation agent solution (0.5 mM diaminobenzene in 200 mM HCl containing 0.5 mM DETAPAC). Samples and standards (2 – 20 pmol) were incubated in the dark at room temperature for 4 hours in order for the derivatisation to take place so the quinoxaline adducts will be analysed by LC-MS/MS and the calibration of the analyte/internal standard response ratio can be established.

4.3.9.2 Preparation of calibration standards

Calibration standards were prepared and derivatized concurrently containing 2 pmol isotopic standards at 400 nM [$^{13}C_3$]MG, [$^{13}C_2$]glyoxal and [$^{13}C_6$]3DG and 0 – 20 pmol methylglyoxal – Tables 6 and 7 (Rabbani and Thornalley, 2014). The cocktails of dicarbonyls were at a concentration of 800 nM. The calibration curves of the dicarbonyls are presented in Figure 54 where the peak area ratio of the analyte/isotopic standard (y-axis) against the analyte concentration (x-axis).

Table 4: Calibration standards for dicarbonyls

There were 6 calibration standards. The stable isotope that comprised of glyoxal, methylglyoxal and 3-DG has a constant concentration of 2 pmol.

Calibration standard	3-DG (pmol)	Glyoxal (pmol)	MG (pmol)	IS (GSS2) Stable Isotope substituted G, MG and 3DG
1	1	1	1	2
2	2	2	2	2
3	4	4	4	2
4	6	6	6	2
5	8	8	8	2
6	10	10	10	2

Table 5: Preparation of calibration standards from stock solution

Standards were treated with ice-cold TCA-saline (10 µl) and were vortexed. An addition of water (25.0 - 0 µl), 3% sodium azide (5 µl) was added and the mixture was vortexed. 800 nM of MG standard was added 0 – 25.0 µl. A constant amount of the [^{13}C]Dicarbonyls stock (5 µl) was subsequently added and the solution was mixed. The samples underwent centrifugation at 6000g and 4 ^{o}C for 10 min. 0.5 mM of DB in HCl-DETAPAC (10 µl) was then added and vortexed. They were then incubated at room temperature for 4 h in the dark.

Calibration	5% TCA-0.9% saline (µl)	Water (µl)	3% Sodium azide (µl)	800 nM MG standard (µl)	400 nM IS (µl)	0.5 mM DB (µl)
0	10	25.0	5.0	0.0	5.0	10.0
1	10	22.5	5.0	2.5	5.0	10.0
2	10	20.0	5.0	5.0	5.0	10.0
3	10	15.0	5.0	10.0	5.0	10.0
4	10	10.0	5.0	15.0	5.0	10.0
5	10	5.0	5.0	20.0	5.0	10.0
6	10	0.0	5.0	25.0	5.0	10.0

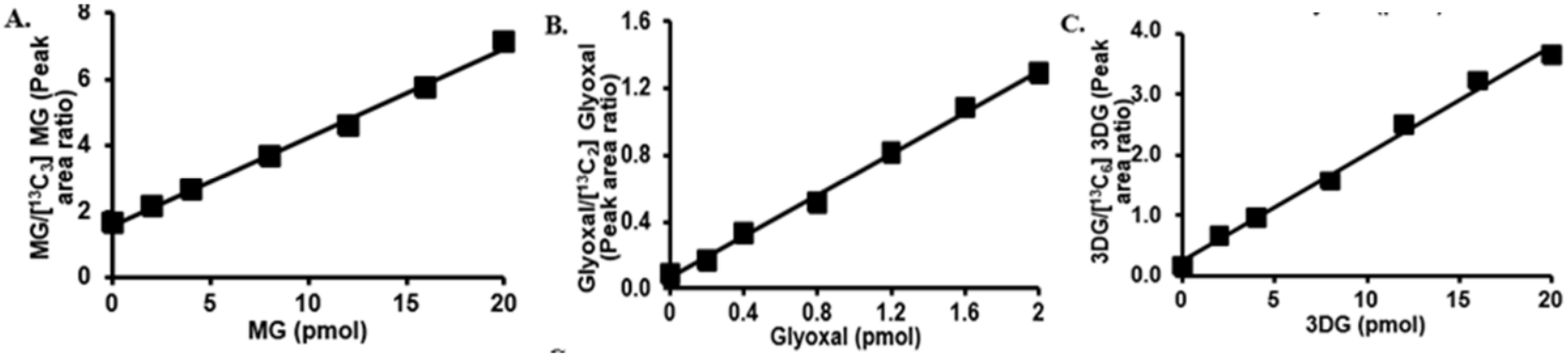

Figure 39: Standard curve for dicarbonyls.

The validated method was applied to determine the concentration of methylglyoxal, glyoxal and 3-DG and was established by the calibration solution of the derivatives of α -dicarbonyl. There was good linearity over the concentration range (0 – 20 pmol). (A) Methylglyoxal. Regression equation: Peak area ratio = ((0.267 ± 0.008) x MG [pmol]) + (1.58 ± 0.09); R^2 = 0.996 (n = 7). (B) Glyoxal. Regression equation: Peak area ratio = ((0.062 ± 0.002)x glyoxal [pmol]) + (0.062 ± 0.017); R^2 = 0.997 (n = 7). (C) 3-DG. Regression equation: Peak area ratio = ((0.169 ± 0.005)x 3-DG [pmol]) + (0.052 ± 0.056); R^2= 0.996 (n = 7).

4.3.9.3 LC-MS/MS conditions

Liquid chromatography was performed by utilizing a reverse phase octadecylsilica (ODS) BEH C18, 1.7 µm particle size column (100 x 2.1 mm) fitted with a 5 x 2.1 mm pre-column. The temperature of the column was 30 °C. The two solvents utilized in the dicarbonyl assay were: 0.1% TFA in water (solvent A) and 0.1% TFA in 50:50 acetonitrile (MeCN) in water (solvent B). The gradient used is displayed in Table 6 below.

Table 6: Chromatographic elution profile in the MG assay.

There are two mobile phases: 0.1% TFA in water (Solvent A) and 0.1% in 50% acetonitrile (Solvent B). The analytical columns need to be conditioned with the mobile phase prior to use and equilibrated between each injection to avoid irreproducible retention times. Isocratic is when the composition of the mobile phase does not alter and remains consistent.

Method phase	Time (min)	Flow rate (ml/min)	Solvent A (%)	Solvent B (%)	Curve
Analysis	0	0.2	100	0	0
	10	0.2	0	100	Linear
Column wash	15	0.2	0	100	Isocratic
Re-equilibration	15	0.2	100	0	Immediate change
	30	0.2	100	0	Isocratic

The instrument utilized in the analysis was Acquity^{TM} UPLC system with eluate directed into the electrospray source of a Quattro Premier XE tandem mass spectrometer. The optimised settings were: capillary voltage was 0.6 kV, ion source temperature 120 °C, desolvation gas temperature 350 °C, the cone gas flow 140 l/h and the desolvation gas flows 140 and 900 l/h respectively. Table 7 shows the optimised multiple reaction monitoring (MRM) conditions used in mass spectrometric detection.

Table 7: Optimised MRMs used to detect and monitor dicarbonyls

The internal standards and the analyte adducts were detected by multiple reaction monitoring (MRM) using LC/MS-MS with a Waters Acquity ODS column (2 x 100 mm).

Analyte	**Retention time (min)**	**Parent ion (Da)**	**Fragment ion (Da)**	**Cone voltage (V)**	**Collision energy (eV)**
MG	7.8	145.1	77.1	24	24
[$^{13}C_3$]MG	7.8	148.1	77.1	24	24
Glyoxal	7.1	131.0	77.1	24	23
[$^{13}C_2$]Glyoxal	7.1	133.0	77.1	24	23
3-DG	5.6	235.2	199.0	21	15
[$^{13}C_6$]3DG	5.6	241.2	205.0	21	15

4.3.10. The assay of glutathione metabolites by LC-MS/MS

The amount of GSH, GSSG and S-D-lactoylglutathione in cultured HEK-293 cells for the detection and quantification of GSH, GSSG and S-D-lactoylglutathione, as previously described (Xue *et al*., 2016).

4.3.10.1 Sample preparation

HEK-293 cells were cultured in 25 mM glucose and treated with and without two-fold the median inhibitory concentration of Mitomycin C and Mechlorethamine for 45 min, 1.5 h and 3 h to determine whether there is an increase in GSH depletion. After the incubation period, media was removed and HEK-293 cells were trypsinised by the routine trypsinisation procedure and were counted by Trypan Blue exclusion assay. HEK-293 cells (*ca.* 0.5 - 1 x 10^6) were sedimented by centrifugation (150 g, 5 min). The medium was removed without disturbing the cell pellet and was re-suspended in 40 µl of a precipitating solution of 10% TCA, 0.15% NaCl and 0.25% sodium azide in water to facilitate the precipitation of proteins and to prevent the enzymatic activities of peroxidases. Samples were then centrifuged (20,000 g, 30 min, 4 ^{o}C) and aliquots of the supernatant (10 µl) was mixed with internal standard/isotopic standard cocktail (10 µl), made up to 50 µl by the addition of 0.1% TFA (aq) and were transferred to vials and analysed by LC-MS/MS for detection of each analyte.

The limit of detection (LoD) was 0.92 pmol, 1.46 pmol and 0.54 pmol for GSH, GSSG and S-D-lactoylglutathione respectively. Analytical recoveries were: GSH, 97.1 ± 1.6%; GSSG, 92.7 ± 5.7%; and S-D-lactoylglutathione, 99.3 ± 14.1%. Intra-batch coefficient of variation was determined by analysis of replicate samples. Intra-batch coefficient of variation was: GSH, 8.8% for GSH (n = 6); and GSSG, 10.9% (n = 6).

4.3.10.2 Preparation of standards

Stable isotopic GSSG was prepared in-house. Stable labelled [*glycine*-$^{13}C_2{}^{15}N_1$]GSH was oxidised using diamide (Kosower, *et al.*, 1969) as shown in Figure 40 to obtain stable labelled [$^{13}C_4{}^{15}N_2$]GSSG to be used in the LCMS/MS method to quantify cellular GSSG. An aliquot of [$^{13}C_2{}^{15}N_1$]GSH solution (3.2 mM, 100 µL) and 10 mM diamide in methanol (30 µL) were added to 100 µL of 10 mM sodium phosphate buffer, pH 7.4 (100 µL) and were incubated at 37°C for 30 minutes. The reaction mixture was purified by elution via a 500 mg strong anion-exchange solid-phase extraction (SAX SPE) cartridge in the formate form. [$^{13}C_4{}^{15}N_2$]GSSG was remained on the SAX-SPE cartridge and the cartridge was washed with 10 mL water to remove the reduced form of diamide. [$^{13}C_4{}^{15}N_2$]GSSG was collected by elution with 100 mM formic acid (5 mL) and underwent lyophilised to dryness. It was then reconstituted in water (1mL) and filtered through a 0.2 µm nylon filter. The concentration of [$^{13}C_4{}^{15}N_2$]GSSG was determined by the isotopic dilution analysis of known amounts of GSSG. The synthesis yield was 28%.

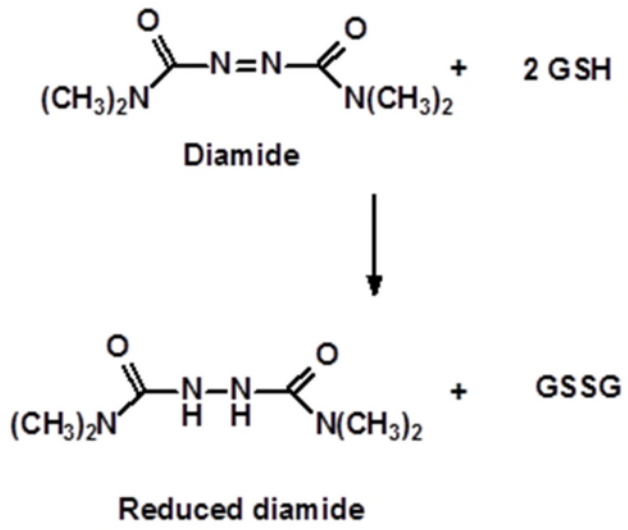

Figure 40: The formation of GSSG from GSH

Tetramethylazodicarboxamide otherwise known as diamide has two amide groups and acts as a thiol-oxidizing agent to oxidize reduced glutathione γ-L-glutamyl-L-cysteinyl-glycine to disulfide (GSSG) stoichiometrically.

Stock solutions (1 mg/ml) of GSH hydrochloride, GSSG and S-D-lactoylglutathione were prepared in water and were filtered. Further dilutions of these stocks were prepared using 0.1% TFA (solvent A) in water. Standards were prepared as shown in Table 8 and 9. S-D-lactoylglutathione was not routinely included in calibration standards since the quantities in test samples were below the limit of detection for the assay. Calibration curves were constructed plotting peak area ratio of analyte/isotopic standard against analyte concentration as shown in Figure 41. The amount of GSH, GSSG and SLG was calculated by utilizing the peak area ratio, calibration curve, cell count and dilution factors involved.

Table 8. Calibration range for glutathione analysis: reduced, oxidized and S-D-lactoyglutathione. Calibration standards were prepared for sample analysis over the range 100-8000 pmol and 5-100 pmol for GSH and GSSG respectively.

Calibration solution	GSH (pmol)	S-D-lactoyl-glutathione (pmol)	GSSG (pmol)	[13C215N1]GSH (pmol)	[13C415N2]GSSG (pmol)
0	0	0	0	100	20
1	200	1	10	100	20
2	400	2	20	100	20
3	800	4	40	100	20
4	1200	6	60	100	20
5	1600	8	80	100	20
6	2000	10	100	100	20

Table 9. Preparation of glutathione standards

The normal standard solution is GSH (100 µM), SLG (0.5 µM) and 5 µM GSSG (5 µM).

Calibration solution	**GSH, SLG & GSSG cocktail (µl) 2 µM**	**0.1% TFA in water (µl)**	**12.5% TCA (µl)**	**Isotopic cocktail (µl)**
0	-	20	20	10
1	2	18	20	10
2	4	16	20	10
3	8	12	20	10
4	12	8	20	10
5	16	4	20	10
6	20	-	20	10

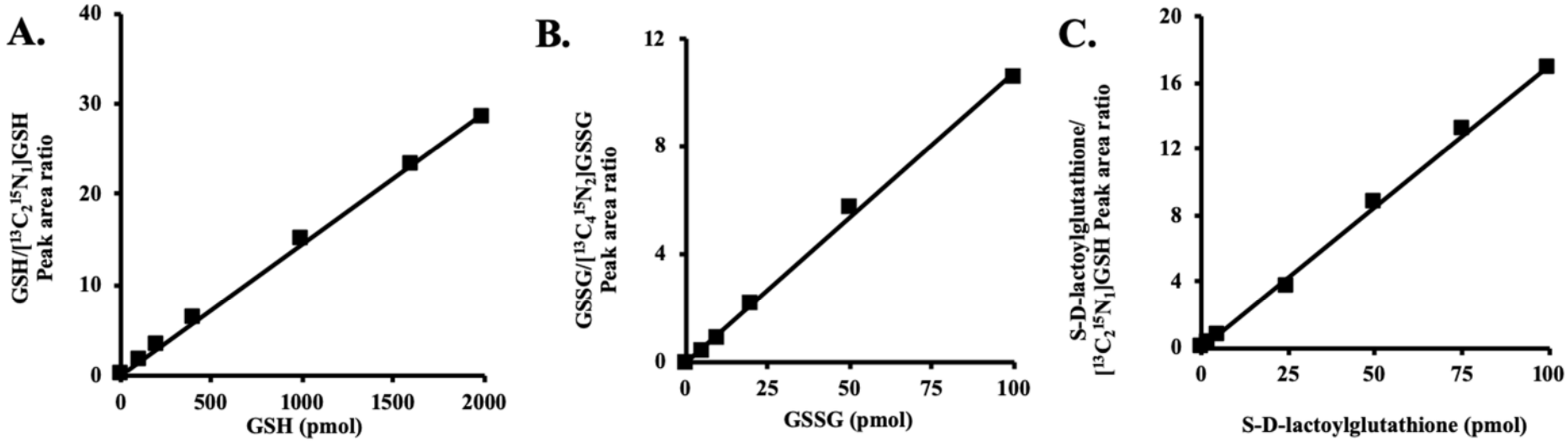

Figure 41. Typical calibration curves of glutathione by LC-MS/MS.

They were constructed utilized unlabelled analyte for GSH (0 – 2000 pmol); GSSG (0 – 100 pmol) and S-D-lactoylglutathione (0 – 10 pmol) and a constant aliquote of isotopically-labelled internal standard of 10 µL. The linearity of the data and the goodness of fit was established by linear regression and the coefficient of determination (R2). A: Standard curve for GSH. Regression of Peak area ratio on amount of GSH (pmol) gave: Peak area ratio = ((0.0145 ± 0.002) x GSH (pmol)) ± 0.180; r^2 = 0.999; n = 7. B: Standard curve for GSSG. Regression of Peak area ratio on amount of GSSG (pmol) gave: Peak area ratio = (0.1072 ± 0.0027) x GSSG (pmol)) ± 0.124; r^2 = 0.998; n = 6. C: Standard curve for S-D-lactoylglutathione. Regression of Peak area ratio on amount of S-D-lactoylglutathione (pmol) gave: Peak area ratio = ((0.1711 ± 0.0032) x S-D-lactoylglutathione (pmol)) ± 0.167; r^2 = 0.998; n = 7.

4.3.10.3 LC-MS/MS

The glutathione assay was conducted using the Acquity^{TM} UPLC-Premier XE tandem mass spectrometer system. The capillary voltage was 3.4 kV. The source ionisation temperature was 120 ^{o}C. The desolvation gas flow was 549 l/h and cone gas flow was 146 l/h. The optimised MRMs used for glutathione analysis and their fragmentation analysis are given in Table 10 and Figure 42. The elution profile for glutathione analysis is presented in Table 11.

Table 10. Optimised MRMs for glutathione analysis

Analyte	Parent ion (Da)	Fragment ion (Da)	Retention time (min)	Cone Voltage (V)	Collision Energy (eV)
GSH	308.2	179.1	11.7	30	13
[13C215N1]GSH	311.2	182.1	11.7	30	13
GSSG	613.2	483.7	14.4	52	18
[13C415N2]GSSG	619.2	489.7	14.4	52	18
S-D-lactoylglutathione	380.2	76.2	13.1	32	35

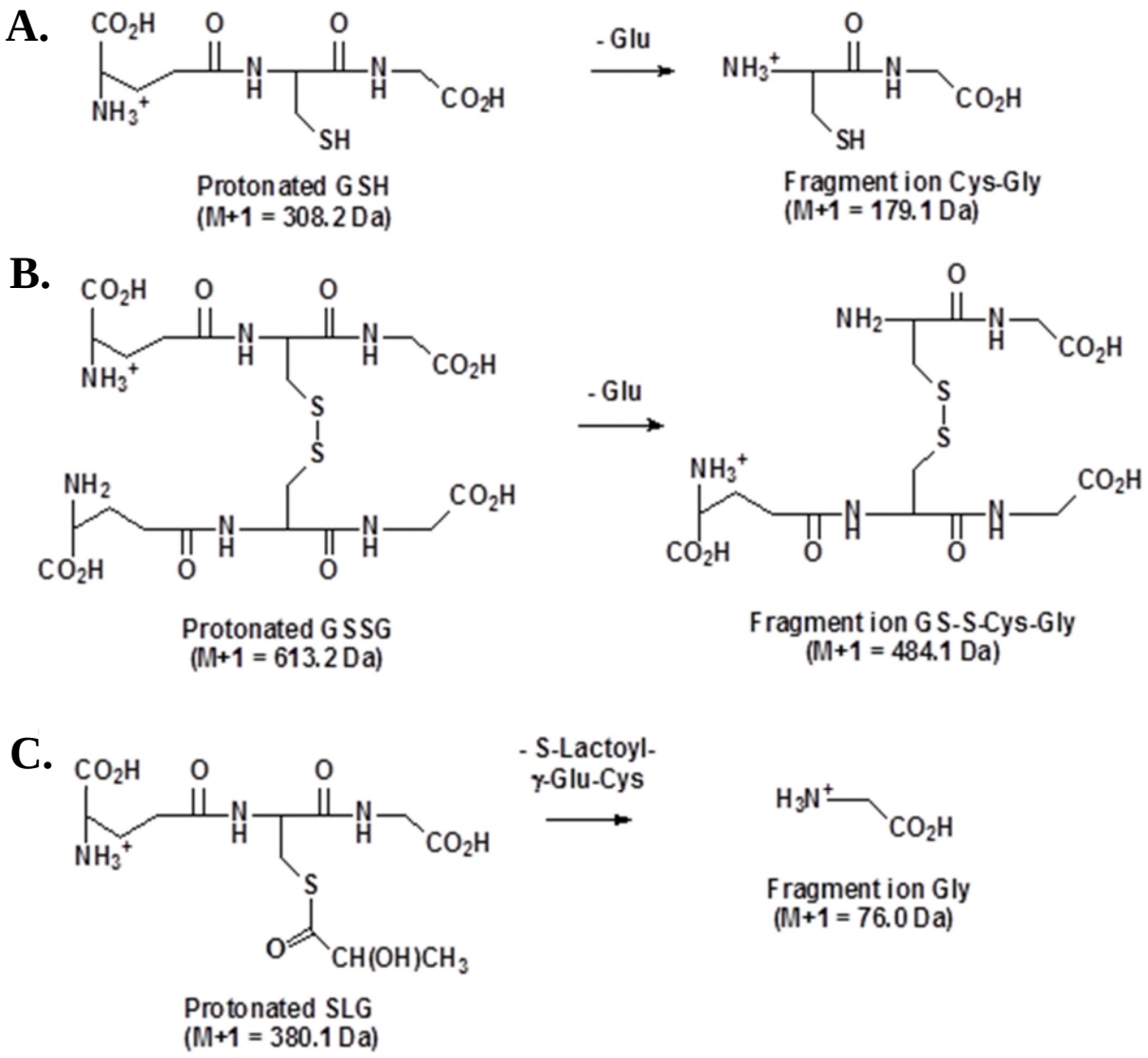

Figure 42. Fragmentation of glutathione.

A. GSH, B. GSSG and C. S-D-lactoylglutathione.

Table 11: Gradient used for glutathione assay on LC-MS/MS

Injection Run					
Time (min)	**Flow rate (ml/min)**	**Solvent A1 (%)**	**Solvent B1 (%)**	**Solvent B2 (%)**	**Gradient**
Initial	0.2	100	0	-	
1	0.2	100	0	-	Isocratic
15	0.2	40	60	-	Linear
16	0.2	40	60	-	Isocratic
Post-run					
Initial	0.4	0	-	100	
10	0.4	0	-	100	Isocratic
25	0.4	100	-	0	Immediate

4.3.11 Assay of GSH conjugates of Mechlorethamine

This assay was conducted to detect and quantify GSH metabolites and GSH conjugates of Mechlorethamine via stable isotopic dilution analysis. The fragmentation of GSH conjugates can be divided into: benzylic, disulfide, aromatic, aliphatic and thioester where they can be determined by high resolution mass spectrometry with specified collision energies (Xie *et al*. 2013).

4.3.11.1 Preparation of samples

Untreated HEK-293 cell pellets (1 x 10^6 cells) were resuspended in 40 µl solution containing 10% TCA, 0.15% NaCl and 0.25% sodium azide in water. This solution precipitates proteins and acts as a preservative by inhibiting peroxidase activity in the sample; residual peroxidase activity otherwise remains in TCA extracts. Samples were centrifuged at 20,000 g for 30 min at 4 °C and aliquots of supernatant (10 µl) transferred to vials for LC-MS/MS analysis with the addition of 10 µl isotopic standard cocktail.

4.3.11.2 Preparation for the Mechlorethamine-GSH adduct

0.5 mM Mechlorethamine with 1 mM GSH was incubated in 10 mM phosphate buffer, pH 7.4, at 37 ^{o}C for 4 hours in a sealed cryovial and is frozen at – 20 ^{o}C.

4.3.11.3 Preparation on standards

The standards and mass spectrometric conditions utilized in Section 4 for the glutathione assay was utilized for this assay. However, there is an addition of optimized MRMs for glutathione the GSH conjugates of Mechlorethamine – Table 12 and 13 respectively. The reactions for the optimized MRMs are illustrated in Figure 43.

Table 12 Optimised MRMs for glutathione metabolite analysis

Analyte	MRM application	Molecular ion (Da)	Fragment ion (Da)	Retention time (min)	Cone Voltage (V)	Collision Energy (eV)	Neutral fragment loss
GSH	Identifier	308.2	84.2	9.74	30	26	Cys-Gly
	Identifier	308.2	162.1		30	17	Glu, NH_3
	Quantifier	308.2	179.1		30	13	Glu
$[^{13}C_2{}^{15}N_1]$GSH	Identifier	311.2	84.2	9.74	30	26	$[^{13}C_2{}^{15}N_1]$Cys-Gly
	Identifier	311.2	165.1		30	13	Glu, NH_3
	Quantifier	311.2	182.1		30	13	Glu
S-D-lactoylglutathione	Identifier	380.2	76.2	10.4	32	35	Glu-S-D-lactoyl-Cys
	Identifier	380.2	148.2		32	22	Glu, Gly, H_2CO_2
	Quantifier	380.2	234.2		32	16	Glu, NH_3
GSSG	Quantifier	613.2	355.5	10.92	52	25	2 Glu
	Identifier	613.2	483.7		52	18	Glu
$[^{13}C_4{}^{15}N_2]$GSSG	Quantifier	619.2	361.5	10.92	52	25	2 Glu
	Identifier	619.2	489.7		52	18	Glu

Table 13 Optimised MRMs for Mechlorethamine glutathione conjugate analysis

Analyte	MRM application	Molecular ion (Da)	Fragment ion (Da)	Retention time (min)	Cone Voltage (V)	Collision Energy (eV)	Neutral fragment loss
MEC-GSH-OH	Identifier	409.3	84.2	9.28	34	43	MEC-OH-Cys Gly
	Quantifier	409.3	280.3		34	15	Glu
MEC-GSHCl_{35}	Identifier	427.3	84.2	9.32	34	39	MEC-Cl-Cys-Gly
	Quantifier	427.3	298.3		34	15	Glu
MEC-GSHCl_{37}	Identifier	429.3	84.2	9.32	34	39	MEC-Cl-Cys-Gly
	Quantifier	429.3	300.3		34	15	Glu
MECGSH_2	Identifier	698.7	84.2	9.50	49	40	MEC-GSH-Cys-Gly
	Quantifier	698.7	404.4		49	23	2 Glu

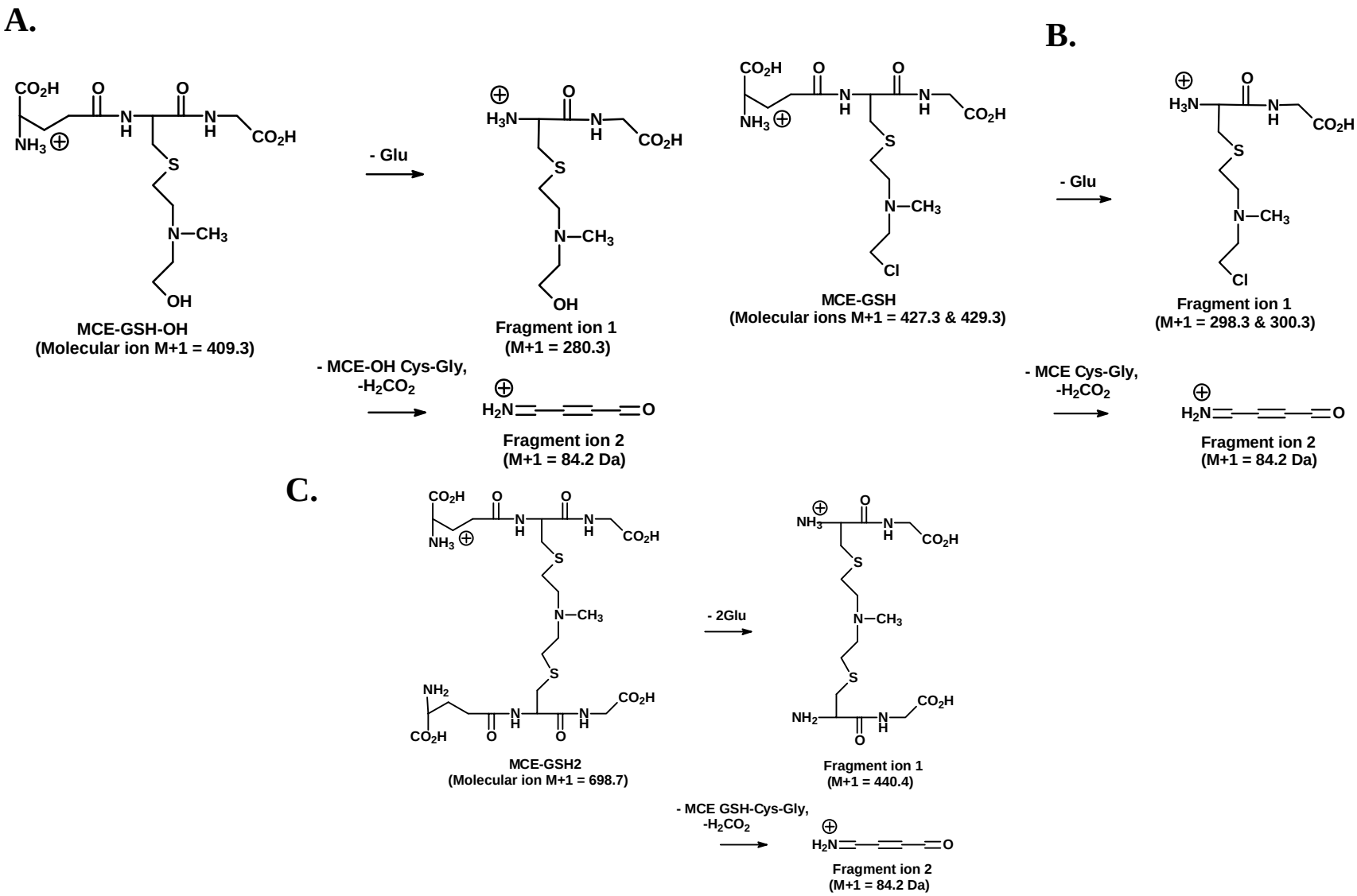

Figure 43 Optimised MRMs for Mechlorethamine glutathione conjugate analysis.

A. Fragmentation of hydrolysed Mechlorethamine-GSH conjugate, MCE-GSH-OH. B. Fragmentation of Mechlorethamine-GSH conjugate, MCE-GSH. C. Fragmentation of Mechlorethamine-biGSH conjugate, MCE-GSH2.

4.4 Data analysis

For the concentration-response curves of anti-cancer drugs, viable cell number (percent of untreated control) V was plotted against drug concentration D and fitted by nonlinear regression to the concentration response equation: $V = 100 \times (GC_{50}^{n})/(GC_{50}^{n} + [D]^{n})$ where GC_{50} is the median growth inhibitor concentration of the drug and n the logistic regression. Non-linear regression was performed using ENZFITTER programme (Biosoft, Cambridge, U.K.). Mass Lynx software was utilized to analyse the data for glutathione, dicarbonyl and GSH conjugate assays. The data was parametric and there is a normal distribution between the two groups. Thus, significant difference between experimental groups was assessed by Student's t-test to predict the form of variance whether equal or unequal variance. Significance was defined as $p \leq 0.05$. Non-parametric analysis were utilized for Glo1 mRNA analysis for three groups.

5.0 RESULTS

5.1 Characterisation of the glyoxalase system and dicarbonyl metabolism in HEK-293 cells *in vitro*.

5.1.1 Growth and viability HEK-293 cell growth in medium containing 25 mM glucose *in vitro*.

HEK-293 cells were cultured in a serum-supplemented basal medium, Dulbecco's Modified Eagle's Medium (DMEM) containing 10 % (v/v) FBS and 25 mM glucose, under aseptic conditions *in vitro*. From the growth curve, HEK-293 cells were in exponential growth up to day 3 of culture and thereafter the rate of cell growth decreased – Figure 44. After 4 days, the cell number had increased to *ca.*1.61 x 10^{6} cells per well. In subsequent experiments, HEK-293 cells were sub-cultured and incubated three days in 25 mM glucose conditions *in vitro*. The mean population doubling time was 0.715 ± 0.08 days (n = 3). This suggests that it has a high proliferation rate which is a characteristic of tumours. The micrographic images are shown in Figure 45.

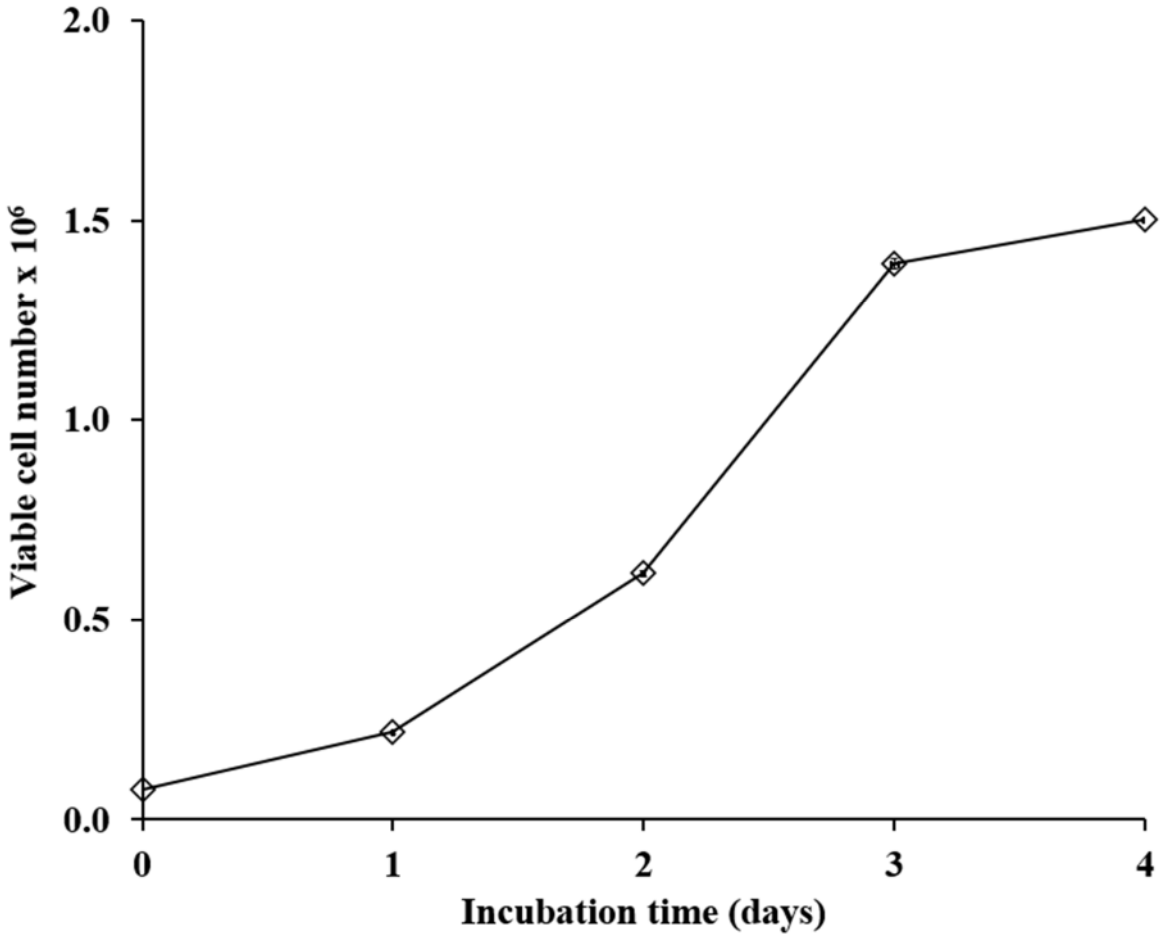

Figure 44: Growth curve of HEK 293 cells in 25 mM glucose *in vitro.*

HEK-293 cells (20,000 cells/cm^2) were incubated in DMEM media with 10% FBS and 25 mM glucose concentrations in 12-well plates that have a diameter of 3.8 cm. This was at 37^{o}C, 5% CO_2 atmospheric conditions. The viable and non-viable cell number were counted using Trypan blue exclusion method every 24 h to construct the growth curve. Data are mean ± SD (n = 3). The log proliferation phase was between 1 – 3 days with a maximal cell number at day 4 of *ca.*1.61 x 10^6 cells per well.

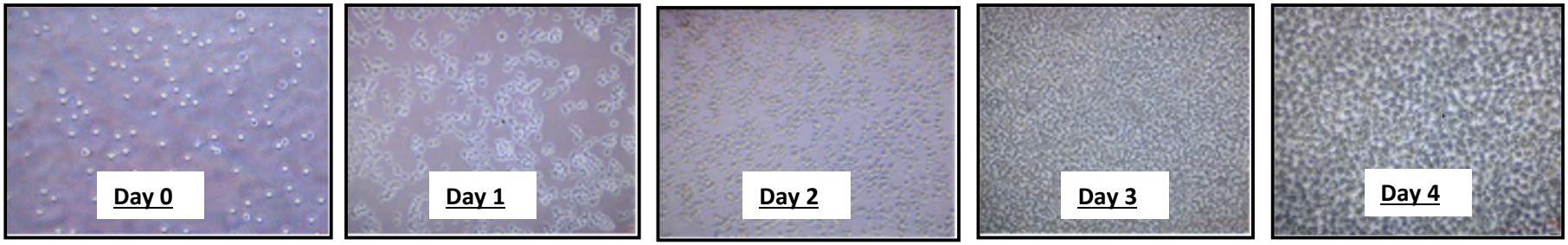

Figure 45: Micrographic images of HEK-293 cells during growth in DMEM medium with 10% FBS.

HEK-293 cells (20,000 cells/cm^2) grown in DMEM medium with 10% FBS at 37^oC, 5% CO_2 atmospheric conditions. Images were taken every 24 h at 20X magnification and presented the epithelial morphology of HEK-293 cells and how their viable cell number and proliferation rate increased over the period of 4 days.

5.1.2 Activity of Glo1, Glo2, MG reductase and MG dehydrogenase in HEK-293 cells in 25 mM glucose *in vitro*.

The activity of Glo1, Glo2, MG reductase and MG dehydrogenase was measured in HEK-293 cell extracts incubated in 25 mM glucose using the protocols described in Section 4.3.3 and the results are presented in Table 14. The enzymatic activity of Glo1 and Glo2 is 3639 ± 21 and 32.0 ± 0.6 mU/mg protein respectively. The MG reductase activity is 1.84 ± 0.10 mU/mg protein and the levels of MG dehydrogenase were undetectable. This reflects the minor role of MG reductase and MG dehydrogenase in the metabolism of MG in HEK-293 cells and emphasises that the major metabolic pathway of MG metabolism is by Glo1 of the glyoxalase pathway.

Table 14: Activity of enzymes of methylglyoxal metabolism in HEK-293 cells *in vitro*. The data presented is the mean ± SD (n = 3). L.O.D, limit of detection.

Glo1 activity (mU/mg protein)	3639 ± 21
Glo2 activity (mU/mg protein)	32.0 ± 0.6
MG reductase activity (mU/mg protein)	1.84 ± 0.10
MG Dehydrogenase (mU/mg protein)	<LOD (0.6)

5.1.3 Glyoxalase 1 protein and mRNA contents of HEK-293 cells incubated in high glucose concentration *in vitro*

The level of the Glo1 protein and mRNA in HEK-293 cells cultured in 25 mM glucose *in vitro* for three days was determined by Western blotting and real-time PCR respectively to provide a molecular and cellular characterization of Glo1 – Figure 46. The Glo1 protein level in HEK-293 cells is 0.683 ± 0.141 whereas the relative GLO1 mRNA expression is 0.904 ± 0.008 normalized to β-actin.

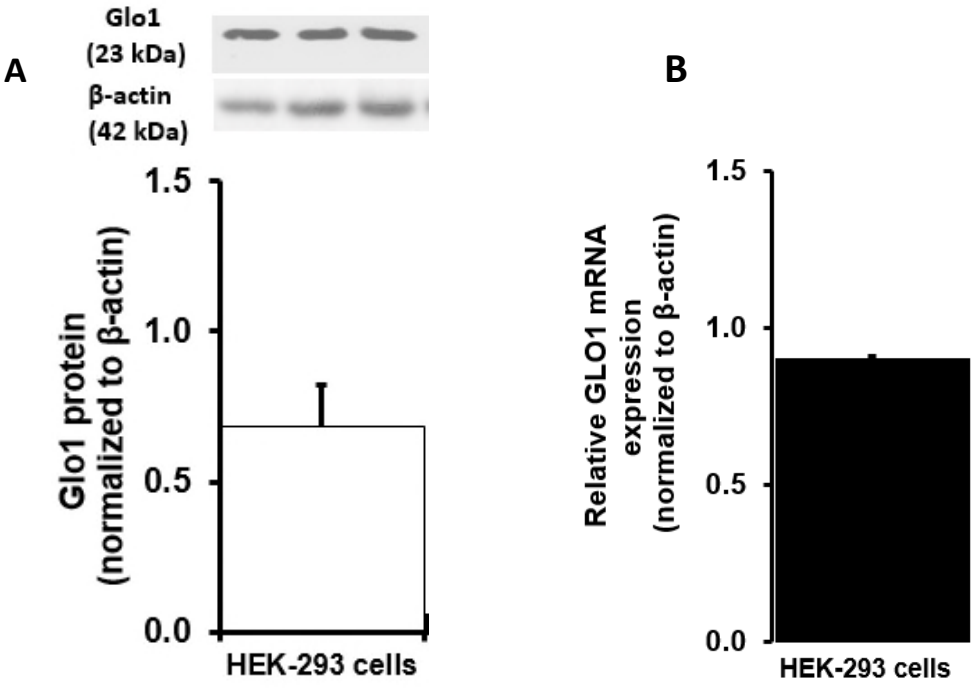

Figure 46: A representation of the relative levels of Glyoxalase 1 protein and mRNA in HEK-293 cells plated at 2 x 10^4 cells/mL incubated in high glucose (25 mM) conditions for three days *in vitro*.

(A) HEK-293 whole cell lysates (20 µg) were analysed by Western blot to detect Glo1 protein using the anti-Glo1 antibody. The Glo1 was detected to be ~ 23 kDa and was stripped and re-probed with the antibody against anti-Beta-actin. Beta-actin was detected to be ~ 43 kDa and was used as a loading control due to its abundance in cells to normalize the relative expression of the protein of interest: Glo1 and ensure the blot is working within detection range to avoid signal saturation and variation. The western blot is representative of three independent replicates Data are mean ± SD (n = 3). (B) Glo1 mRNA expression by real-time PCR in HEK-293 cells normalized to Beta-actin. Data are mean ± SD (n = 3).

5.1.4 The level of dicarbonyl metabolites in HEK-293 cells incubated in high glucose concentration *in vitro*

5.1.4.1 The flux of net L-lactate and D-lactate formation in HEK-293 cells *in vitro*

The flux of D-Lactate formation and the net of L-Lactate formation was determined over three days incubation of HEK-293 cells cultured in high glucose (25 mM) conditions *in vitro*. The media samples were collected on baseline and Day 3 where the flux of D-lactate was calculated by deducting the increase of D-lactate at Day 3 from baseline, normalized to cell number and the number of days of incubation. Thus, it was presented as D-Lactate formation as nmol per million cells per day as shown in Table 15. The net L-lactate formation was determined similar to that of D-Lactate formation; however, it was presented as µmol per million cells per day. HEK-293 cells exhibit characteristics of various tumours where there is high flux of MG formation and elevated Glo1 activity – conditions that are susceptible to toxicity of Glo1 inhibitors (Distler and Palmer, 2012). D-Lactate is a surrogate measure of flux of MG formation and is progressively metabolised by HEK-293 cells.

Table 15: Values of the flux of net L-lactate and D-lactate formation in HEK-293 cells incubated in media containing 25 mM glucose *in vitro*. Data are mean ± SD (n = 3).

Mean metabolic flux	25 mM glucose
Net L-lactate formation (µmol/day/10^6 cells)	6.72 ± 0.24
D-Lactate formation (nmol/day/10^6 cells)	118 ± 10

5.1.4.2 The metabolism of D-lactate in HEK-293 cells *in vitro*

The rate of metabolism of D-lactate by HEK-293 cells was determined by measuring the amount of D-Lactate in the culture medium of HEK-293 cells with and without the addition of exogenous D-lactate (10 µM) at baseline and after incubation for 2 days. This is presented in Table 16. The incremental increase in the rate of D-lactate metabolism on addition of 10 µM D-lactate was 22.7 nmol/day/10^6 cells. The concentration of D-lactate in control cultures at baseline is *ca.* 1 µM, originating from fetal calf serum in the medium. Assuming the rate of D-lactate metabolism is directly proportional to D-lactate concentration, this suggests that the rate of D-lactate metabolism in control cultures is *ca.* 2.3 nmol/million cells/day or 2.5% of the observed rate of D-lactate increase in control cultures. This indicates that the observed rate of increase in amount of D-lactate in HEK293 cultures is approximately equal to the rate of D-lactate formation and hence flux of methylglyoxal formation.

Table 16: D-lactate formation in HEK-293 cells with and without the addition of exogenous D-lactate (10 µM) incubated in media containing 25 mM glucose for 48 hours *in vitro*. Data are mean ± SD (n = 3).

Culture conditions	Rate of increase in D-Lactate formation (nmol/day/10^6 cells)
Control	89.6 ± 8.3
+ Exogenous D-Lactate (10 µM)	112.3 ± 2.9 ($P<0.05$)

5.1.4.3 The flux of glucose consumption in HEK-293 cells *in vitro*

The amount of net glucose consumption by HEK-293 cells can be determined by measuring the culture medium containing 25 mM glucose at baseline and after 3 days – Table 17. This increases the rate of glycolysis and cell survival.

Table 17: The net glucose consumption by HEK-293 cells incubated in media containing high glucose conditions for 3 days *in vitro*. Data are mean ± SD (n = 3).

	HEK-293 cells *in vitro*
Glucose consumption (μmol/day/10^6 cells)	45.2 ± 6.0

5.1.4.4 The concentration of methylglyoxal in HEK-293 cells *in vitro*

The cellular concentration of the main dicarbonyl of MG in HEK-293 cells following three days cultured in medium containing 25 mM glucose *in vitro* was assessed – Figure 47. The concentration was 4.34 ± 1.47 pmol/10^6 cells and the high level suggests that HEK-293 cells have increased dicarbonyl stress under high glucose conditions to increase protein glycation.

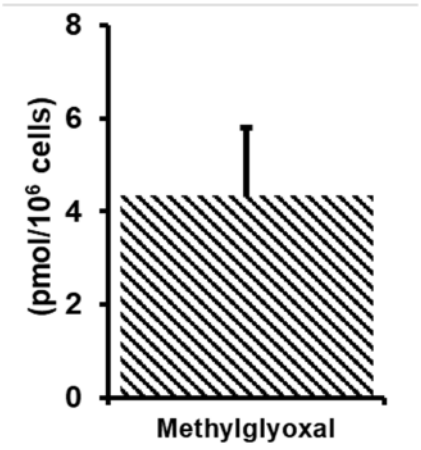

Figure 47: The methylglyoxal concentration in HEK-293 cells in medium containing 25 mM glucose *in vitro*. HEK-293 cells were cultured in DMEM medium containing 25 mM glucose for three days. Data are mean ± SD, (n = 3).

5.1.4.5 The levels of glutathione in HEK-293 cells *in vitro*

The cellular contents of GSH, GSSG and S-D-lactoylglutathione in HEK-293 cells (1 x 10^6) following three days culture supplemented with high glucose concentrations *in vitro* – Table 18. To calculate the levels of total glutathione it is: Total GSH = GSH + (2 x GSSG).

Table 18 The levels of glutathione in HEK-293 cells *in vitro*.
HEK-293 cells were cultured in medium containing 25 mM glucose for three days *in vitro* to determine the levels of glutathione to three independent replicates. Data are mean ± SD, (n = 3).

	HEK-293 cells *in vitro*
GSH (nmol/10^6 cells)	4.40 ± 0.28
GSSG (nmol/10^6 cells)	0.00706 ± 0.00428
Total GSH (nmol/10^6 cells)	4.41 ± 0.28
GSH (% Total GSH)	99.9
GSSG (% Total GSH)	0.122
Cellular S-D-lactoylglutathione (pmol/10^6 cells)	< 1.5 (L.O.D)

5.2 The effect of glucose concentration on HEK293 cells *in vitro*

The concentration of glucose was measured to determine its effect on the HEK-293 cell growth on the glyoxalase system and dicarbonyl metabolism. The hormetic potential of methylglyoxal and its role in causing dicarbonyl stress can then be deduced. The standard protocol for culture of HEK-293 cells used herein has initial glucose concentration of 25 mM. This was compared to incubation with a low glucose concentration of 5 mM under aseptic conditions *in vitro*.

5.2.1 Characterisation of the glyoxalase system of HEK-293 cells incubated in high and low glucose concentration conditions *in vitro*

5.2.1.1 Assessment of HEK-293 cell growth in medium containing 5 mM and 25 mM glucose *in vitro*.

HEK-293 cells were cultured with cell density of 20,000 cells per cm^2, 76,000 cells per well, using a 12 well plate for 4 days. The growth and cell viability of HEK 293 cells was determined via Trypan blue exclusion assay where > 99% in the three independent replicates were viable. From the growth curve, the growth of HEK-293 was exponential to day 3 of culture and thereafter the rate of cell growth decreased. After 4 days, the cell number had increased to *ca.* 1.61 x 10^6 cells per well in 25 mM glucose and 0.82 x 10^6 cells per well in 5 mM glucose *in vitro*. 25 mM glucose was used in MDR studies (supplier recommended conditions) – Figure 48. This is *ca.* 49.0 % decrease in cell growth and suggests that high glucose concentration is a growth advantage for HEK-293 cells and low glucose (5 mM glucose) can decrease cell survival and is reflected on the viable cell number of HEK-293 cells at the stationary phase.

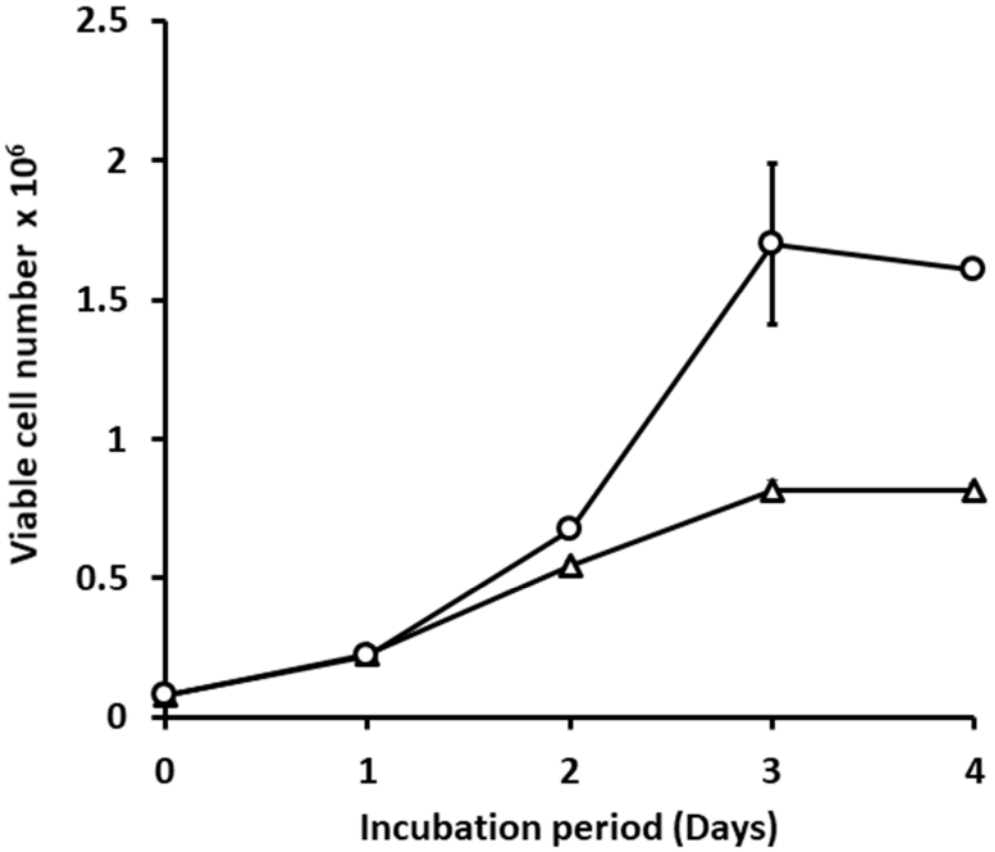

Figure 48: Growth curve of HEK 293 cells in 5 mM and 25 mM glucose for 4 days *in vitro*.

HEK-293 cells (20,000 cells/cm^2) were incubated in DMEM media with 10% FBS and 5 mM 25 mM glucose concentrations indicated for 4 days. Data are mean ± SD (n = 3). Key: low glucose △ ; high glucose ○

5.2.1.2 The activity of glyoxalase 1 of HEK-293 cells in low and high glucose conditions *in vitro*

The enzymatic activity of Glo1 in HEK-293 cells incubated with low D-glucose (5 mM) and high D-glucose (25 mM) conditions for three days was 3350 ± 317 and 2951 ± 106 mU per mg protein respectively. This is *ca.* 11.9% decrease and reflects the metabolic role of high glucose concentration and the increased formation of methylglyoxal as a driver of dicarbonyl stress – Figure 49. An increase in the Glo1 activity is required to protect the proteome of tumours against the high flux of MG formation.

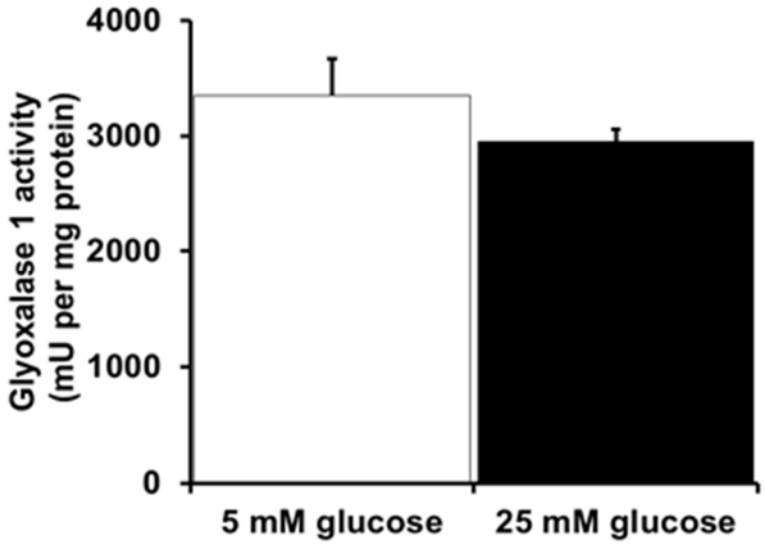

Figure 49: The effect of glucose concentration on the Glo1 activity in HEK-293 cells *in vitro.*

HEK-293 cells were cultured in medium containing low glucose concentration (5 mM) and high glucose concentration (25 mM) for 3 days. Data are mean ± SD (n = 3). Key: low glucose (5mM) □; high glucose (25 mM) ■

5.2.1.3 Flux of glucose consumption, net L-lactate and D-lactate formation in HEK-293 cells cultured in low and high glucose conditions *in vitro*.

Tumour cells require high glycolytic rate and convert most of glucose to lactate in order to grow and proliferate even other oxygenated states; this is known as the Warburg effect (Vander Heiden *et al*., 2009; Vander Heiden, 2011). Therefore, following the Glo1 activity measurement, the effect of glucose concentration on D-Lactate, L-lactate and D-glucose was determined to characterise the energetic metabolism in HEK-293 cells incubated with 5 mM and 25 mM glucose concentrations for three days.

The flux of D-lactate formation was determined in media samples at baseline and after three days and the flux of D-Lactate formation deduced. The flux of D-Lactate formation in HEK-293 cells under low D-glucose concentration conditions was 510 ± 51 nmol/day/10^6 cells whereas under high D-glucose concentration conditions it was 305 ± 18 nmol/day/10^6 cells. This is *ca.* 40.2 % decrease in D-lactate production in high glucose conditions in comparison to low glucose conditions ($p < 0.01$) *in vitro* - Table 19.

Similarly, there was a significant difference in the net formation of L-lactate in HEK-293 cells where under low glucose conditions, the concentration of L-lactate was (70.6 ± 7.5 µmol/day/10^6 cells) ($p < 0.0001$) *in vitro* whereas under high glucose conditions it was (4.82 ± 0.21 µmol/day/10^6), this is *ca*. -93.2% increase in L-lactate formation. The flux of L-Lactate formation was markedly higher regardless of the glucose concentration than the flux of D-Lactate formation. This highlights the concentration of both physiological enantiomers of lactate in HEK-293 cells.

Moreover, there was -41.8 % increase in glucose consumption in HEK-293 cells cultured under low glucose concentration (48.8 ± 3.8 µmol/day/10^6 cells) in comparison to high glucose (28.4 ± 6.1 µmol/day/10^6 cells) ($p <0.01$). This suggests that HEK-293 cells have higher glucose consumption via anaerobic glycolysis that inhibits pyruvate from entering Krebs cycle and increases the conversion of pyruvate to lactate. Increased anaerobic glycolysis also increases

the flux of formation of triose phosphates, DHAP and G3P which in turn increases the flux of MG formation.

To investigate whether the flux of glucotriose degradation to methylglyoxal has occurred in high glucose conditions *in vitro*, the percentage of flux of glucotriose was calculated by dividing the flux of D-Lactate formation of HEK-293 cells by twice the flux of glucose consumption (Hooper *et al*., 1988). This was followed by multiplying the value by 100 to establish the percentage of flux of glucotriose. There was 5.35% increase in the percentage of flux of glucotriose in HEK-293 cells under low glucose conditions 0.523 ± 0.021 in comparison to high glucose conditions (0.551 ± 0.096) *in vitro*. This indicates that glucose has been consumed in the Embden-Meyerhof pathway primarily than other pathway mechanisms such as pentose phosphate pathway in high glucose conditions *in vitro*.

Table 19: The varied analytical assays determining the metabolic fluxes of HEK-293 cells under high and low glucose conditions *in vitro*.

HEK-293 cells were cultured in medium containing low glucose concentration (5 mM) and high glucose concentration (25 mM) for 3 days. Data are mean ± S.D. for independent samples (n = 3). Significance **, $p \leq 0.01$, **** $p \leq 0.0001$ (*t* test, two-tailed, equal variance) with respect to low glucose (control).

HEK-293 cells *in vitro*

Metabolic variable	5 mM glucose	25 mM glucose
Net L-lactate formation (µmol/day/10^6 cells)	70.6 ± 7.5	4.82 ± 0.21 ****
D-Lactate formation (nmol/day/10^6 cells)	510 ± 51	305 ± 18.5 **
D-glucose consumption (µmol/day/10^6 cells)	48.8 ± 3.8	28.4 ± 6.1 **
D-Lactate flux (% Glucotriose)	0.523 ± 0.021	0.551 ± 0.096 **

5.2.2 The effect of exogenous methylglyoxal on the growth and viability of HEK-293 cells *in vitro*

To characterize the response of HEK-293 cells to dicarbonyl stress, HEK-293 cells was treated for 48 h with increasing concentration of exogenous methylglyoxal to evaluate its effect on cell viability and growth. Concentration-cell growth response curves were constructed from 6 different drug concentrations (100 – 2000 μM) and data fitted to deduce 50% of maximal inhibitory concentration (GC_{50}) and logistic regression coefficient (n). Low concentrations of methylglyoxal were insufficient to induce a response. At ≥ 100 μM of methylglyoxal there was a decrease in viable cell number in HEK-293 cells *in vitro*. As the concentration of exogenous methylglyoxal increases, cell growth arrest increases - Figure 50. The dose of methylglyoxal (X-axis) and drug response (Y-axis) was plotted on a logarithmic scale. The resulting methylglyoxal concentration-response curve is inverse sigmoidal. The GC_{50} value for methylglyoxal is 887 ± 40 μM and the logistic regression coefficient was 0.565 ± 0.024.

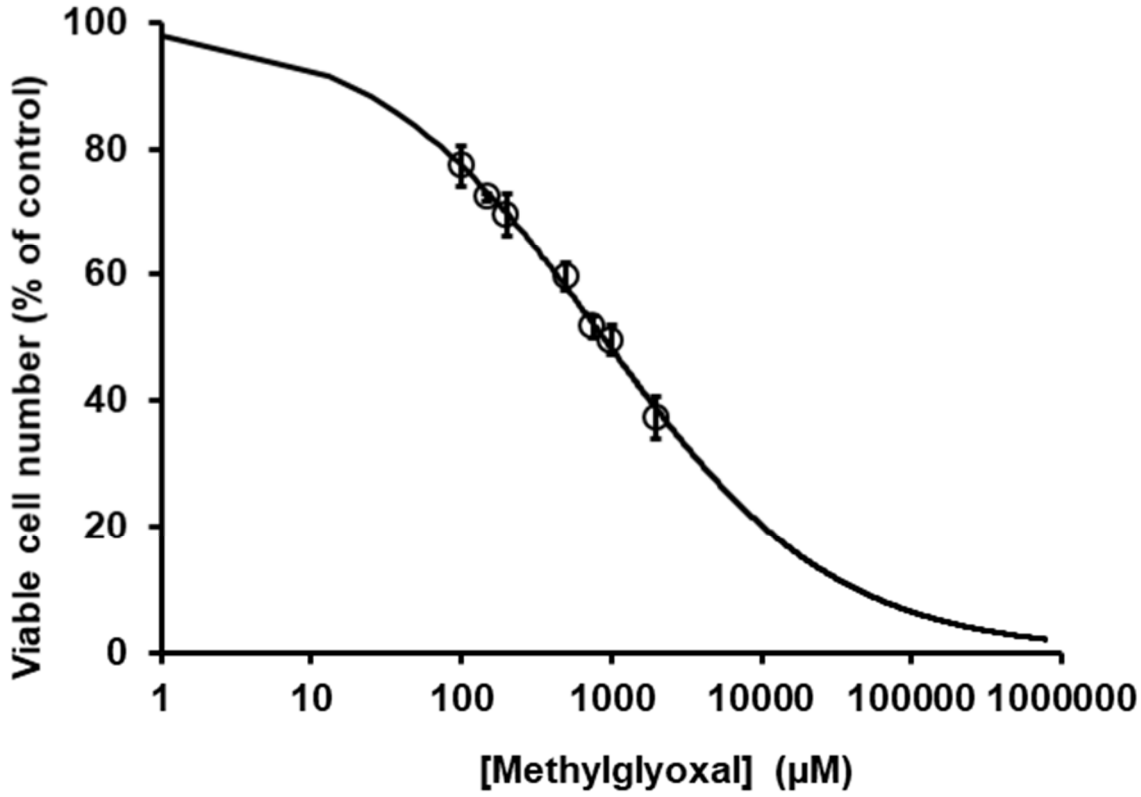

Figure 50: Methylglyoxal concentration-response curve for HEK-293 cell growth incubated under high glucose (25 mM) conditions *in vitro*.

Data are mean ± SEM, n = 3 for Methylglyoxal concentrations 100, 150, 200, 500, 750 and 1000 and 2000 µM. Repeated measurements were conducted to establish the pharmacological profile of methylglyoxal. MG concentration-viable cell number (% of control) were fitted to the dose-response equation = $100 \times 887^{0.565}/(887^{0.565} + [\text{Methylglyoxal}]^{0.565})$. GC_{50} (887 ± 40 µM) and the logistic regression coefficient (0.565 ± 0.024; n = 21)

5.2.2.1 The effect of 887 µM methylglyoxal on the growth of HEK-293 cells in DMEM medium containing 25 mM glucose concentration *in vitro*

To study time course of effect of MG on HEK-293 cell growth, a growth curve of HEK-293 cells was constructed form incubations with and without 887 µM methylglyoxal under high glucose conditions – Figure 51. For the control, the growth of HEK-293 cells was exponential to Day 3 of culture. After 3 days, the cell number had increased to *ca.* 0.982 x 10^6 cells per well. The addition of 887 µM methylglyoxal decreased cell growth of HEK-293 cells *in vitro* and after 3 days, the cell number had decreased to *ca.* 0.536 x 10^6 cells per well. This is *ca.* 45% decrease which validates the GC_{50} value obtained from the dose-response study. Paradoxically, this illustrates how highly proliferating cells such as HEK-293 cells under high glucose conditions presents a resistant phenotype towards treatment with exogenous methylglyoxal and may reflect the level of Glo1 activity and accumulation of MG-derived protein adducts.

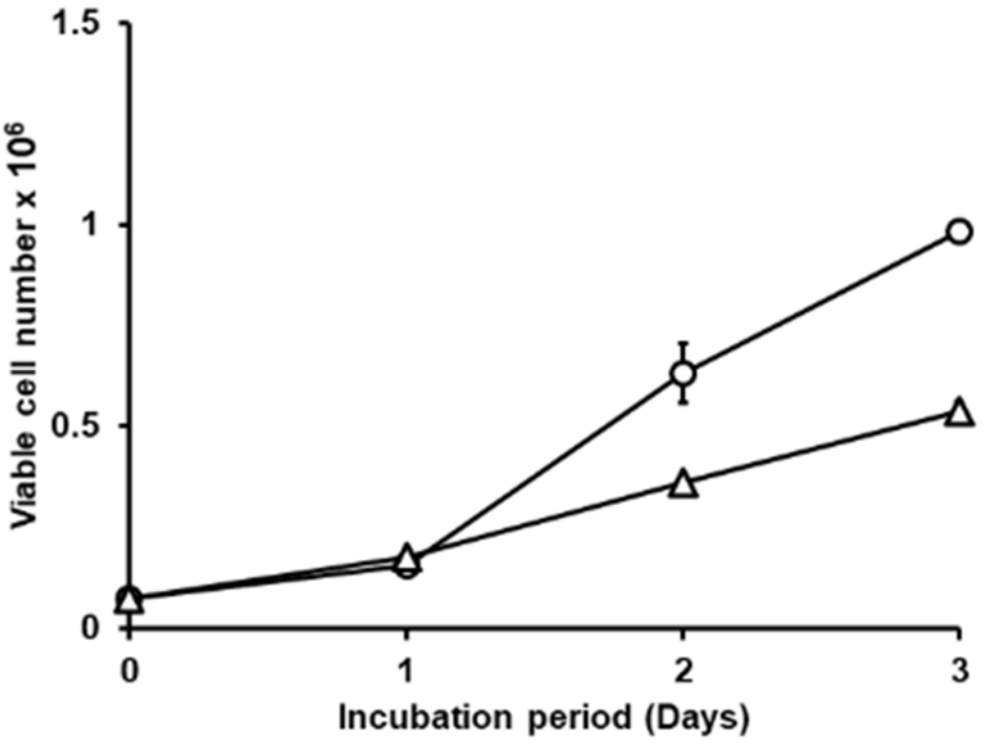

Figure 51: Time-course study of the effect of 887 µM methylglyoxal on the growth of HEK-293 cells under high glucose conditions (25 mM) for three days *in vitro*. Data are mean ± SD (n = 3). ○ Key: Untreated (control); △ 887 µM methylglyoxal

5.3 Stable transfection of HEK-293 cells for overexpression of glyoxalase 1

5.3.1 Comparative analysis of transfected versus non-transfected HEK-293 cells on Glo1 activity.

HEK-293 cells were transfected with vector expressing human Glo1 (pIRES2-GLO1-EGFP) using Lipofectamine 2000 in OptiMEM media. Empty plasmid (pIRES2-EGFP) was used as control. Transfected cells were selected with G-418 disulphate; transfected cell colonies were selected using cloning glass cylinder and cultured further with 2 mg/ml G-418 disulphate in high glucose (25 mM) conditions *in vitro*. The efficiency of the transfection was assessed by visual quantification of EGFP-expressing cells using fluorescence microscopy (excitation maximum, 488 nm; emission wavelength, 507 nm). This is followed by the measurement of Glo1 activity by spectrophotometry and Glo1 protein by western blotting using cytosolic cell extracts. Cell lysates (5×10^6) of cells transfected with pIRES2-GLO1-EGFP plasmid, pIRES2-EGFP plasmid and wild type cells were analysed for Glo1 activity and protein levels. GLO1-overexpressed transfectant cell line had 4 – 5-fold (>90%) increased Glo1 activity, with respect to empty vector stable transfectant control over the ten passages studied – Figure 52.

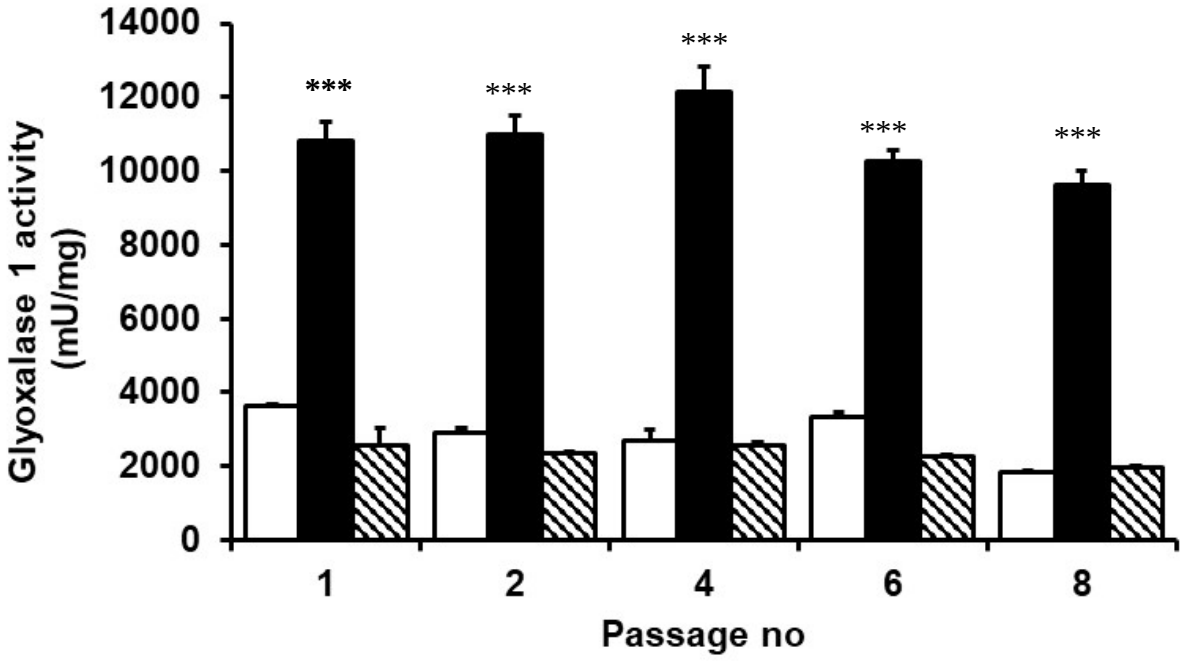

Figure 52: Glyoxalase 1 enzymatic activity of stable transfectant HEK293-derived cell lines for overexpression of Glo1 and empty vector control *in vitro.* HEK-293 cells were cultured in medium containing high glucose (25 mM) conditions *in vitro* for 3 days. Data are mean ± SD (n = 3). Significance testing for paired data were assessed by two-tailed Student t-test for two study groups with equal variance (homoscedastic): Glo1 overexpression with respect to empty vector control ***, P<0.001. Key: wild-type □ ; Glo1-overexpressed ■; Empty vector ▨

5.3.2 Glyoxalase 1 protein content of stable transfectant HEK293-derived cell lines for overexpression of Glo1 and empty vector control incubated in high glucose (25 mM) conditions *in vitro*

The level of the Glo1 protein of HEK-293 cells of wild-type and HEK-293 cells transfected with vector expressing human Glo1 (pIRES2-GLO1-EGFP) and empty plasmid (pIRES2-EGFP) cultured in medium containing 25 mM glucose *in vitro* was determined by Western blotting. GLO1-overexpressed transfectant cell line had 4 – 5 fold (>90%) increased Glo1 protein, with respect to empty vector stable transfectant control over the ten passages studied – Figure 53.

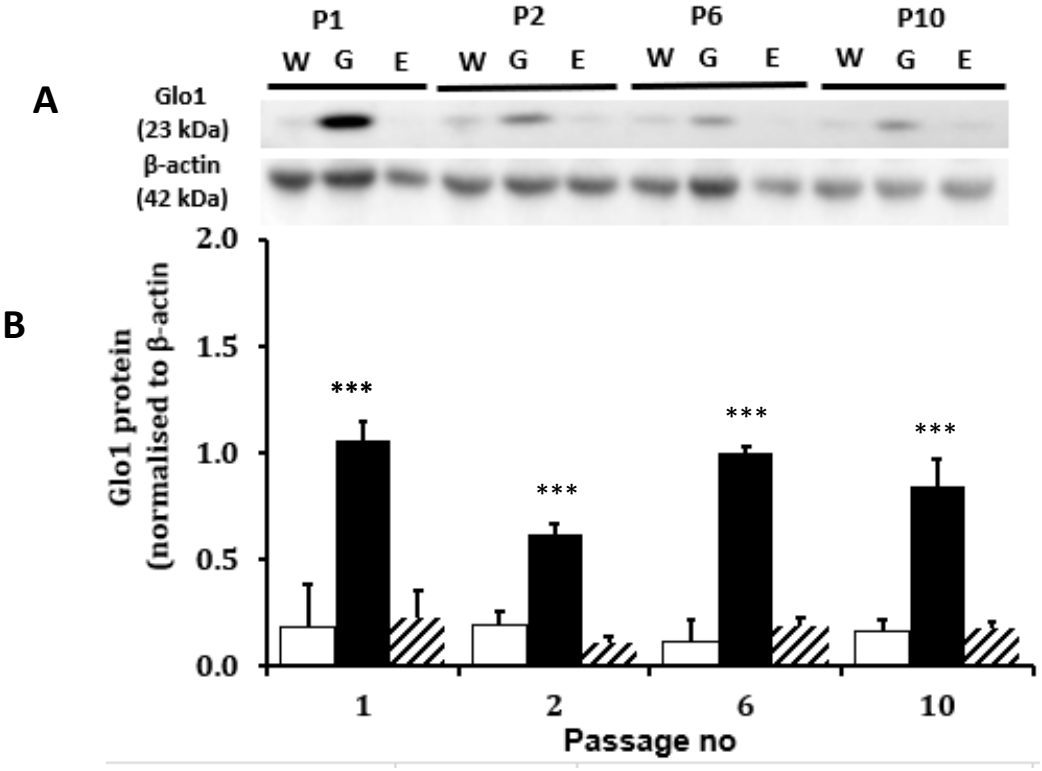

Figure 53: Glyoxalase 1 protein content of wild-type and stable transfectant HEK293-derived cell lines *in vitro*. HEK-293 cells were cultured in medium containing 25 mM glucose *in vitro* for 3 days. (A) Glo1 protein blot, (B) Glo1 protein blot quantitative analysis. Each lane contained 20 µg protein. Beta-actin 1:8000 dilution and the anti-rat Glo1 antibody was used at a 1:10000 dilution. The mean values are plotted and the error bars represent the standard of the mean. Data are mean ± SD of three independent experiments (n = 3). Statistical significance was determined by two-tailed Student's t-test for Glo1 overexpression: ***, P<0.001 with respect to empty vector control. Key: W, wild-type □ ; G, Glo1-overexpressed pIRES2-GLO1-EGFP) ■; E, Empty vector (pIRES2-EGFP) ▨

5.3.3 Assessment of HEK-293 cell growth in wildtype and stable transfectant HEK-293-derived cell lines *in vitro*.

HEK-293 cells were cultured with cell density of 20,000 cells per cm^2, 76,000 cells per well, using a 12 well plate in medium containing 25 mM glucose *in vitro*. From the growth curve, HEK-293 wild type cells were exponential to day 3 of culture and thereafter the rate of cell growth decreased. pIRES2-GLO1-EGFP and pIRES2-EGFP stable transfectant cells lines had slightly lower cell growth rate than untransfected control – Figure 54. After 4 days, the cell number for wild type, pIRES2-GLO1-EGFP and pIRES2-EGFP had increased to *ca.*1.5, 0.977 and 0.868 x 10^6 cells per well respectively. The micrographic images of the three forms of cell lines subjected to fluorescence microscopy are shown in Figure 55. There is green fluorescence in the Glo1 overexpressed and Empty vector stable transfected cells whereas no GFP protein is indicated in the wild-type HEK-293 cells. The morphology of HEK-293 cells has altered from an epithelial-like phenotype in wild-type cells to round cell phenotype in Glo1 overexpressed HEK-293 cell. The cellular defect is due to the toxicity following the introduction of highly efficient plasmid DNA in which the target protein, Glo1 is overexpressed under a cytomegalovirus promoter despite a concentration of 1 µg of DNA was used (Mori *et al*., 2020).

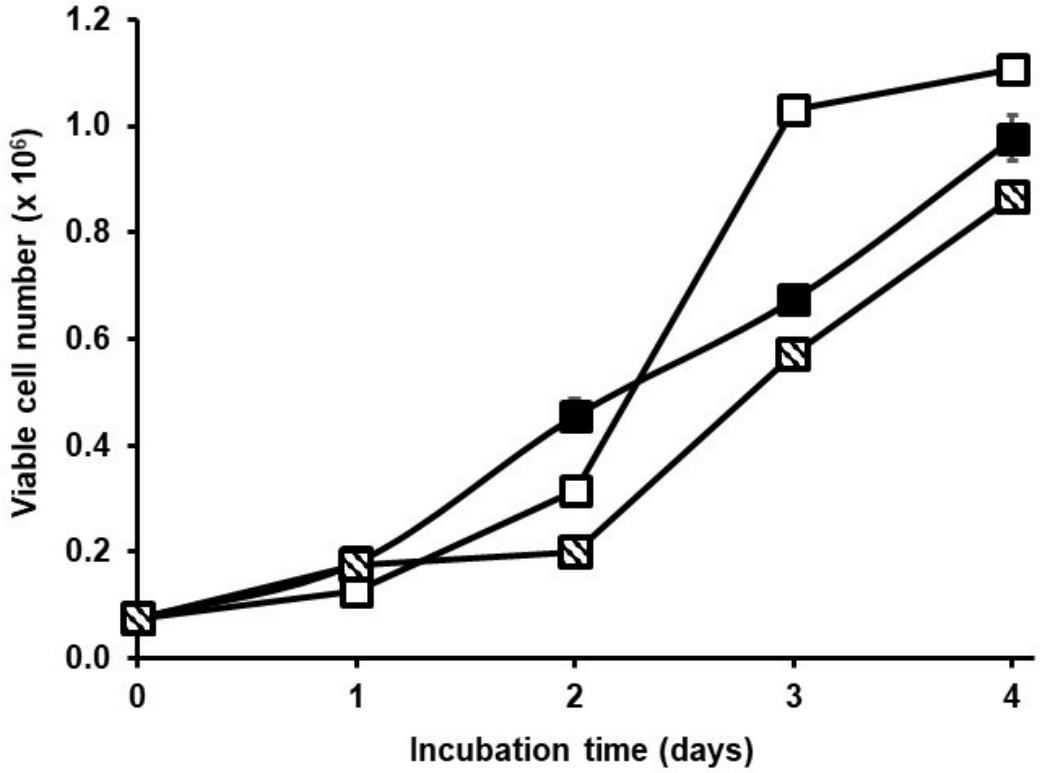

Figure 54: Growth curve of stable transfectant HEK293-derived cell lines for overexpression of Glo1 and empty vector control under high glucose conditions *in vitro*. Data are mean ± SD (n = 3). There was an effect of genotype x time (P = 0.007; ANOVA repeated measures).Key: wild-type ; Glo1-overexpressed pIRES2-GLO1-EGFP) ; Empty vector (pIRES2-EGFP)

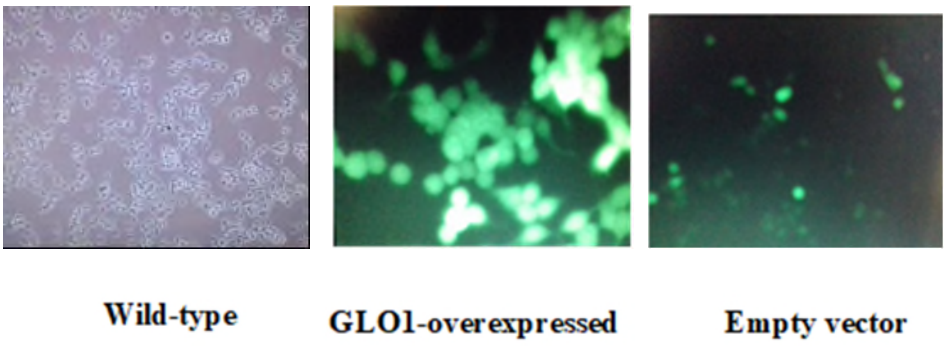

Figure 55: Micrographic images of HEK-293 cells during growth in DMEM medium with 10% FBS under 25 mM glucose conditions *in vitro*: wild-type, GLO1 overexpressing pIRES2-GLO1-EGFP and empty plasmid pIRES2-EGF utilizing phase-contrast bright field and fluorescence microscopy. A 20x objective lens was used and the total magnification was 400x.

5.3.4 The flux of metabolites in wild-type and stable transfectant HEK293-derived cell lines *in vitro*

The flux of glucose consumption and flux of D-lactate formation was measured in HEK-293 cells: wild type and stable transfectant Glo1 overexpressing pIRES2-GLO1-EGFP cells and empty vector control pIRES2-EGFP cells – Table 20. Glucose consumption was decreased 27% in pIRES2-GLO1-EGFP cells and unchanged in pIRES2-EGFP cells, with respect to wild type control. Glucose consumption was decreased in pIRES2-GLO1-EGFP cells by 28%, compared to pIRES2-EGFP cells.

The formation of D-lactate was decreased 58% and 37% in pIRES2-GLO1-EGFP and pIRES2-EGFP cells, respectively, with respect to wild type control. The formation of D-lactate was decreased in pIRES2-GLO1-EGFP cells by 33%, compared to pIRES2-EGFP cells. The formation of D-lactate expressed as a percentage of glucose metabolism is a measure of percentage of glucose metabolism forming methylglyoxal. This was decreased 41% and 38% in pIRES2-GLO1-EGFP and pIRES2-EGFP cells, respectively, with respect to wild type control but unchanged in pIRES2-GLO1-EGFP cells with respective to pIRES2-EGFP cells. This suggests that the Glo1 overexpressing transfection cells line has decreased glucose consumption and proportionate decreased flux of MG formation, compared to empty vector transfectant control. Stable transfection tended to decrease the proportion of glucose leading to MG formation in both stable transfectants with and without Glo1 overexpression.

Table 20: Glucose consumption and formation of D-lactate by wild type and stable transfectant HEK293-derived cell lines cultured in medium containing 25 mM glucose for three days *in vitro*.

Metabolic variable	Wild-type	Glo1-overexpressed (pIRES2-GLO1-EGFP)	Empty vector (pIRES2-EGFP)
D-Glucose consumption (µmol/day/million cells)	39.4 ± 1.2	28.6 ± 1.3 ***,ooo	40 ± 1
Flux of formation of D-lactate (nmol/10^6/day)	89.7 ± 12.3	38.1 ± 4.6 **,o	56.6 ± 10.2 *
Flux of formation of D-lactate (% glucotriose)	0.114 ± 0.017	0.067 ± 0.007 *	0.071 ± 0.009 *

Data are mean ± SD, n = 3. Significance *, ** and ***, P<0.05, P<0.01 and ***, P< 0.001 with respect to wild-type control; o and ooo, P<0.05 and P<0.001 with respect to empty vector transfectant control.

5.4 Effect of anti-cancer drugs on HEK-293 cell growth

5.4.1 Dose-response for the effect of anticancer drugs on HEK-293 cell growth *in vitro*.

Wild-type, empty vector (empty) and Glo1 overexpressing (Glo1+) stable transfectant lines of HEK-293 cells were incubated with and without anti-tumour drugs for 48 h with six different drug concentrations. Viable and non-viable cell number was assessed by Trypan blue exclusion assay. Data was fitted in concentration-response curves to deduce GC_{50} and n values – Figure 56 for topoisomerase inhibitors, 57 for alkylating agents and 58 for other anti-tumour drugs and the experimental anti-tumour drug cell-permeable Glo1 inhibitor. The GC_{50} values for the anti-cancer drugs are given in Table 21. The anti-cancer drugs that had most resistance was Doxorubicin, Mechlorethamine, mitomycin c, paclitaxel and methotrexate. Cisplatin is attracted to cells overexpressed with pIRES2-EGFP-GLOI plasmid. Vincristine, Camptothecin and Glo1 inhibitor had the least resistance.

Table 21: Effect of anti-cancer drugs on the growth of HEK-293 cells (Wild-type, empty vector and Glo1 overexpressing) *in vitro*: GC_{50}. Data are mean + S.D. (n = 3)

Anticancer drug	GC_{50} (wild-type)	GC_{50} (empty)	GC_{50} (Glo1+)	Fold MDR
Mechlorethamine (µM)	2.42 ± 0.36	1.90 ± 0.11	12.70 ± 0.90	7
Mitomycin C (nM)	158 ± 54	174 ± 29	2541 ± 360	15
Cisplatin (µM)	4.17 ± 0.18	3.17 ± 0.35	0.73 ± 0.05	0.2
Methotrexate (nM)	3.83 ± 0.36	4.02 ± 0.35	28.5 ± 0.9	7
Camptothecin (nM)	18.5 ± 0.6	21.8 ± 2.2	37.6 ± 3.3	2
Doxorubicin (nM)	2.99 ± 0.34	3.54 ± 0.28	55.9 ± 3.4	16
Etoposide (nM)	161 ± 11	500 ± 32	1170 ± 169	2
Taxol (nM)	10.5 ± 1.2	6.8 ± 1.0	56.4 ± 7.2	8
Vincristine (nM)	35.2 ± 1.5	63.4 ± 5.2	83.7 ± 3.3	1.3
Glo1 inhibitor BBGD (µM)	3.68 ± 0.20	4.78 ± 0.18	7.37 ± 0.30	1.54

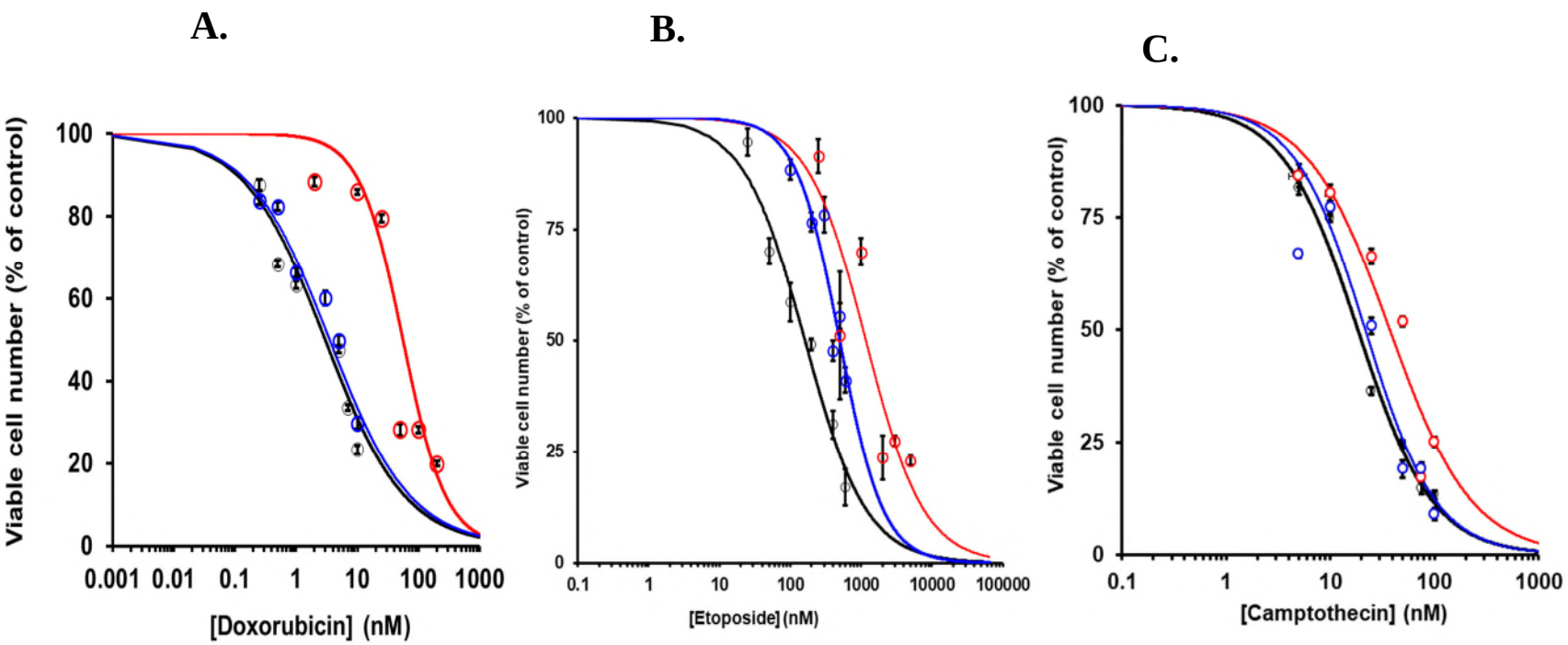

Figure 56: Inhibition of growth of wildtype and stable transfectant HEK-293 cell lines by topoisomerase inhibitors.

A. Doxorubicin B. Etoposide C. Camptothecin. Data were fitted to dose response equation and were solved for GC_{50} and n by non-linear regression (n = 18) which relates to 6 concentrations in triplicates. Wildtype, ■, empty vector ■, Glo1 overexpressed ■

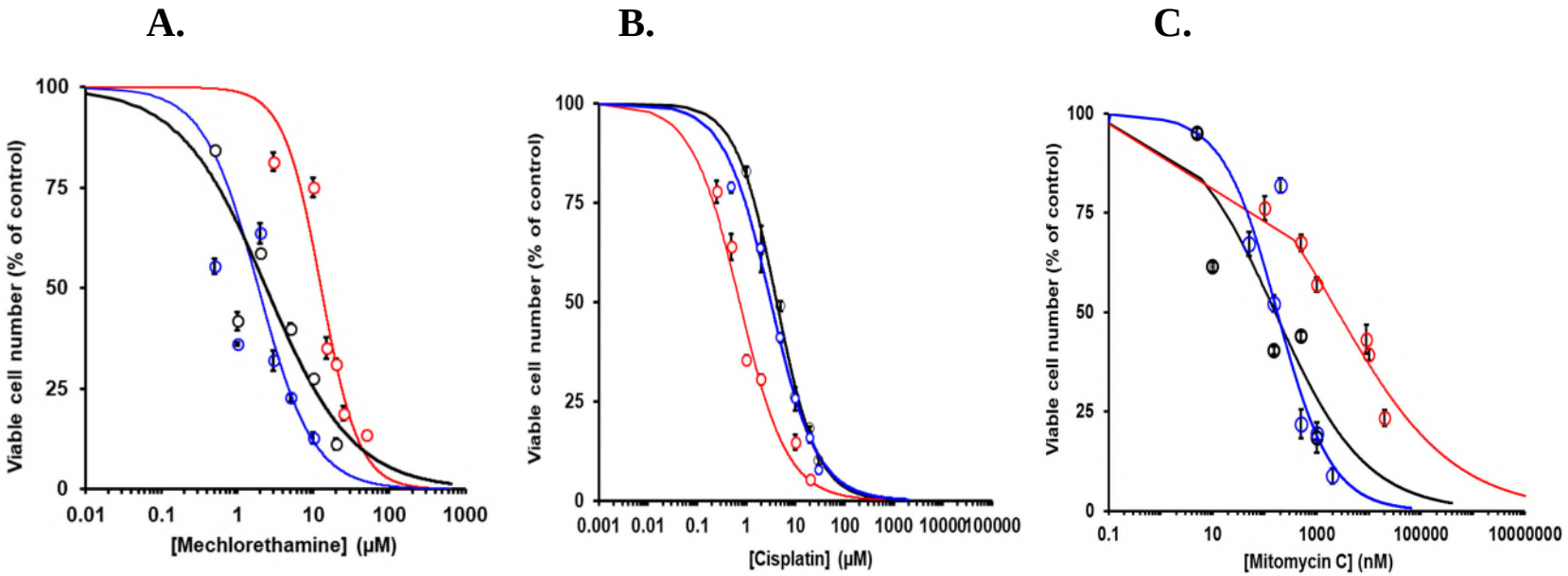

Figure 57: Inhibition of growth of wildtype and stable transfectant HEK-293 cell lines by the alkylating agents. A. Mechlorethamine B. Cisplatin. C. Mitomycin C Data were fitted to dose response equation and were solved for GC_{50} and n by non-linear regression (n = 18) which relates to 6 concentrations in triplicates. Wildtype, ■ ,empty vector ■ , Glo1 overexpressed ■

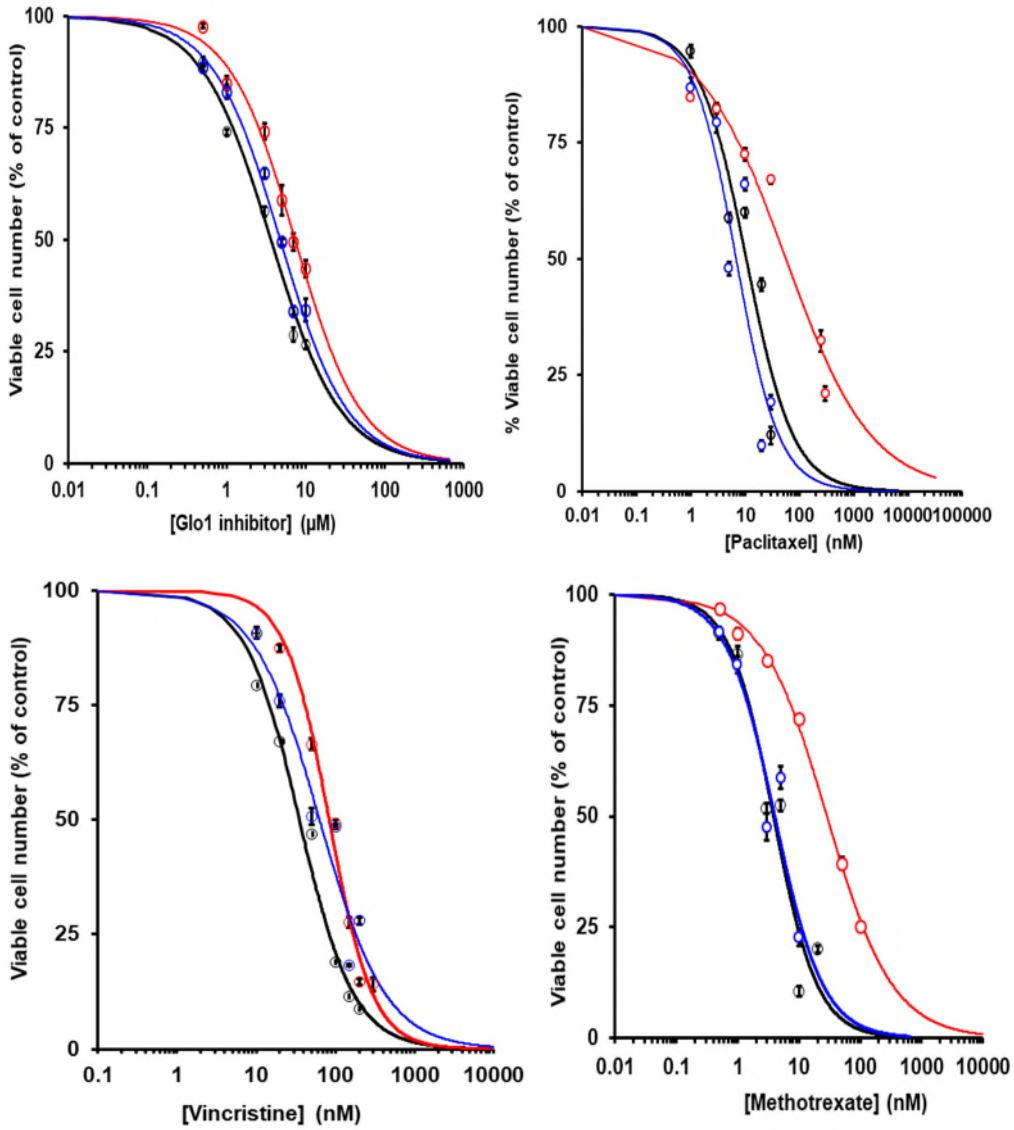

Figure 58: Inhibition of growth of wildtype and stable transfectant HEK-293 cell lines by other anti-tumour drugs. A.Glo1 inhibitor. B. Paclitaxel C. Vincristine. D. Methotrexate Data were fitted to dose response equation and were solved for GC_{50} and n by non-linear regression (n = 18) which relates to 6 concentrations in triplicates. Wildtype, ,empty vector , Glo1 overexpressed

5.4.2 Time-course studies on HEK-293 cells incubated with the anti-cancer drugs that caused high Glo1-MDR.

To investigate the time dependence of the growth inhibitory effects of anti-cancer drugs on HEK-293 cells, time course studies were conducted on wild-type HEK-293 cells *in vitro* incubated with and without mechlorethamine, mitomycin C, methotrexate and paclitaxel at the GC_{50} concentration where as Doxorubicin was conducted at two-fold the GC_{50} – Figure 59. There was minimal cell death after 24 h in drug-treated cells whereas on the second day of incubation there was *ca*. 55% decrease cell death and was significantly decreased on the third day of incubation *ca.* 67% decrease in most cases. HEK-293 cells treated with Methotrexate and Mitomycin C had *ca.* 38% decrease in the third day of incubation. This correlates with the micrographic images in Figure 60 where it presents the time course of changes in cell morphology and growth of HEK-293 cells with and without 5.98 nM Doxorubicin. The drug-treated cells had a round cell phenotype whereas the control maintained its epithelial-like phenotype. This suggests how the anti-tumour drugs that mediated MDR can decrease cell proliferation and induce changes to the morphology of HEK-293 cells.